AD/A-001 819

ABSORPTION SPECTRA OF HIGH-TEMPERATURE SOLID PROPELLANT FLAMES

Richard M. Gross, et al

Utah University

Prepared for:

Air Force Office of Scientific Research

August 1974

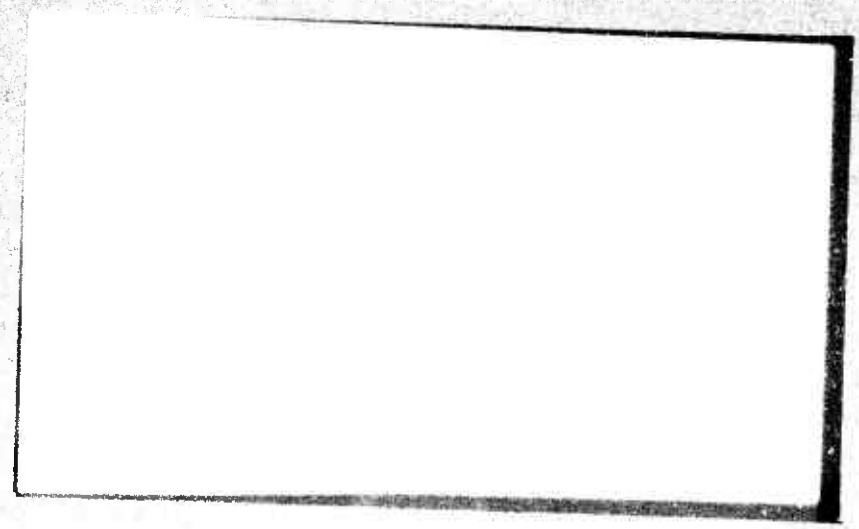

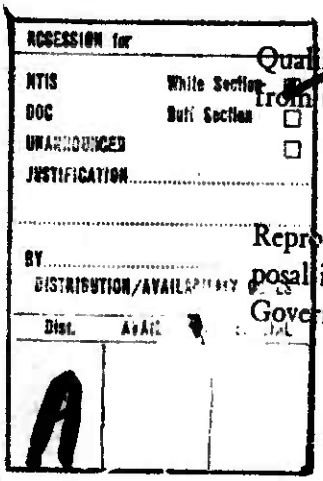

Qualified requestors may obtain additional copies from the Defense Documentation Center.

Conditions of Reproduction

Reproduction, translation, publication, use and disposal in whole or in part by or for the United States Government is permitted.

UNCLASSIFIED

SECURITY CLASSIFICATION OF THIS PAGE (When Data Entered)

REPORT DOCUMENTATION PAGE	READ INSTRUCTIONS BEFORE COMPLETING FORM
1. REPORT NUMBER: AFOSR - TR - 74 - 1905 / 2. GOVT ACCESSION NO.	3. RECIPIENT'S CATALOG NUMBER: AD/A-001 819
4. TITLE (and Subtitle): ABSORPTION SPECTRA OF HIGH-TEMPERATURE SOLID PROPELLANT FLAMES	5. TYPE OF REPORT & PERIOD COVERED: FINAL 1 Jan 73-30 Jun 74
	6. PERFORMING ORG. REPORT NUMBER
7. AUTHOR(s): RICHARD M GROSS, NORMAN W RYAN, ALVA D BAER	8. CONTRACT OR GRANT NUMBER(s): AFOSR-73-2470
9. PERFORMING ORGANIZATION NAME AND ADDRESS: UNIVERSITY OF UTAH, DEPARTMENT OF CHEMICAL ENGINEERING, SALT LAKE CITY, UTAH 84112	10. PROGRAM ELEMENT, PROJECT, TASK AREA & WORK UNIT NUMBERS: 681308, 9711-01, 61102F
11. CONTROLLING OFFICE NAME AND ADDRESS: AIR FORCE OFFICE OF SCIENTIFIC RESEARCH/NA, 1400 WILSON BOULEVARD, ARLINGTON, VIRGINIA 22209	12. REPORT DATE: Aug 1974
	13. NUMBER OF PAGES: 294
14. MONITORING AGENCY NAME & ADDRESS (if different from Controlling Office)	15. SECURITY CLASS. (of this report): UNCLASSIFIED
	15a. DECLASSIFICATION/DOWNGRADING SCHEDULE

16. DISTRIBUTION STATEMENT (of this Report)

Approved for public release; distribution unlimited.

17. DISTRIBUTION STATEMENT (of the abstract entered in Block 20, if different from Report)

18. SUPPLEMENTARY NOTES

19. KEY WORDS (Continue on reverse side if necessary and identify by block number)

INFRARED SPECTROMETER
GAS-PHASE ABSORPTION
COMBUSTION
SOLID PROPELLANT COMBUSTION
COMBUSTION INSTABILITY

20. ABSTRACT (Continue on reverse side if necessary and identify by block number)

A new, high-temperature, infrared radiation source was used in conjunction with a rapid-scanning spectrometer to obtain absorption spectra at an 800 percent rate from composite solid propellant flames during both constant and varying pressure. The propellants studied were AP-HTPB composites. The 3.17 micron H_2O, 4.26 micron CO_2, and 4.72 micron CO absorption bands were calibrated so that the time-dependent variations in the gas phase concentration of these combustion products could be measured. High-frequency oscillations (200-300Hz) were present even in constant pressure tests and are believed to be associated with

DD FORM 1 JAN 73 1473 EDITION OF 1 NOV 65 IS OBSOLETE

UNCLASSIFIED

SECURITY CLASSIFICATION OF THIS PAGE (When Data Entered)

inhomogenieties along the optical path length in the flame. During forced oscillation pressure tests at frequencies of 20 to 100 Hz., the composition and temperature of the propellant flame oscillated in phase with the pressure. The CO2 and CO concentration oscillations were 180 degrees out of phase. The CO2 concentration increased and the CO concentration decreased during periods of pressure increase, and vice versa. The amplitude of these oscillations were many times those observed during the constant pressure tests, and were directly dependent on the rate of pressure change. A study of the variation in the absorption spectra for the major combustion products indicates that prior interpretations of flame emission data during transient pressure conditions were incorrect; however, a principal conclusion of this earlier study was confirmed. Significant gas phase composition variations are produced by pressure changes.

UNIVERSITY OF UTAH

Department of Chemical Engineering

Scientific Report

ABSORPTION SPECTRA OF HIGH-TEMPERATURE SOLID PROPELLANT FLAMES

to Combustion Energetics Division, AFOSR

August 1974

Approved for public release;
distribution unlimited.

Work performed under sponsorship of the Combustion Energetics Division of the Air Force Office of Scientific Research
Grant AFOSR 73-2470A

Report prepared by R. M. Gross
Report approved by Norman W. Ryan and Alva D. Baer

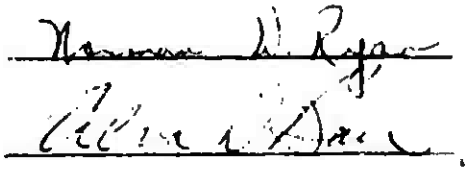

TABLE OF CONTENTS

LIST OF FIGURES

LIST OF TABLES

ABSTRACT

A new high-temperature infrared radiation source was used in conjunction with a rapid-scanning spectrometer to obtain absorption spectra from composite solid propellant flames during both constant and transient pressure tests. Also, an electro-optical, hot-gas pyrometer was used simultaneously to measure flame temperatures. A secondary variable-area nozzle was used to impose either pressure oscillations of controlled amplitude and frequency or single pressure pulses in the combustion chamber pressure. The oscillatory pressure tests had a frequency range of 10 to 100 Hz. and an amplitude range of 2 to 10 psi. The propellants studied were exclusively composites of ammonium perchlorate (AP) and hydroxyl-terminated-polybutadiene (HTPB).

The new, high-temperature, infrared radiation source was operated at a brightness temperature of 2727°K. The rapid-scanning spectrometer scanned the 2.5 to 5.5-μm region in approximately 0.50 msec. at a repetition rate of 800 scans per second. The electro-optical hot-gas pyrometer. operated in the visible spectrum in accordance with the Schmidt method, yielded data at a rate to give 4500 temperature measurements per second.

The 3.17-μm H_2O, 4.26-μm CO_2, and 4.72-μm CO absorption bands were quantitatively calibrated so that variations in the gas phase concentration of these major combustion products could be simultaneously measured. A modified absorbance term, which included the relatively

low intensity flame emission, was used as the calibration parameter. A Beer-Lambert type plot of the modified absorbance versus the respective specie concentration resulted in linear calibration curves over the concentration ranges studied.

The axial concentration profiles revealed CO_2 and CO concentration gradients in the region between 3 mm and 14 mm from the propellant surface. The H_2O concentration was observed to be constant over this same region. These concentration profiles are similar to those observed in hydrocarbon-oxygen flames, and indicate a non-equilibrium condition close to the surface.

The time-varying nature of the composition and temperature at given axial locations in the flame was studied for constant and transient pressure tests. The constant-pressure profiles contained both high and low-frequency oscillations. The high-frequency oscillations (200-300 Hz.) were also present in the transient pressure tests and are believed to be associated with inhomogenieties along the optical path length in the flame, and were not phase correlated. The low-frequency oscillations were not continuous like the high-frequency oscillations, but rather were random in nature. These low-frequency fluctuations were typically in the range of 20 to 80 Hz., with no preferred frequency being apparent. These random fluctuations in the composition profiles are an indication of local changes in the composition of the pyrolysis products leaving the propellant surface.

During the 20 to 100 Hz. oscillatory pressure tests, the composition and temperature of the propellant flame oscillated in phase with the pressure. The CO_2 and CO concentration oscillations were 180° out of phase, and the H_2O oscillation was usually in phase with the

CO oscillation. The CO_2 concentration increased and the CO concentration decreased during periods of pressure increase, and vice versa. The amplitude of these oscillations were many times those observed during the constant pressure tests, and were directly dependent on the rate of pressure change.

The single-pressure-pulse tests further confirmed this pressure effect on the relative specific gasification rates of the AP and HTPB. A single pressure-increase pulse caused an initial oxidizer-rich period which was followed by random fluctuations in the gas phase composition. These random fluctuations varied in frequency and amplitude from test to test and within individual tests, and were apparently independent of the rate of pressure change over the range studied. The single pressure-decrease pulse caused an initial fuel-rich period which was followed by an AP-rich period. This alternating composition condition was continuously repeated during the depressurization. The characteristic time associated with the initial composition change was 15-20 msec and was very reproducible from run to run. Although the magnitude of this initial composition fluctuation was directly dependent on the rate of depressurization, the characteristic time was independent of the rate of depressurization over a range of 300 to 700 psi per second. Even though the rates of pressure change were comparable to those of the oscillatory pressure tests, the composition changes during these single-pressure-pulse tests were much smaller than those of the oscillatory pressure tests.

The characteristic time for composition adjustment corresponds to a characteristic frequency of approximately 25 Hz., which is consistent with the observed difference in the concentration profiles

for oscillatory pressure tests below approximately 20 Hz. At these low frequencies, the concentration oscillations appeared to oscillate at a frequency slightly different than that of the pressure.

The absorption spectra for the three major combustion products obtained in this study indicate that an earlier interpretation of flame emmision data during transient pressure conditions leads to invalid conclusions, even though the general features of the observed phenomena were similar to those reported in this study.

CHAPTER I

INTRODUCTION

Simple composite solid propellants are made by dispersing a finely divided crystalline oxidizer, such as ammonium perchlorate, in a polymeric fuel. The resulting heterogeneity of composite solid propellants has long been recognized as playing an important role in both the steady and the transient combustion processes. Over the years, many studies have attempted to relate the scale of inhomogeneity, the oxidizer particle size, to the burning characteristics of composite propellants. However, almost without exception these studies were aimed at the gross characterization of various propellants. There have been relatively few fundamental studies of the effect of propellant heterogeneity on the combustion processes, and most of them have been limited to stable combustion. Also, almost all of the theoretical modeling of oscillatory combustion has been done with the assumption of a homogeneous condensed phase.

Derr and Osborn [1] observed a change in the steady-state flame structure, as indicated by temperature measurements, adjacent to the solid propellant surface when the oxidizer particle size was changed. Several studies [2, 3, 4] have dealt with the effect of the composite propellant heterogeneity on the propellants' surface structure during stable combustion. These studies revealed that there is a difference in the steady-state gasification rates of the ammonium perchlorate (AP) oxidizer

crystals, and the fuel-binder matrix of composite solid propellant. Also, both of these gasification rates have different steady-state pressure dependencies.

A recent study [5] has shown that there are gas composition variations in composite solid propellant flames during rapid depressurization. These composition variations are caused by changes in the apparent gasification rates of the oxidizer and fuel-binder, due to different pressure-rate dependencies. This phenomenon could result in significant gas composition variations in composite solid propellant flames during oscillatory combustion.

The objective of this work was to characterize this change in the gasification rates of the various components of composite propellants due to pressure oscillations. A rapid-scanning infrared spectrometer was used to quantitatively measure the absorption by propellant flames during externally imposed pressure oscillations.

Gasification Rates: Related Studies

The previous investigations concerning the gasification rates of the two major components of composite solid propellants, the oxidizer and the fuel-binder, employed two kinds of experiments: 1) steady-state pressure tests, and 2) transient pressure tests.

This gasification-rate phenomenon was originally observed by Bastress [2, 6] during a comprehensive investigation of the steady-state burning rates of composite propellants. Bastress examined the extinguished burning surface from steady-state pressure tests. Burning propellant strands were extinguished by means of a rarefaction wave, and the propellant surfaces were studied by means of microscopic

examination and photomicrography. A series of uncatalyzed, unmetallized, AP-polysulfide propellant samples, both unimodal and bimodal oxidizer size distributions, were extinguished over the pressure range from 15 to 1000 psia. This technique produced some interesting information regarding the heterogeneity of composite propellants.

At low pressures, the oxidizer crystals were observed projecting above the fuel-binder surface. However, at intermediate pressures the crystals were flush with the fuel-binder surface, and at high pressures the AP crystals were below the fuel-binder surface. Although this trend was observed for all oxidizer particle sizes studied (9 μm to 265 μm), it was obviously easiest to observe with the larger particle sizes. In the case of a bimodal propellant sample burning at low pressures, the course oxidizer particles were observed projecting above the surface of the fuel-binder containing the fine oxidizer particles. At high pressures the large particles were again observed to be below the fuel-binder surface.

During steady combustion the regression rates of the two propellant components must be the same. However, the gasification rate can be represented as vA for each component, where v is the gasification rate per exposed surface area of the component, and A is the exposed surface area of the component per total propellant surface area. For a given propellant, during steady burning,

$$\frac{\bar{v}_{ox}\,\bar{A}_{ox}}{\bar{v}_{fuel}\,\bar{A}_{fuel}} = \text{constant} \quad , \tag{1}$$

where the bar denotes the time-average values. At high pressure, $(\bar{v}_{ox}/\bar{v}_{fuel})$ is large, and $(\bar{A}_{ox}/\bar{A}_{fuel})$ is small with the AP crystals being exposed only at the bottom of the observed holes. At low pressure,

($\bar{v}_{ox}/\bar{v}_{fuel}$) is small and ($\bar{A}_{ox}/\bar{A}_{fuel}$) is large with the oxidizer crystals protruding above the propellant surface.

Recent work [3, 4] using a scanning electron microscope (SEM) to study the extinguished burning surfaces of composite solid propellants has confirmed the observation reported by Bastress. Boggs et al. [3] studied uncatalyzed, unmetallized composite solid propellants consisting of ammonium perchlorate (AP) and either polyurethane (PU) or carboxy-terminated polybutadiene (CTPB) fuel-binder. Small strands of these propellants were burned over a pressure range from 15 to 800 psia. Once steady-state conditions were attained, the propellant flame was extinguished by a rapid depressurization of the combustion chamber. The SEM used to study the extinguished surfaces provided magnifications up to 100,000 X. Also, high-speed, high-magnification motion pictures were taken while the strands were burning. A comparison of surface structures observed in the motion pictures and those of the extinguished samples indicated that any artifacts introduced by the extinguishment method were minor. The results of propellant strands (25% PU, 74% 200-μm AP) extinguished at both 100 and 800 psia, clearly showed that at the low pressure the specific gasification rate of the AP particles is less than that of the fuel-binder, and vice versa at the high pressure. The low pressure sample also indicated that the AP particles were apparently undermined. Another propellant sample (22% PU, 78% 50 μm AP) showed this same undermining when extinguished at 100 and 200 psia. Tests designed to explore any possible effect of the fuel-binder type on the surface structure were conducted with a propellant containing CTPB fuel-binder. The tests revealed the same type of results, except the AP particles did not appear to be undermined. These studies clearly revealed that the steady-state gasification rates of the AP particles

and the fuel-binder matrix have different pressure dependencies.

Schulz [5, 7] studied the spectral emission (1.7 to 4.8 μm) and temperature of various composite propellant flames during extinguishment by rapid depressurization of the combustion chamber. Propellant samples were burned in a combustion chamber which was mounted on the end of a rarefaction tube. The propellant samples were allowed to burn stably for a short time before the cellulose-acetate diaphragm in the rarefaction tube was ruptured. Spectral measurements were made by means of the same Warner and Swasey Model 501 Rapid-Scanning Spectrometer used in the present study. The emission spectra, at the rate of 800 per second, and a pressure transducer signal were photographically recorded from an oscilloscope display. Flame temperature measurements were made by means of the emission-absorption technique at the sodium D-lines. The flame temperature measurements were not made simultaneously with the spectral measruements but during separate "identical" tests.

Schulz used the 2.5-um H_2O and the 4.4-μm CO_2 emission band intensities as a measure of changes in the flame gas-composition. Because of the rapid depressurization rates, which also produced large flame temperature excursions, it was impossible to relate the individual emission band intensities directly to the flame species concentrations. However, equilibrium calculations showed that the ratio of the H_2O-to-CO_2 in the propellant flame for these fuel-rich systems decreased as the AP level increased. This was confirmed with steady-state emission tests run for various propellants containing different levels of AP. Since the temperature effect on the H_2O and CO_2 emissions would be similar, the use of the intensity ratio approximately compensates the temperature effect. Also, by comparing the transient ratios from depressurization tests with

the measured steady-state ratios at the same pressures, Schulz approximately treated the pressure effect. In this manner Schulz was able to detect changes in the effective fuel-to-oxidant ratio in the propellant flames during rapid pressure decays.

During the initial depressurization, the intensity ratio indicated that a more oxidizer-rich gas was being produced. However, after only several milliseconds, as the pressure decay proceeded, a more fuel-rich gas was generated. Schulz states, "this recovery is probably due in part to the depletion of AP on the propellant surface." For many of the tests, extinguishment occurred during this period of apparent fuel-rich gas generation. The flame temperature decreased rapidly during the initial depressurization, lagging behind the initial drop in the spectral intensity ratio only slightly. The flame temperature recovered at about the same time as the spectral intensity ratio. Schulz postulated that during the rapid pressure decay, the rate of AP gasification increases relative to the fuel-binder rate of gasification. Then, as the pressure decay rate decreases, the relative rates of gasification reverse.

In an effort to obtain direct evidence of the postulated independent gasification rates during depressurization, Schulz tried to separately tag the oxidizer crystals and the fuel-binder with different metallic additives. The spectrometer was operated in the visible region for this work, and the spectral emission intensities from the various metals were measured. Originally, either sodium or potassium permanganate was co-crystallized with AP to form homogeneous crystals. Finely-ground sodium chloride or sodium oxalate was used to tag the fuel-binder. The manganese emission level at 0.403 μm, and the sodium emission at

0.589 μm were used to monitor the relative gasification rates of the AP and fuel-binder respectively. These tests seemed to confirm the postulate of independent gasification rates but were far from being conclusive. However, the infrared emission intensity ratio studies of these propellants containing nonalkali metallic salts failed to confirm the postulate.

These metallic compounds apparently produce a coupling of the oxidizer and fuel-binder gasification, notwithstanding the observations in the visible region. Further tests indicated that only the monovalent alkali metals did not affect the combustion processes. The range of the spectrometer did not allow Schulz simultaneously to tag both the AP and the fuel-binder with different alkali metals. Therefore, separate "identical" tests were run with differently tagged propellants. The AP-tagged propellant was tagged by co-crystallizing sodium perchlorate and AP. The fuel-binder tagged propellant again used very fine sodium chloride. Comparison of the sodium emission intensities from these separate "identical" tests does not allow a firm conclusion, but the results are consistent with the postulated independent gasification rates. Although Schulz's study was very qualitative, it is one of only two fundamental studies to date regarding this variation in gas-composition due to independent gasification rates of the AP and fuel-binder. The other study, by Eisel, is discussed in a following section.

The new high-temperature infrared radiation source developed in this laboratory now permits quantitative absorption measurements to be made of flame gas compositions.

Infrared Absorption Spectroscopy in Flames

The temperatures of most flames of interest exceed the effective temperatures (1500-1700°K) of conventional infrared sources. Therefore, the majority of the spectral studies of flames have been either emission studies, or absorption studies in the ultra-violet and visible regions where high-temperature sources are available.

Emission spectroscopy of flames will not be discussed in detail. The reader is referred to references 8 and 9 for an excellent review of flame emission spectroscopy. Emission is largely due to the small fraction of the molecules or atoms that are in an excited state. These data are a measure of the concentration of the unexcited atoms or molecules only when their excited companions are in thermal equilibrium and there is no self-absorption. Also, the correlation of the emission intensity and the concentration is a difficult matter and can be realized in only a few special cases. Thus, although emission spectroscopy is a powerful qualitative tool, it is almost impossible to obtain quantitative information from emission data.

Absorption spectroscopy requires a background source which has a bright continuous spectrum. For absorption work in flames, this source must have a brightness temperature which is greater than the effective brightness temperature of the flame. This requirement has limited most absorption spectroscopy work in flames to the ultra-violet and visible regions, where very high temperature sources are available. The two most common sources used for the ultra-violet and visible regions are the tungsten strip-filament lamp (2800°K) and the xenon high-pressure arc lamp (5000°K). Many of the stable products of combustion (H_2O, CO_2, CO) do not possess the electronic energy levels necessary to produce

appreciable absorption of radiation in the ultra-violet and visible regions. But since many fuels and intermediate combustion products (i.e., acetylene, formaldehyde, propionaldehyde, benzene, NH_3, NH_2, OH, C_2, CH, NH) do have absorption bands in these regions, ultra-violet and visible absorption spectroscopy has been used to study the reaction mechanisms in flames [10, 11, 12, 13].

Many of the stable products of combustion (i. e., H_2O, CO_2, CO, NO), as well as many unburned hydrocarbons, have absorption bands in the near and middle infrared region (0.70 - 25 μm), making infrared absorption spectroscopy an ideal in-situ method of studying many combustion phenomena. This method eliminates the need for sampling probes, quenching systems and the like associated with the analytical methods requiring a representative gas sample. Unfortunately, the two conventional near and middle infrared background sources, the Nernst glower and the Globar, have maximum operating temperatures of approximately 1700°K to 1500°K respectively. The Nernst glower is an electrically-heated rod of fused rare-earth oxides, and the Globar is an electrically-heated rod of bonded silicon carbide. This relatively low source temperature has restricted the use of infrared absorption spectroscopy to studies of low temperature flames [14, 15]. Cole and Minkoff [16, 17] report doing infrared absorption spectroscopy work in methane-oxygen and ethylene-oxygen flat diffusion flames. They report that the flames studied have maximum temperatures approaching 3000°K, but the operating temperature of the Nernst glower is not reported.

There have been several attempts [18, 19, 20, 21] at developing a new high-temperature infrared source, all of which have resulted in varying degrees of failure. None of them, with one exception, are known

ever to have been used for spectroscopic studies. The exception is the carbon-arc lamp (3800°K) which has been used as a far infrared source. There are several problems associated with using the carbon-arc lamp as a background source: band emission superimposed on the continuum, and atmospheric H_2O and CO_2 interference when operated in its normal mode are just a couple. Thus, the carbon-arc lamp has been limited to specialized applications. The new high-temperature (2800°K) infrared radiation source developed in this laboratory is not plagued by these problems and is ideal for quantitative absorption work in high temperature flames.

Spectroscopic Studies of Composite Propellant Flames

Almost all of the spectroscopic investigations of solid propellant flames have been emission studies, and the majority of these emission studies are for stably-burning double-base solid propellants. These studies are reviewed in reference 22 and will not be discussed. There is but one absorption-spectroscopy study [23] of solid propellant flames reported in the literature, and this study is for a double-base propellant. Only four spectroscopic studies [7, 24, 25, 26] of solid propellant flames during unstable burning are reported, including the work of Schulz [7] already discussed.

Heath and Hirst [23] studied stably burning cordite strands, both photographically and spectroscopically. Besides measuring the dimensions of the different flame zones, they recorded both emission and absorption spectra in the ultra-violet and visible regions. In the dark zone immediately above the propellant surface, they observed some absorption, which they attributed to aldehydes and other organic molecules. They

did not observe the atomic lines of sodium and potassium in this dark zone, indicating that these metal atoms were probably not in the gas phase yet. The absorption in the explosion zone was continuous and complete. They concluded that the explosion zone had a sufficiently large concentration of carbon particles to cause the explosion-zone to be a blackbody.

All of the spectroscopic studies of unstable solid propellant combustion were emission studies, and one of them is of double-base solid propellants. Diederichsen and Gould [24] recorded the photographic spectrum of the near ultra-violet region of double-base solid propellants during mechanically-imposed pressure oscillations. They did not identify any of the spectral bands, but they did observe that the amplitude of the flame radiation oscillations increased toward shorter wavelengths. They suggested that stability grading of various propellants could be done using this short wavelength radiation.

Kimball and Browlee [25] have reported preliminary studies of composite-solid propellant flame emission during unstable burning. Their work was in the visible region, and they reported NH, CN, CH, OH, Ca, Na, K, and Fe emission at one atmosphere. But at 76 atm., they were only able to see NH and OH emission above the continuum.

Eisel [22, 26] studied the infrared emission spectra of composite solid propellant flames during L*, or bulk mode (BMI), instability. A series of propellants (80% AP, 20% estane-based polyurethane), differing only in distribution of AP particle sizes, were studied. These various propellants were tailored to be unstable at low pressures (below 60 psia) and at low frequency (10 to 100 Hz.). Eisel used the rapid-scanning spectrometer used in the present study, to record alternate flame

emission and flame emission-absorption spectra (1.7 to 4.8 μm) during unstable combustion.

Eisel used flame emission spectra (400 spectra per second) to monitor the 1.9-μm H_2O, 4.3-μm CO_2, ano 4.6-μm CO emission intensities. A preliminary shock tube study was undertaken to calibrate emission intensities as a function of partial pressure, temperature, and total pressure. These data were used to normalize the raw CO_2 emission data to fixed values of temperature and pressure. Eisel states, "variations then noted in intensity are attributable to a change in concentration." The 4.6-μm CO band was of low intensity and was badly overlapped by strong adjacent bands. Therefore, Eisel states that "the CO data must not be given too much credence," and, in fact, the CO data are not reported. Also, the H_2O data were only reported in the form of raw H_2O/CO_2 intensity ratios. The flame emission-absorption data (400 spectra per second) were only used in the calculation of the flame temperatures, using the emission-absorption technique applied to the 4.3-μm CO_2 band.

Eisel reports observation of at least three different variations of unstable combustion. These are described as bulk mode instability (BMI), "layer frequency" instability, and local intrinsic instability. BMI was noted by oscillations in the apparent CO_2 concentration and the flame temperature at the same frequency as the pressure oscillations, and both were consistently leading the pressure oscillations. The BMI frequency was controlled by the particle size of the smaller AP particles (15-90 μm). These frequencies were only approximately related to the frequencies predicted by Boggs and Beckstead's [27] "layer frequency" concept. However, the predicted frequency (approximately 3 Hz)

associated with the larger AP particles (600 μm) was approximately equal to the observed frequency in the pressure history records of both unstable and stable tests. Eisel observed tests where both the apparent CO_2 concentration and the flame temperature oscillated at the same frequency, but at a frequency different from, and uncorrelated to, the pressure oscillations. He refers to this as intrinsic instability, and explains it as a situation in which isolated randomly phased regions on the propellant surface burn with a distinct periodicity unrelated to the pressure or flow conditions. It should be noted that the measured flame temperatures were typically 600-800°K lower than the calculated adiabatic flame temperatures for this propellant system.

Present Study

The development of a new high-temperature (2800°K) infrared radiation source in this laboratory now permits infrared absorption measurements to be made in high temperature flames. This new source was used in conjunction with a rapid-scanning infrared spectrometer (800 spectra per second) to study gas-phase composition variations in composite solid propellant flames during both steady-state and oscillatory pressure tests. A rotating valve was used externally to impose controlled oscillations in the combustion chamber pressure. The 2.5 to 5.5-μm region was scanned in approximately 0.50 millisecond, and the 3.17-μm H_2O, 4.26-μm CO_2, and 4.72-μm CO absorbances were measured. The system was calibrated for changes in these absorbances as a function of changes in the respective species concentrations. Thus, it was possible to measure variations in the gas-phase composition due to the changes in the pressure-dependent gasification rates of the AP and the fuel-binder. Also,

an electro-optical hot-gas pyrometer was used simultaneously to measure flame temperatures at a rate of 4500 measurements per second.

CHAPTER II

APPARATUS AND EXPERIMENTAL PROCEDURES

The experimental apparatus consisted of five main sections: (1) the combustion chamber, (2) the rapid-scanning spectometer, (3) the high temperature radiation source, (4) the flame-temperature measuring equipment, and (5) the data acquisition equipment. Figure 1 is an overview of this equipment.

Since the development of a combustion chamber which would yield meaningful quantitative spectroscopic data was a primary objective during the initial stages of this study, a complete description of the combustion chamber is given in the following section. The other equipment is only briefly described in this chapter, and a complete description of this equipment is given in the various appendices.

Combustion Chamber

The design of the combustion chamber was dictated by the following considerations:

1) A means of externally imposing oscillations in the combustion chamber pressure, at controllable frequencies and amplitudes.
2) Windows which would permit measurement of infrared absroption in the propellant flame.
3) Also, windows which would allow independent flame temperature measurements with an electro-optical hot-gas pyrometer.

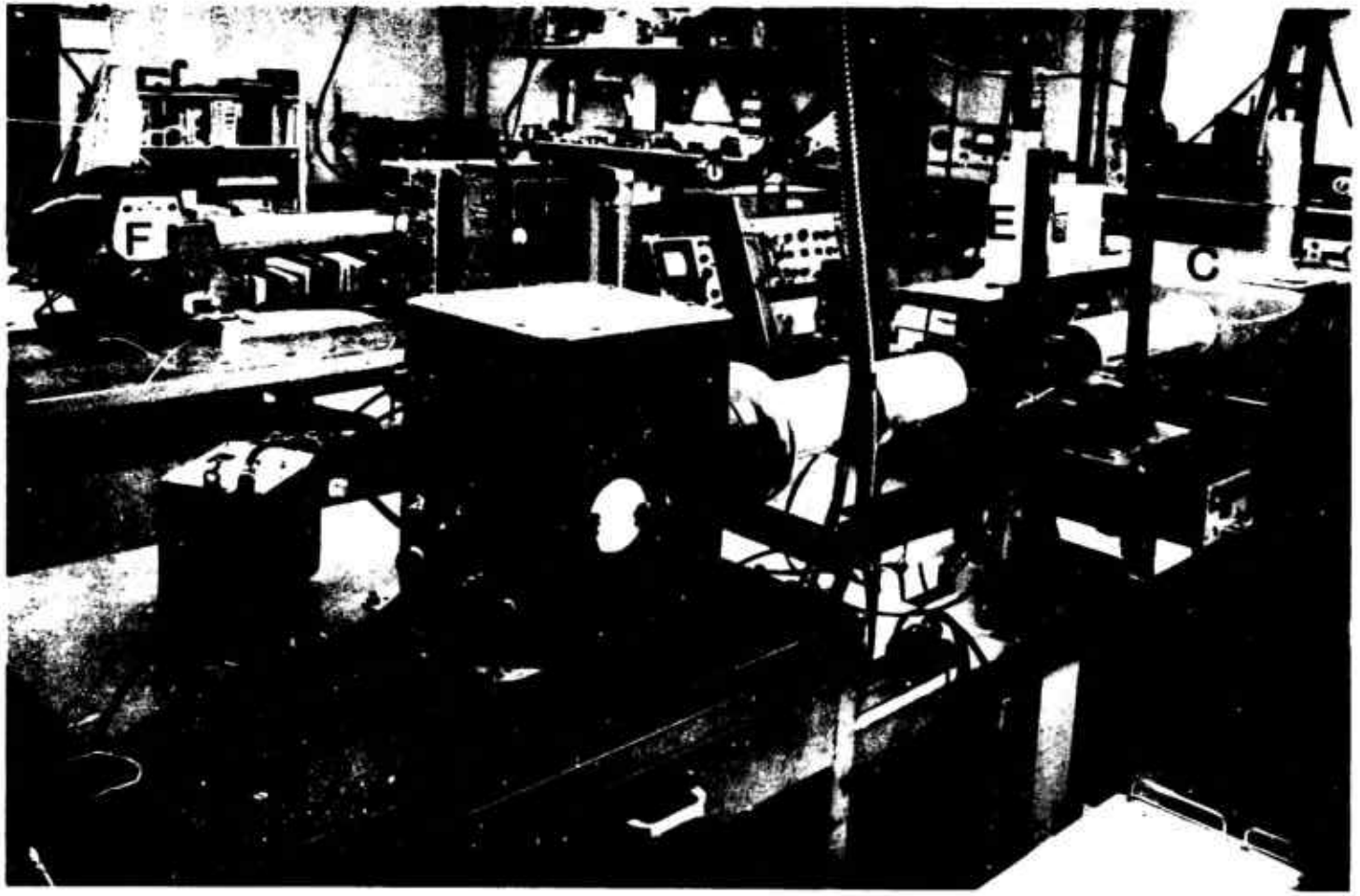

FIGURE 1. AN OVERVIEW PHOTOGRAPH OF THE EQUIPMENT. A. Infrared radiation source. B. Combustion chamber. C. Spectrometer. D. Hot-gas pyrometer source. E. Hot-gas pyrometer detector. F. Fastax camera. G. Fastax controller. H. Spectrometer control console.

4) A gas purging system which would flush all combustion products directly downstream, thus eliminating any recirculation of combustion products through the plane of the spectrometer beam. This purging system must also keep all windows clean during the tests.

The above constraints resulted in the combustion chamber shown in Figures 2 and 3. To facilitate easy modification of the original combustion chamber design, the chamber was built in three separate sections. The central portion of the combustion chamber was machined from a piece of steel 8.9-cm square and 11.4-cm in length. The chamber was equipped with two sets of windows. Two sapphire windows, 5.8-cm in diameter and 3.2-mm thick, were mounted on opposite sides of the combustion chamber and were open to the 3.81-cm internal diameter of the combustion chamber by way of a milled slot, 7.94-mm wide and 3.81-cm in height. This slot was large enough to permit passage of the focused high-temperature infrared source beam. Sapphire was selected as the infrared window material because of its excellent transmittance in the 2.5 to 5.5-μm spectral region and because of its excellent physical properties. Two quartz windows, 2.54-cm in diameter and 4.67-mm thick, were mounted in the other two opposing sides of the combustion chamber to permit the simultaneous use of an electro-optical hot-gas pyrometer to measure flame temperatures. The hot-gas pyrometer was operated at the sodium D-line wavelength, 0.590 μm, and thus, sapphire was not required for the window material. The quartz windows were open to the inside of the combustion chamber by way of a milled slot, 7.94-mm wide and 1.91-cm in height. All windows were sealed by means of O-rings and were provided with gas purging ports necessary to keep the windows clean. Keeping the windows

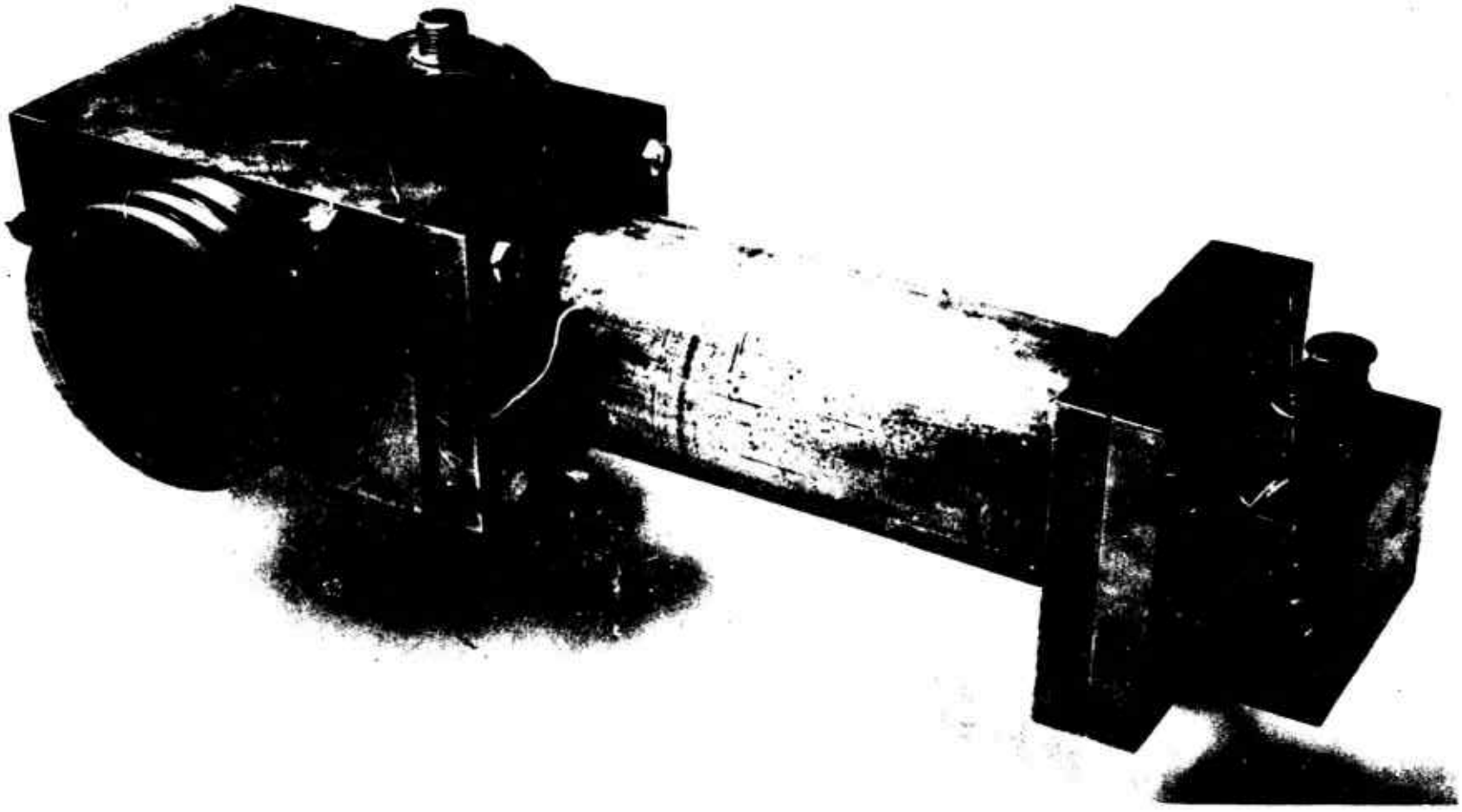

FIGURE 2. A PHOTOGRAPH OF THE COMBUSTION CHAMBER. A. Safety rupture disk assembly. B. Infrared window. C. Hot-gas pyrometer window. D. Pressure transducer. E. Dual-nozzle assembly.

A. Propellant holder
B. Propellant holder mount
C. Central portion of chamber
D. Converging inserts
E. Extension
F. Dual-nozzle assembly
G. Fixed-nozzle inserts
H. Rotating nozzles

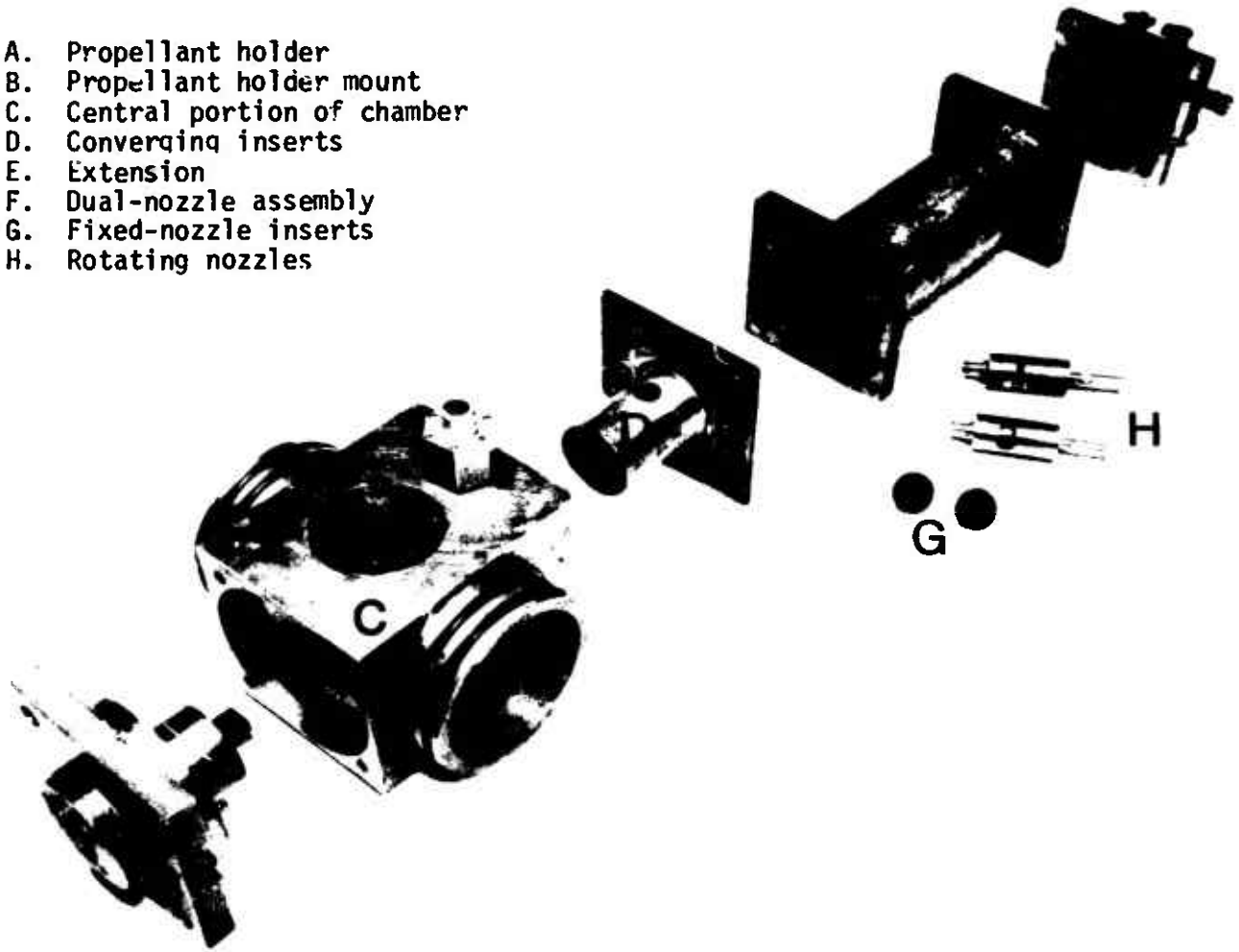

FIGURE 3. AN EXPLODED VIEW OF THE COMBUSTION CHAMBER.

in both optical paths clean was a primary concern, and it was accomplished in the following manner. A 4.75-mm wide and 0.254-mm deep rectangular relief was milled in the surfaces against which the windows mated, and adjacent to the length of each window slot. A series of equally spaced 0.343-mm diameter holes were drilled in this relief area, connecting the relief surface with a set of gas purging channels located in the interior of the combustion chamber body. This configuration provided a continuous stream of gas sweeping over the surfaces of the windows, and then flowing down the optical slots and into the combustion chamber. This technique worked exceptionally well, and thus, the windows could go long periods without cleaning. To permit the necessary purging of the entire optical path between the source and the spectrometer with H_2O-CO_2-free gas, concentric rings, containing O-rings, were welded around the sapphire windows. The extension tubes from the source and spectrometer slipped over these rings and completely sealed the entire system. This central portion of the combustion chamber also contained mounting holes for a Statham pressure Transducer (Model PA285TC-150-350) and a safety rupture disk assembly (BS & B No. SA-8, 195 psig). These holes were located opposite one another on the sides of the combustion chamber containing the smaller quartz windows.

The end of the combustion chamber which served as a mount for the propellant holder is shown in Figure 4. This end-piece also contained the heart of the gas purging system. One central network of channels supplied the purging gas to each of the windows and to a plenum chamber directly behind the sintered-stainless steel frit which filled the annulus between the propellant holder mounting hole and the inside of the combustion chamber. The frit provided a uniform axial purge stream

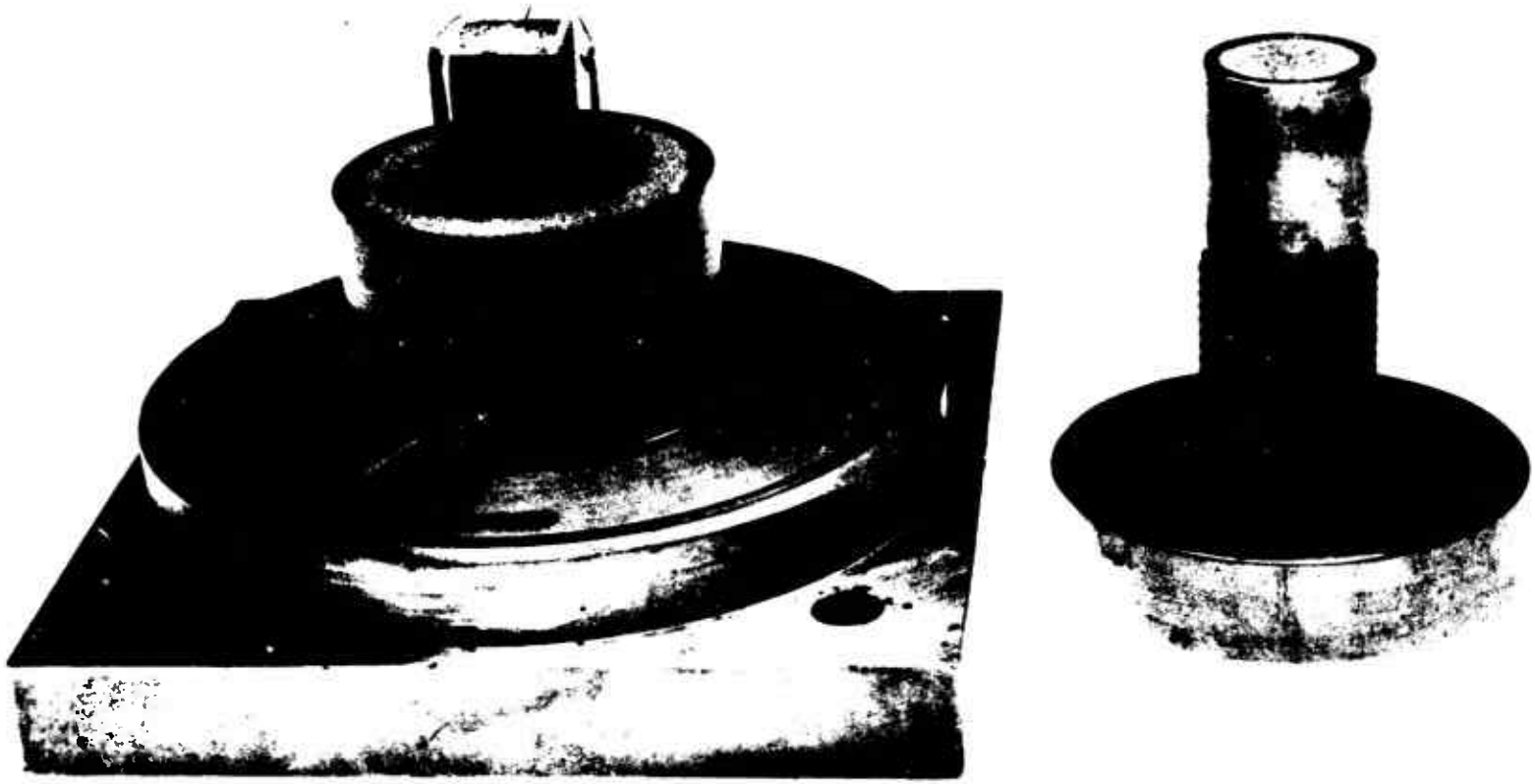

FIGURE 4. A PHOTOGRAPH OF THE PROPELLANT-HOLDER MOUNT AND THE MODIFIED PROPELLANT HOLDER.

which carried combustion products directly downstream.

A rotating nozzle, used in parallel with a fixed nozzle, provided mechanically-imposed oscillations in the chamber pressure. The nozzle assembly is shown in Figures 2 and 3. The mean pressure and the amplitude of the pressure oscillations could be changed by simply changing the size of the fixed and rotating nozzles respectively. The fixed nozzles were made from carbon inserts, and could be changed very quickly. The rotating nozzles were made of brass and had a cylindrical body shape. A hole of the desired nozzle size was drilled through the diameter of the nozzle body, and then the two ends of the hole were milled into 90° arcs around the circumference of the nozzle body. This nozzle configuration produced approximately sinusoidal pressure oscillations, with two pressure cycles for every one revolution of the nozzle. The rotating nozzle was held in place by ball bearings and was continuously lubricated by two oil cups mounted in the top of the rotating nozzle housing. The rotating nozzle was driven by a variable-speed DC motor (Bodine Type NSH-12R) equipped with a Speed Controller (Minarik Electric Co., Model SL14). This motor-controller combination was capable of driving the rotating nozzle over a range from 600 to 6000 RPM. The rotating-valve port in the nozzle housing was threaded so that a small solenoid valve could be attached for some tests. For these tests, the rotating nozzle was opened and used as a fixed nozzle. The solenoid valve was used for rapid opening or closing of this fixed nozzle, and thus cause a single pulse in the chamber pressure. The Fastax Control unit was used to coordinate this valve action with the tests.

The above describes the combustion chamber as it was originally designed and built. Preliminary testing revealed that two modifications

had to be made to eliminate the recirculation of combustion products past the plane of the spectrometer beam. The combustion chamber had to be made longer. This was easily done by placing a 19.0-cm extension between the central portion of the chamber and the end housing the nozzles. Also, it was necessary to divide the chamber into two sections. An upstream section where recirculation was prevented, and a downstream section where recirculation was permitted. These two sections were isolated by means of a tapered insert which made the inside diameter of the chamber converge from 3.81 cm at the edge of the optical slots to 2.54 cm at the start of the 3.81-cm inside diameter extension. This converging section, and then sudden expansion back to the original diameter was successful in separating the two sections. However, a smaller insert was necessary in the middle of this larger converging insert to prevent recirculation in this upstream section. The thin-walled middle insert converged from a 2.54-cm ID to a 1.27-cm ID and was the same length as the larger insert. The smaller insert had three equally spaced studs around its periphery at either end which held it directly in the center of the larger insert.

Both propellant ignition posts were mounted on the propellant holder. One ignition post was silver-soldered directly to the holder, since the chamber was used as one leg of the ignition circuit. A small ceramic tube running the length of the holder insulated the other ignition post from the chamber. The 0.25-mm diameter nichrome ignition wire was embedded in a razor-blade-cut slit in the center of the propellant surface. A fast smooth ignition was produced by applying approximately 12 VDC to the ignition wire.

Spectrometer and High Temperature Source

The Warner and Swasey (Controlled Inst. Div.) Model 501 Rapid-scanning Spectrometer used in this study is a single-beam instrument, designed for studying transient spectroscopic phenomena. The spectrometer can be set up to scan various selected spectral regions, of approximately λ to 3λ in length, from 0.30-μm to 14.0-μm. The spectral region scanned is determined by the grating, filters and detectors used. The spectrometer has seven scan rates ranging from 1.0 msec. to 100 msec., with a corresponding repetition rate range of 8 to 800 scans per second. The spectrometer output is linear in time and wavelength. Therefore, wavelength instead of wave number is used in reporting the data. Previous work in this laboratory [7, 22] indicated that the most useful spectral information for composite propellant flames is in the 2.5 to 5.5-μm region. Thus, the spectrometer was set up to scan the 2.5 to 5.5-μm region at a rate of 800 spectra per second.

The high temperature infrared radiation source used with the spectrometer was a modified version of a Warner and Swasey Model 20 Synchronized Radiation Source, utilizing the new vitreous carbon source developed by Robert J. Law [28]. The vitreous carbon source elements were operated at a brightness temperature of 2725°K. This new high-temperature radiation source permitted the use of the specteometer's 0.20-mm entrance and exit slits, which gave good spectral resolution and an excellent signal-to-noise ratio.

The combustion chamber was located at the common focal plane of the spectrometer and the radiation source. The relatively long optical path had to be purged with CO_2-H_2O free gas in order to eliminate

atmospheric CO_2 and H_2O absorption. Both the radiation source and the spectrometer have tunnels which extend from these units and seal to the combustion chamber, which facilitates this necessary purging. A complete description of the spectrometer and the high temperature radiation source is given in Appendix A.

Equipment for Measuring Flame Temperature

Flame temperature measurements, independent of the infrared absorption measurements, were made with an electro-optical hot-gas pyrometer [29]. The pyrometer operation is based on the spectral emission-absorption method of gas pyrometry often called the Schmidt method or Planck-Kirchhoff method [30]. Flame temperatures are determined by simultaneous measurements of spectral radiance and spectral absorptance at one wavelength. Although the sodium D-line wavelength was used in this work, the Schmidt method has no wavelength restrictions.

To achieve optimum emission and absorption at the sodium D-line wavelengths, a small amount (0.10 to 0.50 weight percent) of finely-ground sodium chloride was added to the propellant formulations. A tungsten-strip lamp was used as the pyrometer's background radiation source, and a chopper wheel containing 64 slots around its periphery was used to prechop this background radiation. The chopper speed was set to produce 4500 interruptions of the source beam per second, yielding a maximum of 4.5 temperature measurements per millisecond. An RCA 7102 photo-multiplier was used as the radiation detector, while an interference filter, transmitting radiant energy only from 0.5884 to 0.5914 μm, provided the very narrow spectral band necessary in the Schmidt method. A complete description of the electro-optical hot-gas pyrometer and the

Schmidt method is given in Appendix B.

Data Acquisition Equipment

The output signal from the spectrometer, the electro-optical hot-gas pyrometer, and the pressure transducer had to be recorded simultaneously. This combination of equipment generated data at a tremendous rate, requiring special recording and measuring equipment. Precision tape decks can be used when the spectrometer is operated at its slower scan speeds. However, at its fastest scan speed, 800 scans per second, the frequency response requirement prevents the use of tape decks.

The problem of simultaneously recording these data was solved by using a high-speed Fastax oscillostreak camera (Wollensak Model WF-225) to record a triple-trace oscilloscope display. The developed 16-mm films were analyzed on a modified Recordak microfilm reader. An electro-mechanical device used to measure the oscilloscope deflections recorded on the film was added to the reader. The electrical signal from this electro-mechanical device was a direct measure of vertical distances on the display screen and was used to drive a digital printer. The printout from the digital printer was used to punch up data cards, and all the data reduction was done on a Univac 1108 digital computer. A complete description of the data acquisition and reduction techniques is given in Appendix C.

Miscellaneous Equipment

The pressure transducer (Statham PA285TC-150-350) used throughout this work was a nonbonded strain gage type transducer, with a 0 to 150 psia range. A nickel-cadmium battery was used to supply the 7.0 VDC

excitation voltage during most of this work. The transducer output was linear over the above pressure range, and with the 7.0 VDC excitation voltage it had a sensitivity of 0.380 mv/psi.

Due to the hazardous nature of this work, all tests were remotely controlled from outside of the testing area. A solenoid valve in the gas line provided remote control of the combustion chamber purging. A double pole switch was used as the chamber purge switch and the ignition switch. The camera-on switch of the Fastax controller was also located outside the laboratory. In addition, the mean pressure transducer signal was recorded on a strip chart recorder (Leeds and Northrup, Speedomax XL Series 600). The Speedomax XL has a 1/3 sec. response time, thus for the oscillatory pressure tests only the mean pressure signal was recorded on the strip chart recorder. Since the Speedomax XL is a two-pen recorder, it was possible to record a signal from the Fastax controller indicating the segment of an oscillatory pressure test during which the Fastax camera was recording data.

In addition to the 565 oscilloscope used to record the data, another oscilloscope (Tektronix Type 502) was used as a monitor. The Type 502 is a dual-beam oscilloscope and was used to monitor the spectrometer and the electro-optical hot-gas pyrometer signals. An oscilloscope camera (Tektronix Model C-12) was used to record information from this monitor oscilloscope.

Two motion picture cameras were used to study the nature of the propellant flames investigated. During the preliminary recirculation studies, a 16-mm Cine-Kodak Special camera was used. The Cine-Kodak Special is a framing camera which can take a maximum of 64 pictures per

second. Also used to study the propellant flames was a 16-mm high-speed combination framing-oscillographic Fastax camera (Wollensak Model WF-17T). The Wollensak WF-17T was also used with the Fastax controller, and it has a maximum speed of 9000 pictures per second. This camera has two lenses mounted normal to one another. Thus, making it possible to photograph the propellant flame (framing mode) and the pressure transducer signal on the oscilloscope (oscillographic mode) simultaneously. Eastman Kodak Ektachrome EF film was used with both of these cameras.

Propellant Sample Preparation

All the work in this study was done with uncatalyzed, nonmetallized composite propellants. Ammonium perchlorate (AP) and hydroxy-terminated polybutadiene (HTPB) were used exclusively as the oxidant and fuel-binder respectively. A complete description of the propellants and the mixing procedure used in their preparation is given in Appendix F.

The propellant was cast in slabs approximately 2.5-cm thick from which samples were cut. Initially cylindrical samples, 15.5-mm in diameter, were cut from the slabs. However, a square cross-section sample was decided upon for the following reason. A slight misalignment with a cylindrical sample can cause changes in the effective optical path length in the flame from run to run. With a rectangular or square sample, this same misalignment does not change the optical path length. Cylindrical samples were used for only part of the preliminary tests, and all the data runs were made with square cross-section samples.

When the change from the cylindrical to square samples was made, the size of the samples had to be reduced so that the square samples would fit on the same propellant holder. Both 12.7-mm and 11.1-mm square

cross-section samples were tried. The 12.7-mm samples were harder to mount on the propellant holder and caused more melting of the ignition posts. Therefore, the 11.1-mm samples were used even though they were approximately the same size as the height of the projected image of the spectrometer's entrance slit. The propellant flame is considerably larger than the sample. Analysis of the high-speed motion pictures (1500 pictures per second) on the film reader revealed that the central core of the flame from the 11.1-mm samples was at least 15-16 mm across.

A specially machined cutter and a small arbor press were used to cut 11.1-mm square and 2.5-cm long samples from the slab. The sides of the fresh samples were leached free of AP by placing the samples in a beaker of water for ten minutes. This procedure leached just a very thin surface layer of AP. Once the sample was dry, the sides of the propellant were coated with a thin acrylic coating (Krylon, Borden Chem. Co.). This method of inhibiting the sides of the sample resulted in a very flat burning of the propellant surface. The samples were then stored in sealed containers until used. Just before the samples were mounted on the propellant holder, they were cut to the desired length, exposing a fresh surface for ignition. A quick-setting epoxy cement was used to fasten the samples to the propellant holder.

Procedure

The spectrometer was continuously purged with H_2O-free air when not in use. Two hours before tests were run, this purge was switched to H_2O-CO_2 free air at approximately 10-15 LPM. One hour before tests were run, the argon purge (5 LPM) of the high-temperature source and all the

electronic equipment was turned on. Just prior to a test, the internal source in the spectrometer was used to check the background CO_2 level.

A data sheet for each run was used to record the following information: 1) the date, the run number, and the film roll number, 2) the type of propellant and its dimensions, 3) the type of run, 4) the oscilloscope and the electro-optical pyrometer settings, 5) the Fastax settings, 6) the infrared source temperature, and 7) miscellaneous comments.

After the propellant was mounted in the combustion chamber, the following sequence of events occurred:

1) the spectrometer scan wheel was started,
2) the electro-optical pyrometer was turned on,
3) the infrared source was turned on and adjusted,
4) the traces of the 565 oscilloscope were adjusted for both intensity and position,
5) the Fastax camera was run for a short period to record the baseline and intensity of the pyrometer's background source,
6) the settings on the Fastax controller were changed for the run conditions,
7) a small purge of the combustion chamber was started using a small bypass valve in the gas line,
8) the ignition-circuit wires were attached to the combustion chamber,
9) the strip chart recorder was started,
10) the ignition and full chamber purge switch was closed,
11) when ignition was indicated by the pressure trace on the strip chart recorder, the camera-on switch from the Fastax controller was closed,

12) after the burn was over, the ignition-purge switch was opened, and the strip chart recorder was turned off,

13) the pyrometer source and the infrared source temperatures were checked; the difference, if any, was noted on the data sheet,

14) the spectrometer scan wheel, the electro-optical pyrometer, and the infrared source were turned off, and

15) the small combustion chamber purge was turned off and the propellant holder was removed.

The burn times of these tests were approximately 5-10 seconds depending on the type of propellant, the length of the sample, and the chamber pressure. The time interval between step #10 and step #11 was approximately one second. The length of time between step #5 and step #12 was approximately one minute, and the time interval between step #1 and step #15 was typically six to eight minutes. All tests were remotely fired; that is, events 9 through 12 were controlled from outside the testing area.

The temperature of the tungsten strip lamp, the electro-optical hot-gas pyrometer's source, was checked with the Leeds and Northrup optical pyrometer only at the beginning and end of a set of runs made each day. It was found that the lamp's current was an excellent measure of the filament temperature. Therefore, the ampere meter on the lamp's power supply was used to check the filament temperature before and after each run.

Closing the camera-on swit h in step #11 started two different sequences of events depending on the type of test. For the oscillatory and steady-state pressure tests, closing the switch caused the camera to

run for a length of time determined by the Fastax control unit. This interval was recorded on the strip chart recorder, along with the overall pressure history of the test. The camera timer was usually set for 1.5 to 2.0 seconds. At the end of this time, the camera started to slow down, taking about another 0.50 second to stop. It took the camera approximately one second to get up to a film speed which was adequate for analyzing the films. This resulted in 1.0 to 1.5 seconds of usable data. In the case of the pressure step-change tests, the closing of this switch again caused the camera to run for a set length of time. However, a predetermined length of time after the camera started, the Fastax control unit activated the solenoid valve. After the preset camera time interval had expired, the solenoid valve would return to its original position and the camera would start to slow down.

CHAPTER III

PRELIMINARY WORK

Recirculation Studies

Developing a system which would yield meaningful quantitative spectroscopic data was a primary objective during the initial stages of this study. The principal task was to eliminate the recirculation of combustion products past the spectrometer's beam, so that only the freshly generated products in the flame were in the spectrometer's view. The recirculation patterns in the original and modified combustion chamber were studied both photographically and spectroscopically.

Initially, cold flow spectroscopic studies were made using the modified propellant holder shown in Figure 4. The sintered stainless-steel frit of this modified propellant holder allowed the introduction of an infrared absorbing gas at the normal location of the burning propellant strand. The optical slots separating the infrared-passing windows from the interior of the combustion chamber were purposely made extra long so that the spectrometer beam could be located above or below the location of the propellant strand surface to detect the recirculation of the infrared absorbing gas. During these tests compressed air was used as the purging gas (O_2 and N_2 are both infrared inactive), and carbon dioxide was introduced through the sintered-stainless steel frit. The strong 4.26-μm CO_2 absorption band was used to monitor the recirculation of CO_2 during different compressed air and CO_2 flow rate

conditions. It was this type of testing which lead to modification of the original combustion chamber, as discussed in the preceding chapter.

Burning propellant strands were also studied in the above manner, as well as photographically. The major finding from the photographic studies was the effect of the purging gas type on the nature of the combustion process. A Cine-Kodak Special camera was used to photograph (32 pictures per second) the burning propellant strand through the large infrared window and optical slot. When compressed air was used as the purging gas, large fingers of flame were observed propagating upstream of the burning propellant surface, along the sides of the propellant strand. This observed phenomenon explained why even inhibited propellant strands coned badly when compressed air was used as the purging gas. Motion pictures of tests made with a nitrogen purge did not reveal these large fingers of flame propagating upstream. The use of nitrogen as the purge gas, and inhibiting the sides of the propellant strands as discussed in the previous chapter, resulted in a very flat regression of the propellant surface. Spectroscopic studies above and below these burning propellant strands, in the final combustion chamber, showed no signs of recirculation of combustion products. Due to the symmetry of the combustion chamber, this finding should also be true for the other sides not observed.

Spectral Characteristics

The absorption spectrometry was done entirely in the middle infrared from 2.5 to 5.5 μm. Since many of the common combustion products possess absorption bands in this infrared region, it is ideal for flame studies. Preliminary information concerning the expected composition of

the combustion products from the propellants being studied was obtained from an equilibrium computer program. A complete description of this equilibrium program and its use during this study is given in Appendix E. These equilibrium calculations revealed that the major gas-phase combustion products are H_2O, CO_2, CO, HCl, H_2, and N_2. All of these species, except H_2 and N_2, have absorption bands in the 2.5 to 5.5-μm region. These absorption bands are listed in Table 1. The strong H_2O and CO_2 bands in the 2.66 to 2.72-μm region overlap, and absorbances in this region are complicated functions of both the CO_2 and H_2O concentrations. Also, these bands were very close to the cut-on wavelength, 2.5 μm, of the filter used with the InSb detector. Both of the above conditions made it impossible to use these H_2O and CO_2 bands for any type of quantitative work. Although the 4.82 and 5.17-μm CO_2 absorption bands are isolated, they are only of medium strength and fall in a region of rapidly declining infrared source intensity, due to the spectral characteristics of the source, the spectrometer, and the sapphire windows. These bands were barely detectable in this study and were not used. The medium-strength 3.17-μm H_2O absorption band, the $2\nu_2$ overtone of the symmetric bending mode, is well isolated and was used to measure changes in the H_2O concentration. The 3.46-μm HCl absorption band, the fundamental stretching band, is very broad and extends from 3.3 to 3.8-μm. Even though the equilibrium calculations indicated that a large amount of HCl would be present in the propellant flames, this band was almost impossible to detect. The reason for this is the relative weakness of this band, and the characteristic spectral shape of the infrared source spectrum. No attempt was made to use this absorption band during this

TABLE 1

SPECTRAL ABSORPTION BANDS OF THE MAJOR EQUILIBRIUM COMBUSTION PRODUCTS OF AP/HTPB COMPOSITE PROPELLANTS
(Hertzberg [33])

Wavelength at band head (μm)	Species	Band Strength
2.66	H_2O	very strong
2.69	CO_2	strong
2.74	H_2O	strong
2.77	CO_2	strong
3.17	H_2O	medium
3.46	HCl	medium
4.26	CO_2	very strong
4.66	CO	medium
4.82	CO_2	medium
5.17	CO_2	medium

study. The very strong 4.26-μm CO_2 absorption band, the fundamental ν_3 antisymmetric stretching band, is well isolated and was used to measure changes in the CO_2 concentration. Finally, the fundamental CO band at 4.66-μm was used to monitor changes in the CO concentration. The spectrometer resolution allowed identification of both the R branch at approximately 4.62-μm and the P branch at approximately 4.72-μm. The 4.72-μm branch was the easiest to measure and was used throughout this study. A complete description of these absorption bands in the middle infrared is given by Hertzberg [31].

These above absorption bands along with other characteristic absorption bands in the 2.5 to 5.5-μm region were used to perform a wavelength calibration of the spectrometer's output. The output of the spectrometer is linear in both time and wavelength. Although the Fastax camera used to record the spectra was rarely up to constant speed during a test, its speed was essentially constant during the 1.25-msec time interval between adjacent spectrometer timing marks on the film. A variable scale (Gerber Model TP007100B) was used to divide this linear time-wavelength scale between adjacent timing marks into 100 equal divisions. The resulting wavelength calibration curve is given in Figure 5.

The 3.17-μm H_2O, the 4.26-μm CO_2, and the 4.72-μm CO absorbances, $\ell n \frac{P^\circ_\lambda}{P_\lambda}$, were calibrated as a function of the respective species concentration in the flame. Where P°_λ is the incident radiant power at wavelength λ, and P_λ is the transmitted radiant power at wavelength λ. Beer-Lambert type calibration curves were obtained. The full details of this calibration work are given in Appendix A.

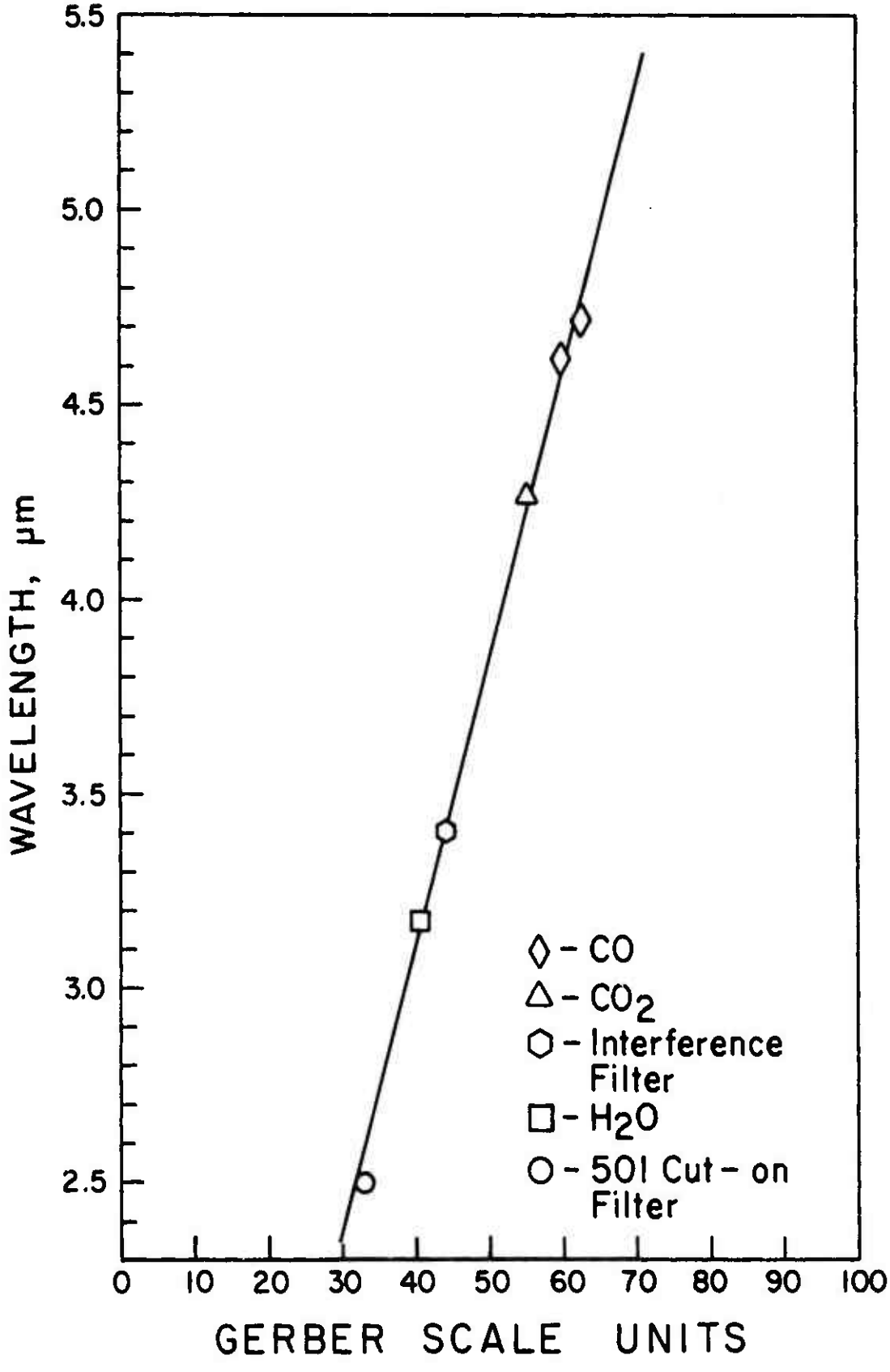

FIGURE 5. WAVELENGTH CALIBRATION OF 2.5 TO 5.5-μm SPECTRAL REGION.

CHAPTER IV

RESULTS AND DISCUSSION

During this study spectrometric data were taken in well over one hundred runs, not including the large number of preliminary tests. It was virtually impossible to reduce all of the data into final form, and it was equally impossible to report all the reduced data. The reported results are typical in that the phenomena presented were observed in other tests as well. However, tests were selected to display best the reported phenomena.

The spectroscopic nature of this work required that the flames studied be as optically clean as possible, and thus only unmetallized, uncatalyzed composite propellants were studied. Preliminary tests were made with different propellants having ammonium perchlorate (AP) contents ranging from 78 to 87 weight percent. Emission tests with the 78 and 80 weight percent AP propellants revealed a high level of continuum emission attributed to carbon particles in the flame. Although the 85 and 87 weight percent AP propellants had a very low level of continuum flame radiation, these near-stoichiometric propellant flames also have a very low concentration of CO, making it very hard to detect and measure accurately the CO absorption band on the absorption spectra. Very early in this work, it became apparent how valuable it was to monitor simultaneously the changes in both the CO_2 and CO concentrations. The 82 weight percent AP propellant was ideal.

The continuum flame radiation was relatively low, indicating a low concentration of particulate matter, and the CO absorption band was well defined and easily measured. Therefore, the majority of the tests in this study were made with one propellant formulation (82% AP, 17-17.25% HTPB-IPDI, 1/2% carbon black, and 1/4 - 1/2% of finely-ground NaCl). A series of tests were also made with 80 and 85 weight percent AP propellants. A full description of the propellant formulations used in this study is given in Appendix F, along with the mixing and curing procedures used in their preparation.

Three different types of propellant combustion conditions were studied: 1) steady-state pressure tests, 2) mechanically driven oscillatory pressure tests, and 3) externally-imposed single-pressure-pulse tests.

Steady-State Pressure Tests

Although the primary objective of this investigation was to study the effect that externally imposed pressure changes had on the gas-phase composition of composite propellant flames, a necessary foundation for this work was the study of the gas-phase composition of composite propellant flames during steady-state pressure tests. In particular, the study of the axial profiles of both composition and temperature as a function of distance from the burning propellant surface, and also the study of non-steady composition and temperature fluctuations at a given location in the flame as a function of time.

Axial Concentration and Temperature Profiles

The axial profiles of both composition and temperature were studied by letting an extra-long strand burn past the position of the

spectrometer's beam. Since the propellant strand completely blocked the optical paths of the spectrometer and electro-optical pyrometer, the time at which the regressing propellant surface reached the plane of the spectrometer's beam was easily detected on the film. The repetition rate of the spectrometer and the burning rate of the propellant were used to calculate approximate distances. Figure 6 shows the results of this type of a steady-state pressure test, where the profiles were measured at four different axial locations. Although this is described as a steady-state-pressure test, the chamber pressure did slowly rise, approximately two psi during the several seconds over which the data were recorded. Also, the pressure trace of this particular run contains some 60 cycle noise, which was only occasionally observed in the pressure traces throughout this study. The most striking feature of these data is that the CO_2 concentration increases with distance from the propellant surface, and the CO concentration decreases with distance from the surface. The H_2O concentration remains fairly constant over the interval measured. These observed CO_2, CO, and H_2O concentration gradients are typical of those observed in hydrocarbon-oxygen flames [32, 33].

Relatively fast reactions produce H_2O, CO, H_2, various radicals (OH, H, O), and other intermediates in the initial part, or primary reaction zone, of the flame. The majority of the H_2O is produced by the following relatively fast reaction

$$RH + OH \longrightarrow H_2O + R \quad , \tag{2}$$

where R can be H, CH_3, C_2H_5, etc. The CO_2 is produced by the relatively slow reaction,

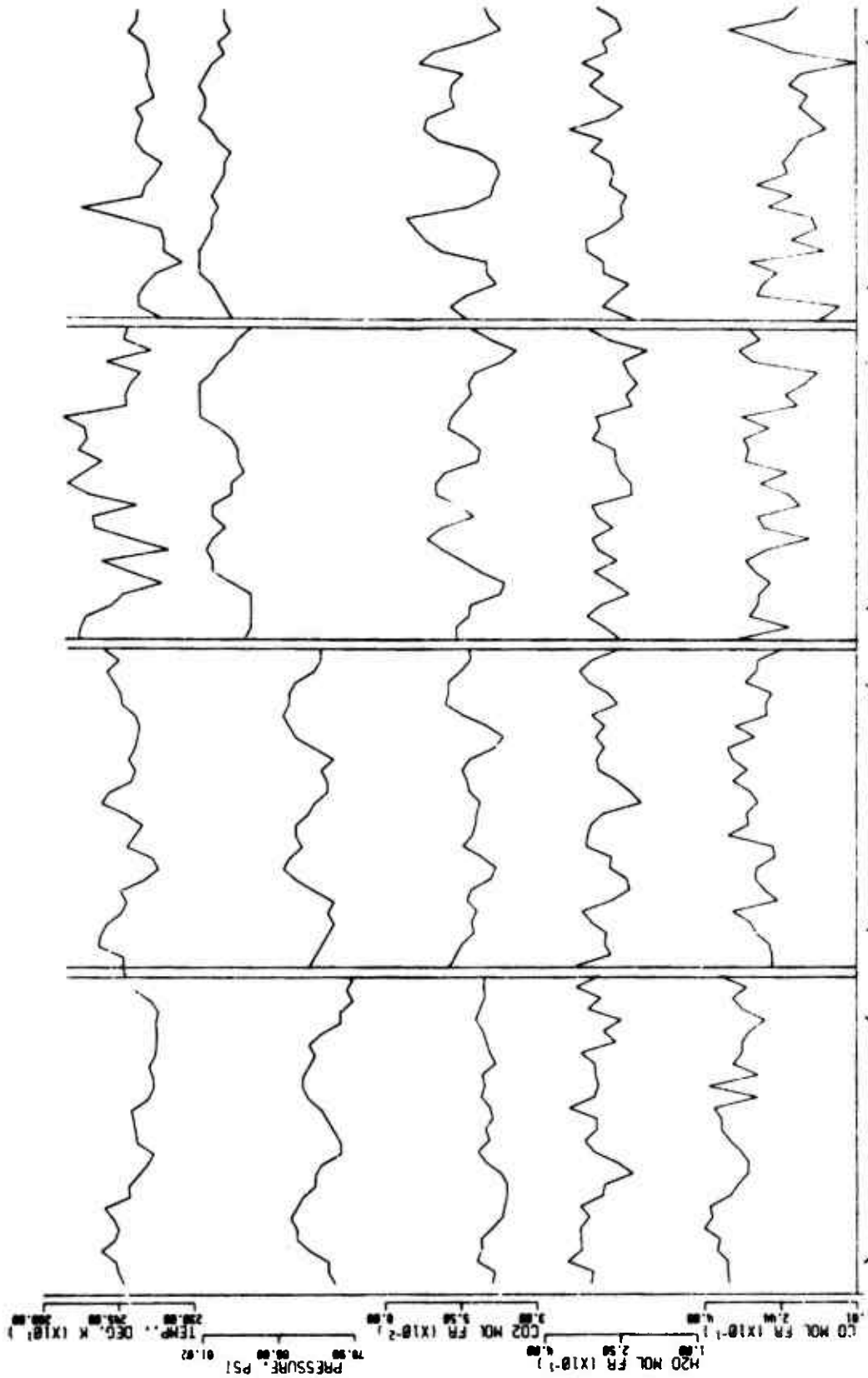

FIGURE 6. TEMPERATURE AND CONCENTRATION MEASUREMENTS AT FOUR AXIAL LOCATIONS DURING A CONSTANT-PRESSURE TEST. (82 wt. % AP propellant [UFN], Run No. 1-3774)

$$CO + OH \longrightarrow CO_2 + H \quad , \qquad (3)$$

in the latter part, or secondary reaction zone, of the flame [33, 34]. These axial CO_2 and CO concentration gradients are evidence of a non-equilibrium condition at distances of up to at least 1.5 cm from the propellant surface.

These observed axial concentration gradients were further confirmed with data from calibration tests using various-length propellant strands. The calibration data consisted of numerous time-averaged values measured at various axial positions in the flame, and they also revealed axial concentration gradients for the CO_2 and CO, but not the H_2O. The calibration data are discussed in Appendix A.

With the limited amount of temperature data for any one axial location presented in Figure 6, it is difficult to detect any trend in the axial temperature profile. However, it is clear that the flame temperature does not change appreciably over the measured distance. More extensive temperature measurements at the 3 - 5 mm and 12 - 14 mm locations, which are discussed in the next section, show that the temperature actually decreased 30-50°K over this distance.

The relatively high frequency (200-300 Hz.) oscillations in the concentration and temperature profiles of this test were universally observed in both the constant and transient pressure tests. The nature of these high frequency oscillations will be discussed later. However, even though this "noise" was of a much higher frequency than most of the phenomena being studied, it partially obscured the phenomena. Therefore, a digital-filter algorithm was incorporated in the data-reduction computer program to eliminate this high frequency "noise" in the final processed data. A complete description of this digital

filter algorithm is given in Appendix D. With the exception of the material in Appendix D and a few of the initial plots in this chapter, all of the data presented are filtered data. The raw, unfiltered data appear in tabular form in Appendix H. The initial-value transients associated with this filtering algorithm are apparent at the beginning of many of the filtered data plots. Thus, the filtered data during the first five or ten milliseconds are not considered to be valid and were not used.

The effectiveness of the filtering algorithm is clearly shown in Figure 7, where the data presented in Figure 6 are replotted in filtered form. These filtered data reveal information, regarding the nature of the concentration fluctuations at any given axial location, which is not easily detected in the unfiltered data. Almost without exception, observed increases in the CO_2 concentration occur simultaneously with observed decreases in the CO concentration and vice versa. These correlated concentration variations are similar to those observed when the effective oxidant/fuel ratio of a flame changes. Although the H_2O concentration also fluctuates, these fluctuations appear to be unrelated to the fluctuations in the CO_2 and CO concentrations. This observation is discussed in more detail in the following section.

Measurements at Individual Axial Locations

The time-varying nature of the flame temperature and composition at given axial locations was studied for a large number of steady-state pressure tests. No attempt was made to keep the spectrometer and pyrometer beams at a fixed position with respect to the propellant surface. Therefore, during the typical 100-125 msec. interval of data-taking, the

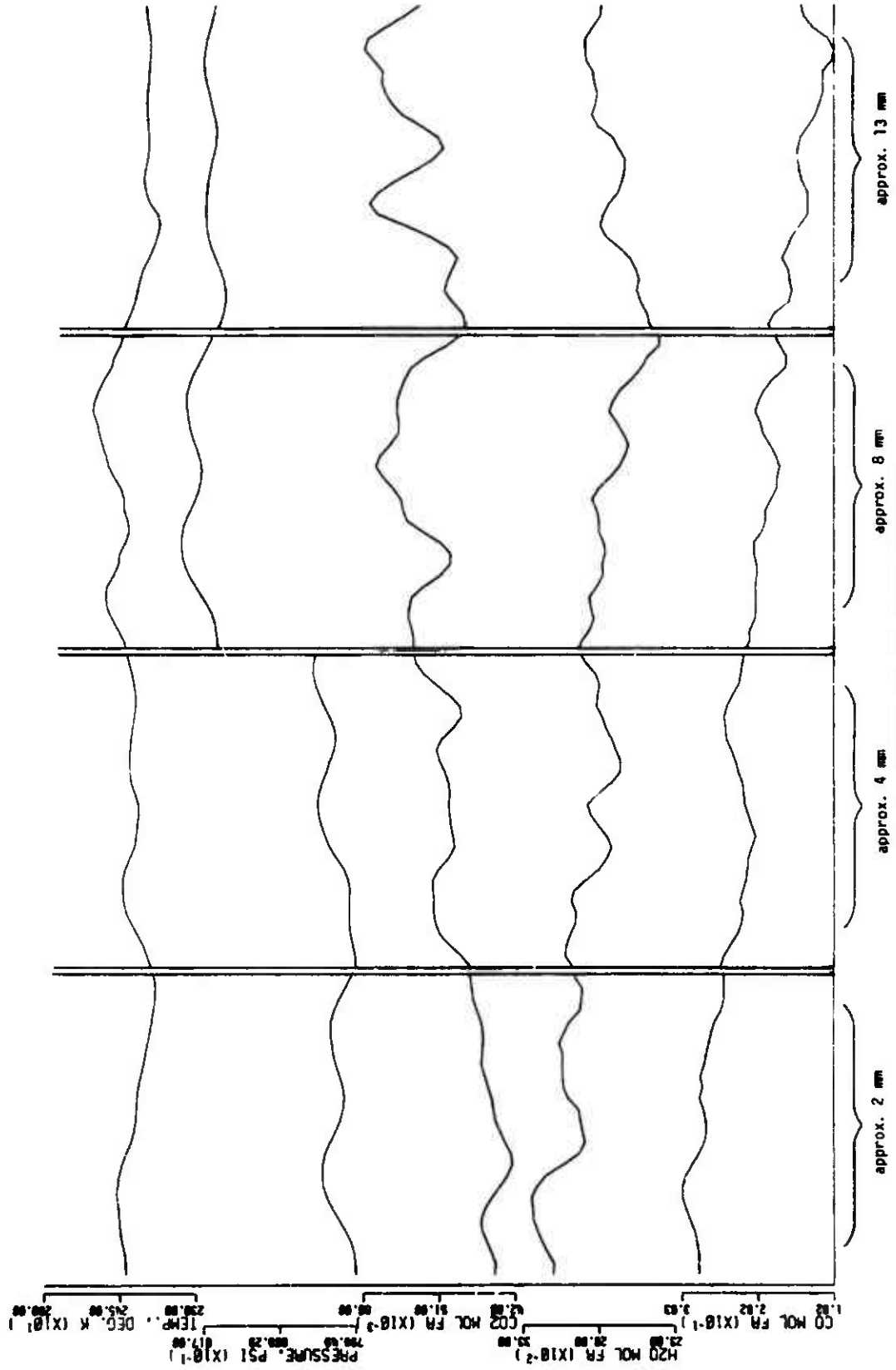

FIGURE 7. FILTERED FORM OF THE TEMPERATURE AND CONCENTRATION DATA PRESENTED IN FIGURE 6.

propellant surface regressed approximately 0.25-0.50-mm. Since this is such a relatively small distance, the axial concentration gradients will not be noticeable within individual tests. These data not only produced information about the steady-state combustion process, but also established a basis of comparison for the transient pressure data. The data plotted in Figures 8 through 11 are representative of the temperature and concentration fluctuations observed in the constant pressure tests. These data are from the same test as those plotted in Figures 6 and 7 and are more extensive measurements at the 3-5 mm and 12-14 mm axial locations. Before the filtered data are interpreted, a further discussion of the high frequency oscillations is necessary.

High Frequency Oscillations. As was noted earlier, the high frequency oscillations appear in the temperature profiles, as well as in the three species concentration profiles. Although the oscillations in each of these profiles are approximately of the same frequency (200-300 Hz.), the relatively slow scan speed of the spectrometer (800 spectra per second) prevented exact definition of the concentration profiles. The excellent time resolution of the electro-optical hot-gas pyrometer permitted a detailed mapping of the unfiltered temperature oscillations. The detailed temperature profiles of two steady-state pressure tests are shown in Figures 12 and 13. The data of Figure 12 are most representative of the nature of the oscillations observed in the majority of the tests. The temperature decrease over this relatively short time interval is not associated with an axial gradient, but instead is part of a low frequency temperature oscillation. The magnitude of this decrease is slightly atypical of the majority of the constant pressure tests.

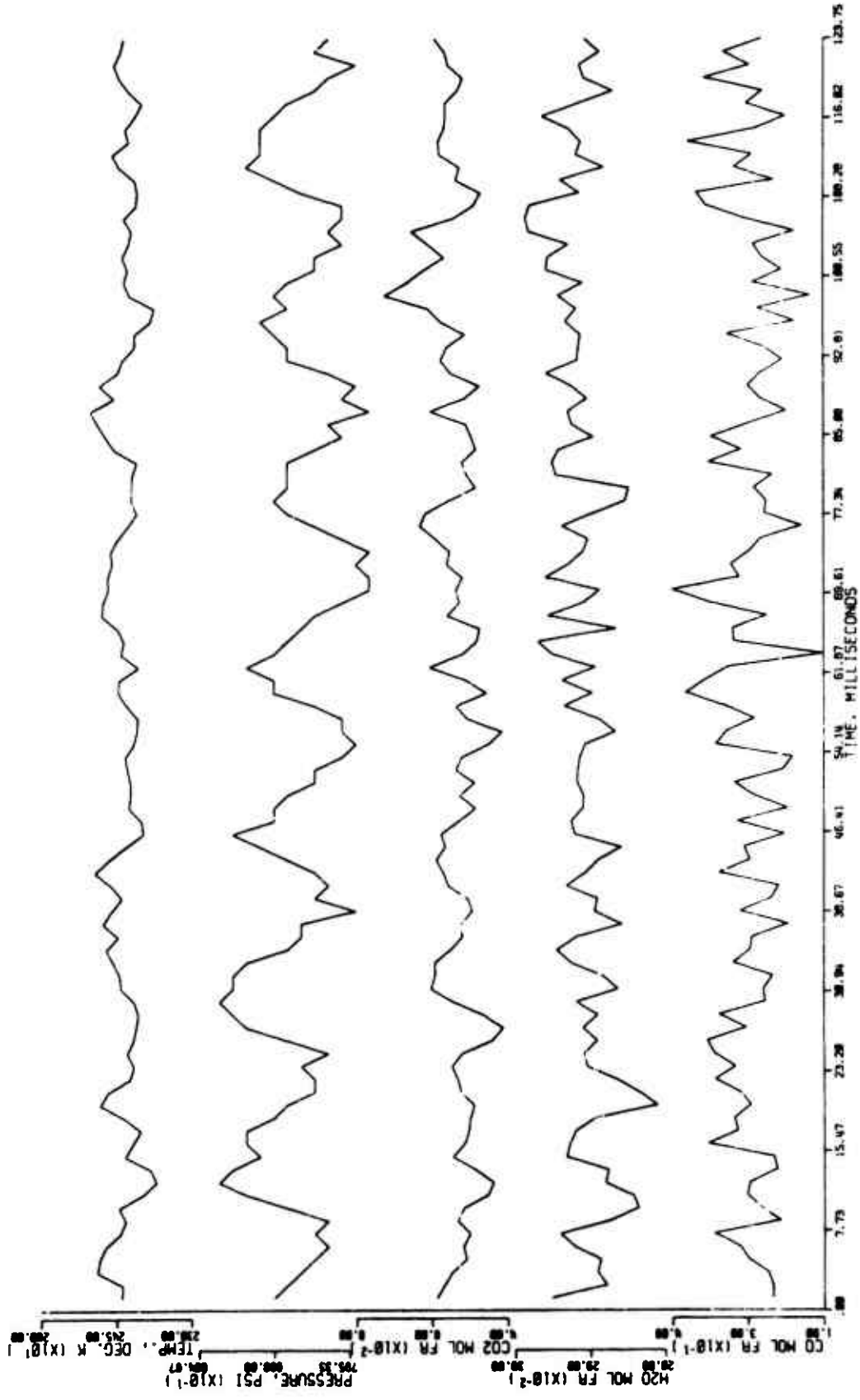

FIGURE 8. TEMPERATURE AND CONCENTRATION PROFILES AT 3-5 mm FROM THE PROPELLANT SURFACE DURING A CONSTANT-PRESSURE TEST. (82 wt. % AP propellant [UFI], Run No. 1-3774)

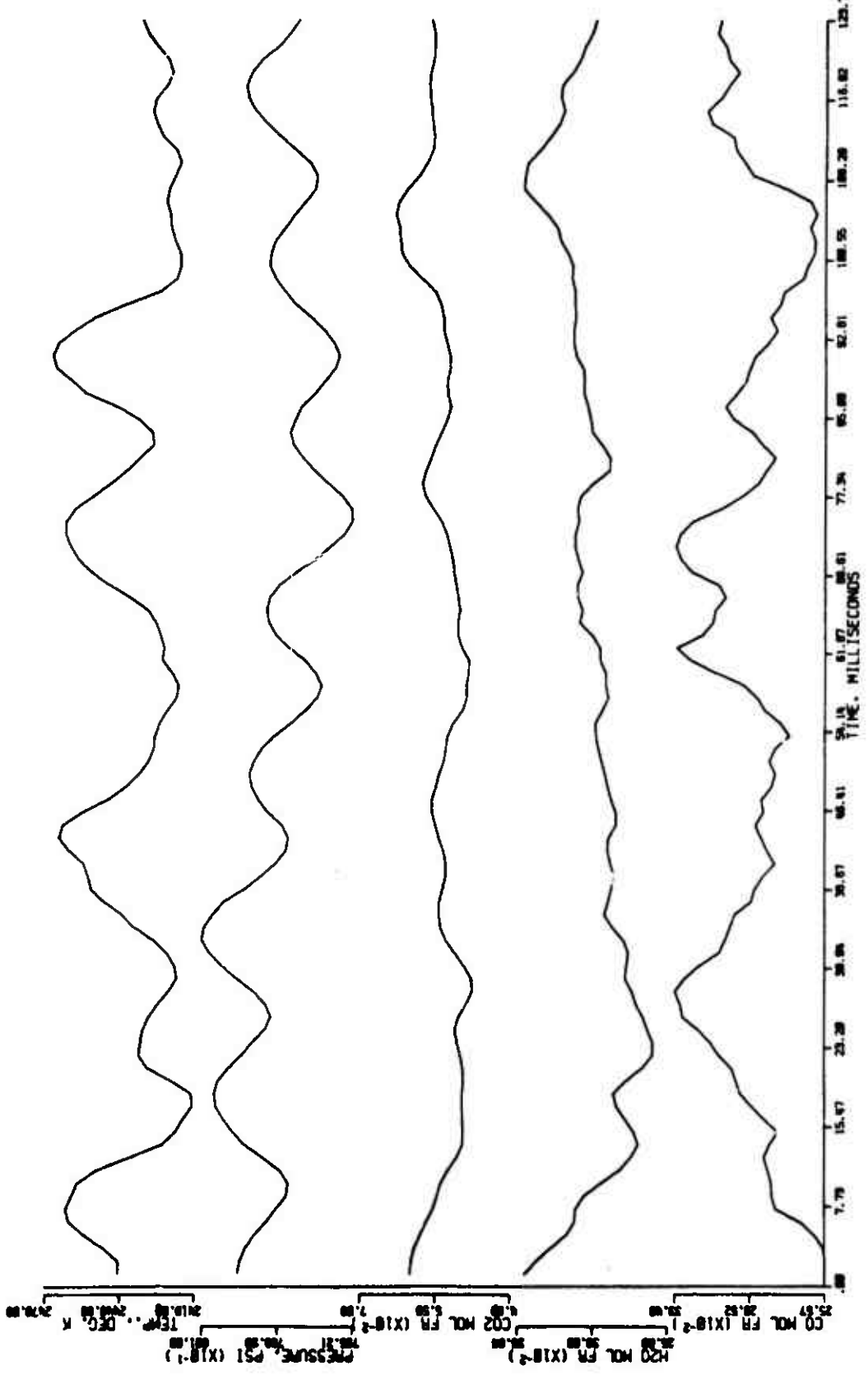

FIGURE 9. FILTERED FORM OF THE TEMPERATURE AND CONCENTRATION PROFILES PRESENTED IN FIGURE 8.

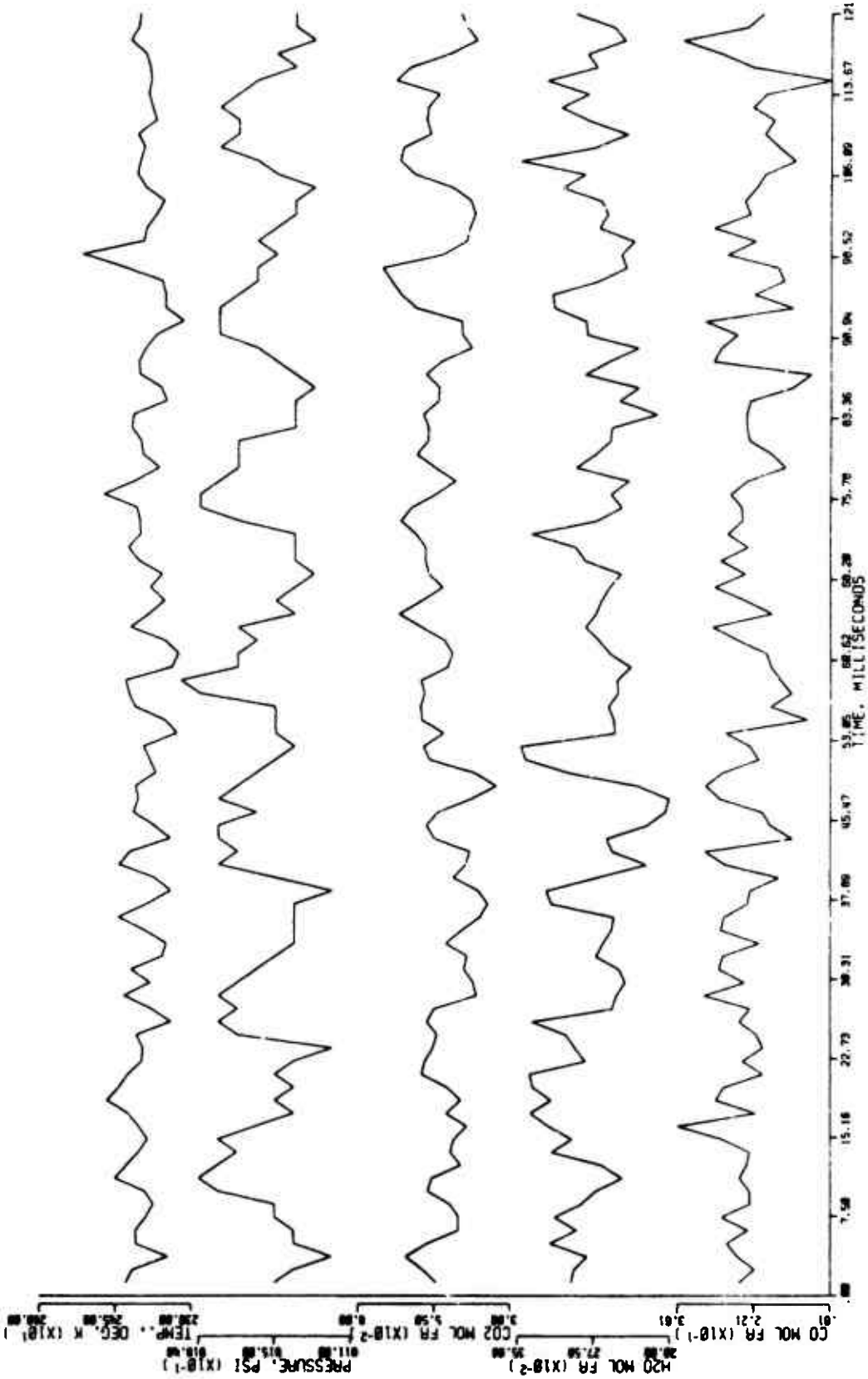

FIGURE 10. TEMPERATURE AND CONCENTRATION PROFILES AT 12-14 mm FROM THE PROPELLANT SURFACE DURING A CONSTANT-PRESSURE TEST. (82 wt. % AP propellant [UFN], Run No. 1-3774)

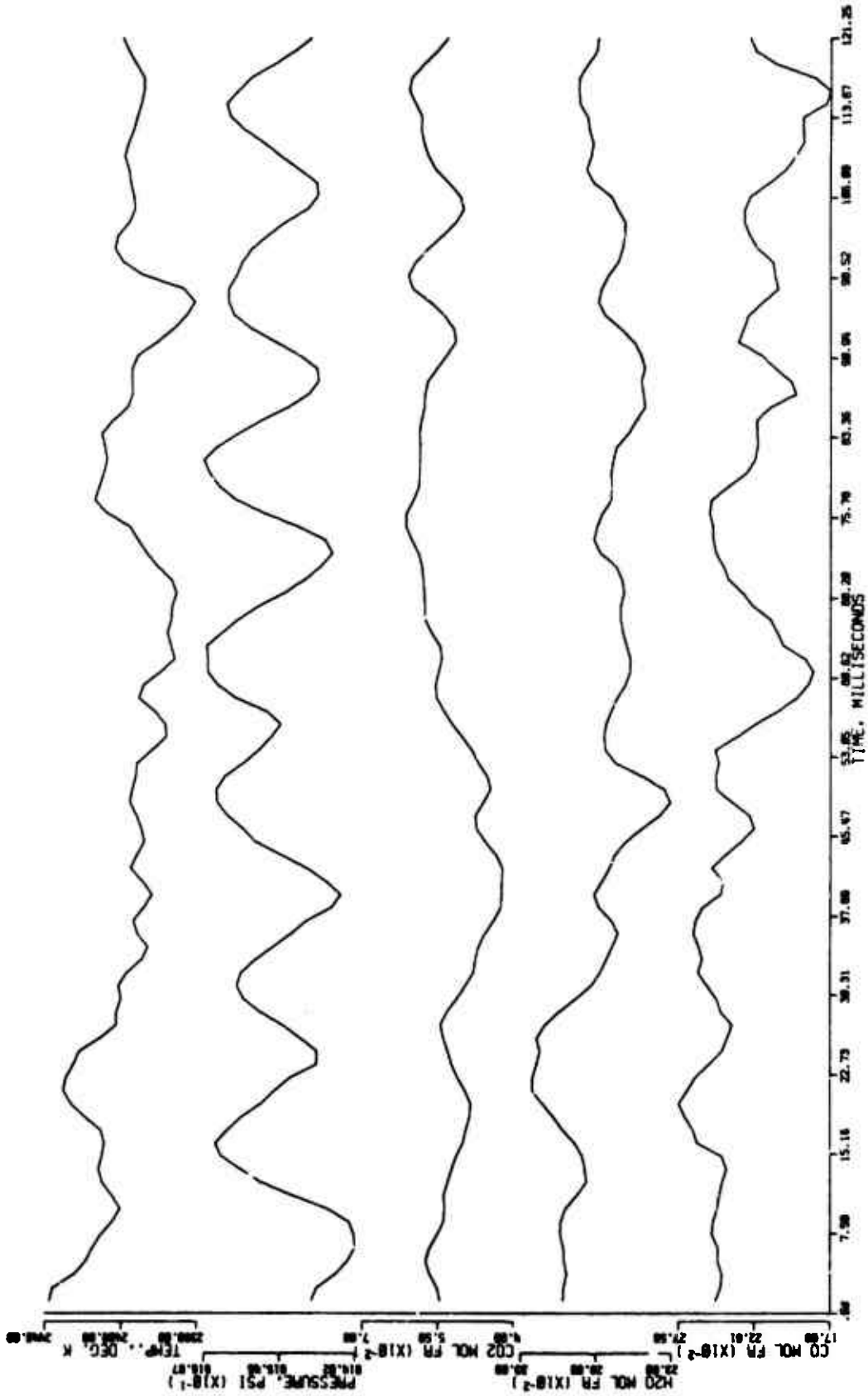

FIGURE 11. FILTERED FORM OF THE TEMPERATURE AND CONCENTRATION PROFILES PRESENTED IN FIGURE 10.

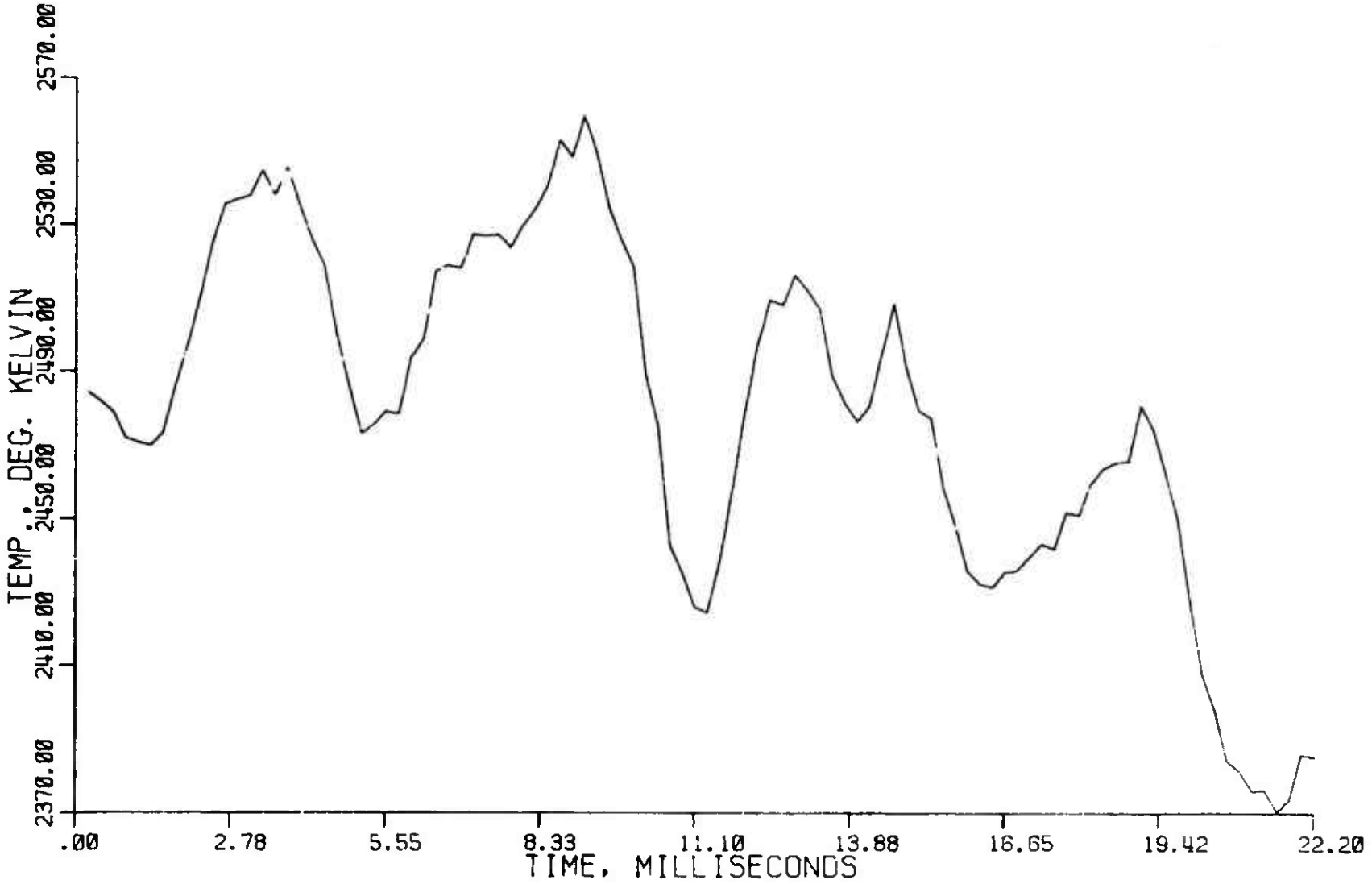

FIGURE 12. TEMPERATURE PROFILE AT 3-5 mm FROM THE PROPELLANT SURFACE DURING A CONSTANT-PRESSURE TEST. (82 wt. % AP propellant [UFP], Run No. 1-31574)

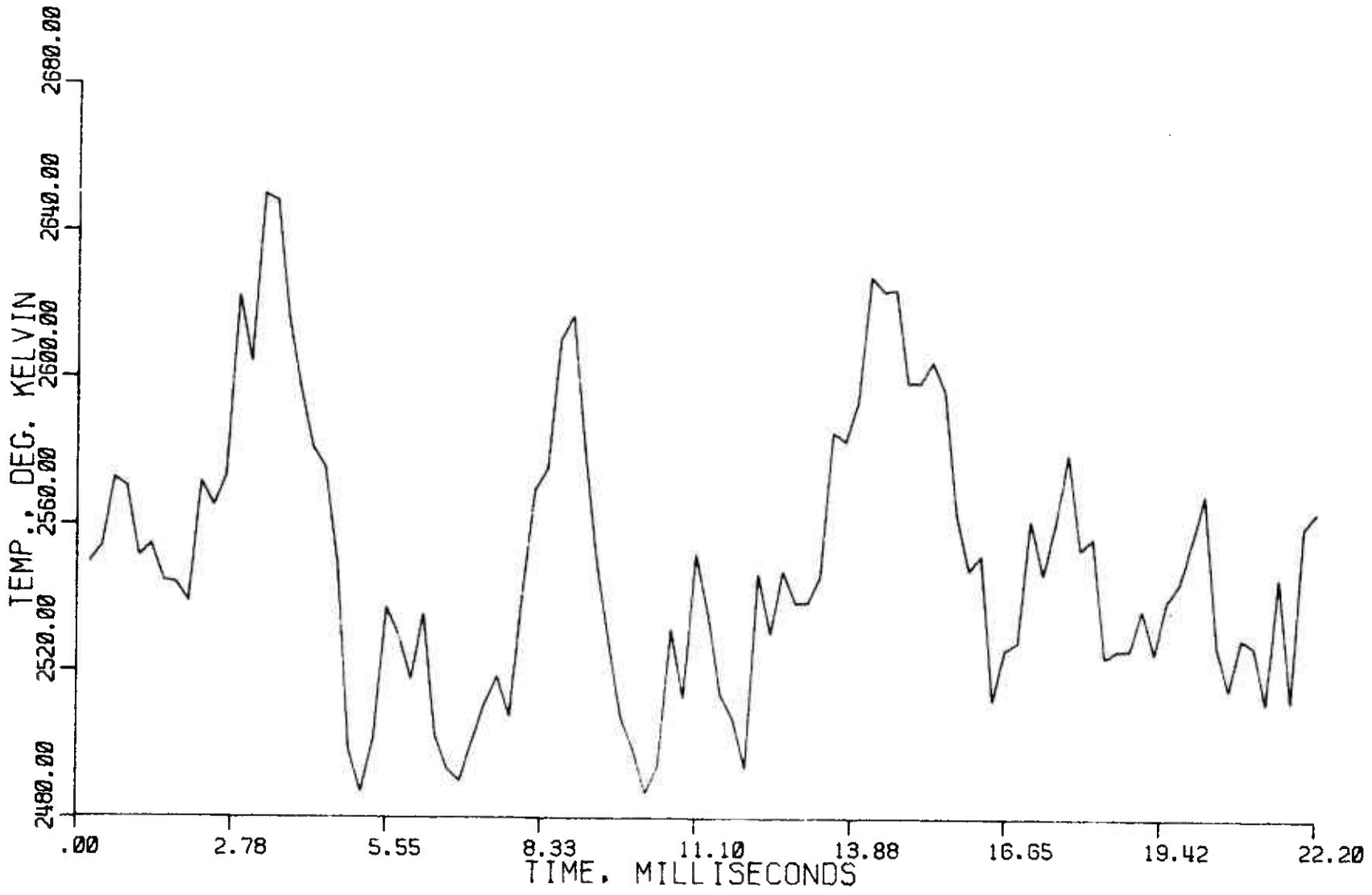

FIGURE 13. TEMPERATURE PROFILE AT 3-5 mm FROM THE PROPELLANT SURFACE DURING A CONSTANT-PRESSURE TEST. (82 wt. % AP propellant [UFP], Run No. 5-31474)

Several major questions need to be answered with regard to these high frequency oscillations. Are the oscillations real, or just manifestations of this particular experimental system? In either case, what is the cause of these oscillations? The various aspects of the experimental equipment which could cause apparent temperature and concentration fluctuations will be discussed first. Since these oscillations have been detected with two completely separate pieces of equipment, the spectrometer and the electro-optical hot-gas pyrometer, the oscillations apparently are not electrical or physical manifestations of the individual pieces of equipment. The presence of common mode noise in both output signals is always a possibility. However, since this "noise" did not appear in either signal during no-flame conditions, this possibility is eliminated.

Are the oscillations related to the scale of propellant heterogeneity, like the layer frequency oscillations postulated by Boggs and Beckstead [27]? For the propellants and pressures used in this study, the Boggs and Beckstead model predicts layer frequencies of approximately 4-7 Hz. and 50-90 Hz. associated with the course (approximately 225 μm) and fine (15 μm) ammonium perchlorate (AP) respectively. Since the observed oscillations were the same order of magnitude as those predicted for the 15-μm AP, tests were made with a unimodal propellant of the course AP (approximately 225 μm). These data also had the same high frequency oscillations. Therefore, we have no grounds for an affirmative answer.

Recirculation of cool combustion products between the flame and the windows could produce oscillations in both the temperature and

concentration profiles. As is discussed in the previous chapter, considerable effort was devoted to eliminating large-scale recirculation flows. Special spectroscopic studies showed that large-scale recirculation of this type was not present in the combustion chamber as finally modified.

An oscillation of the flame shape could also produce fluctuations in the profiles. High-speed motion pictures (1300 pictures per second) revealed a flickering of the propellant flames during both steady and unsteady combustion. This flickering can produce oscillations by two different mechanisms. Local recirculation at the edge of the flame can provide eddies of gas which are unlike the mean gases in the combustion zone. Fluctuations caused by such small scale eddies would most likely not be phase correlated. This flickering could also produce changes in the optical path length in the flame, which would appear as apparent fluctuations in the species concentrations. Apparent concentration oscillations of this type would be phase correlated. Even though the relatively slow scan speed of the spectrometer prevented exact definition of the concentration profiles, there is no hint of the observed concentration oscillations being in phase with one another. The visually observed flickering of the flames appeared to increase in both frequency and amplitude with increasing distance from the propellant surface. Thus, the visual flame structures at the 3-5 and 12-14-mm axial locations were radically different. However, the observed high-frequency oscillations in the concentration profiles at these two axial locations, Figures 9 and 11, are not appreciably different. It is possible that although there were visual differences at the two axial locations, spectroscopically they were similar.

This flickering of the flames could produce an oscillation in the observed flame temperature, if the effective absorptivity of the flame was altered. The temperatures measured are average temperatures (not a path-length arithmetic average), and self-absorption tends to increase the weight of the region closest to the detector. Therefore, if the flickering causes the absorptivity on the detector side of the flame to fluctuate, a resultant oscillation in the flame temperature could be observed. Segments of the temperature profiles of Figures 8 and 10 are presented in detailed form in Figures 14 and 15. Again, there is no appreciable difference between the profiles at the 3-5 and 12-14-mm axial locations. The one large temperature spike in Figure 15 is not representative of the temperature profile at this axial location, as is shown in Figure 10.

High frequency oscillations were also observed in the flame-emission-intensity profiles from flame-emission-only tests. However, these oscillations were in phase with one another and appeared to be aspectral in nature. Changes in the flame's optical path length due to the observed flame flickering is believed to be one possible explanation of these aspectral flame radiation fluctuations. These tests are discussed in Appendix A.

The large temperature fluctuations at fixed axial positions above the surface of composite propellants observed by Oerr and Osborn [1] were attributed to inhomogeneities in the reaction zone. Previous temperature profiles in propellant flames had been obtained by letting the propellant strand burn past the measurement point, such that only a single scan of the temperature profile was obtained. Oerr and Osborn

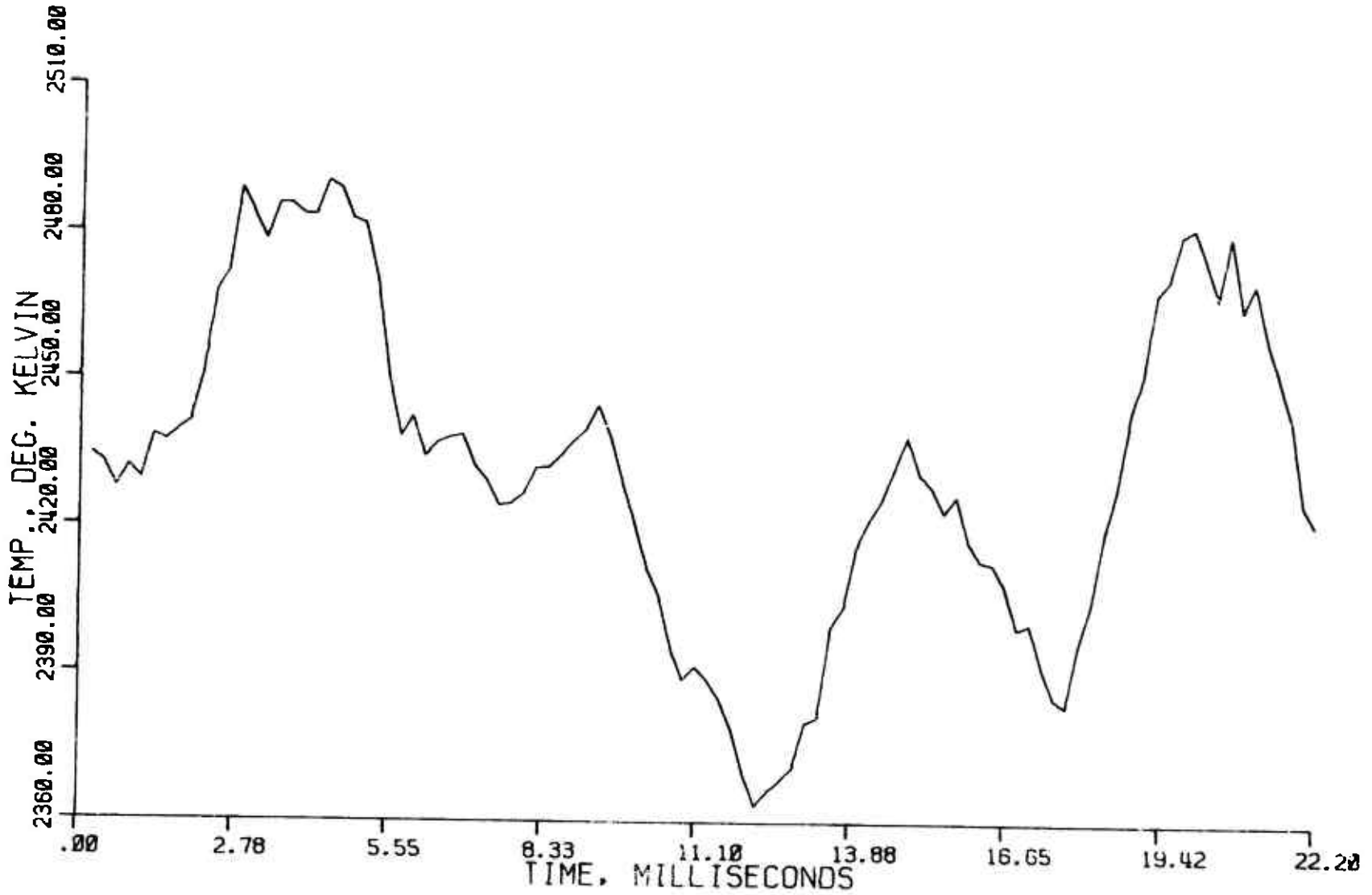

FIGURE 14. TEMPERATURE PROFILE AT 3-5 mm FROM THE PROPELLANT SURFACE DURING A CONSTANT-PRESSURE TEST. (82 wt. % AP propellant [UFN], Run No. 1-3774)

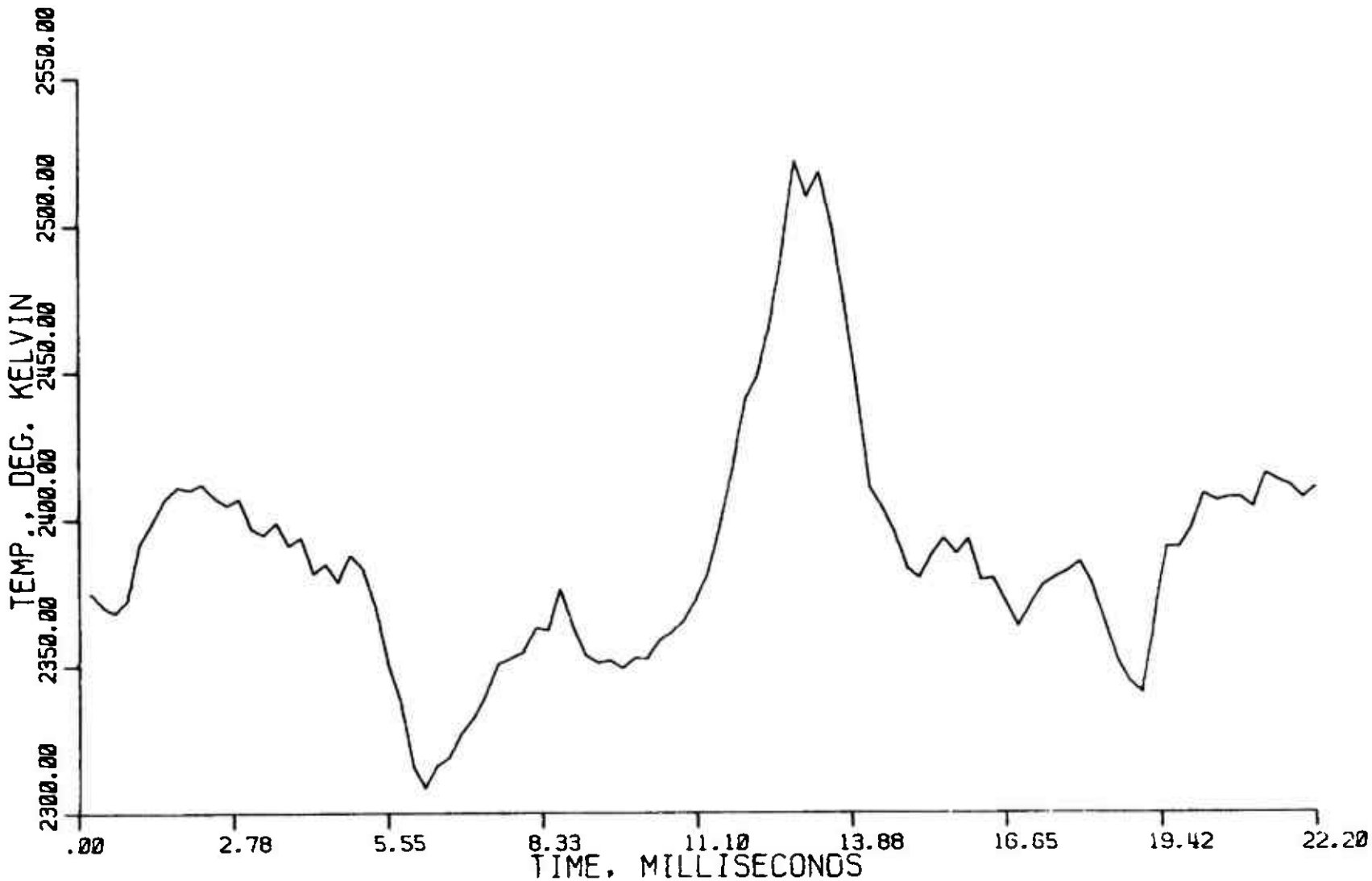

FIGURE 15. TEMPERATURE PROFILE AT 12-14 mm FROM THE PROPELLANT SURFACE DURING A CONSTANT-PRESSURE TEST. (82 wt. % AP propellant [UFN], Run No. 1-3774)

used a servo-controlled feed-shaft to advance the propellant strand toward the temperature measurement zone at the same rate at which the strand burned. Thus, temperature measurements at a fixed axial position in the flame could be made for controlled periods of time. The temperature measurements were made with a modified line-reversal pyrometer, which was capable of one temperature measurement every two milliseconds. The scanning range of the equipment limited the temperature measurements to within one millimeter of the burning propellant surface. Various AP-polysulfide propellants were studied over a pressure range from 1 to 15 atmospheres. The results of the temperature measurements indicated that no one-dimensional temperature profile exists above the burning surface of the propellant. Derr and Osborn observed temperatures, at fixed axial positions in the flame, that varied from the lower limit of accurate temperature measurement (1800°K) to the adiabatic flame temperature of the polysulfide propellant (2200°K).

The high frequency temperature and composition oscillations observed in the present study possibly indicate that these inhomogeneities observed by Derr and Osborn close to the propellant surface still exist at distances of approximately one centimeter from the surface, and are inhomogeneities in both temperature and composition. The optical path length in the flames investigated in the present study was seven times that used by Derr and Osborn. Since both the temperature and spectroscopic measurements yield an average value for the entire optical path length in the flame, the inhomogeneities would tend to average out for longer optical path lengths. Consistent with this fact is that the temperature fluctuations observed in this study were generally smaller than those observed by Derr and Osborn. Also, there

is little chance that any of the oscillations would be phase correlated with one another. This is exactly the condition observed with the high-frequency temperature and concentration oscillations in this study.

In summary, the observed high-frequency temperature and concentration oscillations are believed to be caused by small scale inhomogeneities in the interior and (or) at the edges of the flames. Because these high-frequency oscillations partially obscured the lower frequency phenomena being studied, a digital-filter algorithm was used to eliminate the high-frequency "noise" from the data in final form.

Filtered Data. The filtered steady-state data of Figures 9 and 11 reveal several very interesting features of the steady-state combustion of composite propellants. The flame composition and temperature also fluctuate at a much lower frequency during stable combustion. The lower frequency fluctuations were not continuous like the high frequency oscillations, but rather were random in nature. These low frequency fluctuations were typically in the range of 20 to 80 Hz., with no preferred frequency being apparent. As was previously mentioned, almost all of the observed increases in the CO_2 concentration occur simultaneously with observed decreases in the CO concentration and vice versa. Periodically, this correlation is observed to have minor deviations. The minor deviations are believed to be the result of incomplete filtering of the high-frequency "noise," and thus the unmasking of the low frequency signal was not complete. The digital-filter algorithm was purposely not written for optimum filtering of the high-frequency noise. Instead, it was designed to clean up the data to a minimally acceptable level. The reasons for not using an optimum filtering setting are discussed in Appendix D. The large discrepancies in

the CO-CO_2 correlation in approximately the middle of Figures 9 and 11 are atypical and were very rarely observed. The cause of these particular discrepancies is unknown.

Although the H_2O concentration does fluctuate during steady-state combustion, these fluctuations are apparently unrelated to the CO_2 and CO oscillations. In any event, it is clear that the H_2O fluctuations are not related to the CO_2-CO oscillations in an equilibrium manner. That is, the H_2O and CO_2 oscillations are not in phase. The major sources of H_2O and CO_2 are the free radical reactions involving the OH radical (see equations (1) and (2)). Although the OH radical concentration was not measured in this study, previous studies [33] with fuel-rich systems have shown that the OH radical concentration near the primary reaction zone can be considerably in excess of the equilibrium concentration. This possible superequilibrium OH concentration could have a significant effect on the relatively fast H_2O producing equation. Also, the propellant flame has two fuels, NH_3 from the decomposition of the AP and the fuel-binder pyrolysis products reacting with the decomposition products of the $HClO_4$. Thus, the hydrogen is distributed approximately 60% and 40% between the AP and the fuel-binder respectively. At least two competing reaction paths convert this hydrogen into the stable hydrogen-containing combustion products HCl, H_2 and H_2O. These considerations indicate that the H_2O concentration variation in the flame will not necessarily be a simple function of the changes in the composition of the pyrolysis gases leaving the propellant surface.

The carbon has only one source, the fuel phase. Thus, the carbon containing combustion products CO_2 and CO would be a good indication of changes in the composition of the pyrolysis products leaving the

propellant surface. Since the CO production reactions are relatively rapid, whereas the CO oxidation reaction is relatively slow, the changes in the CO concentration would be the best indication of rapid changes in the composition of the gases leaving the propellant surface.

Because of the very complicated non-equilibrium condition which exists, the equilibrium data were not used to convert the observed CO_2-CO concentration variations into changes in the effective AP-content of the pyrolysis gases leaving the propellant surface, as was originally planned. Instead, these observed concentration variations were used directly for comparing various tests.

The typical CO_2, CO, and H_2O concentration variations for the constant pressure tests were 1-2 mole percent, 4-6 mole percent, and 3-5 mole percent (of the total gas) respectively. The observed temperature fluctuations for these constant pressure tests were only 30-60°K and were only occasionally phase-correlated with the CO and CO_2 concentration oscillations. The magnitudes of these variations occurring during constant-pressure burning, what is called "steady-state burning" for propellants of this kind, are part of the background against which data taken during pressure transients can be analyzed.

Oscillatory Pressure Tests

The oscillatory pressure tests were conducted to see what effect externally-imposed pressure oscillations had on the specific gasification rates of the two composite propellant components. Both the frequency (10-100 Hz.) and the amplitude (2-10 psia) of the pressure oscillations were varied for mean combustion chamber pressures of approximately 25 to 65 psia. For brevity and clarity, only sufficient data to describe the

major findings are presented in this section. The data for other tests are presented in Appendix G. Only the 82-wt.% AP-propellant data are reported in mole fractions. Calibration curves were not established for the 80- and 85-wt. % propellants (see Appendix A); thus, only pressure-corrected absorbances are reported. However, since the temperature corrections for these data are negligible, the pressure-corrected absorbances are directly related to concentration changes. The measurements for the tests reported were made at either the 3-5 mm or 12-14 mm region in the propellant flame, and each test is appropriately labeled. Due to the observed CO_2 and CO axial concentration gradients, the mean concentrations of these species will vary accordingly. All of the data presented in this section and in Appendix G are filtered data.

The data from a 31 Hz. pressure oscillation test are given in Figure 16. The mean combustion chamber pressure was 45 psia, and the peak-to-peak pressure oscillation was approximately 6 psia. Flame temperature measurements were not made for this particular test. With infrequent exceptions, the CO_2 and CO concentration oscillations were at the same frequency as the pressure oscillation and were 180° out of phase with one another. The CO_2 concentration decreased and the CO increased during periods of decreasing pressure, and the opposite condition occurred during periods of increasing pressure. The typical CO_2 and CO oscillations were 2.5-4.0 mole percent and 10-18 mole percent respectively. These amplitudes are approximately three times greater than those of the corresponding steady-pressure test oscillations. The H_2O concentration oscillation is approximately in phase with the CO concentration oscillation and has a magnitude of 9-16 mole percent. Again,

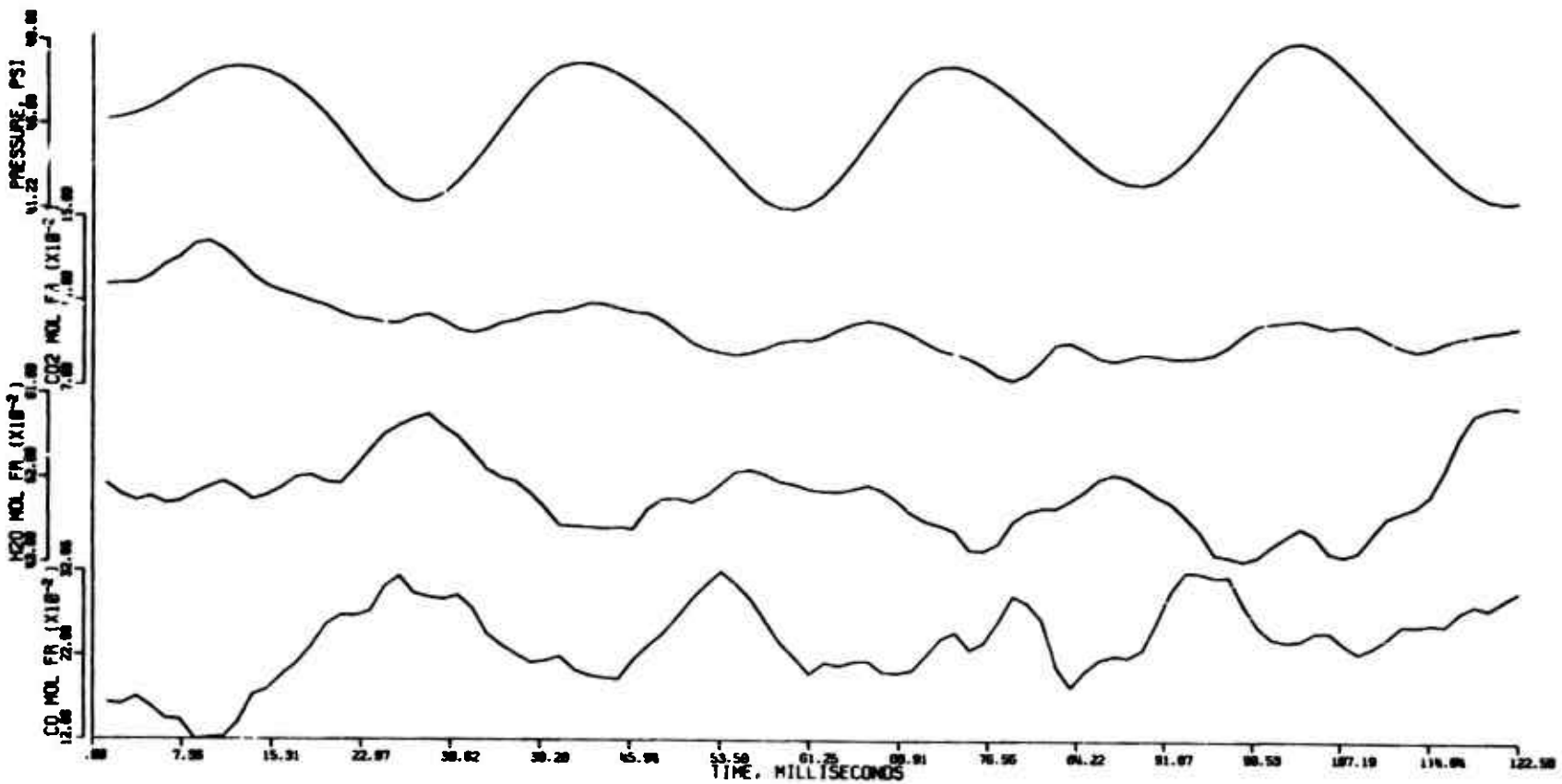

FIGURE 16. CONCENTRATION PROFILES FOR A 31 Hz. OSCILLATORY PRESSURE TEST. (82 wt. % AP propellant [UFN], 12-14 mm, Run No. 2-22174)

this magnitude of the H_2O oscillation is approximately three times greater than the steady-pressure H_2O oscillation. Note that this H_2O-CO correlation is directly opposite to that predicted by the equilibrium calculations. It is assumed that a simultaneous increase in the CO_2 concentration and a decrease in the CO concentration corresponds to an increase in the effective AP concentration of the pyrolysis products leaving the propellant surface. Thus, the specific gasification rate of the AP appears to increase relative to that of the fuel-binder during periods of increasing pressure and vice versa.

Several observations regarding the mean CO_2, the H_2O and CO concentrations require discussion. For this run both the CO_2 and H_2O mole fractions are approximately 167% of the steady-pressure test concentration levels. While the CO concentration is the same as the steady-pressure test value. This excessive H_2O concentration was present in approximately half of the tests run and was not always accompanied by an excessive CO_2 concentration. This phenomenon also occurred in a few steady-pressure tests and is presented in the H_2O calibration curve given in Appendix A. Because almost all the other calibration points fell on the same curve, these few high values were disregarded in the calibration work. The reason for this excessive H_2O concentration, especially when it was not accompanied with an excessive CO_2 concentration, is not understood. However, even though some of the mean concentrations were excessive, these tests possessed the same oscillatory phenomena as the tests having reasonable mean concentrations. Thus, the oscillatory phenomena of these otherwise abnormal tests were considered valid.

The basic features of the concentration oscillations described for

the above test were generally present in all the oscillatory test data. The following data will be used to illustrate other observed characteristics, as well as observed deviations from the above basic features.

The data from several lower frequency tests are presented next. The 7-8 Hz. test data in Figures 17 and 18 are for an 82- and 80- wt. % AP propellant respectively. In both cases the concentration profiles contain a high frequency oscillation, as well as the lower frequency oscillation associated with the pressure. Since only a couple cycles of data are reported for these lowest frequency tests, and since the high frequency oscillation tends to obscure the lower frequency component, it is very hard to determine the relationship between the low frequency concentration oscillation and the pressure. When all of the lowest frequency data are taken collectively it appears that the CO_2 and CO concentrations generally oscillate at a frequency which is slightly different than the pressure frequency. However, the temperature in Figure 19 appears to oscillate in phase with the pressure.

The observed high frequency concentration oscillations are different than the "noise" discussed earlier in that the CO_2 and CO oscillations are generally correlated and are 180° out of phase. These high frequency CO_2 and CO oscillations in the 82-wt. % propellant test of Figure 17 are approximately 80 Hz. This is approximately equal to the layer frequency predicted by the Boggs and Beckstead model for the 15-μm AP in this propellant. Similar oscillations are present in the 80-wt. % AP propellant data of Figure 18, even though they are less well defined. However, this propellant had a unimodal particle distribution of only the 225-μm AP. Therefore, it appears that the origin of this high frequency concentration oscillation is not related to the AP particle

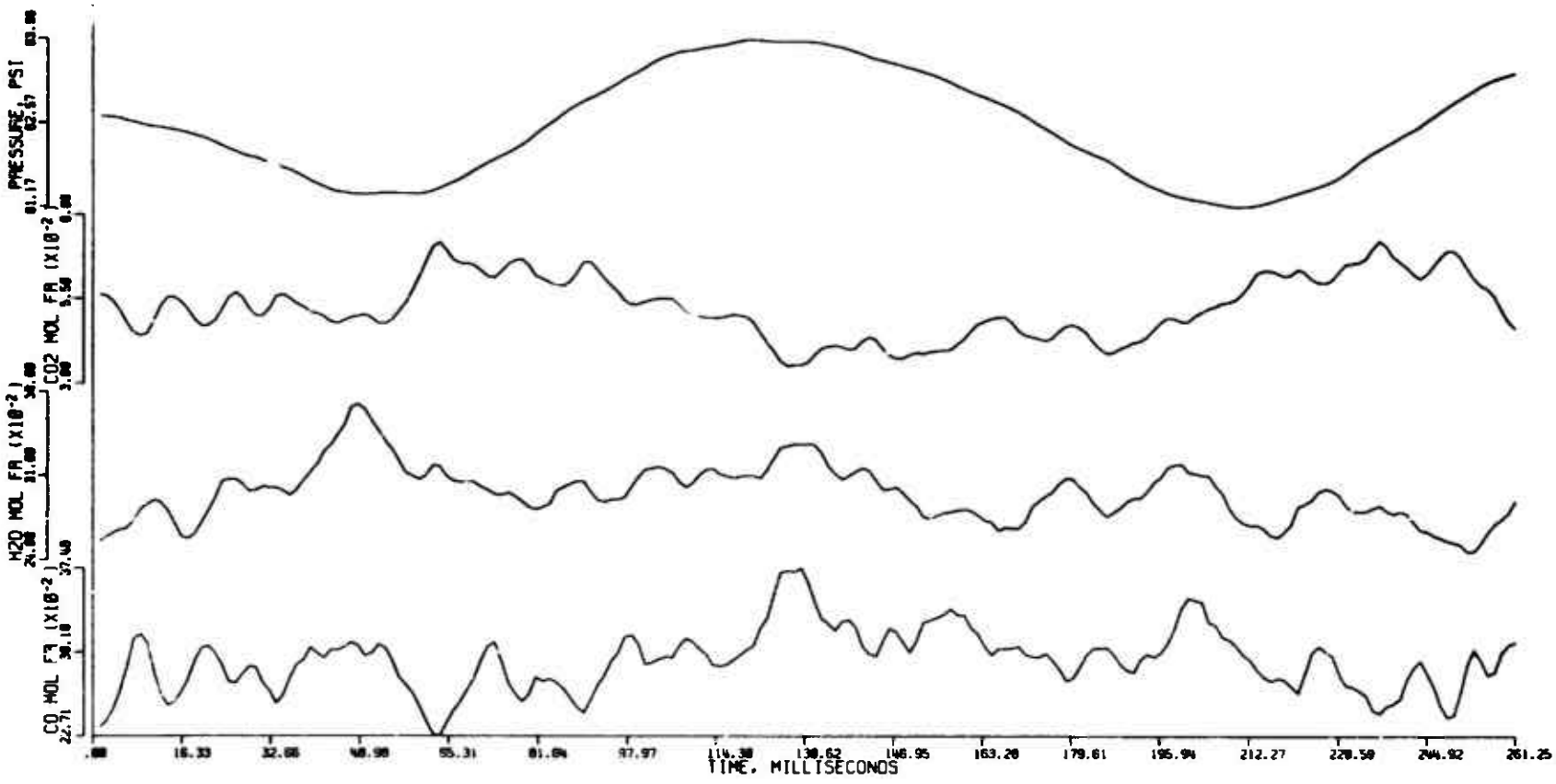

FIGURE 17. CONCENTRATION PROFILES FOR A 7 Hz. OSCILLATORY-PRESSURE TEST (82 wt. % AP propellant [UFN], 12-14 mm, Run No. 2-11174)

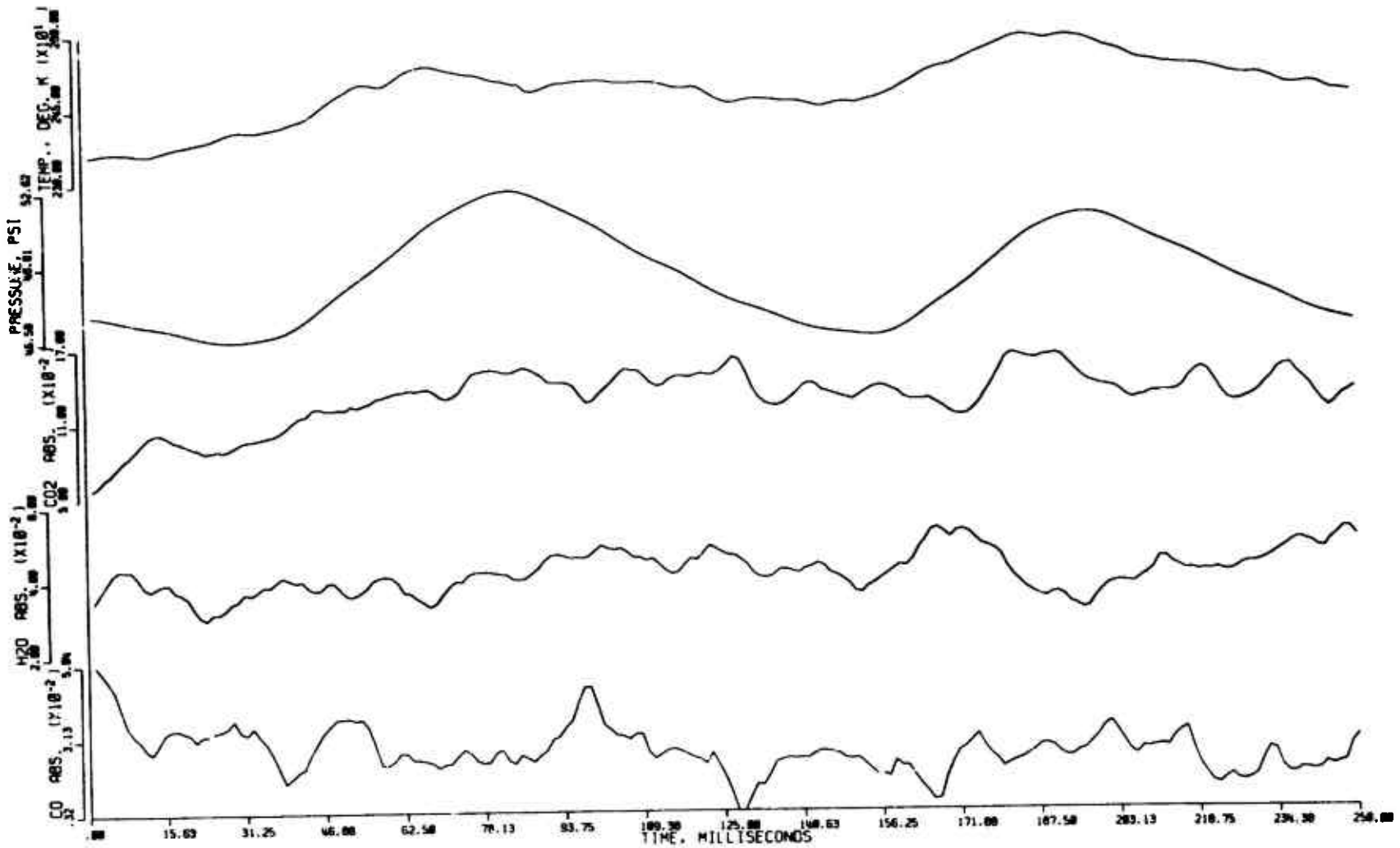

FIGURE 18. TEMPERATURE AND PRESSURE-CORRECTED ABSORBANCE PROFILES FOR AN 8 Hz. OSCILLATORY-PRESSURE TEST. (unimodal 80 wt. % AP propellant [UFO], 3-5 mm, Run No. 2-31474)

size.

The 22 Hz. data in Figures 19 and 20 are for an 82- and 85- wt. % AP propellant respectively. The major significance of these data is that at this slightly higher frequency, the previously observed high frequency concentration oscillations are not present. In both of these tests, the CO_2 and CO concentration oscillations are approximately correlated in the manner described for the 31 Hz data in Figure 16. The 85- wt. % AP propellant data in Figure 20 again shows the CO_2 concentration increasing and the CO concentration decreasing during periods of increasing pressure and vice versa. Again, the H_2O concentration oscillation is in phase with the CO oscillation. Also, the flame temperature oscillation is in phase with this observed gas phase composition oscillation and the pressure.

The correlation between the CO_2-CO oscillations and the pressure less evident for the 82 weight % AP propellant data in Figure 19. The phase shift observed in this test was only occasionally noticed in other tests, and it is not clear if this is a real or just apparent phase shift. The H_2O concentration oscillated slightly during this test, and it appears to be in phase with the CO oscillation for at least part of the run. Again, the mean CO_2 and H_2O concentrations are excessive, while the mean CO concentration is approximately equal to the steady-pressure value.

The data from a 100 Hz. test is plotted in Figure 21. For this test at the highest frequency used, the relatively slow scan speed of the spectrometer does not permit good definition of the concentration profiles. Also, the frequency of the phenomena of interest is approaching that of the "noise," thus, the digital filtering is less effective.

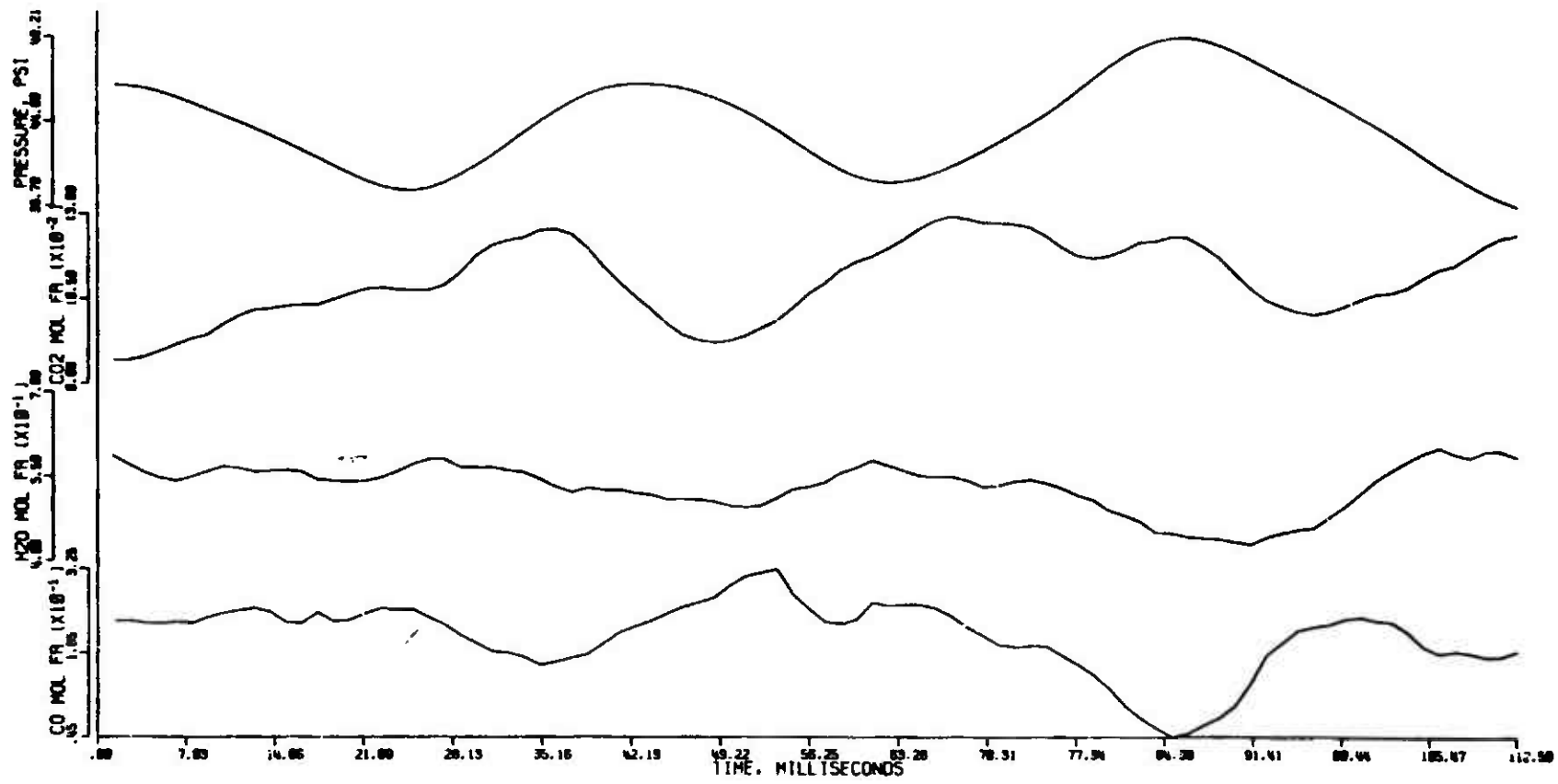

FIGURE 19. CONCENTRATION PROFILES FOR A 22 Hz. OSCILLATORY-PRESSURE TEST. (82 wt. % AP propellant [UFN], 12-14 mm, Run No. 1-22174)

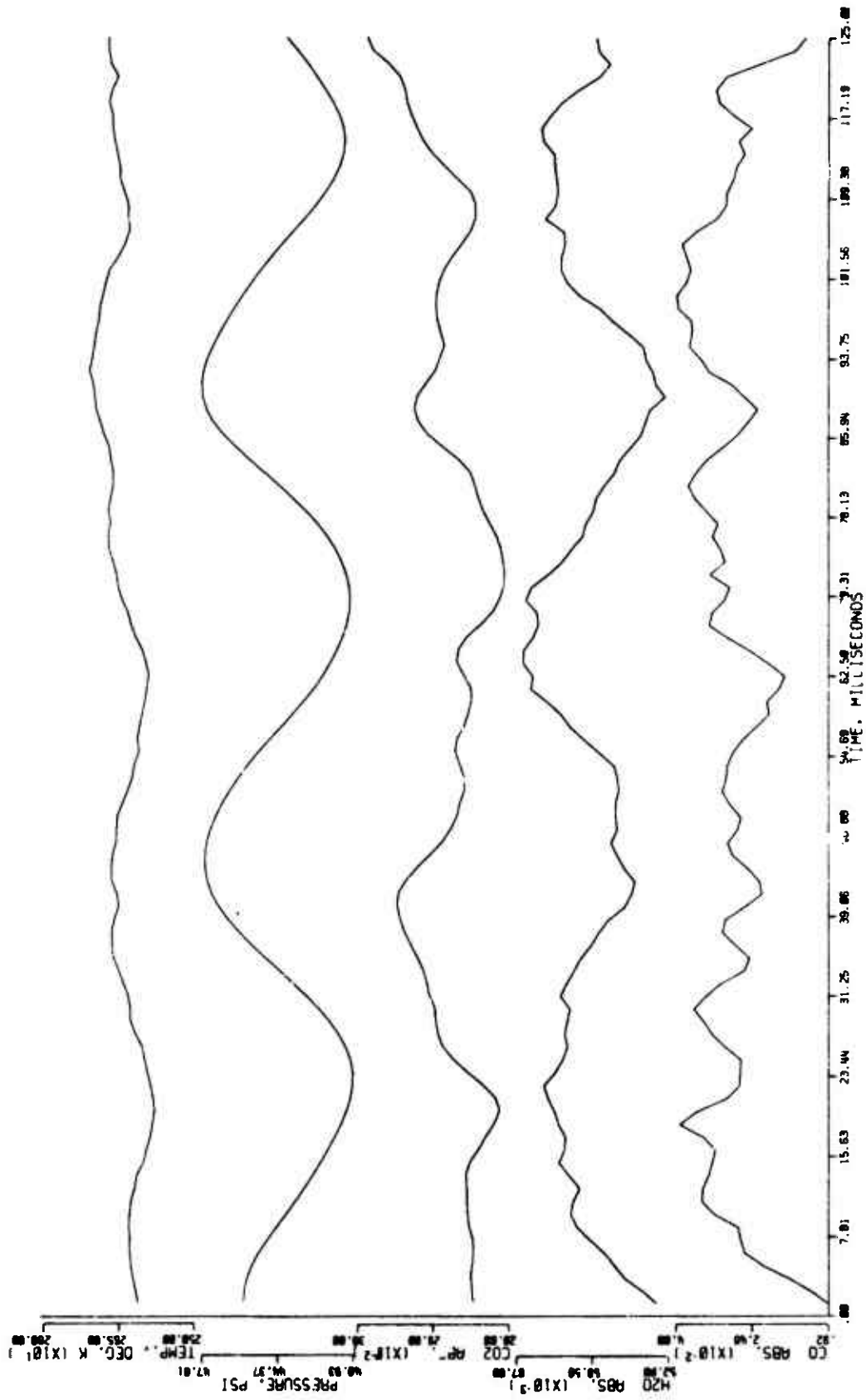

FIGURE 20. TEMPERATURE AND PRESSURE-CORRECTED ABSORBANCE PROFILES FOR A 22 Hz. OSCILLATORY-PRESSURE TEST. (85 wt. % AP propellant [UFR], 3-5 mm, Run No. 11-4474)

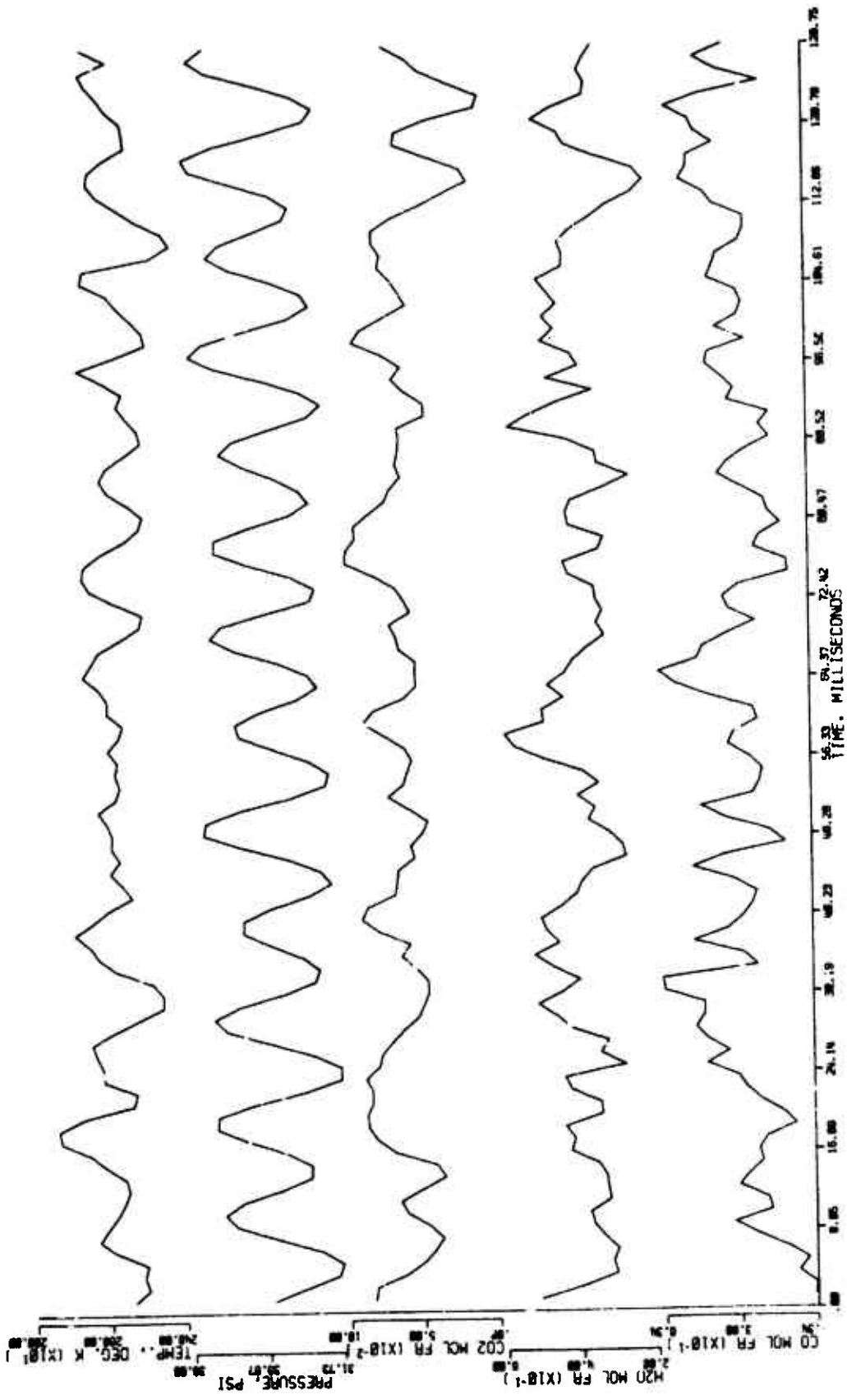

FIGURE 21. TEMPERATURE AND CONCENTRATION PROFILES FOR A 100 Hz. OSCILLATORY-PRESSURE TEST. (82 wt. % AP propellant [UFP], 3-5 mm, Run No. 6-4374)

Although the general characteristics previously described are apparent during portions of the run, the above considerations make it difficult to determine if they are present throughout. However, the major significance of these data is not the correlations between the various profiles but rather the magnitude of the oscillations. The largest temperature and concentration oscillations observed were for this highest frequency. The temperature appears to oscillate in phase with the pressure, with a peak to peak magnitude of 150-200°K. This is 4 to 5 times greater than the temperature oscillations observed for the steady-pressure tests. The CO_2 and CO concentration oscillations are 3-6 mole percent and 30-60 mole percent respectively. The CO_2 oscillation is approximately 3 to 4 times greater than the steady-pressure test CO_2 oscillation, while the CO oscillation is 8 to 10 times greater than the corresponding steady-pressure value. The H_2O oscillation was approximately 15-30 mole percent or 5 to 6 times the steady-pressure value.

Figures 22 and 23 are detailed temperature profiles from two oscillatory pressure tests. The overall temperature changes are associated with the low frequency temperature oscillations which are present in these data. However, comparison of these temperature profiles with those in Figures 12 through 15 for the constant pressure tests reveals a difference in the structure of the high frequency oscillations. These data apparently indicate that the structure of the inhomogenieties in the flame are different for the constant and transient pressure conditions.

The following discussion centers around the oscillatory data presented both here and in Appendix G. In the vast majority of the

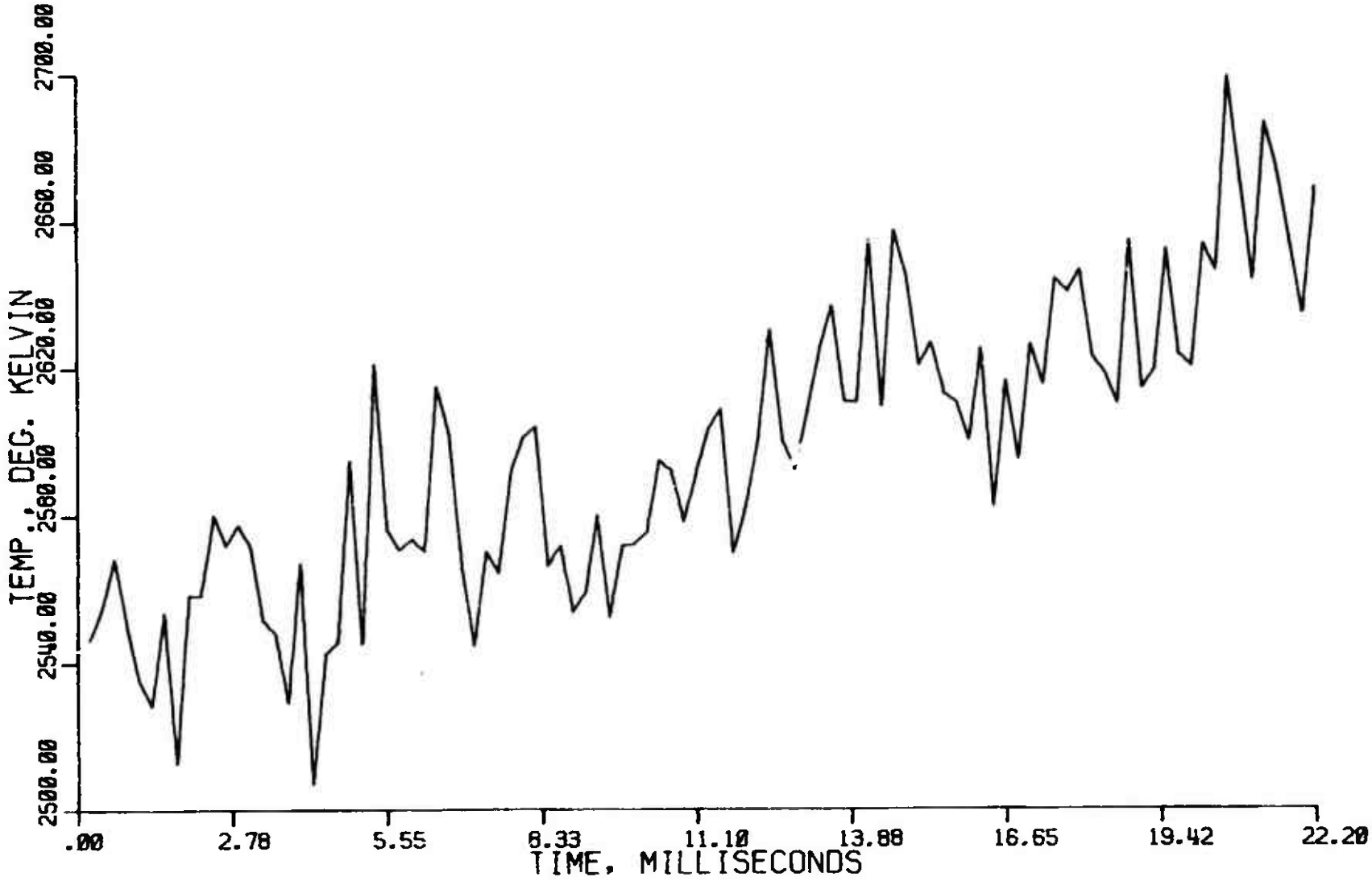

FIGURE 22. TEMPERATURE PROFILE FOR A 35 Hz. OSCILLATORY-PRESSURE TEST. (82 wt. % AP propellant [UFP], 3-5 mm, Run No. 5-4374)

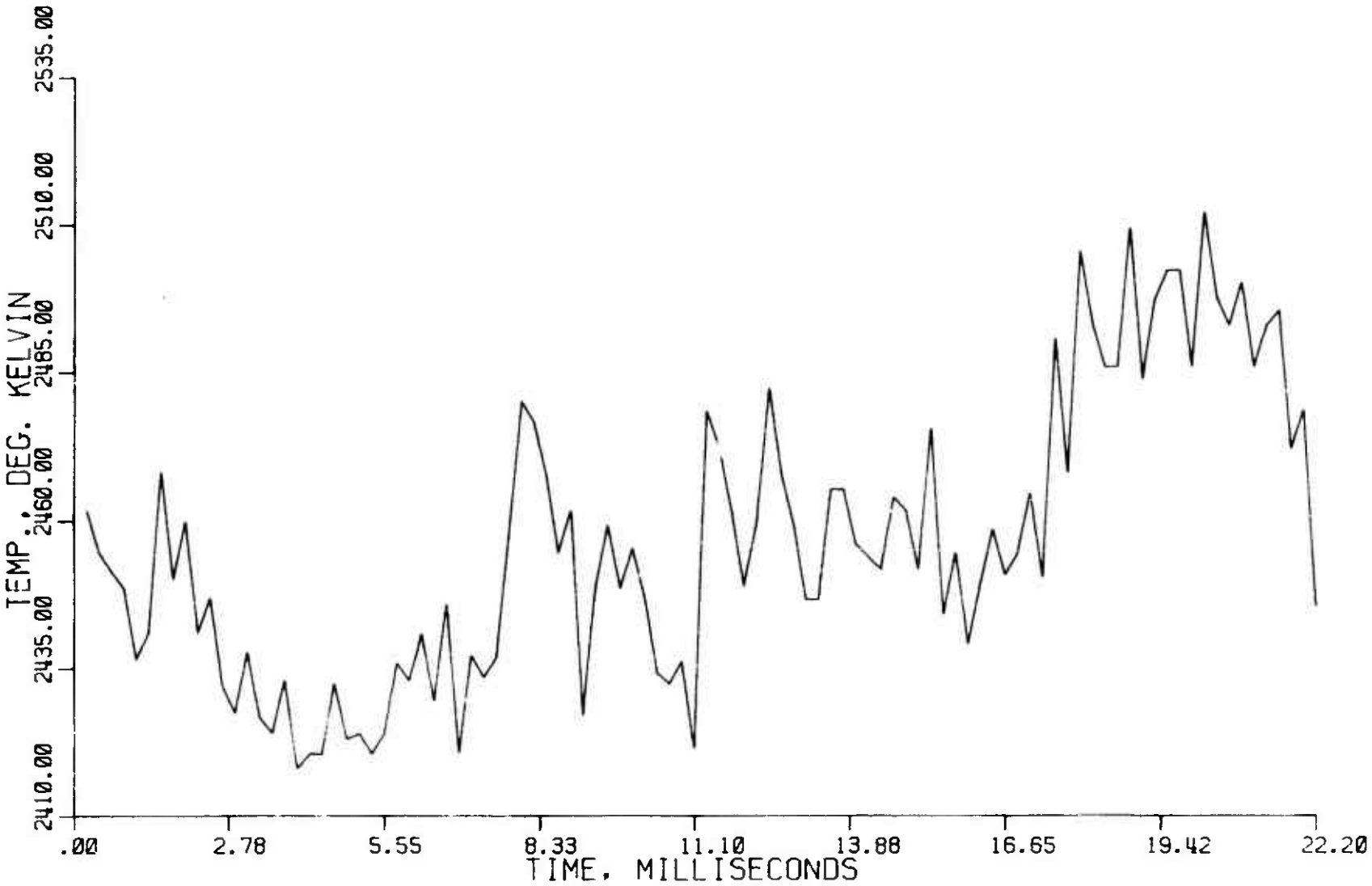

FIGURE 23. TEMPERATURE PROFILE FOR A 50 Hz. OSCILLATORY-PRESSURE TEST. (82 wt. % AP propellant [UFP], 3-5 mm, Run No. 6-31574)

tests, the CO_2 concentration increased and the CO concentration decreased during periods of increasing pressure and vice versa. This observation implies that the specific gasification rate of the AP increases relative to that of the fuel during periods of increasing pressure and vice versa. In the few tests that deviated from this general observation, the origin of the apparent phase shift between the CO_2-CO oscillations and the pressure is not understood.

At a constant mean pressure and a constant frequency, the magnitude of the composition variations in the gas phase increased with an increase in the amplitude of the pressure oscillation. Also, these composition oscillations increased in magnitude with an increase in the frequency of a constant-amplitude pressure oscillation. Over the pressure range studied, 25-75 psia, the mean pressure or the fractional change in the pressure did not appear to have an effect on the composition or temperature oscillations.

Single-Pressure-Pulse Tests

To further clarify the pressure effect on the specific vaporization rates of the two propellant components, several single-pressure-pulse tests were conducted. The data from two pressure-decrease tests are plotted in Figures 24 and 25. In both tests, the CO_2 and CO concentration fluctuations are again 180° out of phase, and the H_2O concentration fluctuations appear at times to be in phase with the CO concentration. During the initial part of the pressure decay the CO_2 concentration decreases and the CO concentration increases for the first 15-20 msec. Then both species concentrations reverse direction, and the CO_2 increases and the CO decreases for approximately the next 30 msec. The data in

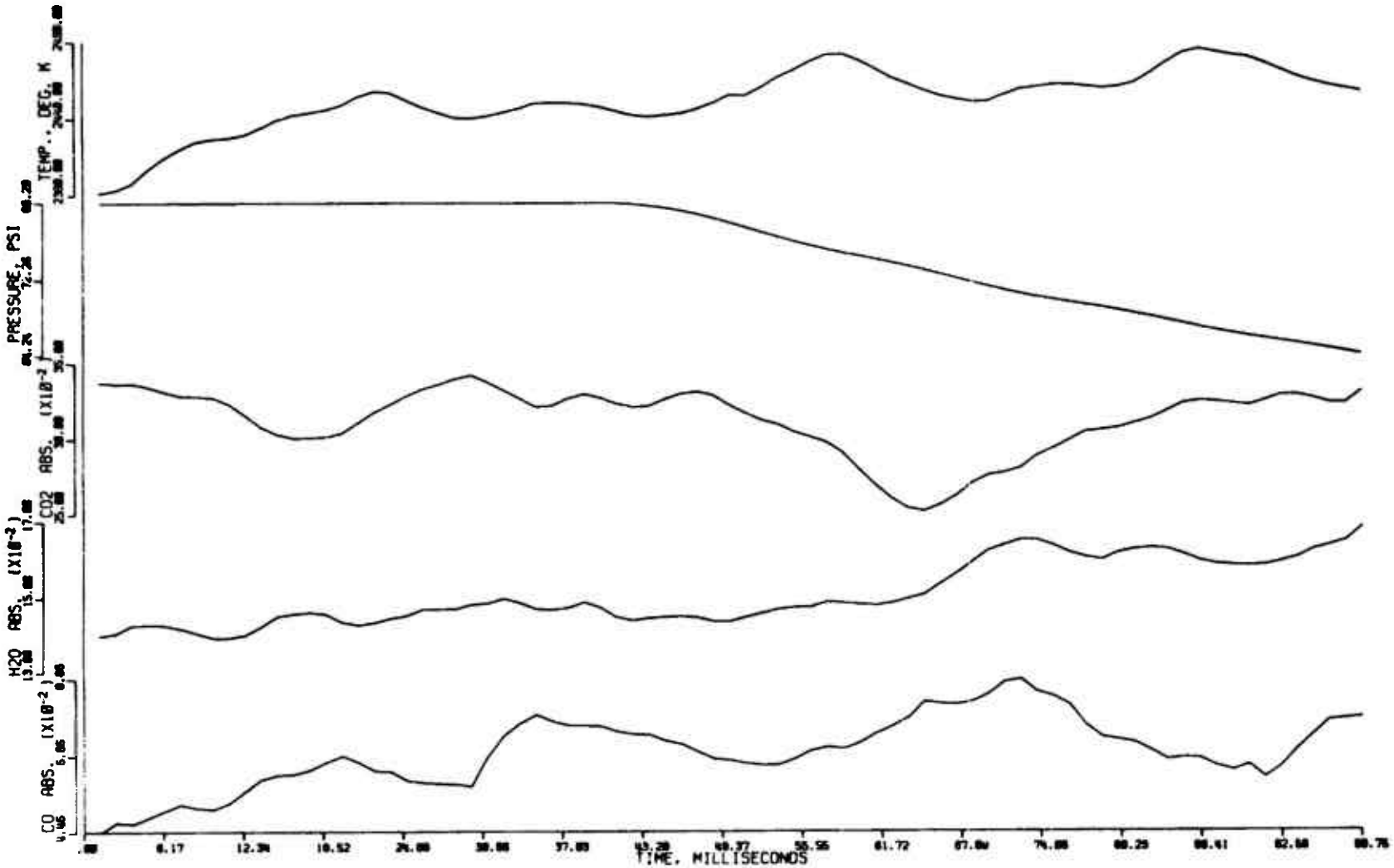

FIGURE 24. TEMPERATURE AND PRESSURE-CORRECTED ABSORBANCE PROFILES FOR A SINGLE-PRESSURE-DECREASE-PULSE TEST. (80 wt. % AP propellant [UFI], 3-5 mm. Run No. 5-4474)

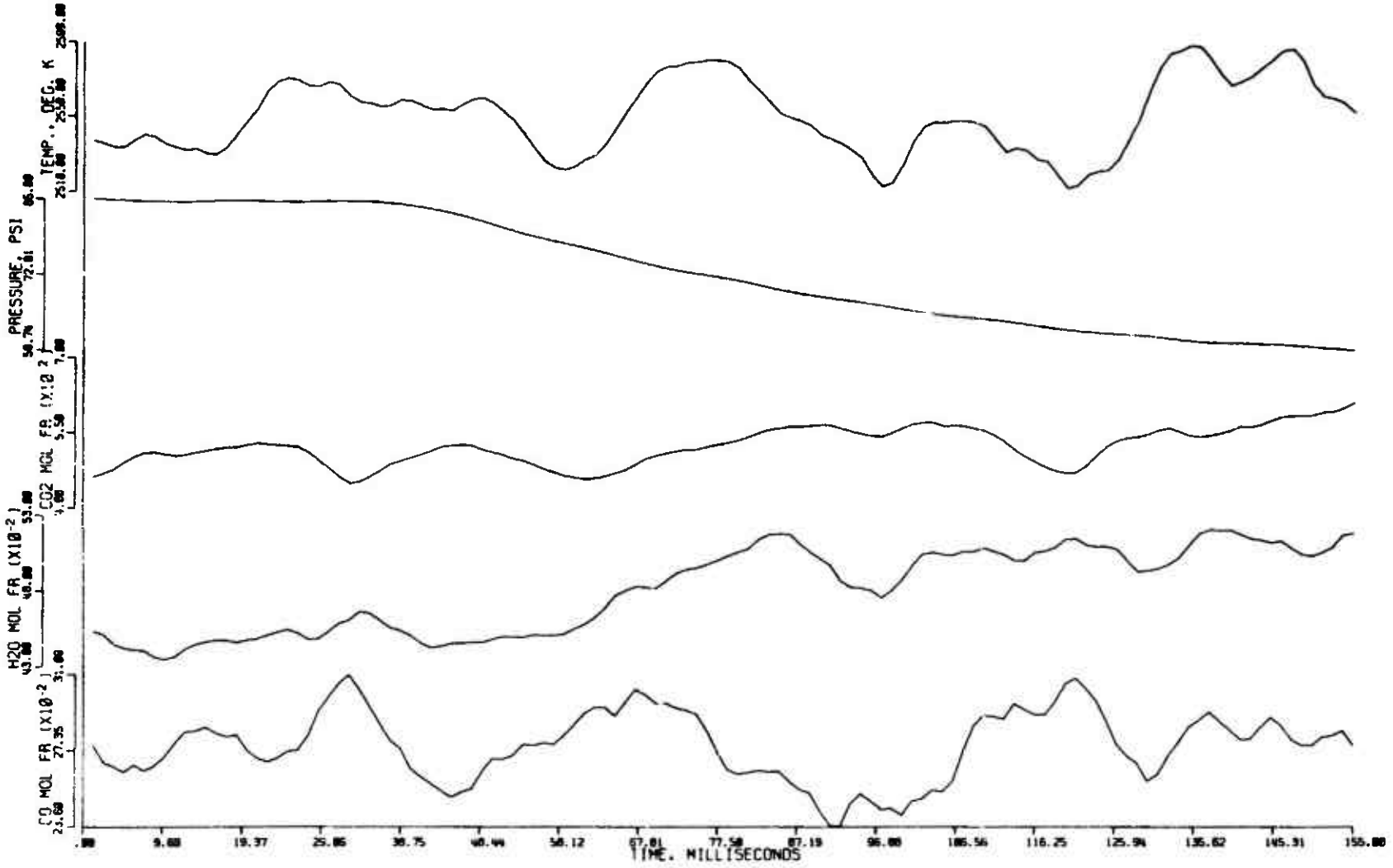

FIGURE 25. TEMPERATURE AND CONCENTRATION PROFILES FOR A SINGLE-PRESSURE-DECREASE-PULSE TEST. (82 wt. % AP propellant [UFN], 3-5 mm, Run No. 8-4374)

Figure 25 shows that this alternating concentration condition continues during a period of continuous pressure decay. Although the temperature oscillated, its magnitude (25-75°K) is approximately equal to the temperature oscillations observed for the steady-state pressure tests. The anomaly just before the pressure decay in Figure 25 is of unknown origin. However, the pressure decay data collectively indicate that it is not associated with the pressure pulse.

Although the characteristic time (15-20 msec.) associated with this initial composition fluctuation was independent of the rate of pressure decay over the range of 300 to 700 psi/sec., the magnitude of this fluctuation was directly proportional to the rate of pressure change. Also, though these rates of pressure decay were comparable to those of the oscillatory pressure tests, the composition changes during these pressure decay tests were much less than those of the oscillatory tests.

Data from two pressure increase tests are plotted in Figures 26 and 27. The nature of the composition fluctuations during pressure increase tests varied from run to run and were not regular like those observed during the pressure decay. However, several general observations regarding these tests can still be made. It appears that initially the CO_2 concentration increases and the CO concentration decreases for an irregular length of time. This is followed by random oscillations in the CO_2 and CO concentrations. Although the H_2O concentration fluctuates, its relationship with either the CO_2 or CO concentration is not apparent. The concentration oscillations for these pressure-increase tests were larger than those observed for the steady-state pressure tests but were again much smaller than the values from oscillatory tests with comparable rates of pressure change.

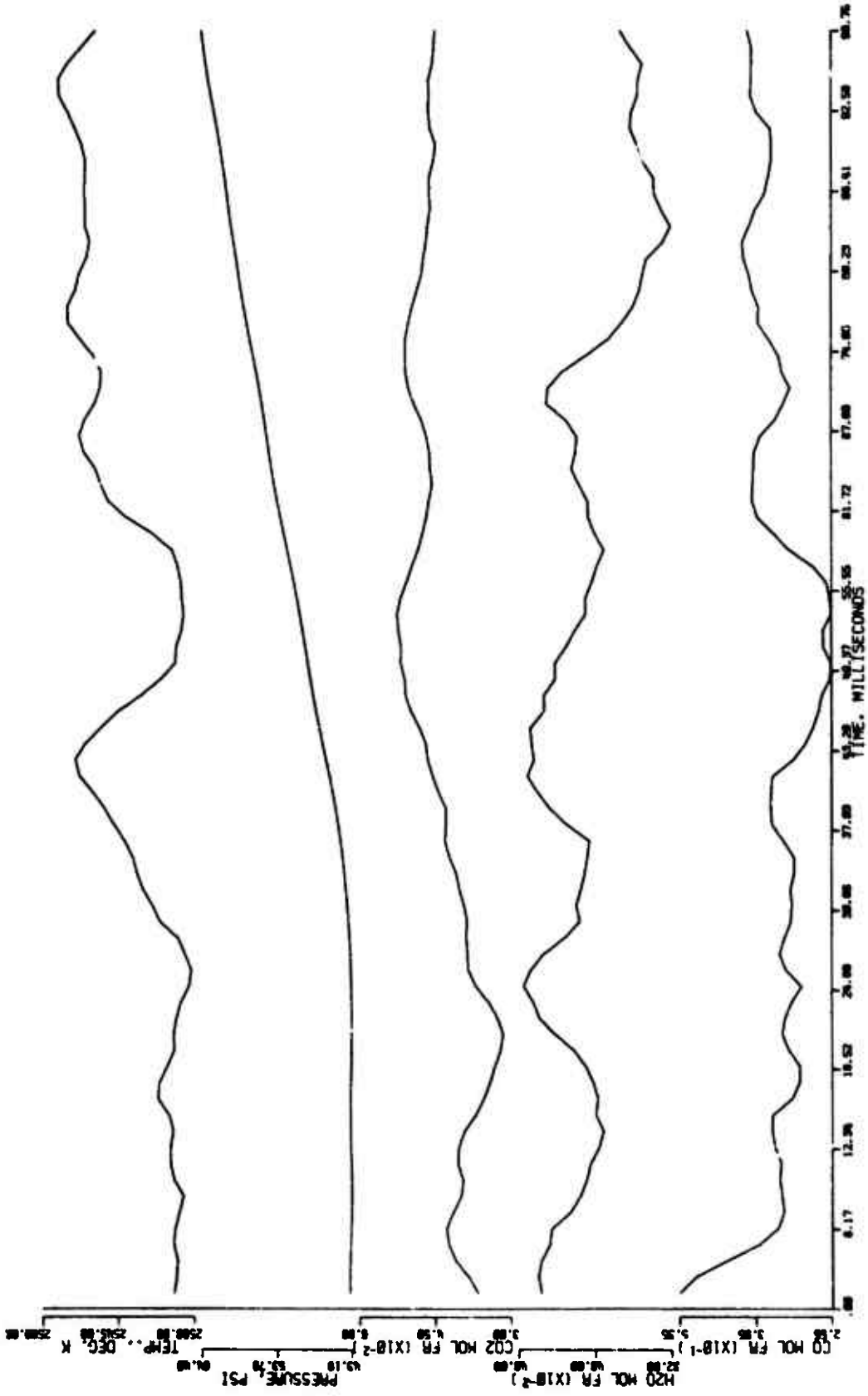

FIGURE 26. TEMPERATURE AND CONCENTRATION PROFILES FOR A SINGLE-PRESSURE-INCREASE-PULSE TEST (82 wt. % AP propellant [UFP], 3-5 mm, Run No. 1-31574)

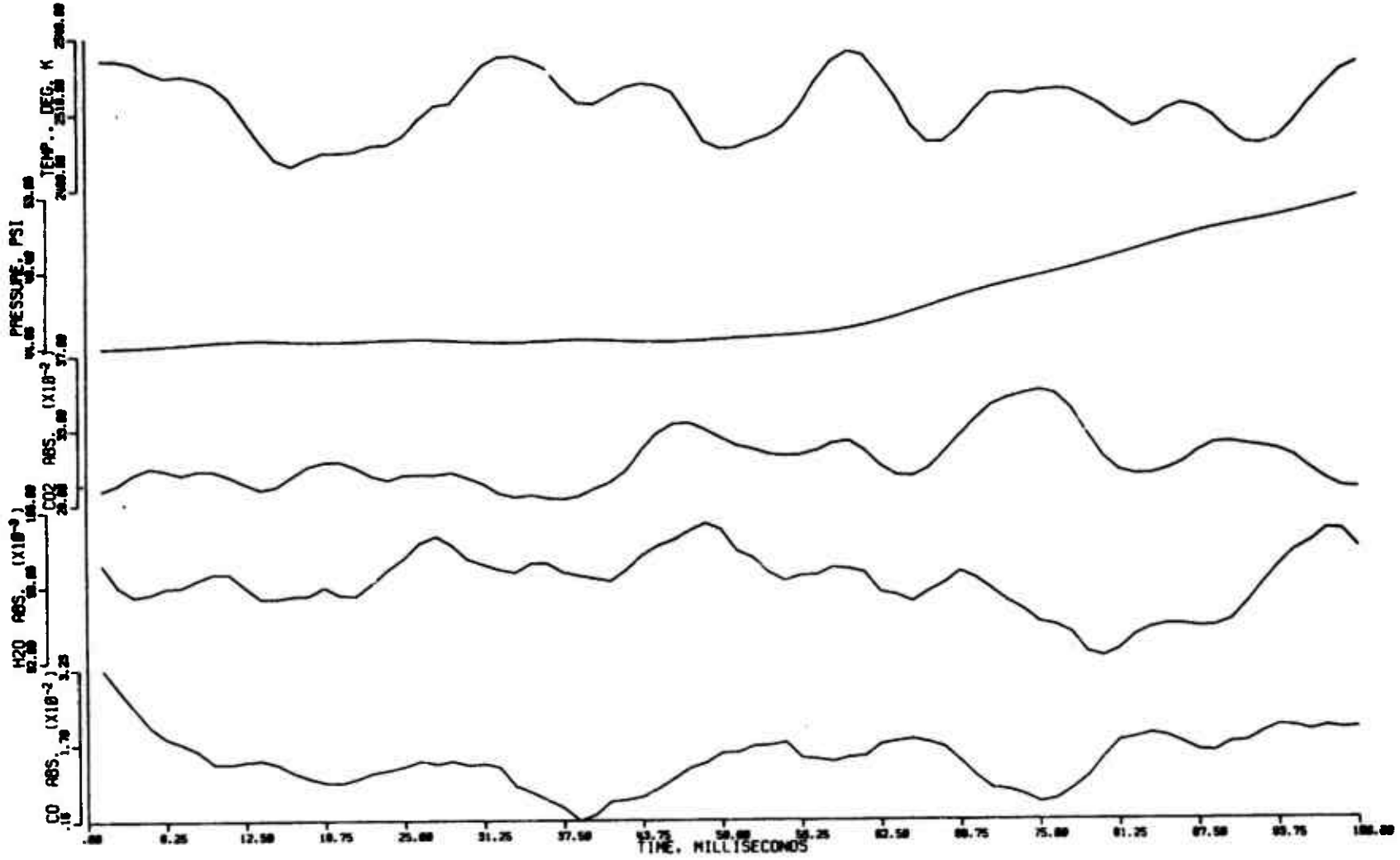

FIGURE 27. TEMPERATURE AND PRESSURE-CORRECTED ABSORBANCE PROFILES FOR A SINGLE-PRESSURE-INCREASE-PULSE TEST. (unimodal 80 wt. % AP propellant [UFO], 12-14 mm, Run No. 7-4474)

Flame-Emission Data

The general observations and resulting conclusions from this study contradict those reported by Schulz [7]. That is, the present data indicate that the AP gasification rate increases relative to that of the fuel-binder during periods of increasing pressure, whereas Schulz concluded that the AP gasification increased relative to that of the fuel-binder during periods of pressure decay.

Since Schulz's rapid depressurization studies (using rarefaction waves) were very unlike the pressure decay tests of this study, data of the kind Schulz took were obtained under the conditions of the present study. The emission data from a typical oscillatory test are plotted in Figure 28. The bottom profile on this figure is the (H_2O/CO_2) emission intensity ratio. The nature of the intensity ratio oscillation for this present test is identical with that reported by Schulz. The steady-pressure intensity ratio data does not predict this large of an oscillation, thus, the observed intensity ratio overshoots the steady-pressure intensity ratio profile in both directions. Schulz used steady-pressure "equilibrium" data to interpret this intensity-ratio overshooting. However, the non-equilibrium condition known to exist in these flames indicates that using his method of interpreting transient data is questionable. Also, the use of flame-emission data, which is largely due to the small fraction of the molecules that are in the excited state, is likely to introduce additional errors.

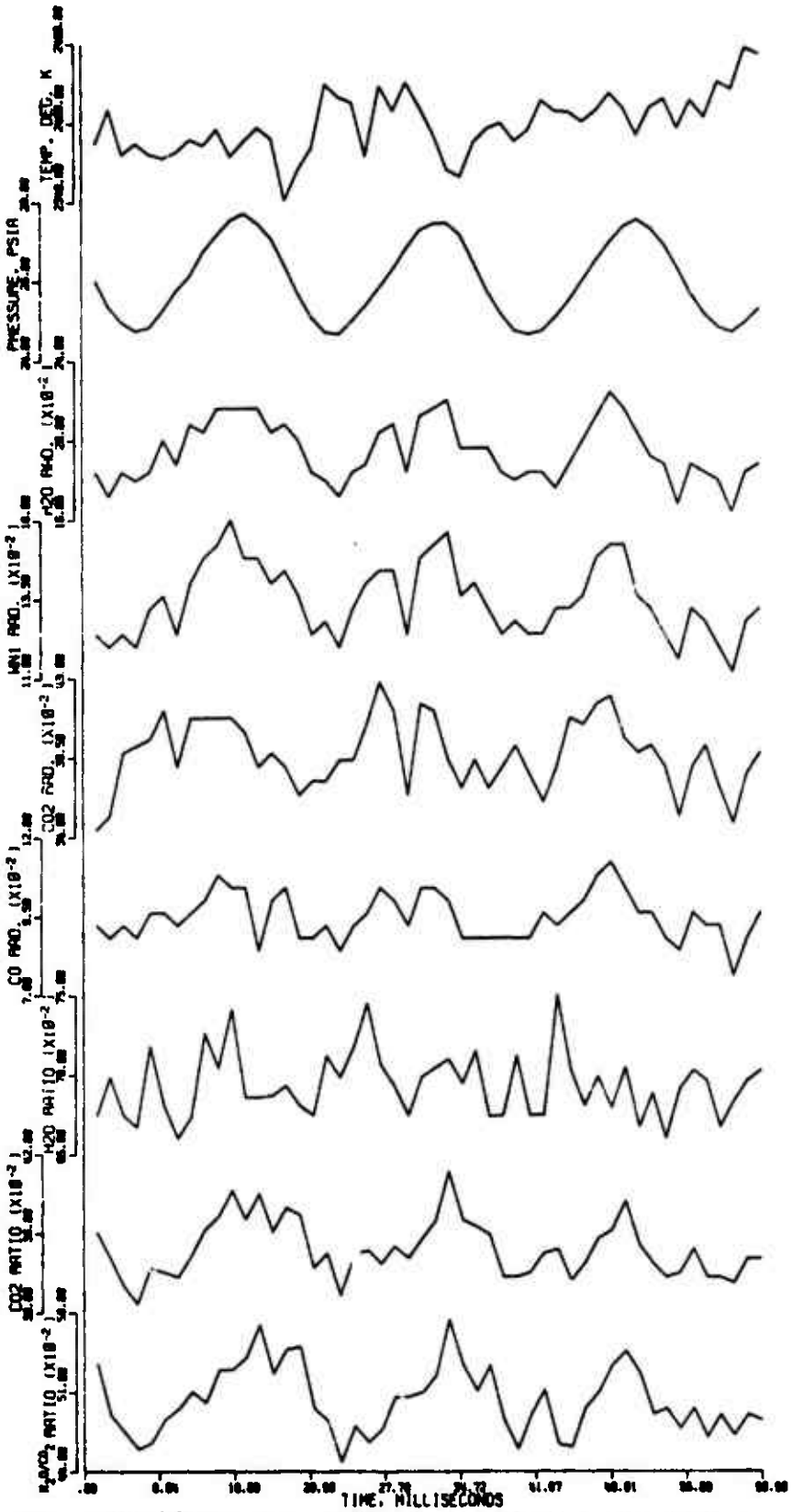

FIGURE 28. TEMPERATURE AND FLAME RADIATION DATA FOR A 54 Hz. OSCILLATORY-PRESSURE TEST. The (window radiation/H_2O radiation), (window radiation/CO_2 radiation), and (H_2O radiation/CO_2 radiation) ratios are also plotted. (85 wt. % AP propellant [UFP], 3-5 mm, Run No. 2-4373, film-reader units are plotted)

CHAPTER V

SUMMARY AND CONCLUSIONS

The objective of this study was to characterize the independent gasification processes of the two components of AP-HTPB composite solid propellants during steady and non-steady pressure tests. In particular, it was to be a study of the independent pressure dependencies of the specific gasification rates of the oxidizer and fuel-binder phases.

A new high temperature infrared radiation source was used in conconjunction with a rapid-scanning spectrometer (800 scans per second) to obtain quantitative absorption spectroscopy data from propellant flames during both steady-state pressure tests and externally imposed transient pressure tests. The system was quantitatively calibrated for the 3.17-μm H_2O, 4.26-μm CO_2, and 4.72-μm CO absorption bands. Also, a fast electro-optical hot-gas pyrometer (4500 measurements per second) was used to obtain simultaneous flame temperatures. A variable-area secondary nozzle was used to impose the pressure transients to otherwise stable burning propellant strands.

The following summary is organized according to the three types of tests conducted: a) steady-state pressure tests, b) oscillatory pressure tests, and c) single-pressure-pulse tests.

Summary of the Constant Pressure Data

The axial composition and temperature profiles as a function of

distance from the burning propellant surface were studied in the region between 3 mm and 15 mm from the propellant surface. The composition profiles revealed gradients in the concentrations of CO and CO_2 over this region. However, the H_2O concentration was, on the same scale of observation, constant over this same distance. These observations from within individual tests were substantiated with numerous time-averaged values measured at various axial positions in the flame. The axial temperature profile indicated that the flame temperature only decreased 25-50°K over this distance, probably due to entrainment of the cold purging gas and radiation to cold surroundings.

The observed concentration profiles are typical of those observed in hydrocarbon-oxygen flames [32, 33]. Relatively fast reactions produce CO and H_2O, however, the CO oxidation reaction which produces the CO_2 is relatively slow [33, 34]. We find that, over the pressure range studied (25-100 psia), a non-equilibrium condition existed at distances of up to at least 1.5 cm from the propellant surface. Consideration of this non-equilibrium condition is most important when interpreting composition data from transient pressure tests. It probably has relevance to considerations of combustion instability.

The time-varying nature of the composition and temperature at a given axial position in the flame produced considerable information concerning the steady-state combustion processes. A 200-300 Hz. oscillation in both the composition and temperature profiles was observed. None of the observed high frequency oscillations were phase-correlated with one another. These high frequency oscillations are believed to be caused by inhomogeneities in the propellant flame, similar to those observed by Derr and Osborn [1] when measuring flame temperatures close

to the surface of a composite propellant.

The flame composition and temperature were also observed to fluctuate at a much lower frequency during stable combustion. These lower-frequency fluctuations were not continucus like the high frequency oscillations, but rather were random in nature. Also, the CO_2 and CO concentration fluctuations were, almost without exception, phase correlated and 180° out of phase. Although the H_2O concentration fluctuated during the steady-pressure tests, these fluctuations were apparently unrelated to the CO_2 or CO fluctuations. These low frequency fluctuations were typically in the range of 20 to 80 Hz., with no preferred frequency being apparent. The average CO_2, CO, and H_2O concentration variations for the steady-state pressure tests were 1-2 mole percent, 4-6 mole percent, and 3-5 mole percent respectively. The observed temperature fluctuations for the steady-state pressure tests were typically 30-60°K and were only occasionally phase-correlated with the CO_2-CO concentration fluctuations.

Summary of the Oscillatory Pressure Data

Oscillatory pressure tests were conducted over a mean pressure range of 25 to 65 psia, a pressure amplitude range of 2-10 psia, and a frequency range of 10 to 100 Hz. The nature of the composition oscillations were generally the same for all the tests between 20 and 100 Hz. The CO_2 and CO concentration oscillations were 180° out of phase. The CO_2 concentration increased and the CO concentration decreased during periods of increasing pressure and vice versa. In several runs, the CO_2 concentration oscillation was out of phase with the pressure,

even though the CO_2 and CO oscillations were still approximately correlated. It is not clear if this observed phase shift was real or just apparent. In either case its origin is unknown. Since this was only an occasional observation, it was considered an anomaly in the otherwise general characterization. In many runs the H_2O concentration oscillation was in phase with the CO concentration oscillation. In the runs where this was not the case, the relationship between the H_2O concentration oscillation and either the CO_2 or CO oscillation was not readily apparent.

Since carbon was only contained in the fuel-binder phase, whereas hydrogen was contained in both the ammonium perchlorate (AP) and the fuel-binder (HTPB) phases, the CO_2-CO concentration variations were considered the best indication of changes in the composition of the pyrolysis gases leaving the propellant surface. Also, an increase in the CO_2 concentration and a simultaneous decrease in the CO concentration was considered as an indication of a more oxidizer-rich gas mixture leaving the propellant surface and vice versa. Thus, for the 20 to 100 Hz. tests, the specific gasification rate of the AP apparently increases relative to that of the HTPB during periods of increasing pressure and vice versa. This finding is directly opposite that postulated by Schulz [7]. The reason for this discrepancy will be discussed later.

The temperature in most of these 20 to 100 Hz. tests oscillated in phase with the pressure with an amplitude greater than that observed for fluctuations during the steady-pressure tests. The adiabatic flame temperature data for the 80, 82, and 85 wt.-%-AP propellants used

indicate that an increase in the effective oxidizer concentration in the flame will result in a temperature increase. That is, the temperature should increase during periods of increasing pressure, which is exactly what was observed in many of the tests. In the few tests where the temperature did not oscillate in phase with the pressure, the temperature fluctuations were generally random in nature and smaller in amplitude. In these tests the temperature profiles resembled those of the steady-pressure tests. The reason for this lack of temperature and composition correlation is not known, but again, this anomaly occurred in only a few tests.

The concentration profiles for the oscillatory pressure tests at the lowest frequencies studied (7-10 Hz.) had a much different character. The concentration profiles for these tests contained a high frequency oscillation as well as the lower frequency oscillation associated with the pressure. The low frequency component of the CO_2 and CO profiles were again generally 180° out of phase. However, when all of the lowest frequency data are taken collectively it appears that the CO_2 and CO concentrations generally oscillate at a frequency which is slightly greater than the pressure frequency. The H_2O concentration oscillation appears at times to be in phase with the CO concentration oscillation, but this is not an observation of sufficient generality to be a prime consideration.

The higher frequency CO_2 and CO concentration oscillations are also generally 180° out of phase. These 70-90 Hz. oscillations were originally thought to be a "layer frequency" associated with the 15-μm AP present in the propellants being used. However, a unimodal propellant

of 225-μm AP also revealed similar high frequency oscillations. The relationship between the higher frequency H_2O oscillations and either the CO_2 or CO concentration oscillation is difficult to determine, although at times it again appears to be in phase with the CO concentration oscillation. The temperature profiles for these low frequency tests did not contain this characteristic high frequency oscillation, and only occasionally oscillated in phase with the pressure.

The following discussion pertains to the temperature and concentration oscillations which are associated with the pressure oscillations. The amplitudes of the concentration and temperature oscillations of the oscillatory pressure tests are at least several times those of the random values seen in constant-pressure tests. The amplitudes of the CO and H_2O concentration oscillations were generally larger with respect to their constant pressure test values than was the corresponding CO_2 oscillation. This is consistent with the reaction kinetics of the various reactions which produce these species. Also, the CO oscillation was generally larger than the corresponding H_2O oscillation which might be due to the dual source of the hydrogen.

At the lowest frequencies (7-10 Hz.) and for pressure amplitudes of only 3-10 psia the magnitude of the concentration oscillations are typically 2 or 3 times greater than the random constant-pressure values. The amplitude of the observed concentration oscillations increased with an increase in the rate of pressure change. Experimentally, this was done by either changing the pressure amplitude at a constant frequency, or by changing the frequency at a constant pressure amplitude. For example, changing the amplitude of a 31 Hz. test from approximately 2 psi

to 8-10 psia resulted in approximately a factor of two increase in the amplitude of the CO_2 and H_2O oscillations, and a factor of three increase in the CO oscillations. Also, the largest temperature and concentration oscillations were observed for the highest frequency studies (100 Hz.). The amplitude of the CO_2 oscillation was approximately 3 to 4 times greater than the constant-pressure value, and the amplitude of the H_2O oscillation was approximately 5 to 6 times greater than the constant-pressure value. The CO amplitude was 8 to 10 times greater than the constant-pressure value.

Summary of the Single-Pressure-Pulse Data

To further clarify the pressure effect on the specific vaporization rates of the two propellant components, single-pressure-pulse tests were conducted. Both pressure increases and decreases were studied.

A single pressure-increase pulse caused an initial increase in the CO_2 concentration and a decrease in the CO concentration. This was followed by an oscillation in the concentration profiles. The magnitude and frequency of these concentration oscillations varied from run to run and within individual runs. Also, there appeared to be no clear correlation between the amplitude of the concentration oscillation and the rate of pressure change, over the range of 25 to 275 psi per second. The H_2O concentration oscillations during these tests at times were in phase with the CO oscillations, but this again was not a general observation. Even though the rates of pressure change for these tests were comparable to those of the oscillatory pressure tests, the amplitudes of the concentration fluctuations were much less than those observed in

the oscillatory pressure tests. The flame temperatures for these tests fluctuated in a random manner very similar to those of the constant pressure tests, and the amplitude of these oscillations was approximately equal to those observed for the constant pressure tests.

The data from the single-pressure-decrease pulse tests were unlike those of the single-pressure-increase pulse tests, in that they were very regular and very reproducible. The pressure decrease caused an initial CO_2 concentration decrease and a CO concentration increase for the first 15 to 20 msec. Then both species concentrations reversed direction and the CO_2 concentration increased and the CO concentration decreased for approximately the next 25 to 30 msec. This initial alternating composition condition was continuously repeated during the pressure decay. Although the temperature oscillated during these tests, its magnitude (25-75°K) was approximately equal to the random temperature oscillations observed for the constant-pressure tests.

The magnitude of this characteristic time (15-20 msec.) associated with the initial pressure decay was independent of the rate of pressure decay over the range of 300 to 700 psi per second. However, the magnitude of this initial concentration fluctuation increased as the rate of pressure change increased. Also, although these rates of pressure change were comparable to those of the oscillatory pressure tests, the composition changes during these pressure decay tests were much smaller than those of the oscillatory-pressure tests.

These present pressure decay data can be compared to the emission data from other depressurization tests reported by Schulz [7]. Schulz, using flame emission intensity ratios, observed the same general

phenomena during depressurization and oscillatory pressure tests as those reported here. However, the interpretation of these emission data lead to the postulate that the specific gasification rate of the AP increased relative to that of the fuel during periods of decreasing pressure, which is in conflict with the conclusions of this study. The reason for this discrepancy will be discussed later; for the moment, only the general features observed by Schulz are of interest. Although Schulz's depressurizations (using rarefaction waves) were considerably different than those investigated in this present study, the same initial composition fluctuation and the subsequent recovery were observed, along with repetition of this alternating concentration condition during the pressure decay. For depressurization rates in excess of 3000 psi per second, Schulz observed initial characteristic times of response of 6-15 msec. Schulz used bimodal propellants with essentially the same AP particle size (15 μm and 200 μm); however, he used different fuel-binders, namely polybutadiene-acrylic-acid (PBAA) and polyurethane (Estane). Although the scale of inhomogeneities should be approximately the same for the propellants used in both studies, it is uncertain how large of an effect the different fuel-binders would have on the characteristic times. For the data reported by Schulz, it appears that the PBAA propellants have the shorter characteristic times (6-10 msec.) and the Estane propellants have longer characteristic times (10-15 msec.). Also, tests made by Schulz with propellants made of AP and carbon black pressed into pellets showed characteristic times in this same region (6-15 msec.). It is interesting to note that for "similar" propellants, changing the depressurization rate by over an order of magnitude apparently results in a relatively small change in the characteristic time. This characteristic

time, τ, has a corresponding characteristic frequency, ω, of 25-33 Hz. This characteristic frequency is consistent with the observation that the nature of the concentration oscillations changed considerably for pressure oscillations below approximately 20 Hz. At the lowest frequency studied (7-10 Hz.), the concentration profiles appeared to oscillate at a frequency which was slightly different than that of the pressure oscillation.

Conclusions

1) The H_2O, CO_2, and CO concentration profiles measured in this study indicate that a non-equilibrium condition exists in composite propellant flames close to the burning surface. Over the pressure range studied (25-100 psia) this non-equilibrium condition was observed to extend out to at least 15 mm from the surface of a stably burning propellant.

2) The flame temperature and composition of stable burning composite propellants are not constant, but rather fluctuate in a random manner and apparently at no preferred frequency. The gasification rate of either the oxidizer or fuel can be expressed as vA, where v is the vaporization rate per exposed area of the respective component, and A is the exposed area of the respective component per total propellant surface area. For steady burning, the average values of these quantities must be such that

$$\frac{\bar{v}_{ox}\,\bar{A}_{ox}}{\bar{v}_{fuel}\,\bar{A}_{fuel}} = \text{constant},$$

where the bar denotes the time-average values. During constant-pressure burning, the respective specific gasification rates, v_{ox} and v_{fuel},

should be constant, therefore changes in the ratio (A_{ox}/A_{fuel}) are believed to cause these observed random fluctuations in the gas phase composition. The random variation in (A_{ox}/A_{fuel}) results from a non-uniform distribution of the crystalline AP in the fuel-binder matrix, and (or) from processes which take place on the surface during the combustion process.

3) A pressure transient will cause a change in the gas phase composition of the composite propellant flames. The CO_2-CO data indicate that the flames become AP-rich during periods of increasing pressure and vice versa. These composition variations are much larger than those observed for the constant pressure burning. The different pressure dependencies of the specific vaporization rates of the oxidizer and fuel result in a change in the (v_{ox}/v_{fuel}) ratio. Until (A_{ox}/A_{fuel}) is sufficiently altered, the change in the (v_{ox}/v_{fuel}) ratio is responsible for the composition changes of the pyrolysis gases leaving the propellant surface. Later, after (A_{ox}/A_{fuel}) has been sufficiently altered, this too can be responsible for gas-phase composition changes.

4) The specific vaporization rates are not only dependent on the instantaneous pressure, but also in some degree on the rate of pressure change. An increase in the rate of pressure change results in an increase in the amplitude of the composition oscillations.

5) For equal rates of pressure change, pressure oscillations produce much larger composition variations than a single-pressure pulse.

6) The characteristic time, τ, associated with the initial fuel-rich period during a pressure decrease test can be represented as L/r, where L is a characteristic length associated with depleting the surface of one ingredient, and r is a characteristic mean regression rate of the

mixture. The initial fuel-rich period is, it is postulated, associated with a change in (v_{ox}/v_{fuel}) whereas the subsequent AP-rich period is associated with a change in (A_{ox}/A_{fuel}).

7) The characteristic time, τ, for the propellants studied, has a corresponding characteristic frequency, ω, of approximately 25 Hz. Above 25 Hz. the changes in the gas phase composition are associated with changes in (v_{ox}/v_{fuel}) whereas below approximately 25 Hz. composition changes can be associated with changes in both (v_{ox}/v_{fuel}) and (A_{ox}/A_{fuel}).

8) Small pressure oscillations can produce large temperature oscillations (200°K), as well as the large gas phase composition oscillations. The temperature oscillates in phase with the pressure, and thus in phase with the composition oscillations. For the small pressure amplitudes studied, the propellant burning rate should not change significantly. Thus, the change in the thermal energy accumulation in the solid phase should also be relatively small. Therefore, the observed temperature oscillations are believed to be primarily associated with flame composition changes and not with changes in the thermal energy accumulation in the solid phase.

9) The H_2O concentration oscillations during transient pressure tests appear to be in phase with the CO concentration oscillations, and thus 180° out of phase with the CO_2 concentration oscillations. This is directly opposite of the equilibrium concentration changes for flames with changing oxidizer-to-fuel ratios. This observed condition could result if the principle reaction were

$$H_2O + CO \longrightarrow CO_2 + H_2 \quad .$$

Also, if there were a large excess (relative to equilibrium) concentration of OH radicals, then the H_2O concentration might increase during fuel-rich periods instead of oxidizer-rich periods.

10) This study strongly suggests that the use of equilibrium data to interprete H_2O-emission-to-CO_2-emission intensity ratios during transient pressure tests leads to invalid conclusions. It is also not clear if this interpretation is solely attributable to a non-equilibrium effect, of if faulty interpretation of emission intensity data must also be considered.

11) The use of infrared absorption spectroscopy as an in-situ method of analyzing transient phenomena in flames should prove most valuable in the future, now that a good high temperature infrared source has been developed.

APPENDIX A

SPECTROSCOPIC EQUIPMENT AND TECHNIQUES

Spectrometer

The Warner and Swasey (Controlled Inst. Oiv.) Model 501 Rapid-Scanning Spectrometer used in this study is a single-beam instrument, designed for studying transient spectroscopic phenomena. The spectrometer can be set up to scan various selected spectral regions, of approximately λ to 3λ in length, from 0.30 μm to 14.0 μm. The spectral region scanned is determined by the grating, filters and detectors used. The spectrometer has seven scan rates ranging from 1.0 msec. to 100 msec., with a corresponding repetition rate range of 8 to 800 scans per second.

The radiant energy of interest is collected by a Cassegrainian optical system, which can be focused on any source 28 cm or more from the spectrometer, and imaged on the entrance slit of a Czerny-Turner monochromator. The wavelength scanning is accomplished by sweeping a sequence of corner mirrors through an intermediate focal plane of the double-pass Czerny-Turner monochromator. As each set of corner mirrors traverses across the dispersed spectrum in the intermediate focal plane, the rays intercepted are laterally displaced and directed back through the monochromator. The symmetry of the corner mirrors produces a simultaneous scanning of a short and a long wavelength region across the separate exit slits associated with the short and long wavelength

detectors. Twenty-four sets of corner mirrors are mounted on the periphery of the dynamically balanced scan wheel which is driven at a constant rate of speed by a hysteresis-synchronous motor. A schematic of the spectrometer is shown in Figure A-1.

Since the moving element is not part of the dispersing train, the optical quality of the spectrometer is not affected by the rapid scanning but is limited by the signal-to-noise ratio of the detector. The spectrometer output is a time-varying voltage, which is preamplified in the spectrometer before going to the spectrometer's control console. The control console has separate gain and filtering controls for the two detector signals. The maximum gain setting and the minimum filtering setting corresponding to no filtering, were used throughout this entire study. The spectrometer output is linear in time and wavelength. Therefore, wavelength instead of wave-number is used in reporting the data.

The nature of the phenomena investigated in this study dictated that the spectrometer be operated at its fastest scan rate of one millisecond. The previous work of Schulz [7] and Eisel [22] indicated that the most useful spectral information for composite propellant flames is in the 2.5 to 5.5-μm region. Thus, the spectrometer was set up to scan the 2.5 to 5.5-μm region using the components listed in Table A-1. Since only one indium antinomide (InSb) detector was needed to scan this region, the scan time was only 0.50 msec. The spectral resolution of the spectrometer is determined by the grating and the entrance and exit slit widths. The seven slit widths available on the spectrometer are 0.025-mm, 0.05-mm, 0.10-mm, 0.20-mm, 0.50-mm, 1.0-mm, and 2.0-mm. Decreasing the slit width increases the spectral resolution, while at the same time it decreases the signal-to-noise ratio. The new

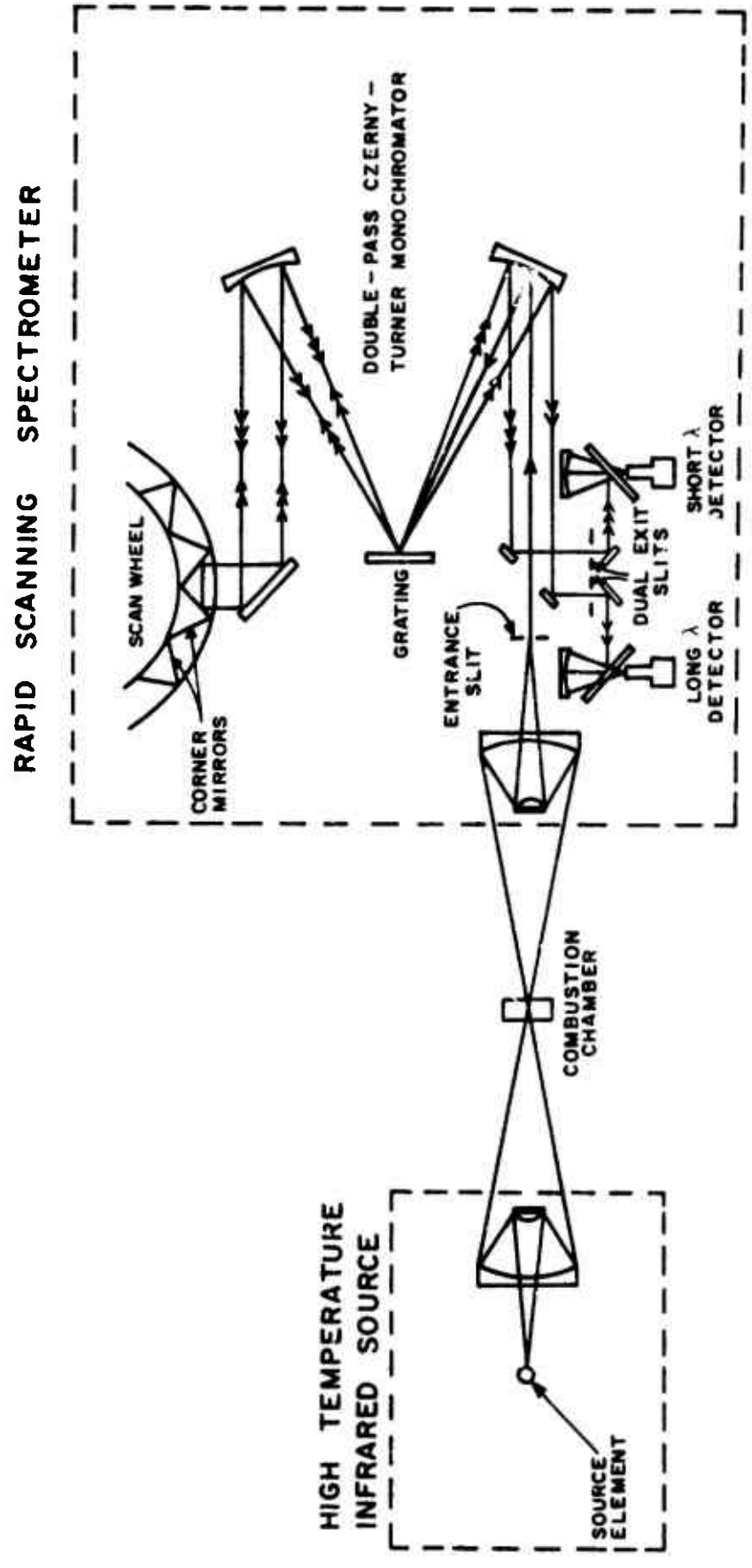

FIGURE A-1. A SCHEMATIC DRAWING OF THE SPECTROMETER.

TABLE A-1

SPECTROMETER COMPONENTS USED TO SCAN

THE 2.5 TO 5.5-μm SPECTRAL REGION

Component	Description	Comments
Detector	InSb-liq N_2 cooled	Barnes Eng. #0101
Diffraction grating	11.58 grooves/mm	Blaze angle: 4.0 μm
Pre-amplifier	PCI-D	
Entrance and exit slits	0.20 mm	Vertical baffles: 9.0 mm
Cut-on filter	2.50 μm	#200176-10

high-temperature radiation source used in this study permitted the use of the 0.20-mm slits, which gave good spectral resolution and an excellent signal-to-noise ratio. The 0.20-mm slits and the 12.5-lines/mm grating gave excellent resolution of the 4.26-mm CO_2 doublet at the 10 and 100 msec scan times. However, the 4.26 CO_2 doublet was not resolved at the 1.0 msec. scan time. The problem appeared to be the relatively large time constant of the new InSb detector (Barnes Eng. #101). Otherwise, the spectral resolution at the 1.0 msec scan time was good. The 9-mm entrance and exit slit baffles were used instead of the normal 12-mm baffles, so that the projected image of the entrance slit was completely inside the central core of the propellant flames.

The combustion chamber was located at the common focal plane of the spectrometer and the radiation source. At this distance, approximately 78 cm, the projected image of the entrance slit was approximately 11.0 mm x 0.25 mm. The relatively long optical path had to be purged with CO_2-H_2O free gas in order to eliminate atmospheric CO_2 and H_2O absorption. Both the radiation source and the spectrometer have tunnels which extend from these units and seal to the combustion chamber. The spectrometer was purged with CO_2-H_2O free air which was dried in a refrigeration air drier (Puregas Model 750) and then passed through cannisters of molecular sieves (13x) to remove CO_2 and remaining traces of water.

Infrared Radiation Source

The high temperature infrared radiation source used for this study was a modified version of a Warner and Swasey Model 20 Synchronized Radiation Source. The infrared source supplied with the Model 20 was a

fused silicon carbide Globar. The radiation from the Globar was focused on the exit slit of the source by means of a spherical and planar mirror. The energy from this exit slit was collected by a Cassagrainian optical system, identical to the one in the spectrometer, and imaged on the common focal plane of the spectrometer and source.

The maximum operating temperature of the Globar is approximately 1500°K, which is not high enough to permit absorption measurements in high temperature propellant flames (2400-2700°K). Fortunately, Robert J. Law [28], while working with this same instrument, developed a new high-temperature infrared radiation source which operates at 2700-2800°K. The Glo-Rod elements were made from vitreous carbon rods, 3.18 mm in diameter and 5.1 cm long. The vitreous carbon was supplied by the Beckwith Carbon Corp. of Van Nuys, Calif. Vitreous carbon properties are intermediate between glass and carbons in respect to thermal and electrical conductivity. Therefore, it is described as a conductive ceramic. The source element was electrically heated to the operating temperature by passing a current of approximately 140 amperes at 10 VAC, supplied by a large step-down transformer. The current to the source elements, and thus its temperature, was set by means of a large autotransformer on the primary winding side of this large step-down transformer. An optical pyrometer (Leeds and Northrup Model 8732-C) was used to measure the element temperature through a window in the outer source housing. The optical pyrometer was calibrated just prior to this study, and this calibration is traceable to an NBS standard lamp. The temperature of the source element was not controlled with a controller circuit. However, in the range 2700-2800°K, the source temperature rarely fluctuated more than

± 20°K. At these high temperatures the source element had to be operated in an argon atmosphere, to keep element degradation to a minimum. The original design used a pool of mercury as the bottom source-element terminal, thus eliminating any potential problems caused by thermal expansion of the vitreous carbon rod. The entire source element mounting assembly was water-cooled. A complete description of this new source is given by Law [28].

The Glo-Rod source used by Law was modified in two ways for use in this study. First, the pool of mercury was eliminated. It was discovered that both ends of the rod could be rigidly mounted, without any deleterious effects due to thermal expansion. However, a stiff leaf spring was added to the top mounting head, which allowed it to move the necessary fraction of a millimeter. Also, since the chopper wheel of the Model 20 Synchronized Radiation source was not going to be used in this study, the exit slit and mirrors of the Model 20 were removed. The Glo-Rod element was located at the old slit location; thus any energy losses associated with the mirrors and exit slit were eliminated. The source element was operated at a brightness temperature of 2725°K during this study, and each element lasted approximately two hours at this temperature. Although each test lasted only a matter of seconds, it was necessary to have the Glo-Rod on an average of five minutes per test; resulting in approximately twenty-five tests per source element.

Spectroscopic Techniques

Quantitative analysis by means of infrared absorption spectroscopy is based on the use of the Beer-Lambert Law,

$$\ell n \frac{P_\lambda^o}{P_\lambda} = K_\lambda \, c\ell \quad , \qquad (1)$$

where P_λ^o is the incident radiant power, P_λ is the transmitted radiant power, c is the the concentration of the absorbing component, λ is the wavelength of the absorption band associated with the absorbing component, ℓ is the optical path length in the absorbing gas, and K_λ is the spectral absorption coefficient. The ratio $\frac{P_\lambda^o}{P_\lambda}$ is called the absorptance and the term $\ell n \frac{P_\lambda^o}{P_\lambda}$ is called the absorbance. This section describes the techniques used to measure P_λ^o, account for flame emission, and quantitatively calibrate the system for the components studied.

Single Beam Spectrometer Data

The Warner and Swasey Rapid-Scanning Spectrometer (Model 501) is a single beam instrument, and thus a technique of measuring the incident radiation, P_λ^o , has to be established. Many of the popular methods described in the literature [35] were not applicable, and they are described only briefly. The empty-cell method could be used by recording radiation spectra before and after each run, and then calculating an average value for P_λ^o. However, the twenty-four sets of rotating corner mirrors do not all have the same reflectivity [28]. This variation is slight, ± 2%, for all but one set of corner mirrors, which is off by 10%. Obviously, this condition has to be considered if the empty-cell method is used. Although this method accounts for the reflection and absorption losses of the two sapphire windows, it does not account for any aspectral attenuation of the source radiation due to reflection and scattering associated with the flame. Also, since the high-temperature infrared source used for this study does not have a temperature controller, there

is the possibility of the source radiation slowly changing with time. The empty-cell method cannot account for this possible variation in the radiance of the source.

The above considerations dictate that the various P^o_λ values should be measured within each scan. The very popular tangent base-line method could be used to measure the CO_2 $P^o_{4.26}$, by drawing a tangent to the window areas on either side of this absorption band. The distance between the spectrometer baseline and the tangent, measured 4.26 μm is $P^o_{4.26}$. This technique would make the data reading process very time consuming, and considering the large quantity of spectra required to be read, it is not a realistic alternative. Also, due to the characteristic spectral shape of the 2.5-μm to 5.5-μm region, and the very broad HCl absorption band (3.3-3.7 μm) adjacent to the 3.17-μm H_2O absorption band, this tangent method would be most difficult to apply successfully to the 3.17-μm H_2O and the 4.6-μm CO absorption bands. A typical absorption spectrum is shown in Figure A-2, with the various bands marked.

Fortunately, the very discernible inflection point at 3.85 μm to 3.95 μm, which is characteristic of the spectrometer, is in a non-absorbing band or "window" area. It is possible to relate the various P^o_λ values to the $P^o_{3.9}$ value by

$$P^o_\lambda = m_\lambda \, P^o_{3.9}, \qquad (2)$$

where the coefficients m_λ are calculated from empty-cell data. Except for the flame attenuation, which will be discussed later, these coefficients are a function only of the spectral characteristics of the spectrometer, the spectral characteristics of the sapphire windows, and the source temperature. The spectral characteristics of the spectrometer

FIGURE A-2a. THE 2.5 TO 5.5-μm SPECTRUM OF THE HIGH-TEMPERATURE INFRARED RADIATION SOURCE. Some atmospheric CO_2 is present.

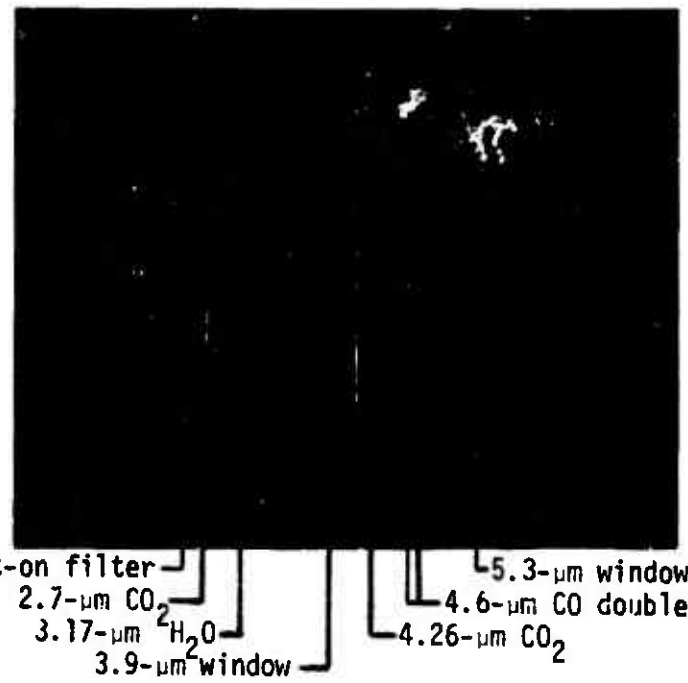

FIGURE A-2b. THE 2.5 TO 5.5-μm SPECTRUM SHOWING THE VARIOUS ABSORPTION BANDS. This was obtained with a gas cell, and the absorption strengths are not representative of the tests. The CO_2 concentration was so great that the 4.26-μm band is almost black and the weak 2.7-μm band is noticeable.

and sapphire windows are fixed and, of course, did not change during this study. The coefficients, ratios of the source's spectral radiance at various wavelengths, are a function of the source temperature in a manner described by the Planck radiation law. As would be expected, the observed source temperature fluctuations of ± 20°K when operating at 2725°K did not produce any measurable changes in these coefficients. Therefore, the coefficients calculated from empty-cell data are constants. The usefulness of these coefficients to calculate the various P^o_λ values from the $P^o_{3.9}$ value measured on absorption spectra depends on the validity of one assumption. That is, the non-absorbing attenuation, reflection and scattering, of the source radiation due to the flame is aspectral in nature.

Because the flame attenuation of the source radiation at 3.9 μm is non-absorbing in nature, this transmitted radiation will be represented by the $P^o_{3.9}$ nomenclature and not $P_{3.9}$. The coefficients relating the transmitted radiation at other "window" areas in the 2.5 μm to 5.5 μm region to $P^o_{3.9}$ were measured for both the empty-cell and the flame absorption conditions. These preliminary tests indicated that the non-absorbing flame attenuation of the source radiation was indeed aspectral. The use of these coefficients in conjunction with the $P^o_{3.9}$ value measured for each scan, provided a convenient and quite accurate method of determining the various P^o_λ values needed for absorption calculations within each scan.

Absorption Measurements in Flames

Flame emission is a major concern. Ideally, the experimenter seeks to distinguish the transmitted source radiation from the flame

radiation. Usually the source radiation is prechopped mechanically [17, 35] thus producing a high frequency AC detector signal associated with the source radiation, while the flame radiation produces a DC signal. The data can be reduced directly, or with the aid of electronic filters the DC signal can be eliminated, leaving only the absorption information. This technique works especially well for monochromatic operation, and can be applied to slow scan operation. However, for the scan time (0.50 msec.) used in this study, this technique is physically impossible.

Separate emission and emission-absorption measurements can be made, and the emission data used to correct the emission-absorption data to absorption only data. The Warner and Swasey Rapid-Scanning Spectrometer is equipped with a Model 20 synchronized radiation source. A chopper wheel in the source unit can be synchronized with the scan wheel in the spectrometer, sc as to block the source radiation on alternate scans. This produces flame emission and emission-absorption spectra on alternate scans of the spectrometer. Although the synchronized source provides continuous, alternating emission and emission-absorption measurements during a run, it also reduces the time resolution of the spectrometer by a factor of two. The phenomena studied required the full time resolution provided by the spectrometer's fastest scan rate, 800 spectra per second. Therefore, the synchronized radiation source was not used.

An alternative method would consist of using average emission values for a given test condition to correct the emission-absorption data. The emission data could be obtained from a separate emission-only run at the same test conditions, or by using a shutter in the source unit, during a segment of the emission-absorption run. In an effort to

see if this method could be successfully applied, the nature of the flame radiation from several different propellants was studied for both steady-state and oscillatory pressure tests. The results of several emission-only tests, which are representative of the more than twenty-five tests made, are shown in Figures A-3 through A-6. The quantities measured on emission-absorption spectra are $(P^o_{3.9} + p_{3.9})$ and $(P_\lambda + p_\lambda)$. $P^o_{3.9}$ is the transmitted source radiation at the 3.9-μm "window" area, and $p_{3.9}$ is the flame emission at this wavelength. P_λ is the transmitted source radiation at the absorption band wavelength, λ, and p_λ is the flame emission at this wavelength. The flame radiation values, p_λ, are fairly constant during constant pressure tests, with the values fluctuating about a mean value. During oscillatory pressure tests the flame emission values oscillated in phase with the pressure. However, even for large pressure oscillations (10-20% change in the mean pressure), the fluctuations in the flame radiation values were usually smaller than those during a constant pressure test.

The p_λ values can be represented as the sum of a mean value, $\bar{p}_\lambda$, and a fluctuating component, p'_λ, where the value of p'_λ can be either positive or negative. Thus, the average value method results in the following absorbance term

$$\ell n \left\{ \frac{m_\lambda \left[(P^o_{3.9} + p_{3.9}) - \bar{p}_{3.9} \right]}{(P_\lambda + p_\lambda) - \bar{p}_\lambda} \right\} = \ell n \left\{ \frac{m_\lambda (P^o_{3.9} + p'_{3.9})}{P_\lambda + p'_\lambda} \right\}. \qquad (3)$$

Equation (2) can be used to simplify the right hand side of equation (3) or

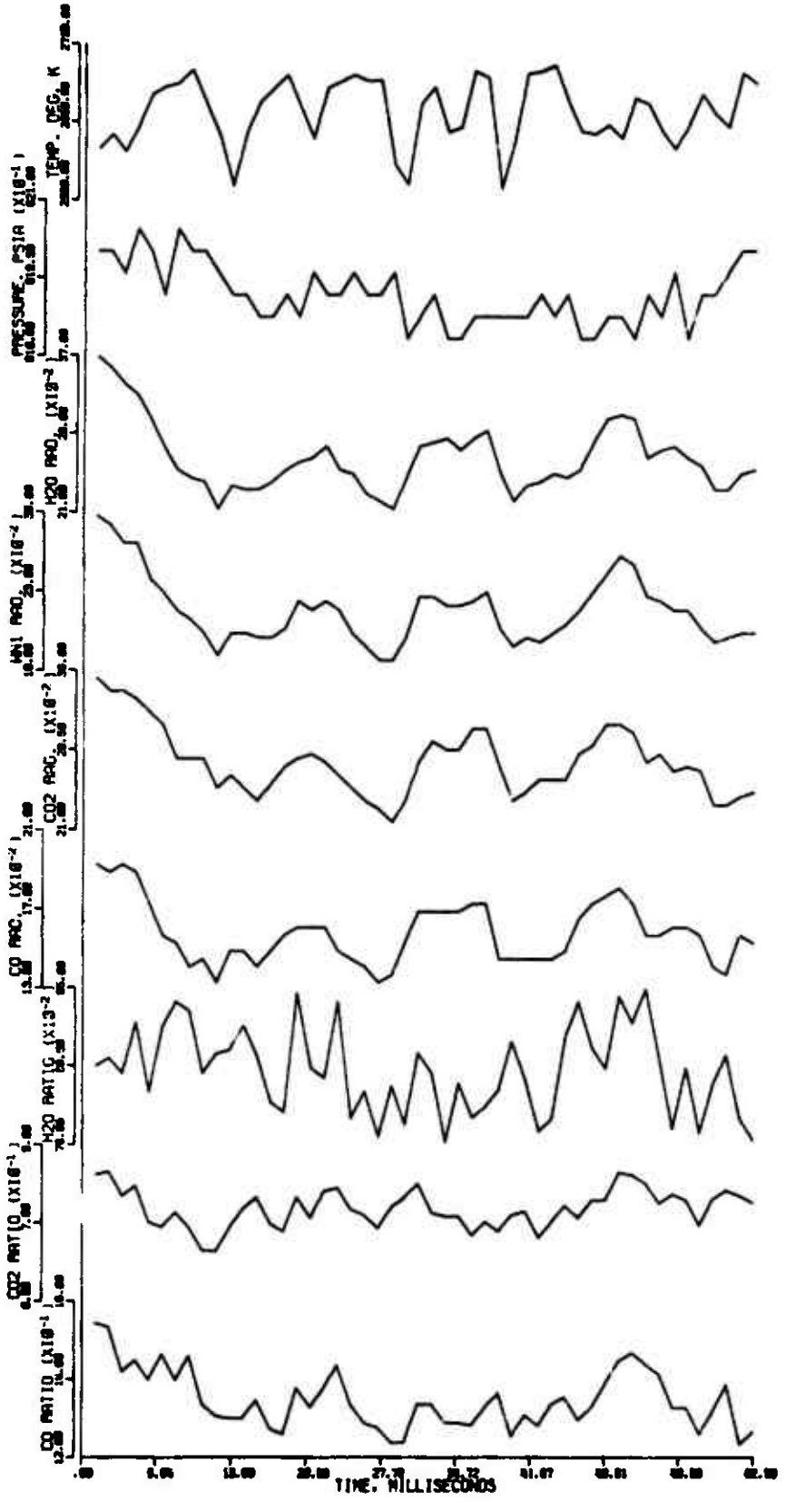

FIGURE A-3. TEMPERATURE AND FLAME RADIATION DATA FOR A CONSTANT-PRESSURE TEST. The ($P_{3,g}/P_{\lambda}$) ratios are also plotted. (82 wt. % AP propellant [UFP], 3-5 mm, Run No. 1-4474, film-reader units plotted)

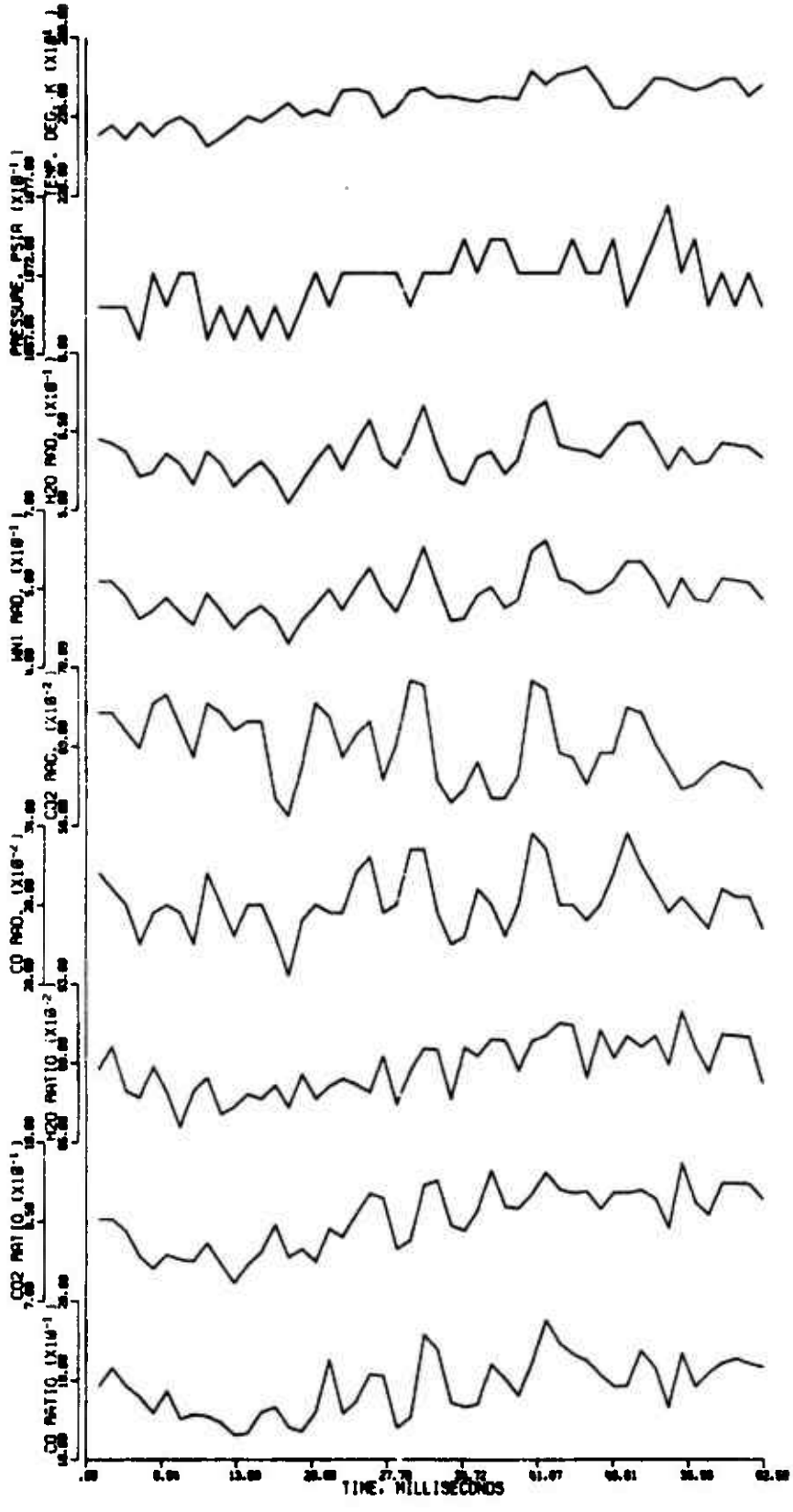

FIGURE A-4. TEMPERATURE AND FLAME RADIATION DATA FOR A CONSTANT-PRESSURE TEST. The ($P_{3.9}/P_{\lambda}$) ratios are also plotted. (82 wt. % AP propellant [UFP], 3-5 mm, Run No. 3-31574, film-reader units plotted)

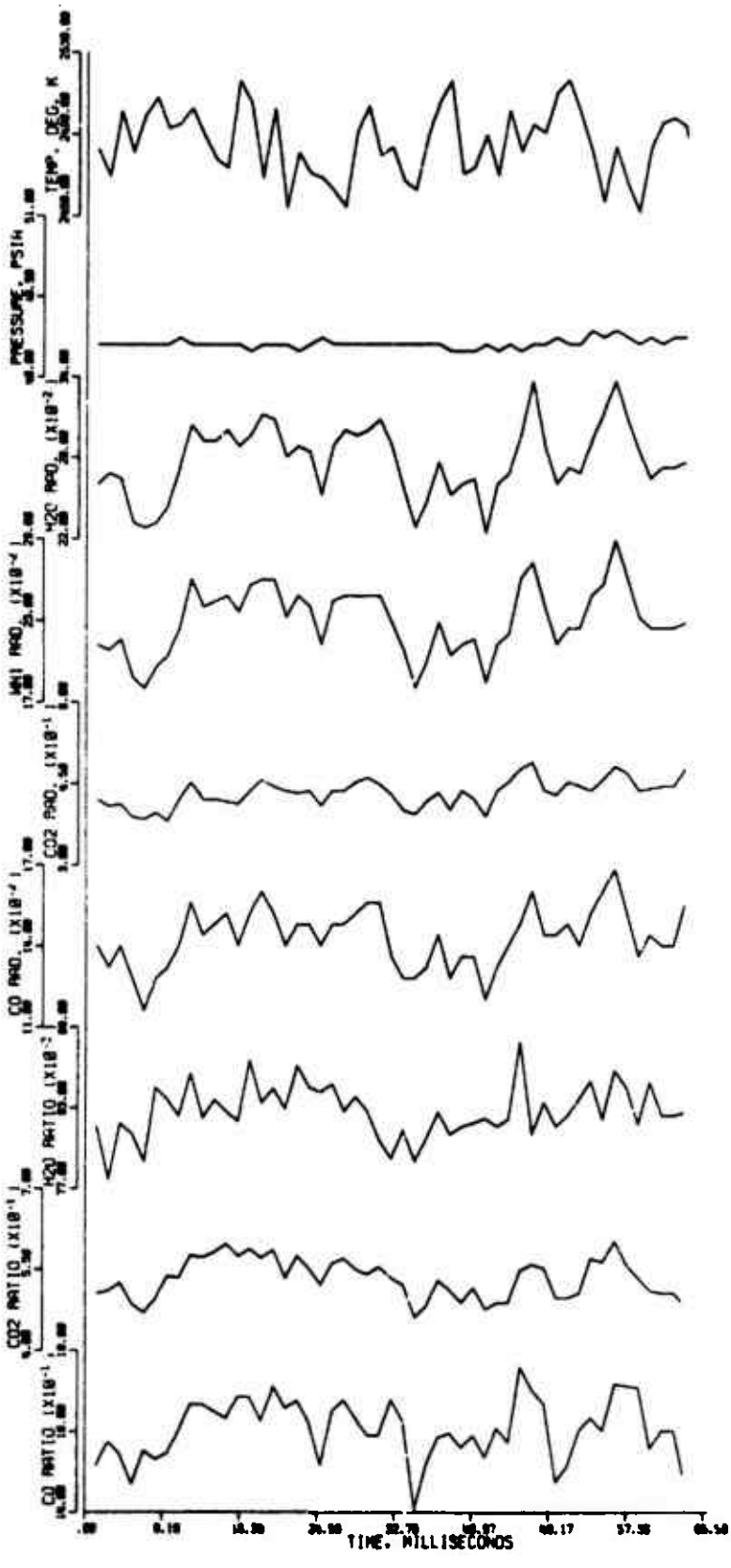

FIGURE A-5. TEMPERATURE AND FLAME RADIATION DATA FOR A CONSTANT-PRESSURE TEST. The ($P_{3.9}/P_{\lambda}$) ratios are also plotted. (82 wt. % AP propellant [UFP], 3-5 mm, Run No. 3-31574, film-reader units plotted)

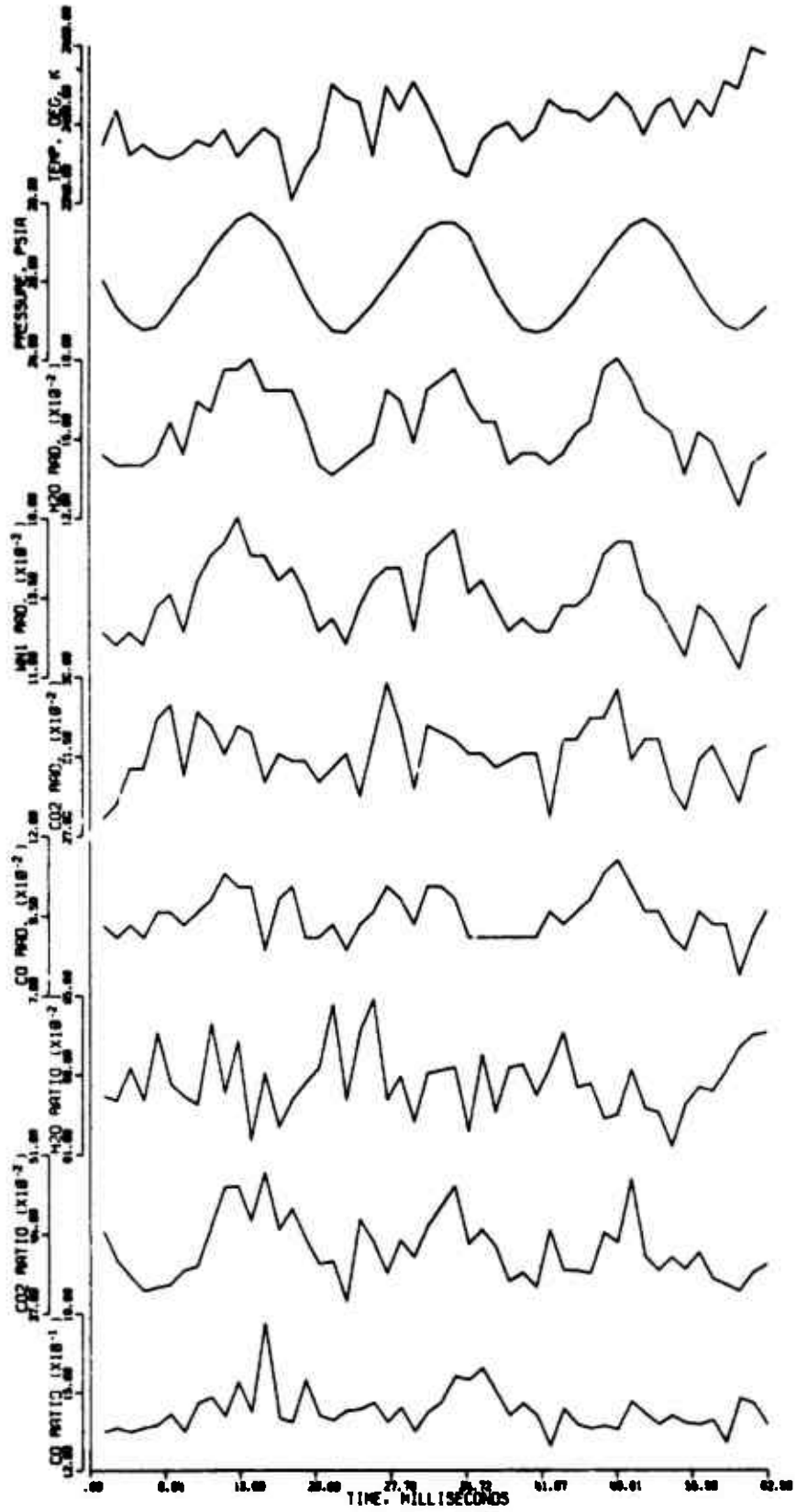

FIGURE A-6. TEMPERATURE AND FLAME RADIATION DATA FOR A 54 Hz. OSCILLATORY-PRESSURE TEST. The ($P_{3.9}/P_{\lambda}$) ratios are also plotted. (82 wt. % AP propellant [UFP], 3-5 mm, Run No. 2-4374, film-reader units plotted)

$$\ell n \left\{ \frac{m_\lambda (P^o_{3.9} + p'_{3.9})}{P_\lambda + p'_\lambda} \right\} = \ell n \left\{ \frac{P^o_\lambda + m_\lambda p'_{3.9}}{P_\lambda + p'_\lambda} \right\} \quad . \qquad (4)$$

Since the fluctuating components, $p'_{3.g}$ and p'_λ, are small compared to P^o_λ and P_λ ,

$$\ell n \left(\frac{P^o_\lambda + m_\lambda p'_{3.9}}{P_\lambda + p'_\lambda} \right) \simeq \ell n \left(\frac{P^o_\lambda}{P_\lambda} \right) \quad , \qquad (5)$$

which is the absorbance term defined by the Beer-Lambert law.

Preliminary calibration work to exploit this method revealed a serious disadvantage. The subtraction operation in the denominator can result in a relatively small number compared to that obtained in the numerator. Thus, the subsequent division yields a number which is large compared to the denominator. While the relative error introduced in the data reading process remains constant, the above operations magnify the absolute error greatly. Fortunately, the emission-only tests revealed several other characteristics of the flame radiation which lead to a different method of interpreting the emission-absorption data. As was discussed earlier, the p_λ values are fairly constant during both steady-state and oscillatory pressure tests, even though the p_λ values do oscillate in phase with the pressure during the oscillatory pressure tests. In a like manner, the p_λ values for constant pressure tests also vary with the total pressure, but not in a way which is easily discernible. Refer to Table A-2. Some of the data indicate that the p_λ values increase directly with the pressure, as might be expected. However, the important point is that the absolute value of these variations is comparatively small with respect to the p_λ values. Also, even though the p_λ values fluctuate during a test, the ratios $\frac{p_{3.g}}{p_\lambda}$ remain constant, indicating

TABLE A-2

AVERAGE FLAME EMISSION INTENSITIES FOR STEADY-STATE PRESSURE TESTS

These data show the effect of total pressure on the various flame emission intensities for a 82 wt.% AP propellant.

Run	Pressure (psia)	Flame Emission Values (film-reader units)					Emission Intensity Ratios			
		H_2O	WN1	CO_2	CO	WN_2	$\frac{WN1}{H_2O}$	$\frac{WN1}{CO_2}$	$\frac{WN1}{CO}$	$\frac{H_2O}{CO_2}$
3-31574	47.0	0.22	0.22	0.42	0.14	0.07	0.83	0.55	1.60	0.64
7-122873	66.0	0.25	0.21	0.39	0.13	0.07	0.86	0.55	1.57	0.64
1-4474	82.0	0.26	0.20	0.34	0.15	0.06	0.80	0.59	1.34	0.76
5-122873	87.5	0.21	0.17	0.38	0.14	0.05	0.80	0.43	1.35	0.55
3-122873	97.5	0.25	0.21	0.35	0.15	0.07	0.85	0.63	1.37	0.71
3-31574	107.0	0.61	0.55	0.61	0.30	0.15	0.90	0.90	1.82	1.00

that the fluctuations are aspectral in nature. Moreover, the value of these ratios are nearly constant from run to run, regardless of the change in the $p_{3.9}$ and p_λ values. The value of these ratios typically vary only 5-10% from run to run, with the maximum variation observed being approximately 20%. The fluctuations in the ratios plotted in Figures A-3 through A-6, almost without exception, fall within the precision of the data reading process. The two most likely causes of these aspectral emission fluctuations are aspectral attenuation caused by particulate scattering in the flame and fluctuations in the optical density of the flame. The non-catalyzed, non-metallized high-AP-content propellants used should be fairly clean and free of large amounts of particulate matter. High speed motion pictures (1000-1500 pictures per second) of these flames showed a flickering on the edges of the flame, which could account for changes in the optical density of the flame. The flame flickering visually appeared to increase in both frequency and amplitude with increasing distance from the propellant surface, however, this was not noticed in the flame emission fluctuations. Although the reason for this discrepancy is unknown, this flickering is believed to be the main cause of the flame emission intensity fluctuations.

Since $p_{3.9} = n_\lambda p_\lambda$,

$$\ell n\left[\frac{m_\lambda(P_{3.9} + p_{3.9})}{P_\lambda + p_\lambda}\right] = \ell n\left[\frac{m_\lambda(P_{3.9} + n_\lambda p_\lambda)}{P_\lambda + p_\lambda}\right] = \ell n\left[\frac{P_\lambda^o + m_\lambda n_\lambda p_\lambda}{P_\lambda + p_\lambda}\right] \quad . \quad (6)$$

For the normal non-radiating spectroscopic sample, $p_\lambda \cong 0$, the above term is just the absorbance, $\ell n\left[\frac{P_\lambda^o}{P_\lambda}\right]$. Therefore, if the $m_\lambda n_\lambda p_\lambda$ and p_λ terms are comparatively small, the above uncorrected emission-

absorption data is approximately equal to the absorbance. In this work, the $m_\lambda n_\lambda p_\lambda$ values are all only 10-15% of their respective P^o_λ values, and the H_2O $p_{3.17}$ is only 15% of the H_2O $P_{3.17}$ values. However, the CO_2 $p_{4.26}$ and $CO_p p_{4.6}$ values are typically 25% and 50% of the CO_2 $P_{4.26}$ and CO $P_{4.6}$ respectively.

For the special case where the p_λ values are constant for all conditions,

$$\ell n \left[\frac{P^o_\lambda + m_\lambda n_\lambda p_\lambda}{P_\lambda + p_\lambda} \right] = \ell n \left[\frac{P^o_\lambda + A_\lambda}{P_\lambda + B_\lambda} \right] \quad , \tag{7}$$

where A_λ and B_λ are constants. Therefore, the above modified absorbance term must also be related to the concentration of the absorbing component by the Beer-Lambert law. This special case was closely approximated over the pressure range covered in the work, 25 psia to 100 psia, suggesting that this uncorrected modified absorbance term could be calibrated and used in the same way as the standard absorbance term. Also, since p_λ appears in both the numerator and denominator, small fluctuations in p_λ result in very small changes in the value of the modified absorbance term.

Qualitative Calibration

Since the early work of Angstrom [36] in 1890, it has been known that the absorption of radiation by gases at room temperature deviates from the Beer-Lambert law. However, recent experimental work by Tourin [37, 38, 39], with two of the gases of interest in this study, H_2O and CO_2, indicates that the Beer-Lambert law is applicable to the spectral absorption of hot gases. Therefore, calibration tests were made to see if the above modified absorbance term also obeyed the Beer-Lambert law.

It is well known that the absorption coefficient, K_λ, depends on temperature. Thus, the calibration work had to be done at the flame temperatures of the propellants studied. Originally, this calibration work was going to be done with hydrocarbon-oxygen gas flames, using equilibrium gas compositions calculated from thermochemical data. A special sintered-stainless steel frit gas burner was made from a spare propellant holder. But it was decided that many potential problems could be eliminated if the propellant flames to be studied were also used for the calibration work. The major problem eliminated was the inherent uncertainty of how much difference there was in the optical path length in the two types of flames. Since the slope of the Beer-Lambert plots is $k_\lambda \ell$, going from one system to the other would require adjustment of the slopes of the calibration curves. High-speed motion pictures indicated that measuring the path length, ℓ, would be difficult at best. By using the propellants for everything, the optical path length, ℓ, was a constant and did not explicitly enter into the calculations.

The calculated adiabatic flame temperature and species concentrations for a B2 wt.% AP propellant are plotted as a function of the combustion chamber pressure in Figure E-3. Since both the flame temperature and the species mole fractions of a given propellent are essentially independent of pressure over the pressure range of interest, a constant temperature calibration can be made by making several tests at different total pressures. Recent studies [40, 41] have shown that calibrations of this type, where the ratio of the absorbing component partial pressure to the total pressure are kept constant, produce a family of linear Beer-Lambert curves. All the curves

go through the origin, but the slopes are a function of the pressure ratio. If this same calibration is done at constant total pressure, instead of constant pressure ratio, a family of curved Beer-Lambert type curves is produced just by changing the total pressure. Effects of this type have been observed at low pressures, atmospheric and below, and can be explained in terms of pressure broadening of the unresolved spectral lines encompassed within the spectral slit width of the spectrometer. Tourin, et al., [42, 43] has shown that this pressure effect is important only at low pressure, atmospheric and below, and that the spectral lines are completely pressure broadened at pressures above two atmospheres. Therefore, the pressure broadening effects on the absorption coefficient should not be observed in this work.

Since the 82-weight-percent AP propellent was used for the majority of the tests, for reasons that are discussed in Chapter IV, this propellant was also used for the calibration tests. The species concentrations used in this calibration work are equilibrium concentrations calculated by the computer program discussed in Appendix E. The calibration curves for the species of interest (H_2O, CO_2 and CO) are plotted in Figures A-7, A-8 and A-9. All of the calibration curves are linear, but they do not pass through the origin as required by the Beer-Lambert law. This is not surprising, considering the definition of the modified absorbance term used in these calibrations. In fact, the relatively small values for all the intercepts is probably an indication of how small of an effect the flame radiation terms, p_λ, really had on the values of the modified absorbance terms. Almost all of the H_2O calibration points fell on the one calibration curve. The two extreme data points in Figure A-7 are typical of occasional tests where the apparent H_2O

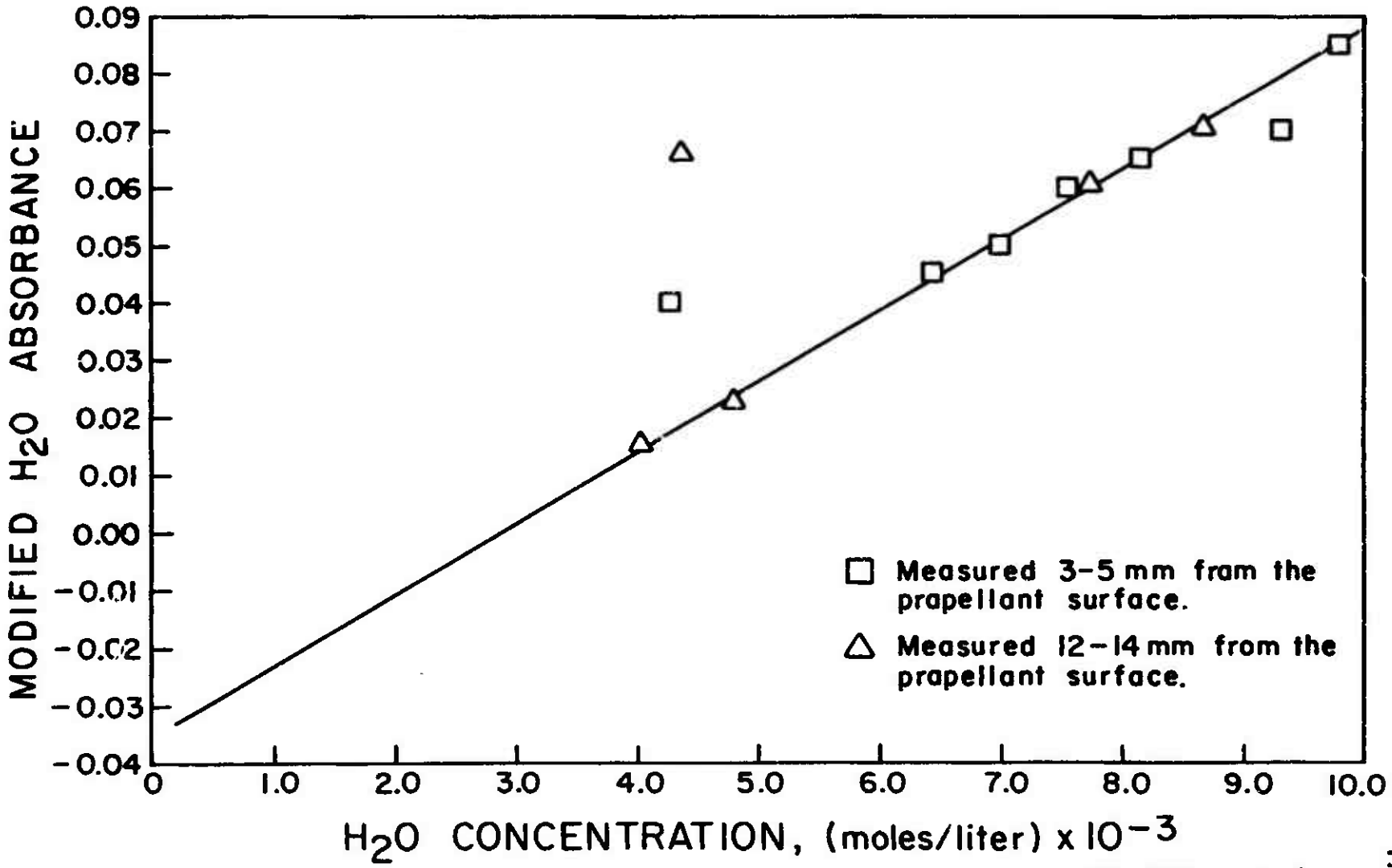

FIGURE A-7. H_2O CALIBRATION CURVE FOR AN 82 WEIGHT PERCENT AP PROPELLANT. (UFN and UFP)

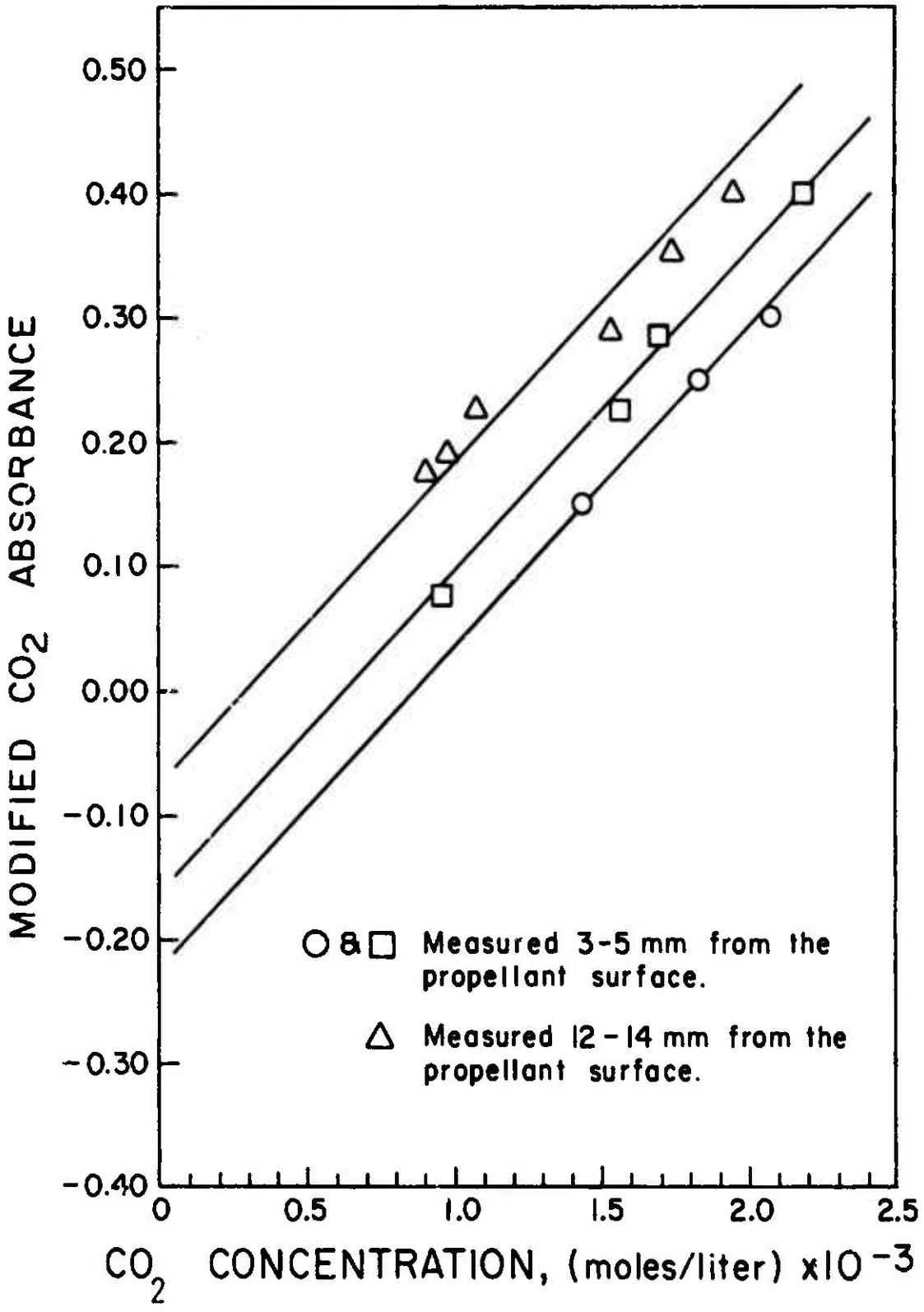

FIGURE A-8. CO_2 CALIBRATION CURVE FOR AN 82 WEIGHT PERCENT AP PROPELLANT. (UFN and UFP)

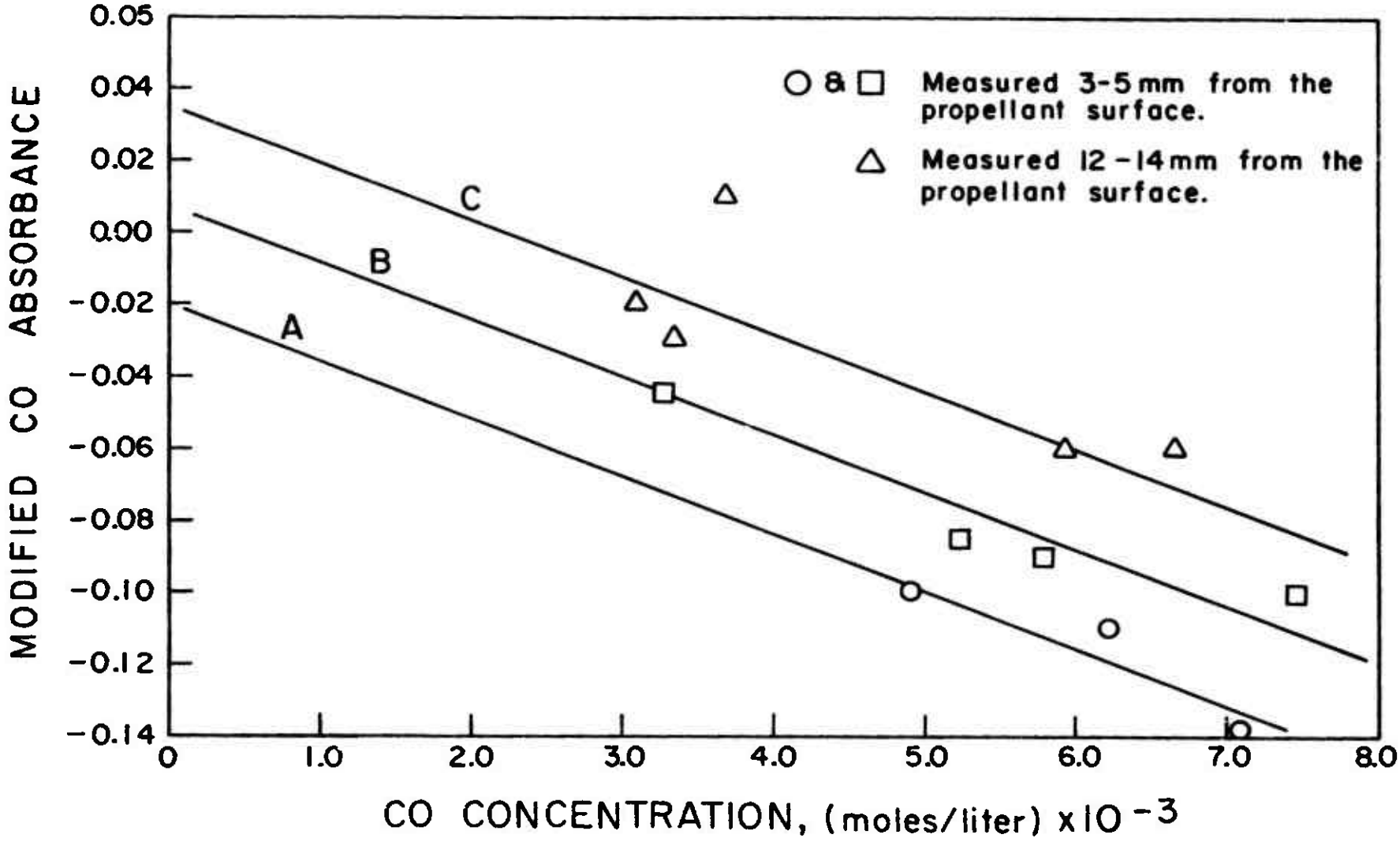

FIGURE A-9. CO CALIBRATION CURVE FOR AN 82 WEIGHT PERCENT AP PROPELLANT. (UFN and UFP)

concentration was excessive. This excessive H_2O concentration was also detected during many of the oscillatory pressure tests. The cause of this apparently large H_2O concentration is not understood. A family of three constant-slope calibration curves existed for both the CO_2 and CO. These sets of curves are a result of a change in CO and CO_2 concentration with increasing distance from the propellent surface. Data showing this effect are plotted in Figure 7 (Chapter IV). Notice that the H_2O concentration is essentially constant throughout the flame region studied, explaining why only one H_2O calibration curve was observed.

In the case of the CO_2 and the CO calibration, curves B and C represent data taken approximately 3-5 mm and 12-14 mm from the propellant surface, respectively. Each curve is made up of data taken on three separate days, over the course of several months, and with propellant strands from two different propellant batches. Curve A also represents data taken close to the propellent surface, and it should coincide more closely with Curve B. The reason for this discrepancy is unknown. However, the fact that all the data for Curve A were taken in one day, a couple of months before the data associated with the other two curves, suggests that some anomaly is present in these earliest data. One possibility is that the propellant strands used for these earliest tests were cut from a portion of the propellant slab that had a slightly different composition than the rest of the batch. In any event, the data reported were taken during the time period covered by Curves B and C, and Curve A was not used to reduce any of the data reported. The important feature of Curve A is that its slope is identical to the slopes of Curves B and C.

These double CO_2 and CO calibration curves are displaced segments of the true calibration curves. This displacement is due to the use of the same equilibrium composition data for both positions in the propellant flame, when in fact a change in the CO_2 and the CO composition has been observed experimentally. For obvious reasons, the gas-phase composition farthest from the propellant surface is likely to be closest to the calculated equilibrium composition. Therefore, it was assumed that curve C was the true calibration curve for both the CO_2 and the CO. Use of this calibration curve with data obtained close to the propellant surface indicates the true fuel-rich nature of this zone adjacent to the burning surface. It should be noted that the difference between curves B and C only produces a difference of 1-3 mole percent and 5-10 mole percent in the absolute CO_2 and CO concentrations respectively. The primary concern in this work was changes in concentrations, which are related to the slopes of the calibration curves.

The slope and location of the H_2O and CO_2 calibration curves are very well defined. However, the scatter in the CO data makes it more difficult to determine the exact CO calibration curve. Although the exact location is in doubt, the slope of the CO calibration curve is fairly well defined. Therefore, the measured changes in the gas phase composition are considered to be quite accurate, even though the absolute values might be in error slightly.

Also, the slope of the CO calibration curves is negative, which is a startling observation at first glance. The reason for this negative slope is apparent when the modified absorbance term

$$\ell n \left[\frac{P_\lambda^o + m_\lambda n_\lambda p_\lambda}{P_\lambda + p_\lambda} \right]$$

is studied. The $m_\lambda n_\lambda$ terms for the H_2O, CO_2, and CO absorption bands are approximately 1.0, 0.40, and 0.45 respectively. For the weak CO absorbing band at 4.6 μm, only 0.40 ($p_{4.6}$) is added to $P^o_{4.6}$ in the numerator, while the entire $p_{4.6}$ is added to the $P_{4.6}$ in the denominator. Since the 4.6 μm CO band is a weak absorber, the denominator in the modified absorbance term increases faster than the numerator, resulting in a negative slope. Even though the CO_2 $m_{4.26}n_{4.26}$ also has approximately the same value, 0.40, the fact that the 4.26 μm CO_2 band is a strong absorber prevents the above from occurring. It should be noted that this negative slope, which was calculated from the average values of many runs, is consistent with several observations. The observed change in the CO_2 and CO concentrations, while the H_2O concentration remains constant, with increasing distance from the propellant surface, is consistent with this negative slope calibration curve. Also, the observed CO_2 and CO concentration fluctuations with time are consistent with the calibration findings.

Because the absorption coefficient, K_λ, is a function of temperature, these 82-weight percent calibration curves may not be used with the data from the 80 and 85-weight percent propellant tests. Separate calibration curves for the 80 and 85-weight-percent propellants were not made. However, a few 80 and 85-weight-percent propellant data points are plotted in Figures A-10, A-11 and A-12, along with the

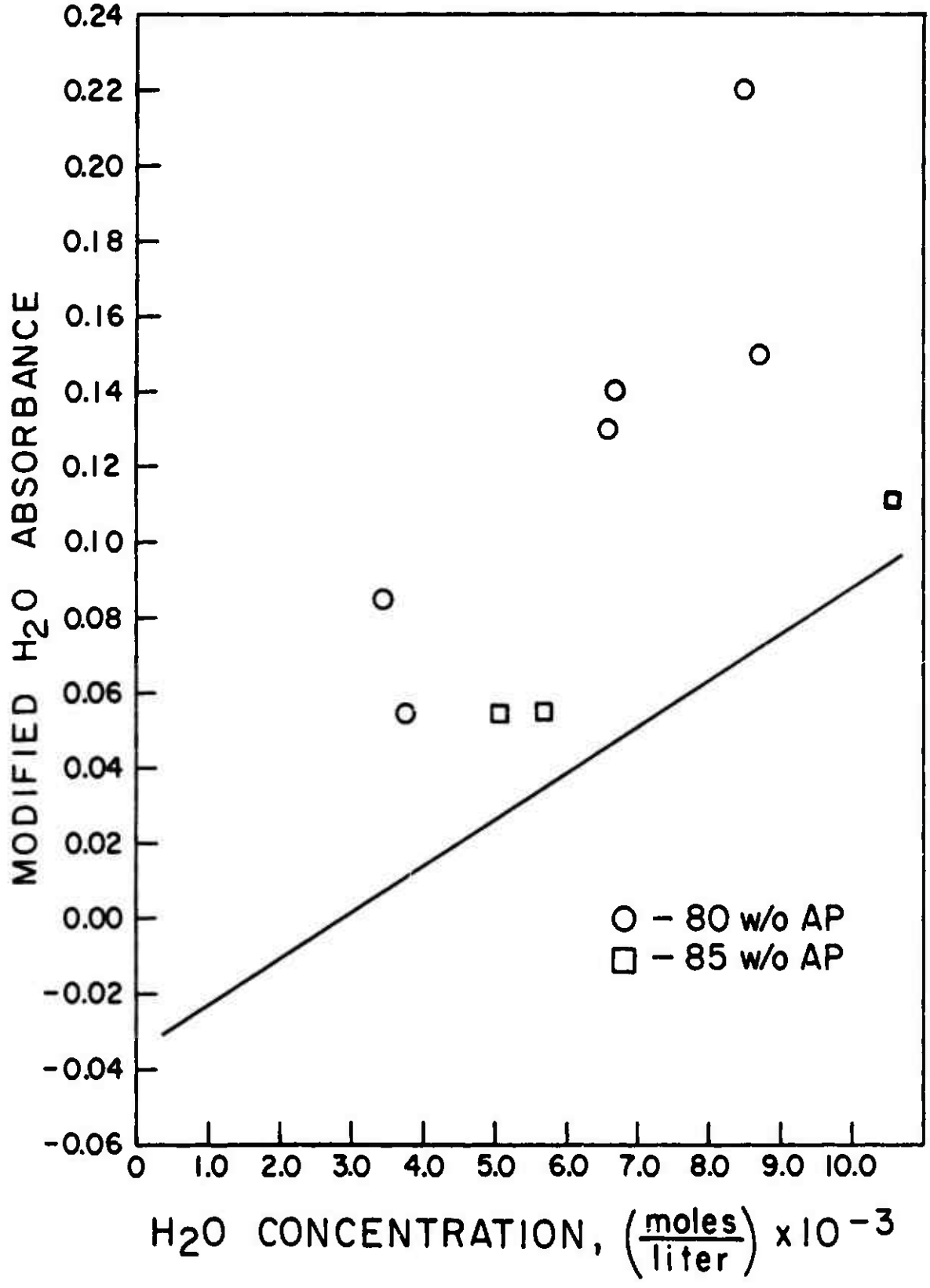

FIGURE A-10. COMPARISON OF H_2O DATA FROM 80 AND 85 WEIGHT PERCENT AP PROPELLANTS WITH THE 82 WEIGHT PERCENT CALIBRATION CURVES.

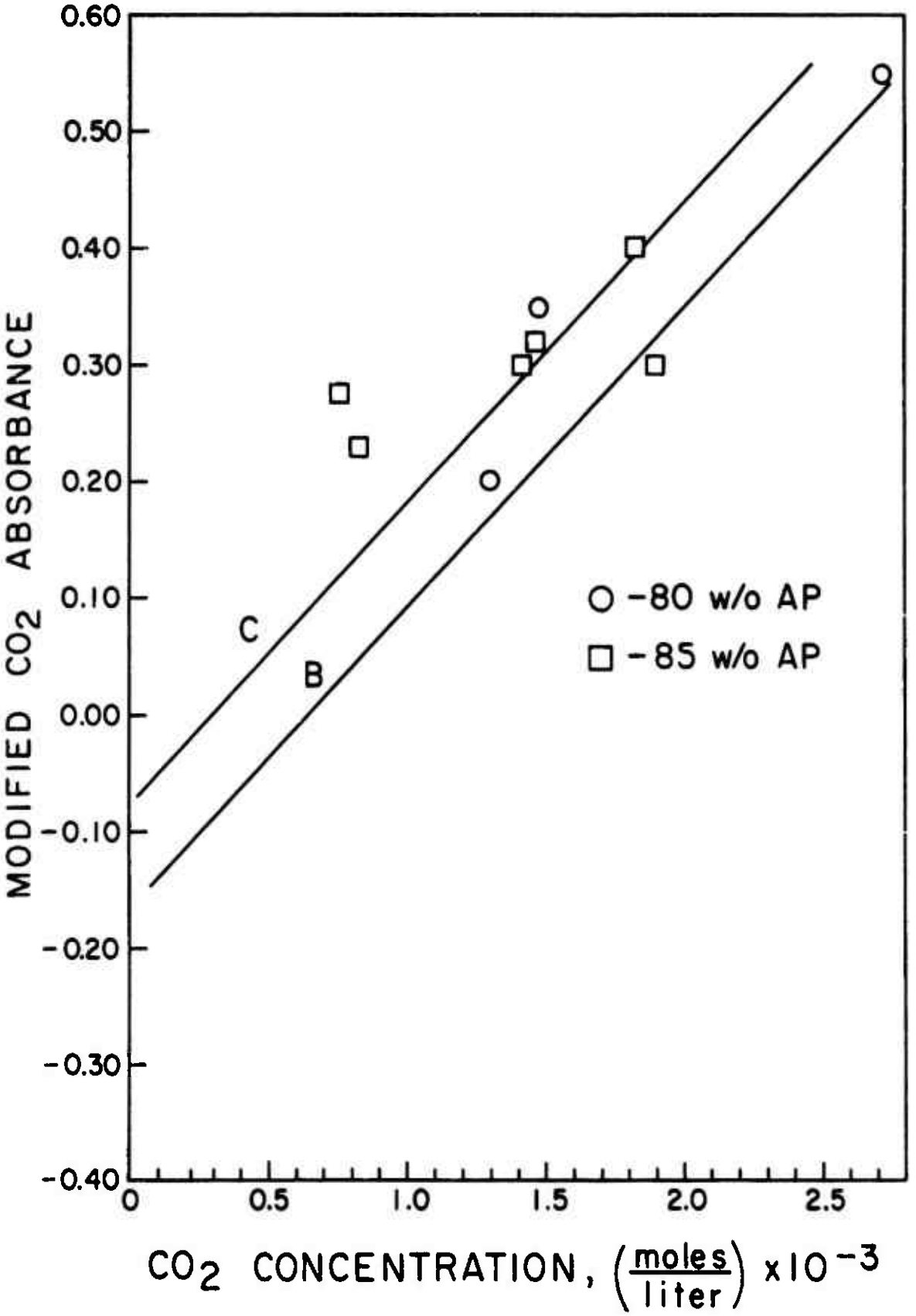

FIGURE A-11. COMPARISON OF CO_2 DATA FROM 80 AND 85 WEIGHT PERCENT (w/o) AP PROPELLANTS WITH THE 82 WEIGHT PERCENT CALIBRATION CURVES.

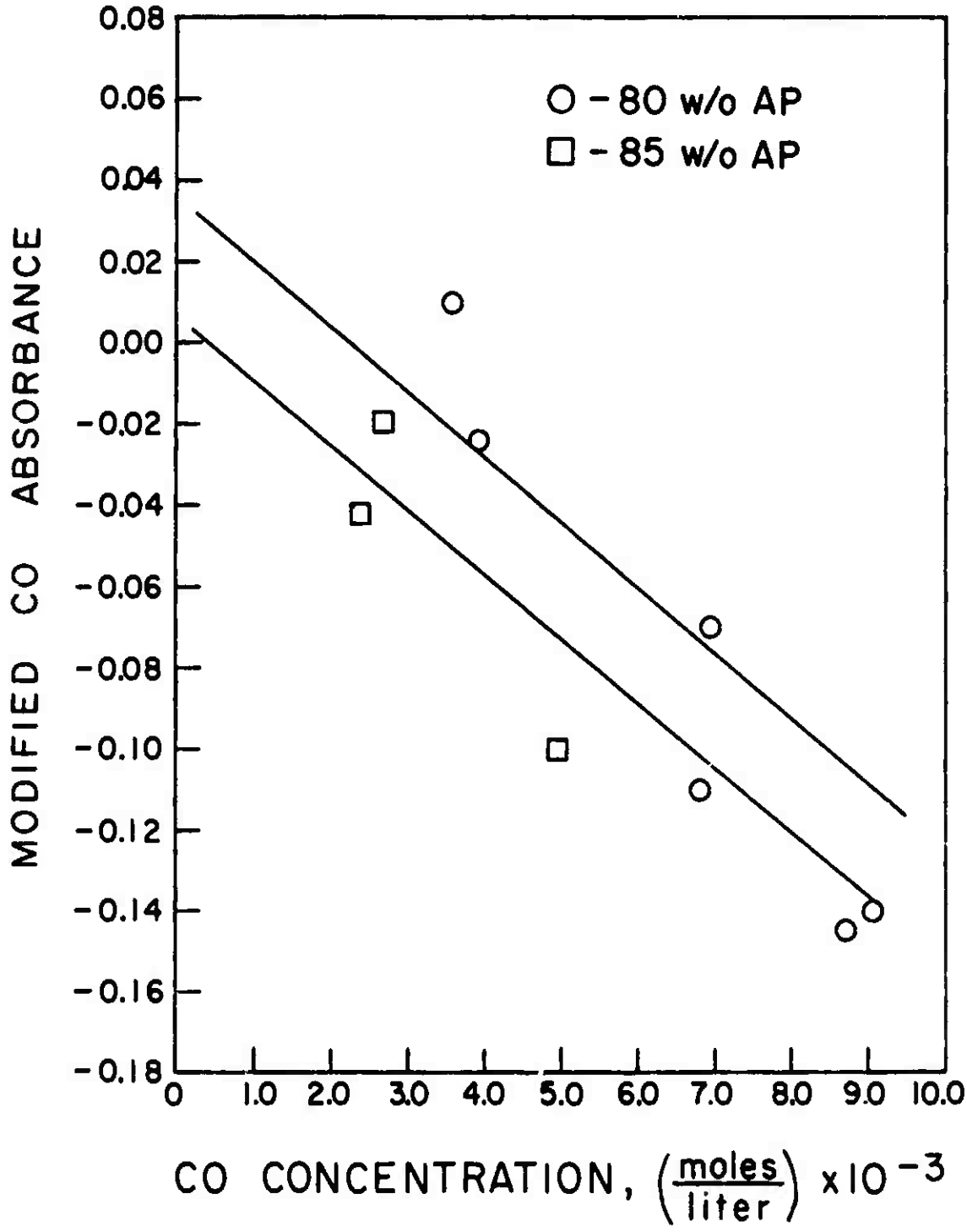

FIGURE A-12. COMPARISON OF CO DATA FROM 80 AND 85 WEIGHT PERCENT (w/o) AP PROPELLANTS WITH THE 82 WEIGHT PERCENT CALIBRATION CURVES.

82-weight-percent propellant calibration curves. It is hard to discern any trend from this limited amount of data. Even though the difference between the calculated adiabatic flame temperatures for the 80 and 82 and the 82 and 85-weight percent propellants is only approximately 175-200°K, no attempt was made to use the 82-weight-percent propellant calibration curves for these other data. Instead, only pressure corrected absorbances are reported for the limited 80 and 85 propellant data.

APPENDIX B

FLAME TEMPERATURE MEASUREMENTS

The flame temperatures were determined by the simultaneous measurements of the flame's spectral radiance and spectral absorptance at one wavelength. This temperature measurement technique was first reported by Schmidt in 1909 [44], and was first used with modern equipment and interpretation by Silverman in 1949 [45]. This radiometric method of gas pryometry is often referred to as the Schmidt or the Planck-Kirchhoff method. Although the sodium D-line wavelengths were used in this work, the Schmidt method has no wavelength restrictions.

Equipment for Flame-temperature Measurements

A schematic of the electro-optical hot-gas pyrometer used to measure the flame's radiance and absorptance is shown in Figure B-1. The radiant energy from the light source was focused on the slit of the chopper wheel assembly by a combination of a plane and a spherical mirror. A Cassegrainian optical system collected the radiant energy from the slit and focused it on the center plane of the combustion chamber. A matched Cassegrainian optical system in the receiver unit collected the combined source and flame radiation and focused it on the detector.

A GE 18A/T10/1P tungsten strip lamp, powered by a Technipower (Model L10-25) power supply, was used as the light source. The strip lamp was operated at an effective black-body temperature of 2553°K. The 22-cm

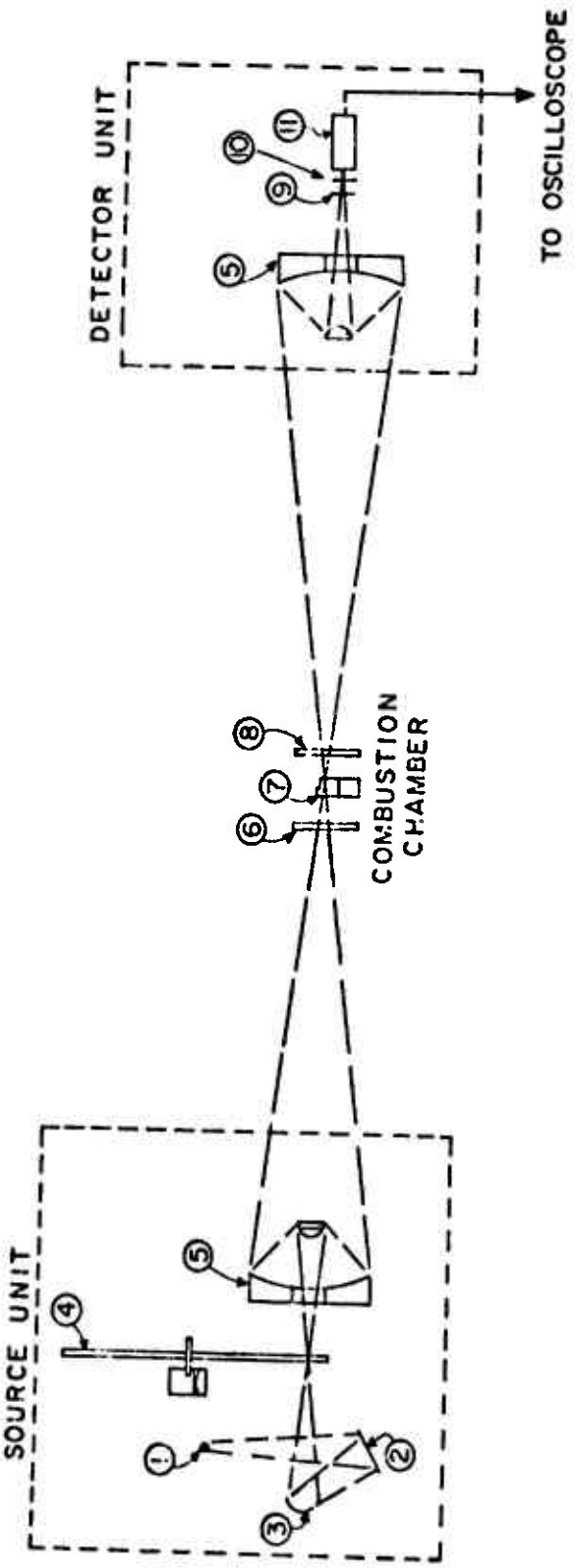

FIGURE B-1. A SCHEMATIC DRAWING OF THE ELECTRO-OPTICAL HOT-GAS PYROMETER. 1) source; 2) plane mirror; 3) spherical mirror; 4) chopper wheel; 5) Cassegrainian optical system; 6 and 8) windows; 7) propellant flame; 9) exit slit; 10) interference filter; 11) photo-multiplier detector.

diameter chopper wheel contained 64 slots around its periphery, and it was driven by a 12-VDC motor. The motor was powered by a Lambda (Model LH 122a FM) regulated power supply, which was used to set the speed of the motor. The motor speed was set to produce 4500 interruptions of the source beam per second, yielding a maximum of 4500 temperature measurements per second.

Prior to entering the RCA 7102 photo-multiplier detector, the light beam passed through a small entrance slit and an interference filter. The entrance slit was 3.18 mm long and 0.50 mm wide, and its projected image in the focal plane of the receiver unit was approximately 4.0 mm long and 0.62 mm wide. This small slit guaranteed that only radiation from the very central core of the propellant flame was measured. The interference filter (Baird Atomic, Inc., Type B-11 (x)) provided the very narrow spectral band necessary in the Schmidt method, transmitting radiant energy only from 0.5883-μm to 0.5914-μm. The transmittance curve for this particular filter is shown in Figure B-2. The RCA 7102 photomultiplier was operated at a voltage of 1150 VDC, supplied by a Hewlett-Packard OC power supply (Model # 6110A). With these operating conditions the photomultiplier output was approximately 8 volts; thus the signal did not require amplification before going to the oscilloscope for recording.

Theoretical Development of the Temperature Equation

The temperature equation used in this work is based on Wien's energy-distribution law instead of Planck's law, and the development of the equation presented follows Millar et al.[29]. Figure B-3 is a schematic

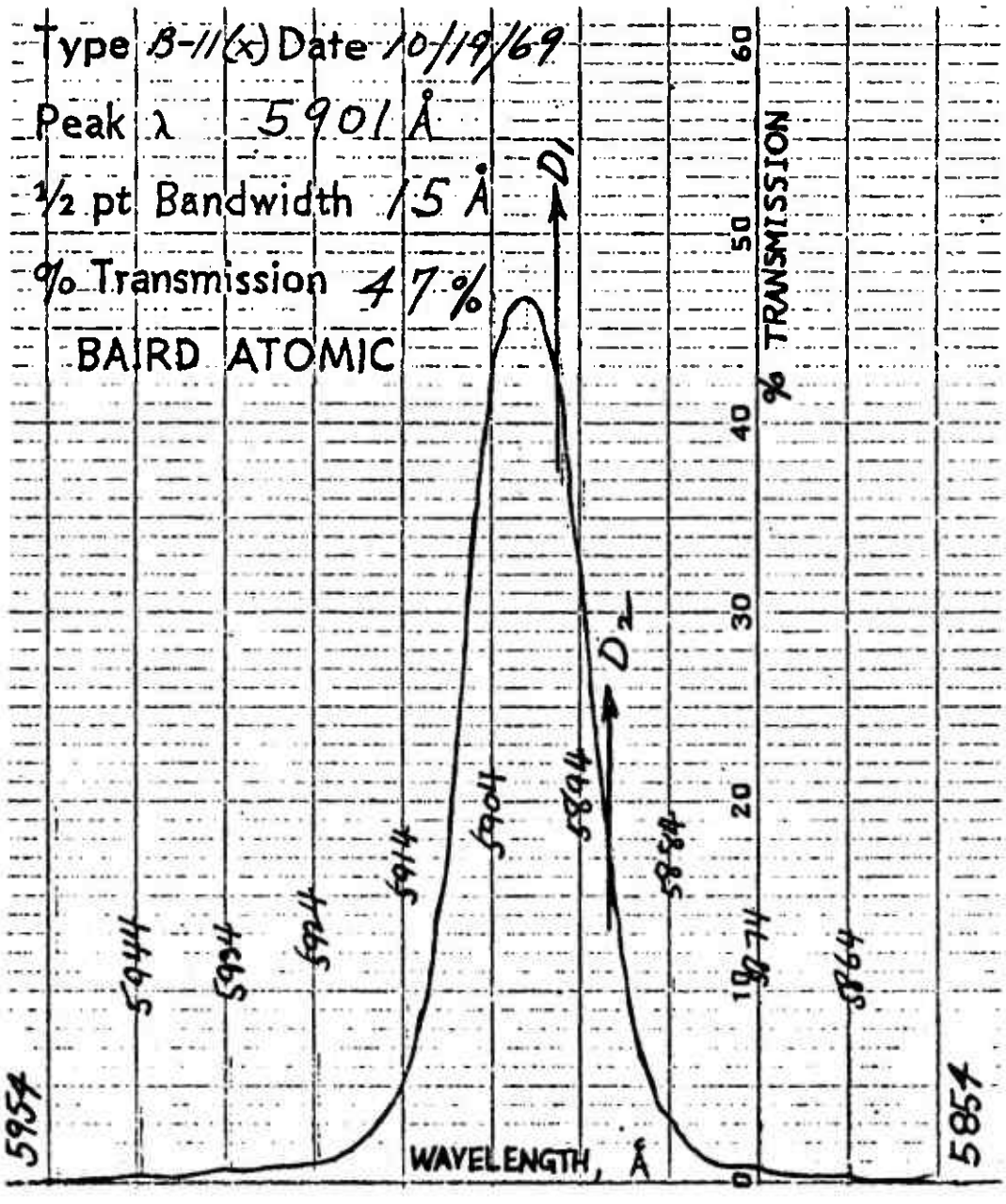

FIGURE B-2. THE TRANSMITTANCE CURVE FOR THE Na D-LINE INTERFERENCE FILTER.

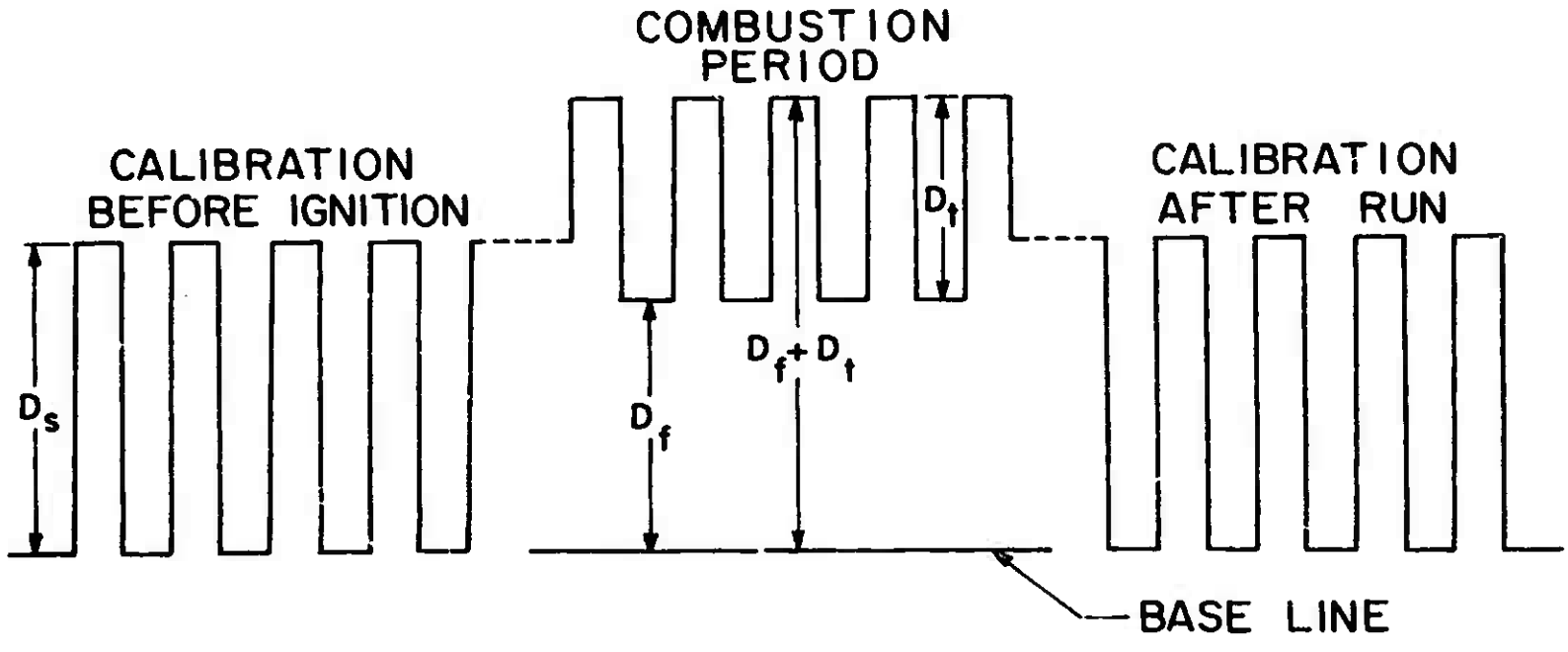

D_s: Signal due to background source radiation.

D_f: Signal due to flame emission.

D_t: Signal due to transmitted background - source radiation.

FIGURE B-3. A SCHEMATIC DIAGRAM OF THE PYROMETER'S OUTPUT SIGNAL.

diagram of the hot-gas pyrometer's output during both no-flame and flame conditions.

If the chopper wheel is not blocking the background-source light beam, and there is no flame present, the detector output, D_s, may be expressed as

$$D_s = C\, N_{pS}(\lambda_D, T_{ps}) \quad , \tag{1}$$

where T_{ps} is the true temperature of the projected-image of the background source, and $N_{pS}\ (\lambda_D, T_s)$ is the spectral radiance of the projected image of the background-source over the very narrow spectral range, $\Delta\lambda_D$, transmitted by the Na D-line filter. The proportionality constant, C, is characteristic of the transmission coefficient of the optical equipment between the flame location and the detector, the detector sensitivity, and the calibration factor for the electronic equipment.

For the flame condition, with the chopper blocking the background-source light beam, the detector output, D_f, is given by

$$D_f = C\, \varepsilon_{f\lambda}\, N^b(\lambda_D, T_f) \quad , \tag{2}$$

where $N^b(\lambda_D, T_f)$ is the spectral radiance of a blackbody at the true temperature of the flame (T_f) over the narrow spectral range $\Delta\lambda_D$, and $\varepsilon_{f\lambda}$ is the effective flame emissivity over this same spectral range.

For the flame condition, with the chopper wheel not blocking the background-source, both flame radiation and the transmitted background-source radiation reach the detector. Thus, the detector output is given by

$$\begin{aligned} D_f + D_T &= C\varepsilon_{f\lambda} N^b(\lambda_D, T_f) + C[N_{pS}(\lambda_D, T_{ps}) - \alpha_{f\lambda}\, N_{ps}(\lambda_D, T_{ps})] \\ &= C[N_{ps}(\lambda_D, T_{ps}) - \alpha_{f\lambda}\, N_{ps}(\lambda_D, T_{ps}) + \varepsilon_{f\lambda}\, N^b(\lambda_D, T_f)] \quad , \end{aligned} \tag{3}$$

where D_T is the detector output signal due to the transmitted radiation, and $\alpha_{f\lambda}$ is the effective absorptivity of the flame over the spectral range $\Delta\lambda_D$.

Equations (1), (2) and (3) can be combined to yield

$$D_f + D_T = D_s - \alpha_{f\lambda} D_s + D_f \quad . \tag{4}$$

Rearranging equation (4) gives

$$\alpha_{f\lambda} = \frac{D_s - D_T}{D_s} \quad . \tag{5}$$

Thus, the average absorptance (absorptivity) of the flame over the spectral range $\Delta\lambda_D$ can be determined from a record of the detector's output.

If Kirchhoff's law holds, the absorptance (absorptivity) of the flame at any wavelength equals the emissivity of the flame at the same wavelength. (The validity of this assumption is discussed later.) Therefore, the average absorptivity over $\Delta\lambda_D$ equals the average emissivity over that same spectral range, or

$$\alpha_{f\lambda} = \varepsilon_{f\lambda} \tag{6}$$

Equations (1), (2), (3), and (6) combine to yield

$$\frac{D_s - D_T}{D_f} = \frac{N_{ps}(\lambda_D, T_{ps})}{N^b(\lambda_D, T_f)} \tag{7}$$

Wien's energy-distribution law is used to determine the flame temperature from the flame radiance. Wien's law for the flame is

$$N^b(\lambda_D, T_f) = \int_{\lambda_1}^{\lambda_2} \frac{C_1}{\lambda^5} \exp\left(-\frac{C_2}{\lambda T_f}\right) d\lambda \tag{8}$$

where $\lambda_2 - \lambda_1 = \Delta\lambda_D$, the spectral range passed by the sodium D-line filter. C_1 and C_2 are known constants. For the projected image of the

background-light source Wien's law is

$$N_{ps}(\lambda_D,T_{ps}) = N^b(\lambda_D,T^b_{ps}) = \int_{\lambda_1}^{\lambda_2} \frac{C_1}{\lambda^5} \exp\left(-\frac{C_2}{\lambda T^b_{ps}}\right) \qquad (9)$$

where T^b_{ps} is the brightness temperature measured at λ_D (the temperature of a blackbody which has the same spectral radiance as the projected image of the background-light source over the spectral range $\Delta\lambda_D$) of the projected image of the background-light source.

Since $\Delta\lambda_D$ is relatively small, the mean value theorem can be used in evaluating both $N^b(\lambda,T_f)$ and $N^b(\lambda,T^b_{ps})$. That is, $N^b(\lambda,T_f)$ and $N^b(\lambda,T^b_{ps})$ may be expressed as the product of $\Delta\lambda$ and the mean value of the integrand in the spectral range $\Delta\lambda_D$, or

$$\frac{N^b(\lambda_D,T^b_{ps})}{N^b(\lambda_D,T_f)} = \frac{\exp\left(-\frac{C_2}{\lambda_D T^b_{ps}}\right)}{\exp\left(-\frac{C_2}{\lambda_D T_f}\right)} \quad . \qquad (10)$$

Equating equations (7) and (10) yields

$$\ell n\left[\frac{D_s - D_T}{D_f}\right] = \frac{C_2}{\lambda_D T_f} - \frac{C_2}{\lambda_D T^b_{ps}} \quad . \qquad (11)$$

Rearrangement of equation (11) results in the temperature equation

$$\frac{1}{T_f} = \frac{1}{T^b_{ps}} + \frac{\lambda_D}{C_2}\ell n\left[\frac{D_s - D_T}{D_f}\right] \quad , \qquad (12)$$

where the constants λ_D and C_2 are 0.5896-μm and 1.439-cm°K respectively, and T^b_{ps} is the brightness temperature of the projected image of the background-source measured at λ_D. Remember that D_s, D_T, and D_f are all measured off the recorded detector output.

The brightness temperature of the projected image of the background-source was measured with a Leeds and Northrup optical pyrometer (Model

8632-C). The temperature measurements were made with the combustion chamber removed, but with one of the quartz combustion chamber windows in the optical path. Two different methods of viewing this projected image were tried. First, the optical pyrometer was mounted in place of the photomultiplier detector assembly and focused on the projected image. This technique gave a brightness temperature of 2358°K when the tungsten strip lamp was operated at a brightness temperature of 2553°K. The second method used a 45° first-surface mirror at the plane of the projected image of the background-source, and the pyrometer was focused on the projected image on the first-surface mirror. This technique gave a brightness temperature of 2273°K when the tungsten-strip lamp was operated at a brightness temperature of 2553°K. The relatively small difference (85°K) obtained by these two methods might suggest the use of a mean temperature value. However, preliminary temperature calculations showed that the 2273°K value resulted in measured flame temperatures that were more consistent with respect to the calculated adiabatic flame temperatures for these propellants. Therefore, 2273°K was used exclusively for all the temperature calculations reported.

Because the optical pyrometer measures brightness temperatures at a wavelength of 0.653 μm (λ_p), it was necessary to correct the pyrometer readings, T^p, to the corresponding sodium D-line (λ_D = 0.5896 μm) brightness temperatures, T^b. The equation used to correct the measured tungsten filament temperature, T_s^p, can be developed by again using Wien's energy-distribution law. If T_s is the true filament temperature, and ε_p is the tungsten filament emissivity at λ_p, then, from Wien's law

$$N_s(\lambda_p, T_s^p) = C_1\lambda_p^{-5}\exp(-C_2/\lambda_p T_s^p) = \varepsilon_p C_1\lambda_p^{-5}\exp(-C_2/\lambda_p T_s) \quad , \qquad (13)$$

and

$$N_s(\lambda_D,T_s^b) = C_1 \lambda_D^{-5}\exp(-C_2/\lambda_D T_s^b) = \varepsilon_D C_1 \lambda_D^{-5}\exp(-C_2/\lambda_D T_s) \quad , \qquad (14)$$

where ε_D is the tungsten filament emissivity at λ_D. Equations (13) and (14) can both be solved for T_s and then equated, yielding

$$\frac{1}{T_s^b} = \frac{1}{T_s^p} + \frac{\lambda_p}{C_2} \ln \varepsilon_p - \frac{\lambda_D}{C_2} \ln \varepsilon_D \quad . \qquad (15)$$

Using ε_p and ε_D values of 0.420 and 0.430 respectively [46], in equation (15) yields a T_s^b value of 2585°K corresponding to the measured T_s^p value of 2553°K.

The following assumption has to be made in order to correct the measured temperature, T_{ps}^p, of the projected-image of the background source: the same fraction of the source radiance at λ_D and λ_p reach the projected-image, or

$$\frac{N_{ps}^b\ (\lambda_D,T_{ps}^b)}{N_s^b\ (\lambda_D,T_s^b)} = \frac{N_{ps}^b\ (\lambda_p,T_{ps}^p)}{N_s^b\ (\lambda_p,\ T_s^p)} \quad . \qquad (16)$$

Use of Wien's law allows equation (16) to be rewritten as

$$\frac{C_1\lambda_D^{-5}\exp\ (-C_2/\lambda_D T_{ps}^b)}{C_1\lambda_D^{-5}\exp\ (-C_2/\lambda_D T_s^b)} = \frac{C_1\lambda_p^{-5}\exp\ (-C_2/\lambda_p T_{ps}^p)}{C_1\lambda_p^{-5}\exp\ (-C_2/\lambda_p T_s^p)} \quad . \qquad (17)$$

Equation (17) can be simplified and rearranged to yield

$$\frac{1}{T_{ps}^b} = \frac{\lambda_D}{\lambda_p}\left[\frac{1}{T_{ps}^p} - \frac{1}{T_s^p}\right] + \frac{1}{T_s^b} \quad . \qquad (18)$$

The above T_s^b value of 2585°K, and the measured T_s^p and T_{ps}^p values of 2553°K and 2273°K respectively were used to calculate a T_{ps}^b value of 2324°K. This calculated T_{ps}^b value and the λ_D and C_2 values can be used to rewrite equation (12) in the final form used to calculate flame

temperature,

$$\frac{1}{T_f} = \frac{1}{2324°K} + \frac{0.5896\text{-}\mu m}{1.439 cm°K}\left[\frac{10^{-4} cm}{\mu m}\right] \ell n\left[\frac{D_S - D_T}{D_f}\right] \quad . \qquad (19)$$

Throughout the derivation of equation (19), Wien's law was used instead of the more exact Planck radiation law. However, for the sodium D-line wavelengths, the discrepancy between Wien's law and Planck's law is less than one percent for temperatures less than 4000°K [47]. Since almost all the flame temperatures in this study were below 3000°K, the use of the simpler Wien's law should not introduce significant error in the values of the calculated flame temperatures.

The accuracy of the above temperature equation depends on the validity of several assumptions made during its derivation. The Schmidt method measures one of the statistical temperatures associated with the internal energy distributions of the radiating specie. All of the statistical temperatures are the same and equal to the kinetic temperature only when there is complete thermal equilibrium. Use of the sodium D-line wavelengths results in the measurement of the electronic excitation temperature of the radiating species. Although there are major departures from equilibrium in the reaction zones of flames, the relatively small departures from equilibrium in the post-reaction-zone region do not usually produce a major difference between the electronic excitation temperature and the kinetic temperature [8]. Therefore, experimentally measured post-reaction-zone flame temperatures (using the sodium D-line wavelengths) have generally agreed well with theoretically predicted flame temperatures, as well as with flame temperatures measured by other techniques.

The Schmidt method assumes equality between the flame's spectral

absorptance (absorptivity) and spectral emissivity, that is, application of Kirchhoff's law to the flame. Because the emission and absorption of a gas vary strongly with wavelength, Kirchhoff's law is applicable to gases only in a sufficiently narrow spectral band [30]. The sodium D-line interference filter used in this study has a one-half peak-height spectral band width of 0.0015-μm, and the application of Kirchhoff's law is assumed to be valid over this very narrow spectral band.

Also, for Kirchhoff's law to hold there must be no nonabsorbing attenuation of the light due to reflection and scattering in the flame. That is, the flame must be clean and free of particulate matter. This same consideration was also important in the infrared absorption measurements, thus, only uncatalyzed, non-metallized propellants with relatively high AP contents were used in this study. Since these propellant formulations do not generate large quantities of particulate matter, the effects of flame reflection and scattering should be negligible. However, the super-adiabatic flame temperatures measured for the lowest AP content (80 wt. %) propellant used are believed to be caused by such particulate effects. This condition is discussed in a following section.

Flame-temperature Measurement Technique

A high-speed camera was used to record the hot-gas pyrometer's signal on an oscilloscope, as is described in Appendix C. The pyrometer signal during combustion is shown in Figures C-1 and C-2. The modified square wave form is the result of the mechanical chopping assembly and the frequency response of the electronic equipment. All measurements were made to the flat minimum and maximum regions of the curve. Originally, the quantity D_s was recorded before and after each run. However, since

no discrepancies were ever observed between the before and after values, subsequently, D_s values were only recorded before each run. The D_s value after each run was checked visually to make sure that it had not changed. The various pyrometer deflections measured from the 16-mm film were used as input data for a computer program, which calculated the D_s, D_T, and D_f values and then calculated the flame temperatures from equation (19). A complete description of the data reduction technique is given in Appendix C.

The sodium emission was obtained by adding a small amount of finely ground sodium chloride to the propellant formulations. Temperature measurements with optimum accuracy are obtained for absorptances above 20% [30]. It was found that 0.10 to 0.50 weight percent of sodium chloride was adequate to produce acceptable absorptances over the pressure range studied (25-100 psia). In fact, at the highest pressures studied, the 0.50 NaCl weight percent produced nearly blackbody conditions ($\alpha_{\lambda f} \cong 0.95$).

Flame-Temperature Results

The time-varying nature of the flame temperatures is described in Chapters IV and V and will not be discussed in this section. However, there are several characteristics of the measured time-averaged flame temperature values which require discussion.

Figure B-4 compares the measured flame temperatures of the three different AP-content propellants used with their respective adiabatic flame temperatures. The experimentally measured values plotted are mean values from steady-state pressure tests. Over the pressure range used, 50 to 100 psia, the adiabatic flame temperatures only increase slightly (20-40°K) with pressure. Therefore, the adiabatic flame

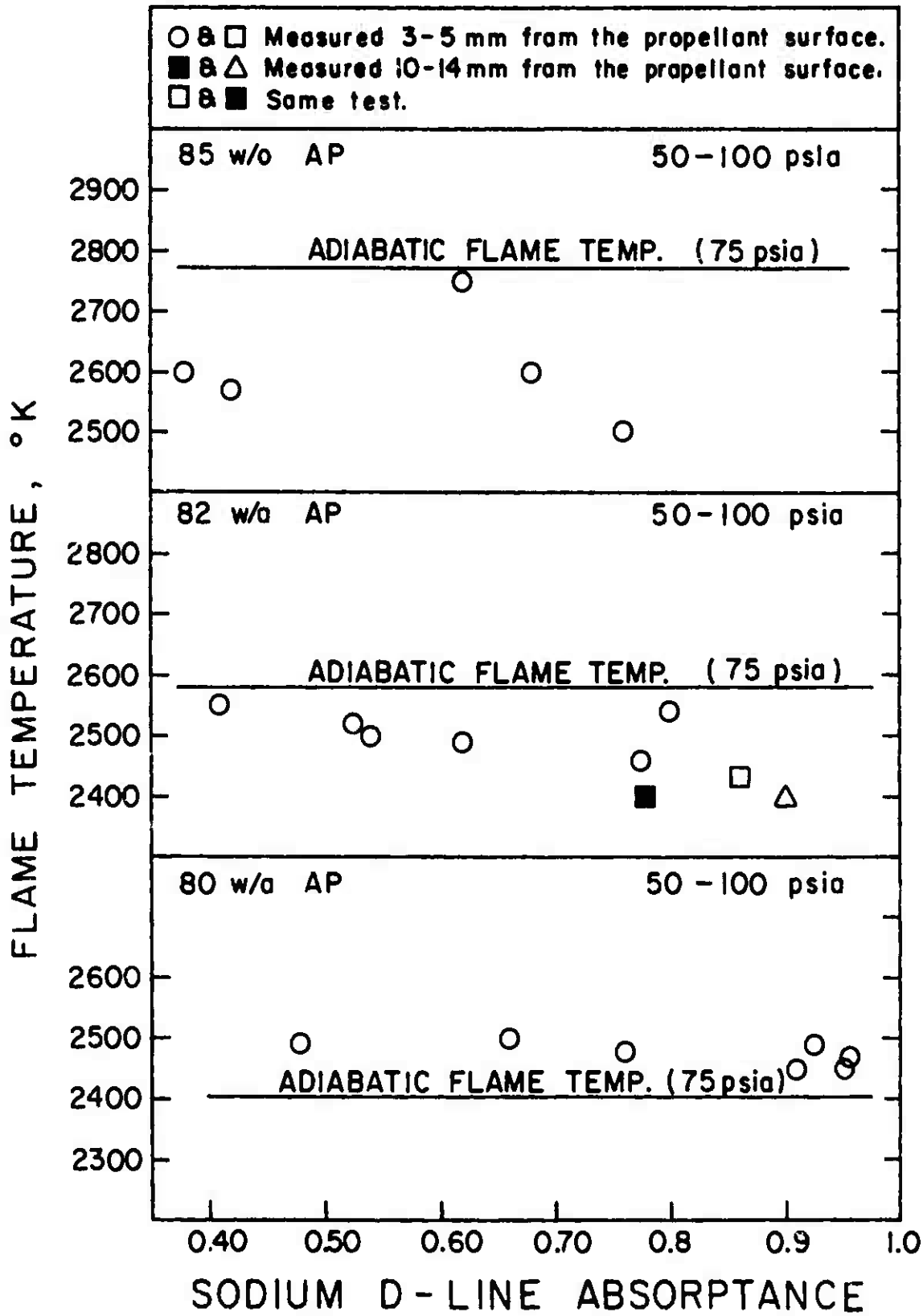

FIGURE B-4. COMPARISON OF MEASURED TIME-AVERAGE FLAME TEMPERATURES FOR 80, 82, AND 85 WEIGHT PERCENT (w/o) AP PROPELLANT WITH THE CORRESPONDING ADIABATIC FLAME TEMPERATURES.

temperature at 75 psia is plotted for reference. With regard to the experimentally measured flame temperatures, increasing the pressure increases the sodium D-line absorptance (absorptivity), thus, the temperatures are plotted as a function of the measured sodium D-line absorptance.

The 82 wt. % AP propellant was used during the majority of this study and it will be discussed first. The measured flame temperatures for this propellant were 2-7% (50-175°K) lower than the adiabatic flame temperature. This deviation is normal and reasonable for this type of non-adiabatic combustion. Also, as is discussed in Chapter IV, the flame temperature appeared to decrease slightly (30-50°K) with axial distance from the propellant surface (between 3 mm and 14 mm). However, the major characteristic of the measured flame temperatures is the absorptance effect. When there is a temperature gradient alone the optical path in the gas, the temperature measured by the Schmidt method is an average value over the path. This is not an arithmetic mean. Regions of higher temperatures are weighted more because of the curvature of the Planck law curve, while regions closest to the detector are weighted more due to self-absorption. The result is that the average value is weighted towards higher temperatures for lower absorption levels and towards lower temperatures at higher absorption levels [30]. This effect is apparently observed in the 82 wt. % AP propellant data, with the temperature decreasing approximately 150°K between an absorptance value of 0.40 and 0.90. Almost without exception, all of the time-dependent temperature profiles reported were measured with an absorptance between 0.40 and 0.80, thus, the run to run difference in the mean temperatures due to this absorptance effect would not be greater than 100°K. Since

the absorptance did not vary greatly during a test, this absorptance effect was not noticed within individual tests.

The measured flame temperatures for the 80 wt. % propellant were all 2-4% (50-100°K) higher than the adiabatic flame temperature. A slight error in the AP-content of the propellant, introduced during preparation, could cause this deviation. However, since the data in Figure B-4 came from tests using two separate propellant batches, this cause of the deviation is unlikely. As is discussed in Appendix A, these flames had a much higher level of continuum flame emission, presumably the result of a large concentration of radiating carbon particles. Carbon particles in a flame reduce the background-source radiation due to scattering and reflection, while only the flame emission from the back side of the flame is weakened. Therefore, the sodium emission is reduced less than the background radiation, resulting in a measured temperature which is artificially high [8]. This is believed to be the cause of the high temperature values for the relatively dirty 80 wt. % AP propellant flames.

The measured flame temperatures for the 85 wt. % AP propellant were 6-10% (170-270°K) lower than the adiabatic flame temperature. Again, these values would be expected to be lower than the adiabatic flame temperature, but not by this great of an amount. The reason for this deviation is not readily apparent.

For both the steady-state and oscillating pressure tests, the mean flame temperatures for the 80, 82, and 85 wt. % AP propellants increased with an increase in the AP content. However, the magnitude of the changes were not those predicted by the adiabatic flame temperature data. Although the mean temperature values are most likely off by 2-5%, it is believed that the magnitude of the observed time-dependent fluctuations are accurate.

APPENDIX C

DATA ACQUISITION AND REDUCTION

Data Acquisition Equipment

The output signals from the spectrometer, the electro-optical hot-gas pyrometer, and the pressure transducer had to be recorded simultaneously. This combination of equipment generated data at a tremendous rate, requiring special recording and measuring equipment. Precision tape decks can be used when the spectrometer is operated at its slower scan speeds. However, at its fastest scan speed, 800 scans per second, the frequency response requirement prevents the use of tape decks.

Five pieces of information had to be measured from each spectral scan. Thus, at a scan rate of 800 spectra per second, the spectrometer generated 4000 pieces of useful information per second. The electro-optical hot-gas pyrometer generated 4500 temperature measurements per second, or 9000 pieces of information per second. The problem of simultaneously recording these data was solved by using a high-speed Fastax camera (Wollensak Model WF-225) to record an oscilloscope display for later analysis.

The three output signals were displayed on a multichanneled oscilloscope (Tektronix Type 565). The Tektronix Type 565, a dual-beam oscilloscope, was equipped with a type 3A3 dual channel differential amplifier and a type 2A63 single-channel differential amplifier. Both the scope and the amplifiers were operated in the DC-coupled mode

and had a bandpass of DC to at least 300 HZ. The Wollensak Model WF-22S camera is a 16-mm oscillo-streak camera. It is equipped with both magnetic and dynamic braking, which allows repeated starting and stopping on the same roll of film. A Fastax control unit (Wollensak Model J-515) was used to coordinate camera operations with the tests.

The oscilloscope was placed on its side, and operated without time base. This produced an oscilloscope display of horizontally deflected dots, with the vertical streaking motion of the film adding the time base. A small reference light was attached to the face of the oscilloscopt to provide a reference line used in the analysis of the films. A small portion of film is shown in Figure C-1. The camera was operated at a film speed of approximately 20 fps, which allowed recording data from four runs on each 100 foot roll of film. Eastman Kodak 4-X Negative Film (4XN430) was used to record most of the data. Some of the initial data were recorded on Eastman Kodak Tri-X Reversal (TRX-430) film. However, in both cases the film was developed to give a negative. Thus, the oscilloscope traces appeared as dark lines on a clear background and were very easy to analyze. Even though only small segments of each run were analyzed, this data recording technique provided a permanent record of each run, without affecting the resolving power of the spectrometer.

The films were analyzed on a modified Recordak microfilm reader, which is shown in Figure C-2. The overall magnification of the Fastax camera and Recordax reader was such that a 1-cm deflection on the oscilloscope corresponded to approximately 2 cm on the film reader. An electro-mechanical device used to measure the oscilloscope deflections recorded on the film was added to the reader. The slider from a precision

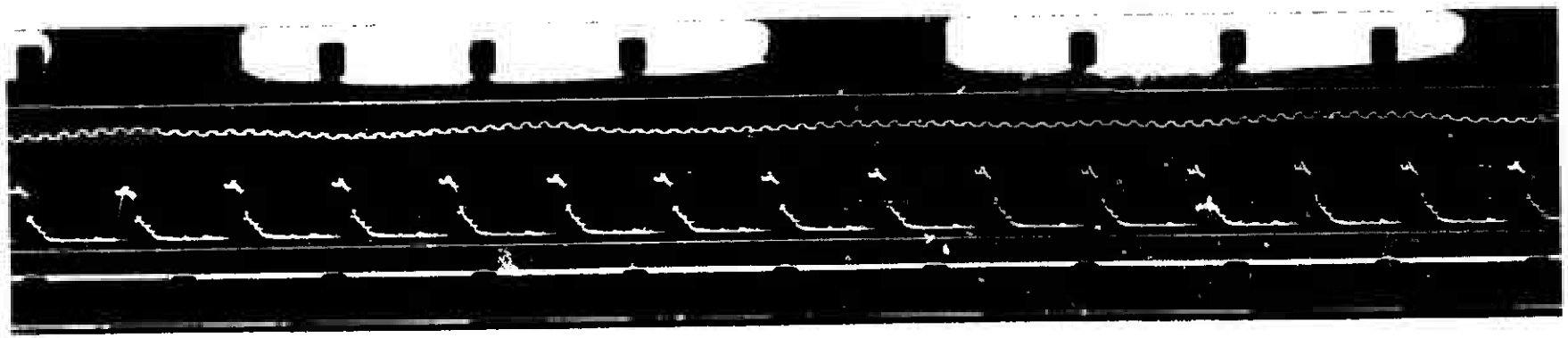

FIGURE C-1. AN ENLARGEMENT OF A SMALL PORTION OF THE 16-MM FILM FOR A CONSTANT PRESSURE TEST WITH A 82 WT.% AP PROPELLANT. Starting at the top of the film, the traces are: pressure, hot-gas pyrometer, spectrometer, and reference line.

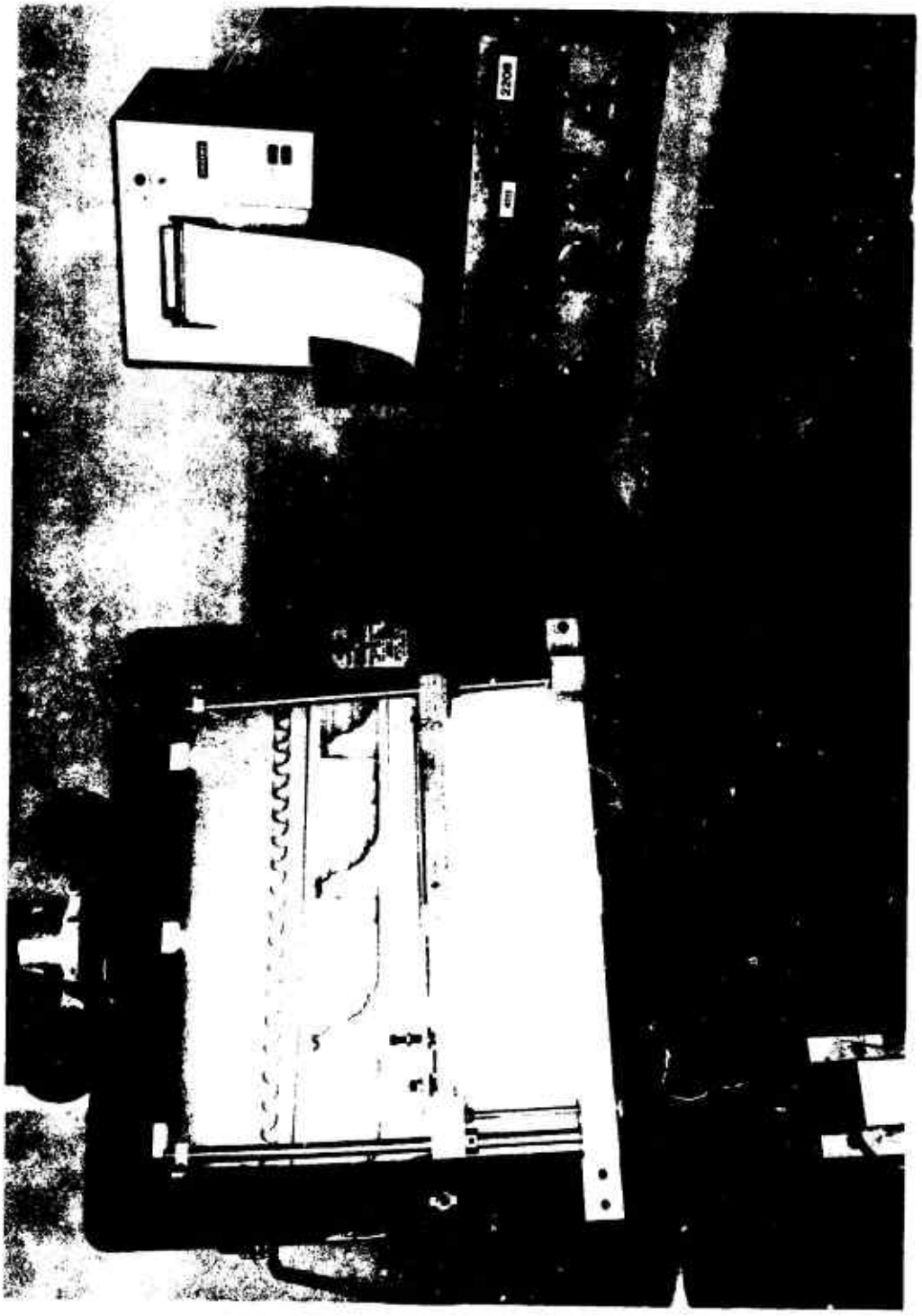

FIGURE C-2. AN OVERVIEW PHOTOGRAPH OF THE FILM READER AND RECORDING SYSTEM.

linear potentiometer (Gamewell 140TS100) was fastened to a moveable hair-line assembly mounted on the display screen of the reader. The potentiometer had a 40kΩ resistance and a 1% linearity. The fourteen-inch linear travel of the potentiometer permitted the hair-line assembly, which was mounted on precision ball bushings, to traverse the entire vertical distance of the display screen. The output from the potentiometer, which was powered by a 12-volt battery, was a direct measure of vertical distances on the display screen. An analog-to-digital (A/D) converter (Teledyne Philbrick Model 4111) was used to convert this voltage signal into its corresponding binary coded decimal (BCD) signal necessary to drive the digital printer (Anadex Model DP-650A).

The following procedure was used when reading the 16-mm films (refer to Figure C-1 and Figure C-2):

1) The reference line immediately below the spectrum being read was lined-up with the measuring hair-line while the hair-line assembly was resting on the fixed stops.
2) The following signals were then recorded:
   a) spectometer baseline just prior to the spectrum
   b) H_2O absorption, 3.90-μm window, CO_2 absorption, CO absorption, 5.3-μm window.
   c) the two adjacent D_f signals directly above the spectrum, and the corresponding $D_f + D_t$ signal
   d) the pressure directly above the spectrum
3) The film was advanced to the next spectrum, and steps 1 and 2 were repeated.

Step 1 in the above procedure was also used when the ten "before-run" Hot-gas-pyrometer baseline and D_s signals were recorded. The

reproducibility of measurements made with this equipment corresponded to ±0.2-mm deflection on the oscilloscope screen.

Data Reduction

The various oscilloscope deflections measured from the 16-mm film, in the form of the digital printout, were used as the input data for a computer program, and all data reduction was done on a Univac 1108 digital computer. The output from the computer program consisted of the reduced unfiltered data in tabular form, and a plot of the various filtered variables as a function of laboratory time. The plots were generated by the University of Utah Computer Center's Gerber plotter (Model #622 Graphic Display System).

APPENDIX D

DIGITAL FILTERING ALGORITHM

This section describes the digital filtering algorithm used to eliminate the high frequency "noise" from the final data. The nature of the "noise" being removed is thoroughly discussed in Chapter IV, thus, only its characteristics relating to the filtering algorithm will be mentioned here. The two most common algorithms used for digital smoothing are the arithmetic average and the numerical equivalent of the first order lag, or simply called digital lag. The digital lag algorithm was used exclusively in this work and will be the only algorithm discussed.

The numerical equivalent of a simple RC low pass filter was first described by Jursik [48] and then later by Goff [49] and Smith [50]. The The differential equation describing the first-order lag for continuous signals is

$$\tau_f \frac{dy(t)}{dt} + y(t) = x(t) \quad , \tag{1}$$

where y(t) is the input signal to the filter, x(t) is the filter output and τ_f is the time constant of the filter.

This equation can be expressed by finite differences and rearranged to yield

$$y_n = \alpha x_n + (1-\alpha) y_{n-1} \quad , \tag{2}$$

where y_n is the present output value, y_{n-1} is the previous output value,

λ_n is the present input value, and α is a weighting function. The time function response of the system relates the weighting function α, to the filter time constant τ_f and the sampling time interval T_{ss}. When τ_f is considerably larger than T_{ss}, $\alpha \cong T_{ss}/\tau_f$. Thus, the filter's bandwidth can be easily varied by changing the value of the weighting function α. If a fixed input is applied, the output of equation (2) approaches the input monotonically at a rate proportional to both the frequency of computation and the value of α.

The basic limitation to digital lag filtering is dictated by Shannon's sampling theorem [50], which states that if the continuous signal is to be completely recovered from its sampled counterpart, the sampling frequency must be at least twice the highest frequency component in the signal. That is not to say the sampling frequency has to be at least twice the highest frequency of interest.

The effective sampling frequency of the equipment was 800 Hz, while the observed "noise" was only 200-300 Hz. Thus, the requirement of Shannon's sampling theorem was met, and digital lag filtering was applicable to the data.

Before the digital filtering algorithm was applied to the data, its performance was tested on some artifically created signals. This preliminary work was done on a Wang 2200 mini-computer equipped with a plotter. Figures D-1 and D-2 show the results of single and double stage filtering respectively. The original signal in both of these plots, $y = \sin(x) + \sin(11x-1) + \sin(17x-5)$, has a "noise" which is typical of that found in the experimental data. The bottom sin(x) curve in each figure is the signal trying to be recovered from the original input signal, and is given for reference only. As would be expected, the two

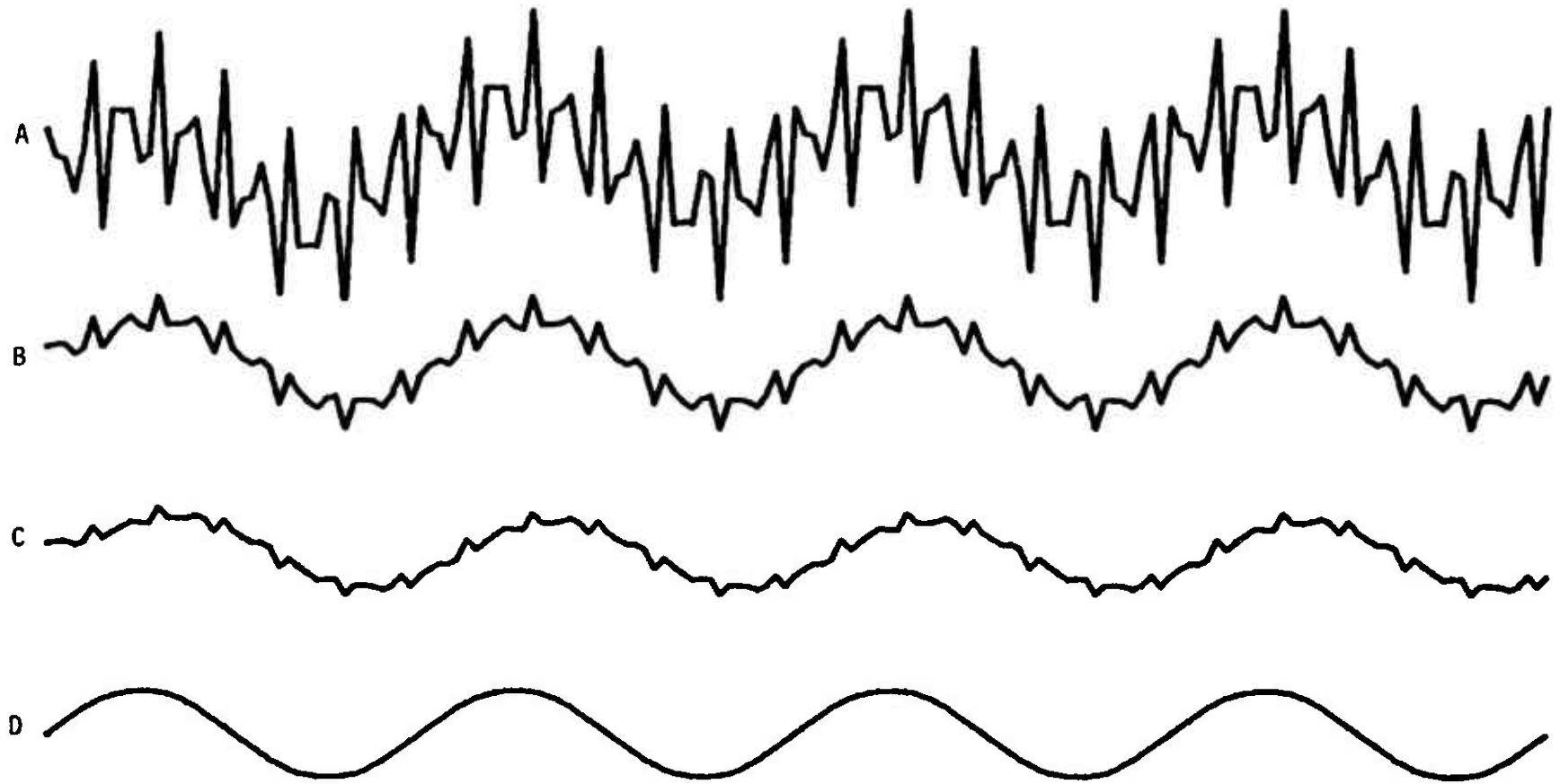

FIGURE D-1. PERFORMANCE TEST OF THE SINGLE-STAGE DIGITAL FILTER. A) input signal: $y = \sin(x) + \sin(11x-1) + \sin(17x-5)$, B) output signal for $\alpha = \pi/10$, C) output signal for $\alpha = \pi/20$, and D) $\sin x$, for reference only. (This work was done on a Wang 2200 minicomputer.)

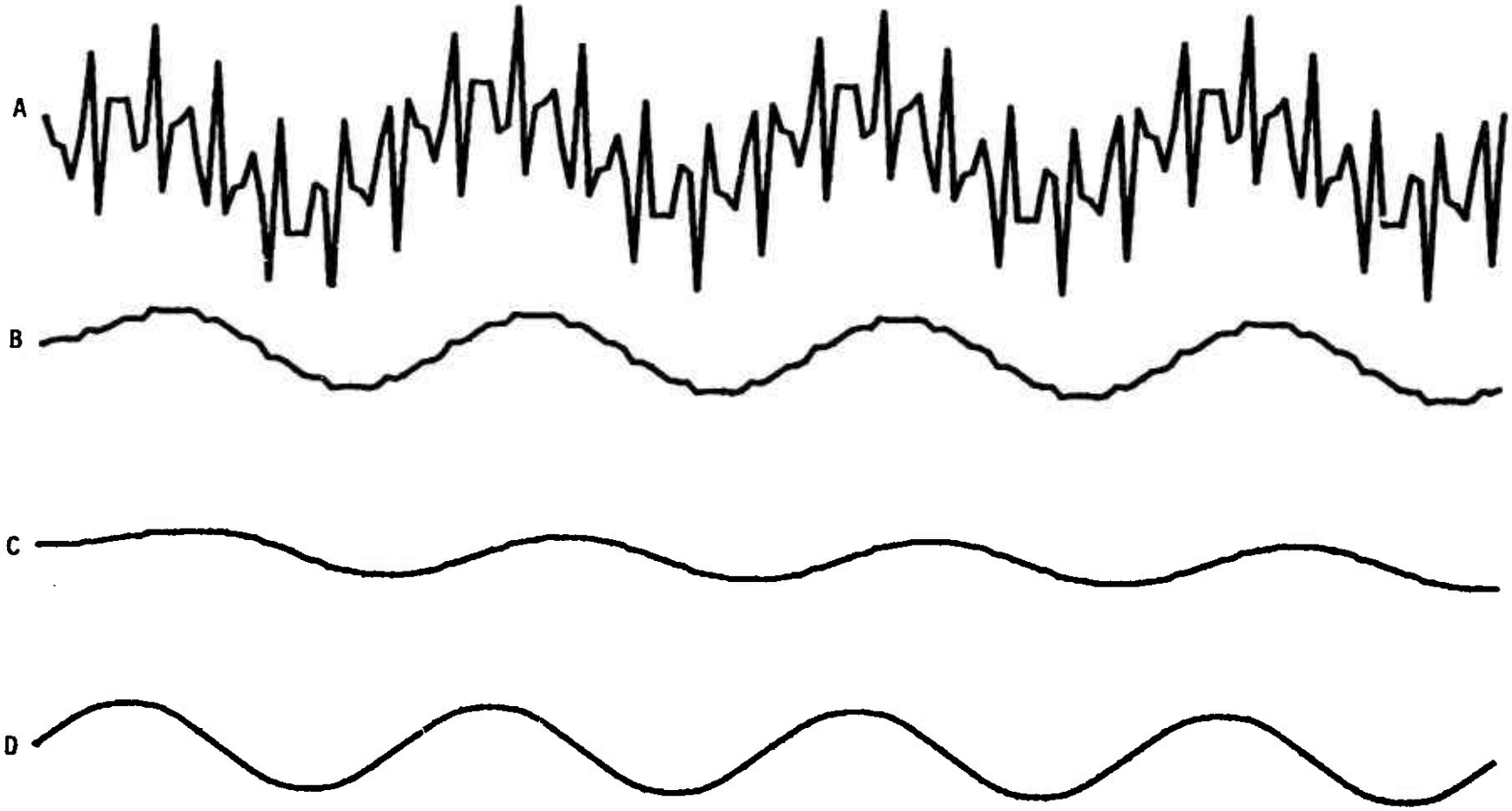

FIGURE D-2. PERFORMANCE TEST OF THE TWO-STAGE DIGITAL FILTER. A) input signal: $y = \sin(x) + \sin(11x-1) + \sin(17x-5)$, B) output signal for $\alpha = \pi/10$, C) output signal for $\alpha = \pi/20$, and D) $\sin x$, for reference only. (This work was done on a Wang 2200 minicomputer.)

stage filter is superior to the one stage filter, and as α is increased, the initial value effects persist for a longer time. The observed gain and phase angle of the digital filter compare well with those predicted by the Bode diagram for the particular systems.

Figures D-3 through D-8 show the results of the two-stage digital filtering of the experimental data. Note that the two α's used, $\pi/10$ and $\pi/20$, are the same as those used in the preceeding preliminary testing. Since all five variables were filtered, the phase lag problem has been implicitly treated. This treatment is only exact when all the variables have the same frequency. However, any errors introduced by slight frequency differences would be small and were not treated. The gain ratios predicted by the Bode diagram were used to approximately adjust the magnitudes of the filtered data. Although the initial value effects persist longer for the larger value of α, the initial portion of the data in all cases must be considered erroneous. Since the $\pi/10$ value of α gave a reasonable degree of filtering, with a minimum amount of initial value effects, this value was used exclusively.

Figures D-9 and D-10 show the unfiltered and filtered data from a single-pressure-pulse test. Again, the digital-lag filter was applied to all the variables. Although the filtering changed the shape of the initial segment of the pressure-pulse, the advantages derived from the approximate treatment of the phase lag which this provided was considered to out-weigh the slight disadvantage of a distortion in the pressure trace.

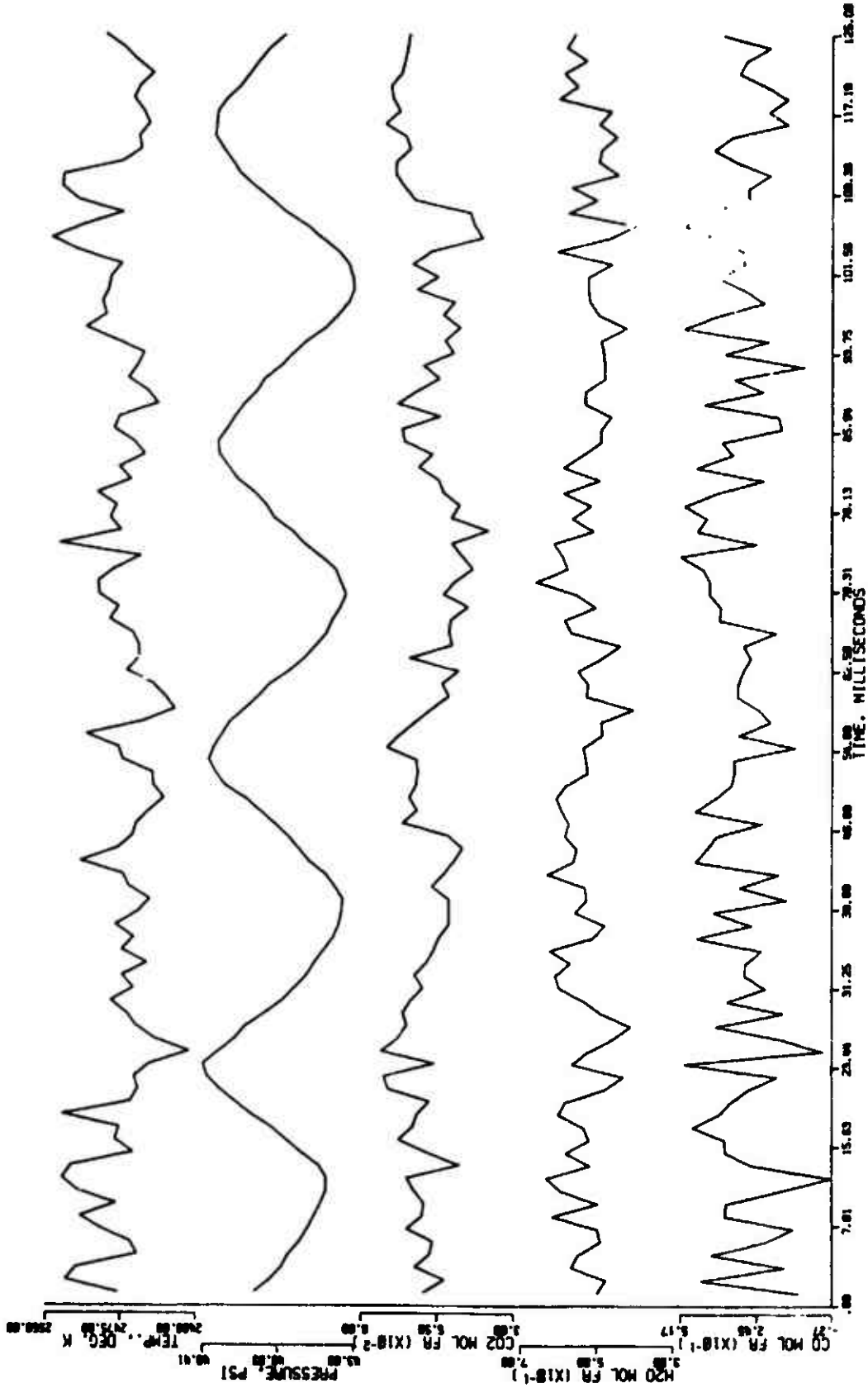

FIGURE D-3. UNFILTERED DATA FROM A 32 Hz. OSCILLATORY-PRESSURE TEST. (82 wt. % AP propellant [UFP], 3-5 mm, Run No. 3-31474)

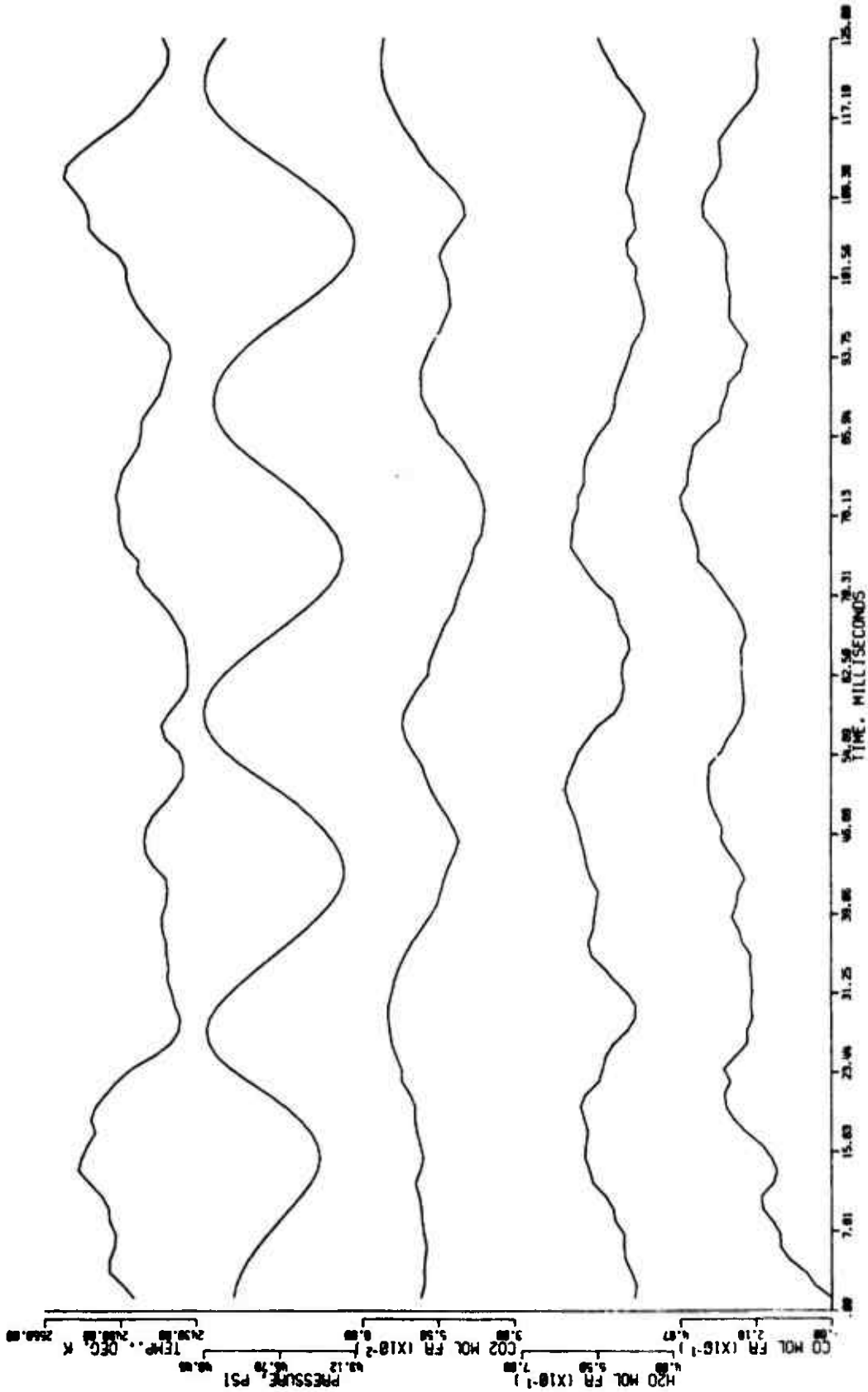

FIGURE D-4. FILTERED FORM OF THE DATA PRESENTED IN FIGURE D-3. (two-stage filter, $\alpha = \pi/10$)

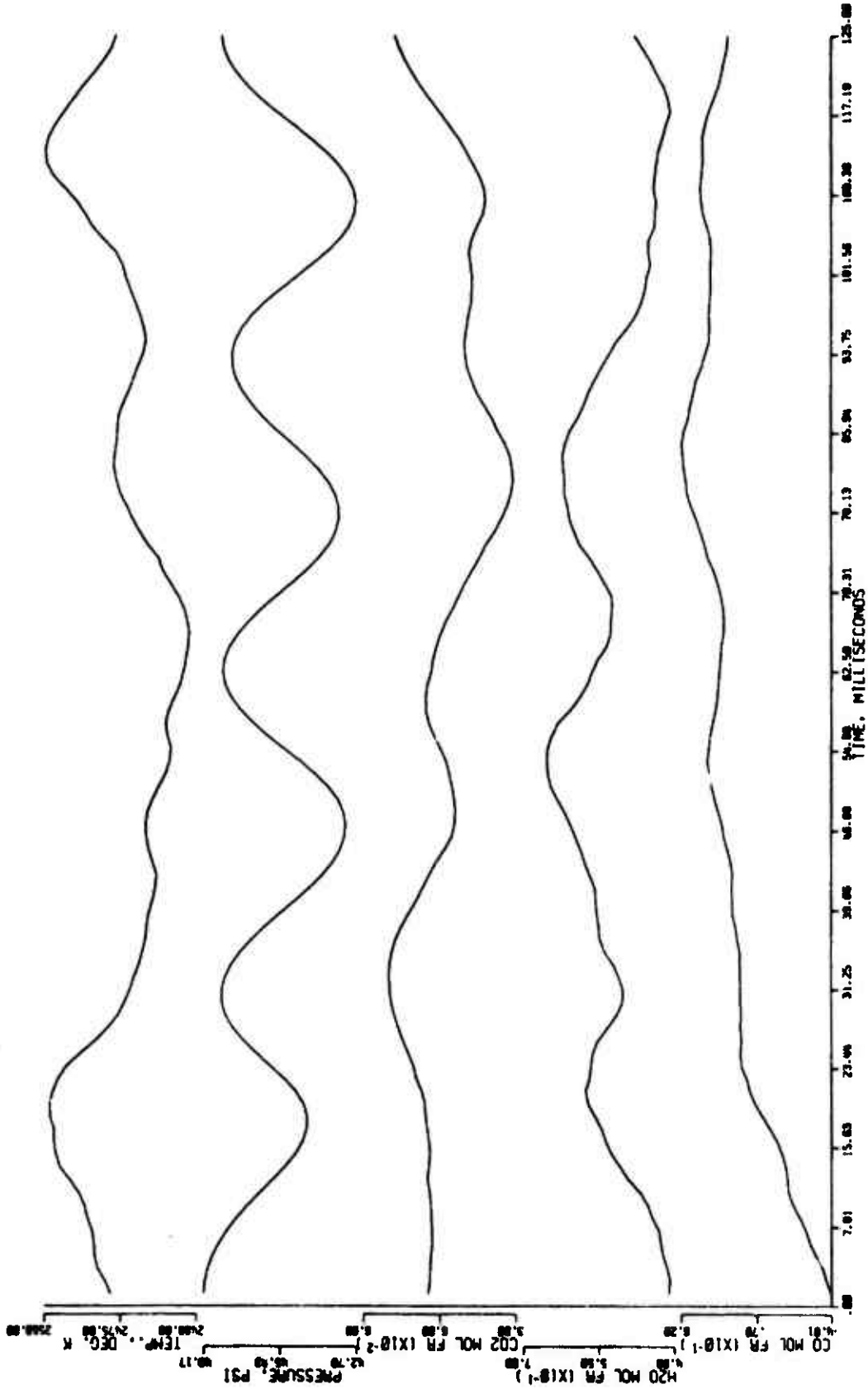

FIGURE D-5. FILTERED FORM OF THE DATA PRESENTED IN FIGURE D-3. (two-stage filter, $\alpha = \pi/20$)

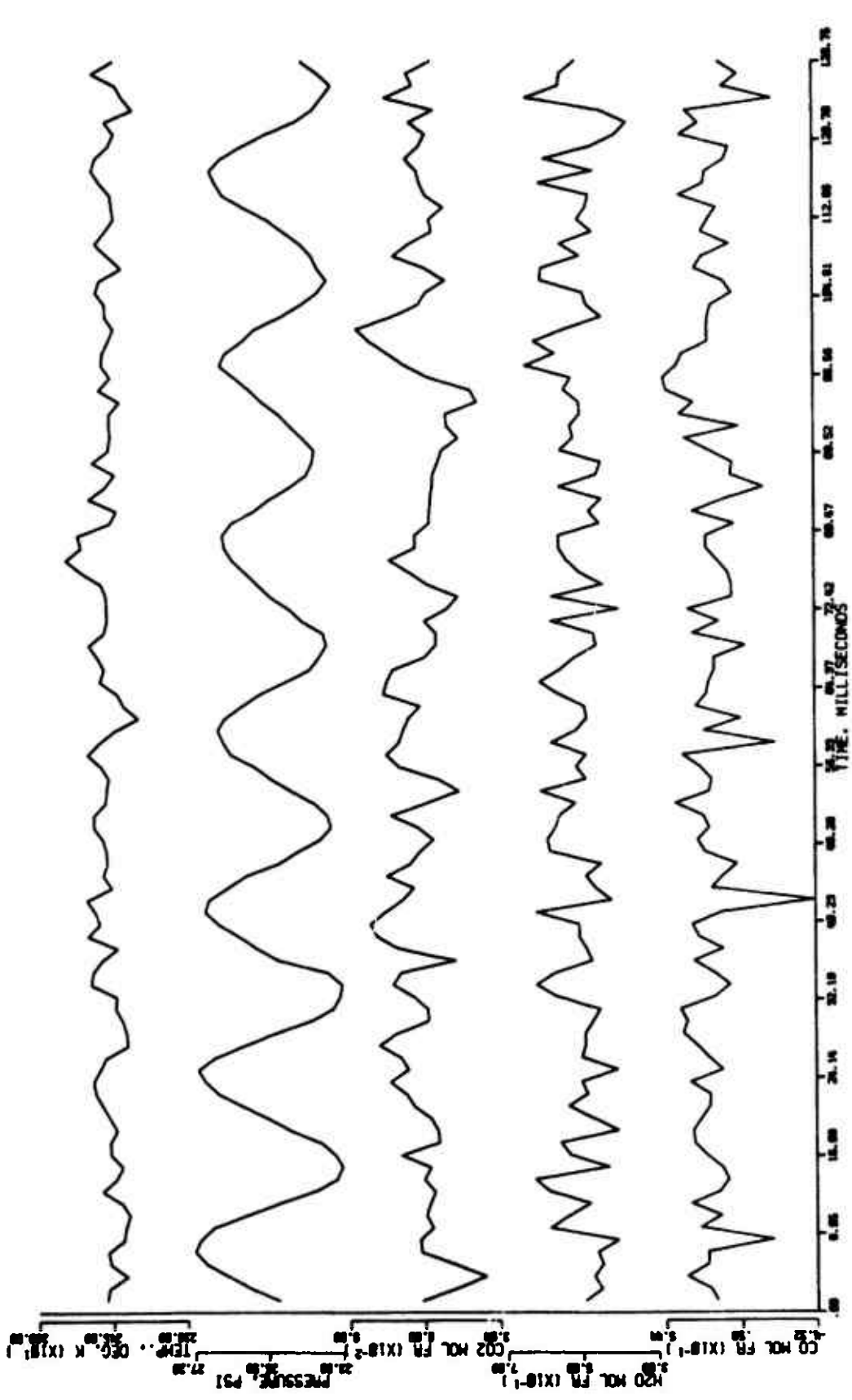

FIGURE D-6. UNFILTERED DATA FROM A 55 Hz. OSCILLATORY-PRESSURE TEST. (82 wt. % AP propellant [UFP], 3-5 mm, Run No. 6-31574)

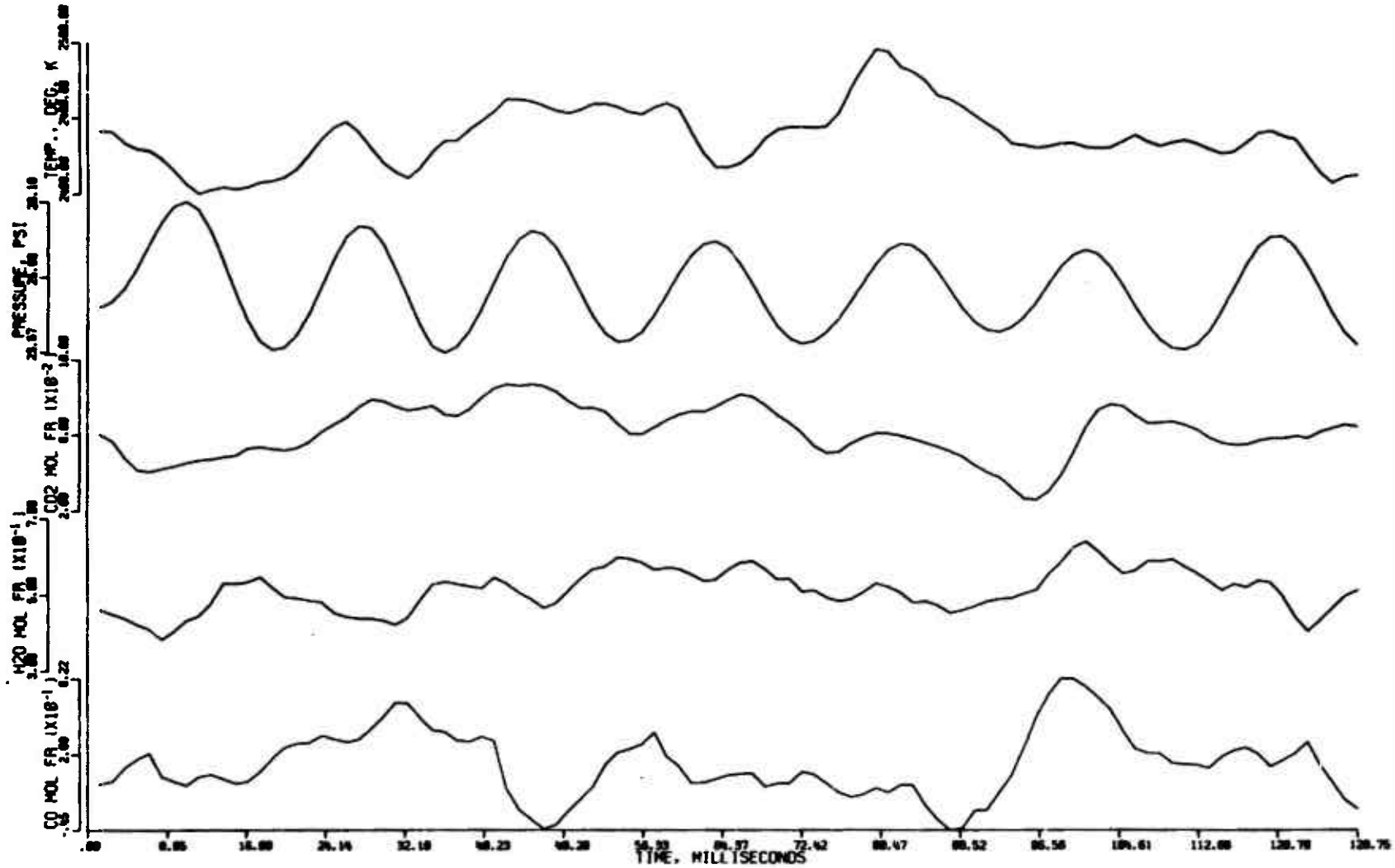

FIGURE D-7. FILTERED FORM OF THE DATA PRESENTED IN FIGURE D-6. (two-stage filter, $\alpha = \pi/10$)

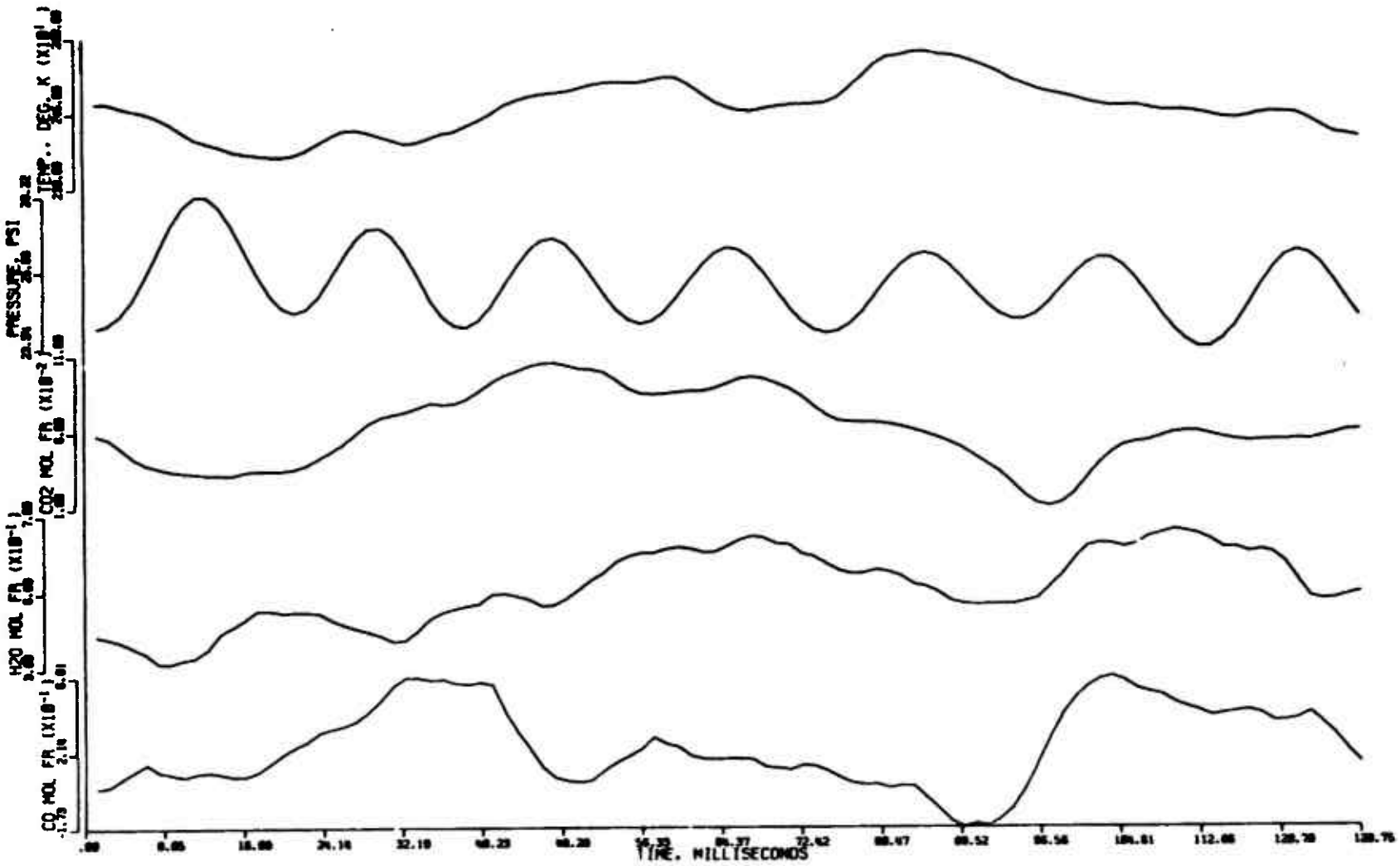

FIGURE D-8. FILTERED FORM OF THE DATA PRESENTED IN FIGURE D-6. (two-stage filter, $\alpha = \pi/20$)

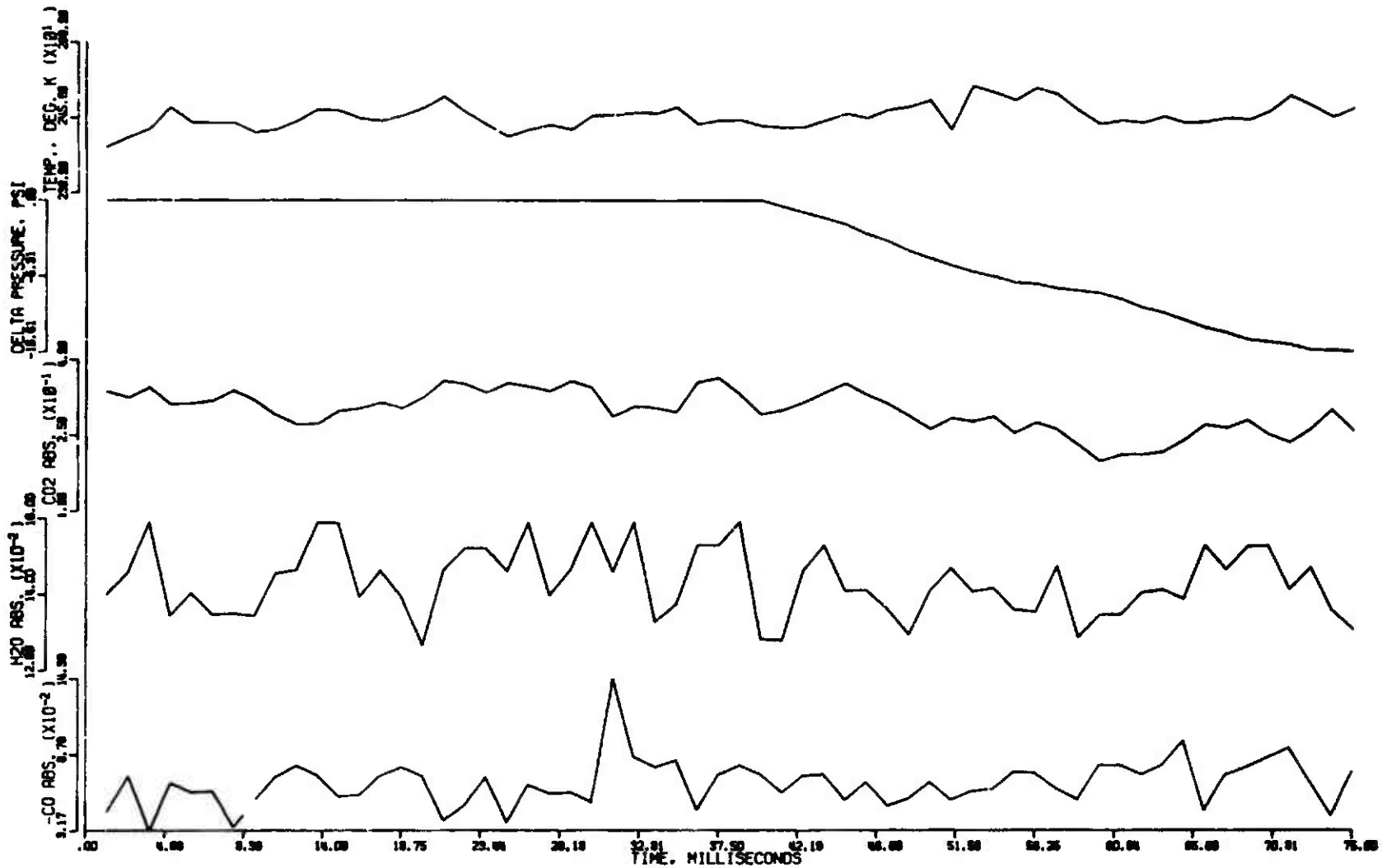

FIGURE D-9. UNFILTERED DATA FROM A SINGLE-PRESSURE-DECREASE-PULSE TEST. (80 wt. % AP propellant [UFI], 3-5 mm, Run No. 5-4474)

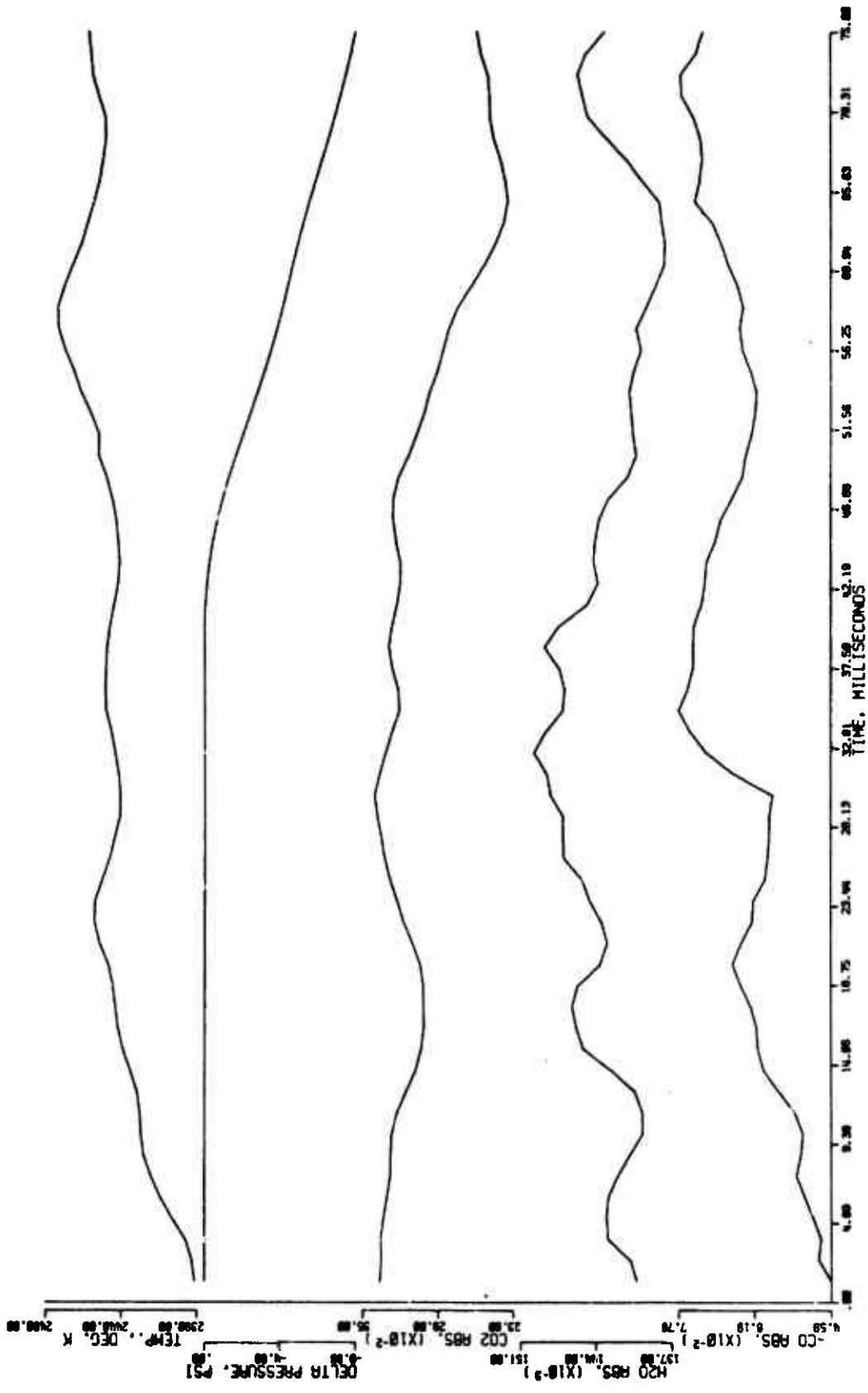

FIGURE D-10. FILTERED FORM OF THE DATA PRESENTED IN FIGURE D-9. (two-stage filter, $\alpha = \pi/10$)

APPENDIX E

EQUILIBRIUM COMBUSTION COMPUTER PROGRAM

An equilibrium combustion computer program was used during various aspects of this study. The computer program used was written by Curtis Selp, Robert Hall, Gerald Cahill and Robert Patton; and it was obtained from the United States Air Force Rocket Propulsion Laboratory, Edwards Air Force Base. The program is very general and it is capable of calculating many of the standard rocket motor parameters (i.e., optimum specific impulse, ionized exhaust products, and equilibrium combustion products in the combustion chamber, throat, and nozzle of a rocket motor). However, in this study the program was only used to calculate the adiabatic flame temperature and the equilibrium combustion products in the chamber. The program will work with a system containing up to thirty-two elements. The following input data were required for each run:

1) A list of propellant ingredients and their respective thermochemical data.
   a) heat of formation, (kcal/formula wt.)
   b) density, g/cc
   c) name and amount of elements making up each ingredient
2) chamber and exhaust pressure.
3) the propellant formulation, in weight percent of the listed ingredients.

A copy of a typical computer output is given in Table E-1. The first column of gas properties is for the combustion chamber, while the second is for the exhaust conditions. Included in the list of gas properties is the adiabatic flame temperature, and the equilibrium specie composition given in moles/100 grams. In addition to this output, the computer program lists the species considered, based on the input ingredients.

The propellants studied in this work were exclusively ammonium perchlorate (AP) and hydroxyl-terminated-polybutadiene (HTPB) based composite solid propellants (see Appendix G). The thermochemical data used for the HTPB was obtained from Thiokol Chemical Corporation in Brigham City, Utah. The HTPB has a heat of formation of 4 kcal/100 gm, a density of 0.899 g/cc, and an elemental composition of $C_{7.271}H_{10.982}O_{0.094}N_{0.007}$.

Table E-2 gives the adiabatic flame temperatures and the major species concentrations for even AP weight percent (wt.%) propellants (between 80 and 92 weight percent) containing 1.2 wt.% NaCl and 1/2 wt.% carbon black. These adiabatic temperature data are plotted in Figure E-1 as a function of the propellant AP content. The species concentrations are plotted as a function of the propellant AP content in Figure E-2. The flame temperature and the species concentration data for the 82 AP wt.% propellant are plotted in Figure E-3 as a function of the combustion chamber pressure.

Since propellants containing 0.10, 0.25 and 0.50 wt.% NaCl were used in this study, the effect of a small change in the NaCl content on the flame temperature and composition was studied. Table E-3 gives the adiabatic flame temperatures and the major species concentrations for 80, 82 and 85 AP wt.% propellants containing 1/2 wt.% carbon black and no NaCl.

TABLE E-1

EQUILIBRIUM COMBUSTION COMPUTER PROGRAM OUTPUT FOR
AN 82 WEIGHT PERCENT AP PROPELLANT CONTAINING
1/2 WEIGHT PERCENT CARBON BLACK. (75 psia)

UNIVERSITY OF UTAH CHEMICAL ENGINEERING DEPARTMENT

PROPELLANT	HF	DENS	WT	MOL	VOL
AP	-69,4200	1,9600	82,0000	,6979	41,8367
HTPB	4,0000	,8990	16,1800	,1618	17,9978
IPDI	-73,5000	1,0860	1,3200	,0059	1,2155
C	,0000	2,2600	,5000	,0416	,2212
NACL	-98,3210	2,1630	,0000	,0000	,0000

GRAM ATOMS /100 GRAMS	C	H	O	N	CL
	1,2894	4,6754	2,8186	,7109	,6979

ENTHALPY = -48,23680 DENSITY =1,632

PRESSURE (PSIA)	75,000	5,000
EPSILON	,000	,000
ISP (SHIFT)	,000	203,165
ISP (FROZEN)	,000	204,350
TEMPERATURE (K)	2557,012	1550,444
MOLECULAR WEIGHT	22,947	23,086
MOLES GAS/100G	4,358	4,332
CF	,000	,000
PEAE/M (SECONDS)	,000	28,579
GAMMA	1,240	1,263
HEAT CAP (CAL)	44,761	41,320
ENTROPY (CAL)	270,330	270,330
ENTHALPY (KCAL)	-48,237	-95,653
C* (FEET/SECOND)	,000	,000
ITERATIONS	6	9
H	,02537	,00010
H2	,73535	,86794
H2O	1,24430	1,12079
N2	,35521	,35545
CO	1,01486	,88091
CO2	,27447	,40847
CLH	,68116	,69782
HO	,00950	,00000
O2	,00015	,00000
CHO	,00005	,00000
CL	,01368	,00007

TA8LE E-2

EQUILI8RIUM FLAME COMPOSITION ANO AOIA8ATIC FLAME TEMPERATURES FOR AP/HTPB COMPOSITE PROPELLANTS CONTAINING 1/2 WT.% NaCl, 1/2 WT.% CARBON BLACK

Pressure	Wt.% AP	Adiabatic Flame Temp. °K	Equilibrium Concentrations, Mole Fraction				
			H_2	H_2O	CO	CO_2	HCl
50	80	2398.4	0.206	0.248	0.258	0.052	0.150
50	82	2567.4	0.159	0.293	0.225	0.066	0.157
50	84	2704.5	0.114	0.335	0.185	0.086	0.162
50	86	2794.1	0.076	0.369	0.142	0.101	0.165
50	88	2823.2	0.047	0.393	0.092	0.118	0.168
50	90	2788.0	0.027	0.407	0.055	0.187	0.172
50	92	2682.1	0.012	0.413	0.023	0.124	0.180
75	80	2404.5	0.206	0.248	0.258	0.053	0.150
75	82	2579.6	0.159	0.294	0.225	0.066	0.158
75	84	2724.9	0.114	0.337	0.186	0.086	0.164
75	86	2822.8	0.075	0.372	0.142	0.102	0.167
75	88	2856.9	0.045	0.396	0.095	0.119	0.170
75	90	2820.8	0.025	0.409	0.053	0.129	0.174
75	92	2708.3	0.011	0.414	0.022	0.126	0.186
100	80	2408.3	0.206	0.248	0.258	0.053	0.150
100	82	2587.5	0.159	0.295	0.225	0.066	0.158
100	84	2738.5	0.114	0.338	0.186	0.083	0.165
100	86	2842.6	0.074	0.373	0.141	0.102	0.169
100	88	2880.6	0.044	0.398	0.094	0.121	0.171
100	90	2844.0	0.024	0.411	0.052	0.131	0.176
100	92	2726.5	0.010	0.416	0.021	0.127	0.183

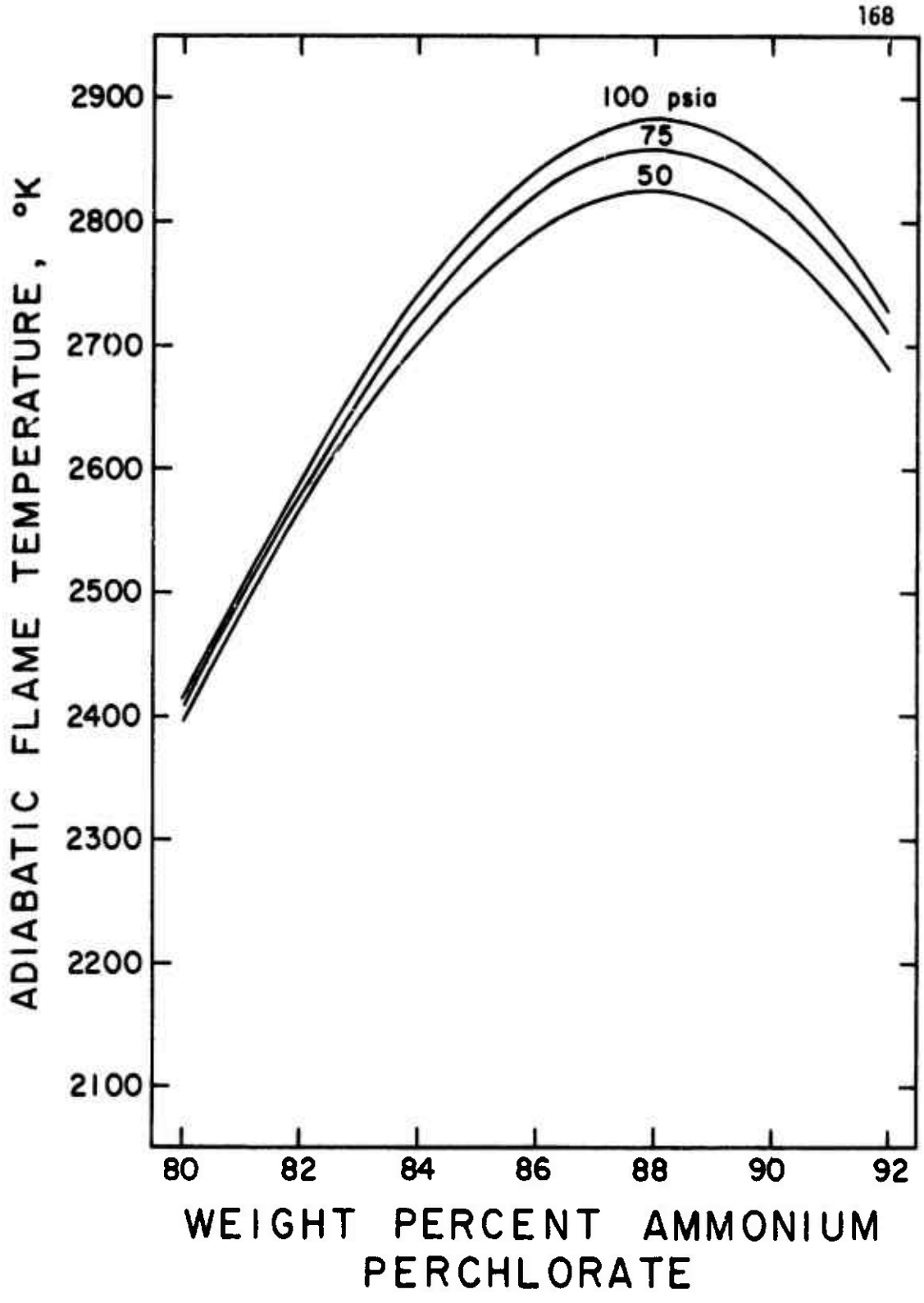

FIGURE E-1. ADIABATIC FLAME TEMPERATURES FOR AP-HTPB PROPELLANTS WITH VARIOUS AP CONTENTS. (1/2 wt. % NaCl, 1/2 wt. % carbon black)

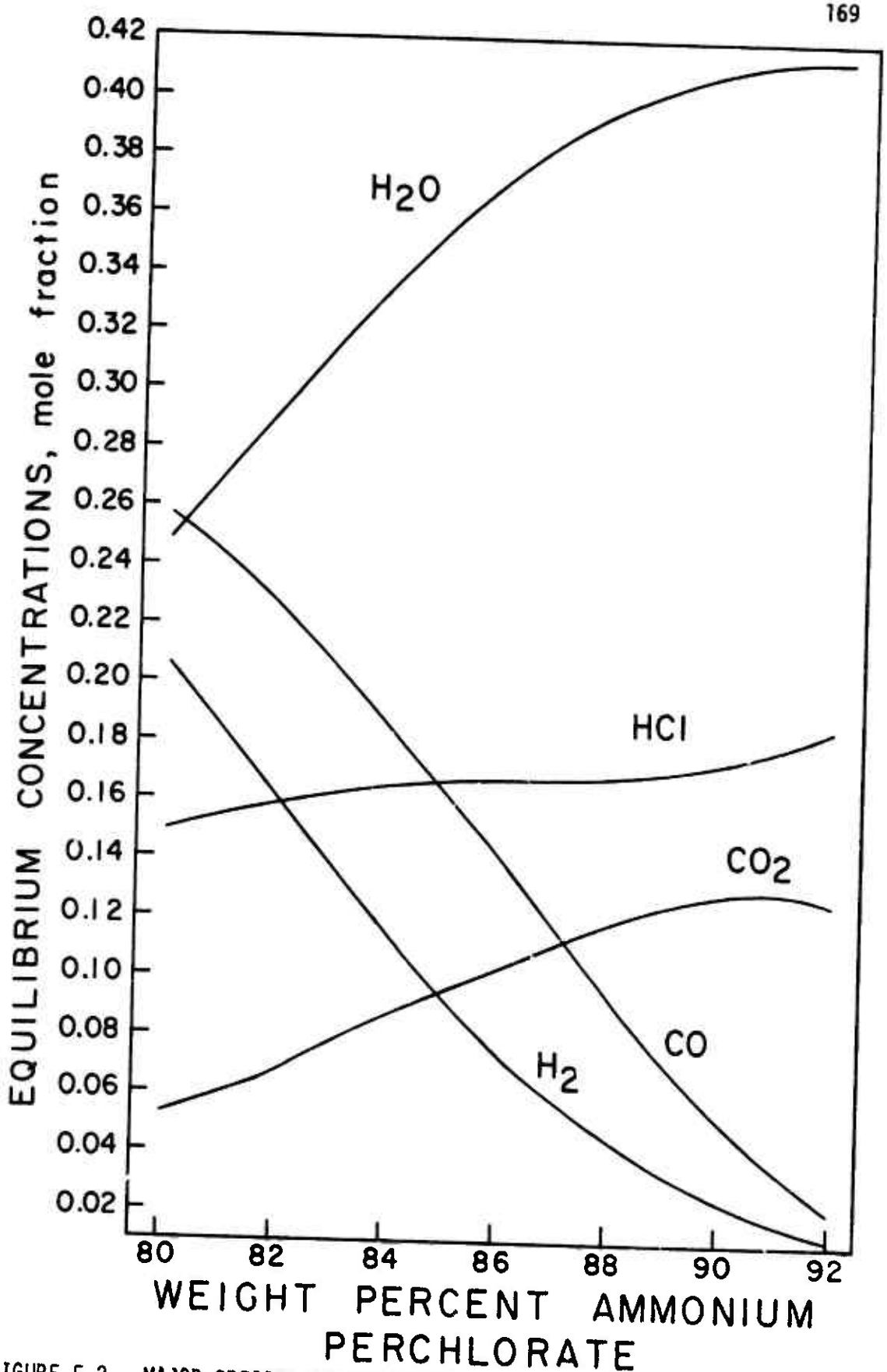

FIGURE E-2. MAJOR SPECIES CONCENTRATIONS FOR AP-HTPB PROPELLANT WITH VARIOUS AP CONTENTS. (1/2 wt. % NaCl, 1/2 wt. % carbon black)

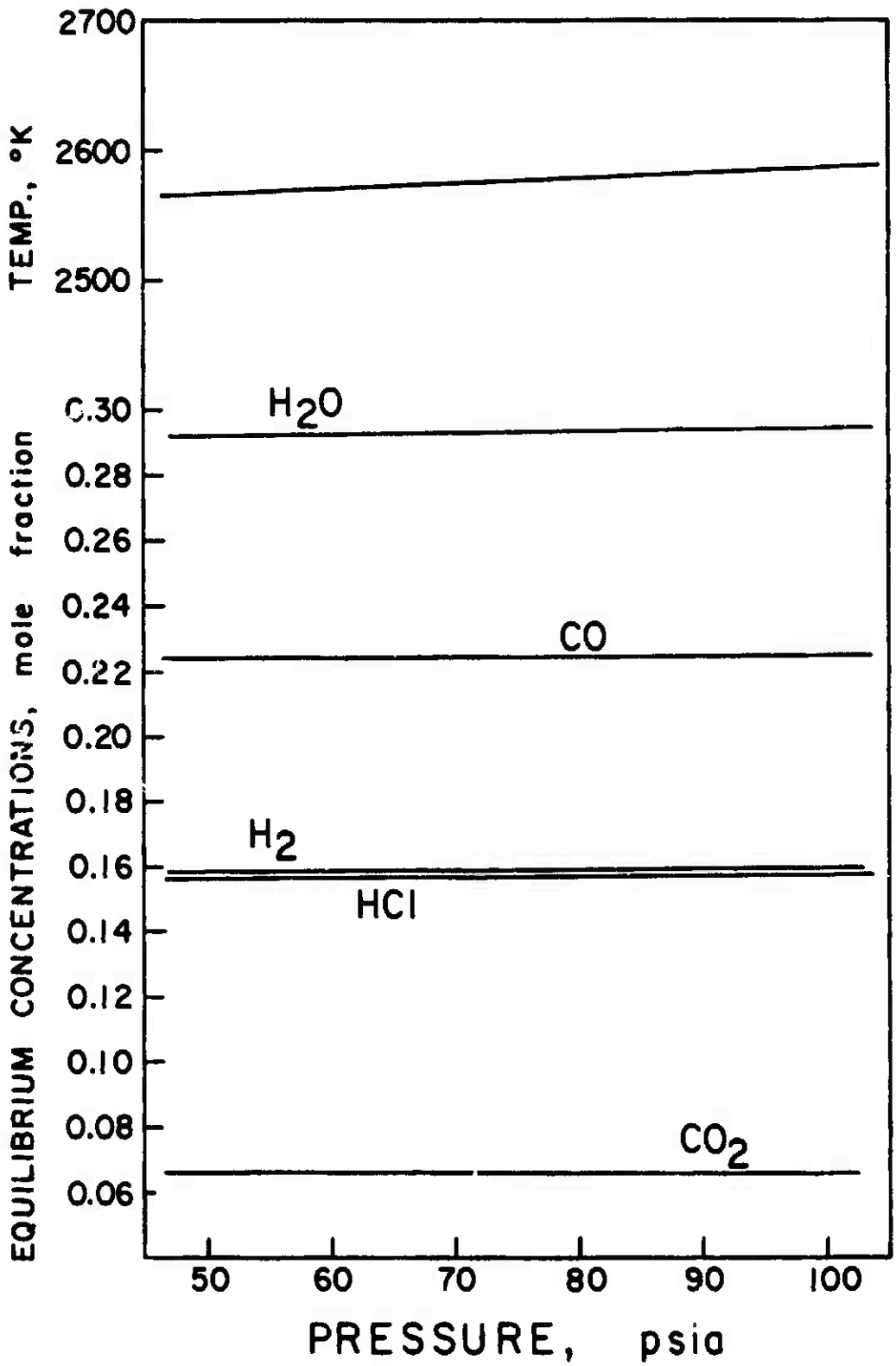

FIGURE E-3. TEMPERATURE AND CONCENTRATION DATA FOR AN 82 WEIGHT PERCENT AP PROPELLANT AT VARIOUS COMBUSTION CHAMBER PRESSURES.

TABLE E-3

EQUILIBRIUM FLAME COMPOSITION AND ADIABATIC FLAME TEMPERATURES FOR AP/HTPB PROPELLANTS CONTAINING 1/2 WT.% CARBON BLACK AND NO NaCl

Pressure	Wt.% AP	Adiabatic Flame Temp. °K	H_2	H_2O	CO	CO_2	HCl
50	80	2374.1	0.215	0.239	0.264	0.051	0.148
50	82	2545.8	0.169	0.285	0.233	0.063	0.156
50	85	2744.0	0.103	0.346	0.174	0.087	0.163
75	80	2379.5	0.215	0.239	0.264	0.052	0.148
75	82	2557.0	0.169	0.286	0.233	0.063	0.156
75	85	2767.4	0.102	0.348	0.174	0.088	0.165
100	80	2382.9	0.216	0.240	0.265	0.051	0.149
100	82	2564.2	0.169	0.286	0.233	0.063	0.157
100	85	2783.1	0.102	0.349	0.175	0.088	0.166

The data in Tables E-2 and E-3 set the upper and lower limits for the NaCl wt.% range used in this study. Comparison of these data clearly indicates that this 1/2 wt.% NaCl change has a relatively small effect on both the flame temperature and composition. Therefore, the effect of the smaller NaCl content variation of the propellants used was assumed to be negligible.

APPENDIX F

PROPELLANT FORMULATIONS AND PREPARATION

The propellants used in this study were exclusively composite propellants consisting principally of ammonium perchlorate (AP) and hydroxyl-terminated-polybutadiene (HTPB). All of the propellants were prepared at the University of Utah in the Chemical Engineering Department's propellant mixing facility.

The propellants, with one exception, had a bimodal AP particle distribution. The exception was one propellant that had a unimodal particle distribution. However, in all cases, only two AP particle size distributions were used. The course AP was -48 + 100 mesh (150-300 μm) and was sieved at the University of Utah's propellant mixing facility in Tyler standard screens. The fine AP was ground by the Thiokol Chemical Corporation and was classified as 15-μm. The course AP/fine AP weight ratio was 60/40 for all the bimodal propellant formulations.

Thiokol Chemical Corp. supplied the HTPB (Arco Chemical Co., R-45) and its thermochemical data (see Appendix E) used in the equilibrium combustion calculations. Isophrone diisocyanate (IPDI), manufactured by the Midland Div. of the Dexter Corp., was used as the HTPB curing agent. An HTPB/IPDI weight ratio of 92.53/7.47 was used for all the propellant formulations. The carbon black used was manufactured by the Cabot Corporation (Regal SR, GP-6406), and the sodium chloride (Baker Chemical

Co., reagent grade) was ground and sieved to -325 mesh (less than 43 μm).

Approximately a dozen different propellant formulations were made and used during various aspects of this study. The compositions of the propellants used for the majority of the tests, including all of the reported tests, are given in Table F-1.

Mixing Procedures

A water-heated sigma-blade mixer, equipped with a variable-speed drive and enclosed in a vacuum chamber, was used to mix the propellants. Although the mixer could handle propellant batches from 300 to 700 grams, the batches were typically 500 or 600 grams. All propellant ingredients were weighed on a triple beam balance. The following procedure was followed each time a batch of propellant was prepared:

a) Several hours prior to preparing a batch of propellant the mixer's constant-temperature, circulating-water bath and the heated vacuum oven were turned on and allowed to reach steady-state. Both were operated at a temperature of 60°C.

b) The AP was weighed and added to the mixer. The course AP was added first.

c) The carbon black and sodium chloride were weighed and added to the mixer.

d) The HTPB and then the IPDI were weighed and added.

e) The vacuum chamber was sealed and the vacuum pump started.

f) The chamber was held at a low pressure for 15 to 20 minutes in order to de-aerate the mixture.

g) The mixer was started and operated for fifteen or twenty minutes.

h) The mixer was turned off and the vacuum released.

TABLE F-1

PROPELLANT FORMULATIONS

Prop. Code	Weight Percent						
	Fuel-Binder		AP				
	HTPB	IPDI	Total	Course Particles	Fine Particles	Carbon Black	NaCl
UFI	18.04	1.46	80.0	58.0	43.0	0.50	—
UFN	15.73	1.27	82.0	49.0	33.0	0.50	0.50
UFO	17.85	1.44	80.0	80.0	—	0.47	0.24
UFP	15.96	1.29	82.0	49.0	33.0	0.50	0.25
UFR	13.32	1.08	85.0	51.0	34.0	0.50	0.10

i) The sides and blades of the mixer were scraped with a spatula.

j) Steps e through h were repeated.

k) The propellant was examined to make sure that it was homogeneous. If not, steps e though h were repeated once more.

l) The propellant was placed in a preheated aluminum pan to form a slab approximately 2.5 cm thick.

m) The pan of propellant was placed in the 60°C vacuum oven and held at a low pressure for approximately 10 to 15 minutes in order to de-aerate the propellant slab.

n) The pan of propellant was then placed in an atmospheric curing oven at 58°C for four to five days.

The cured propellant slab was properly marked and then stored in the propellant locker. The procedure used for cutting propellant strands from these propellant slabs is discussed in Chapter II.

APPENDIX G

ADDITIONAL DATA FROM CONSTANT AND TRANSIENT PRESSURE TESTS

The additional data presented in this section are from the type of tests described in Chapter IV, and they supplement the discussion regarding constant-pressure, oscillatory pressure, and single-pressure-pulse tests found in that chapter. The individual figures are clearly labeled so that the data can be easily interpreted.

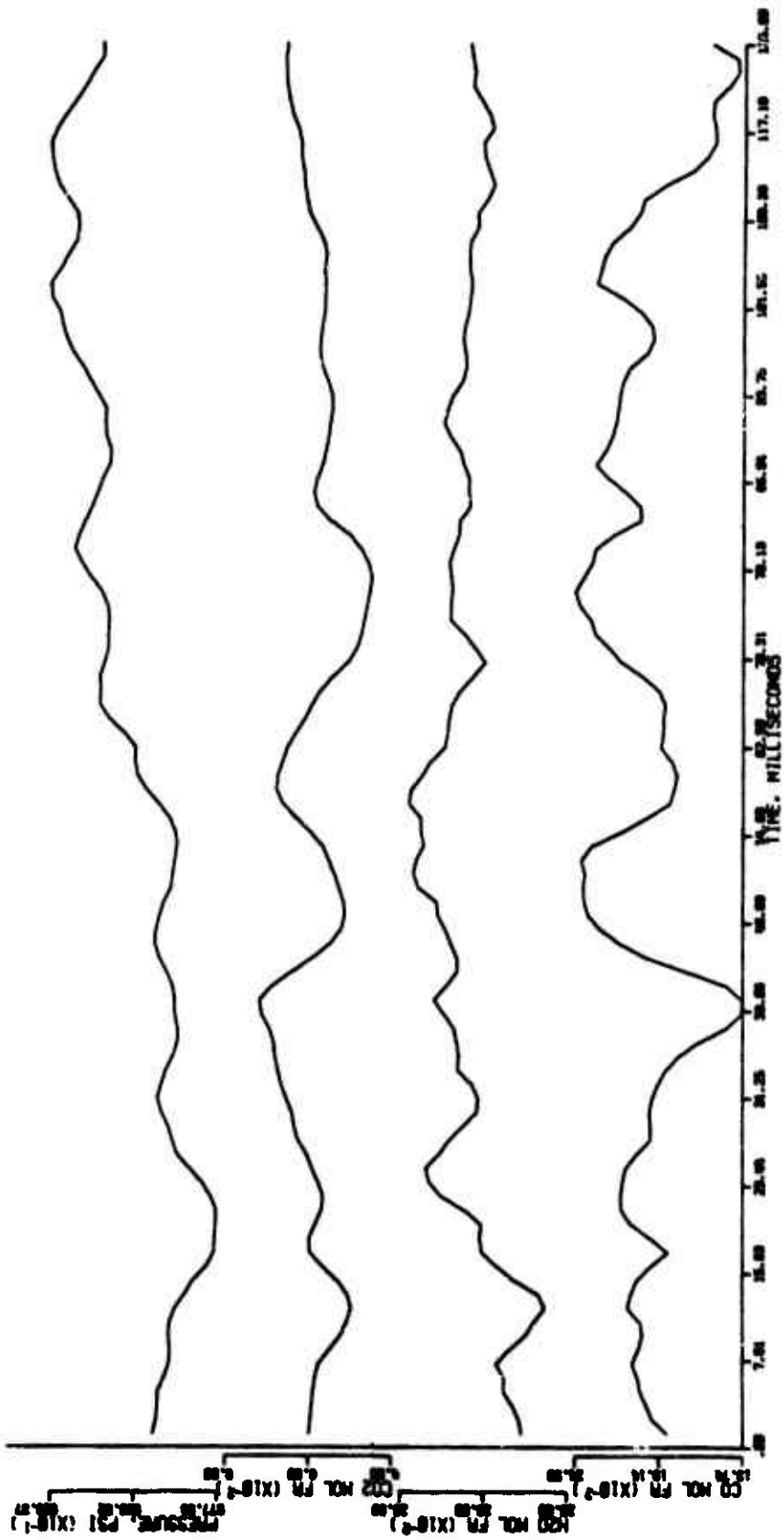

FIGURE G-1. CONCENTRATION PROFILES FROM A CONSTANT-PRESSURE TEST. (82 wt. % AP propellant [UFN], 3-5 mm, Run No. 4-122873)

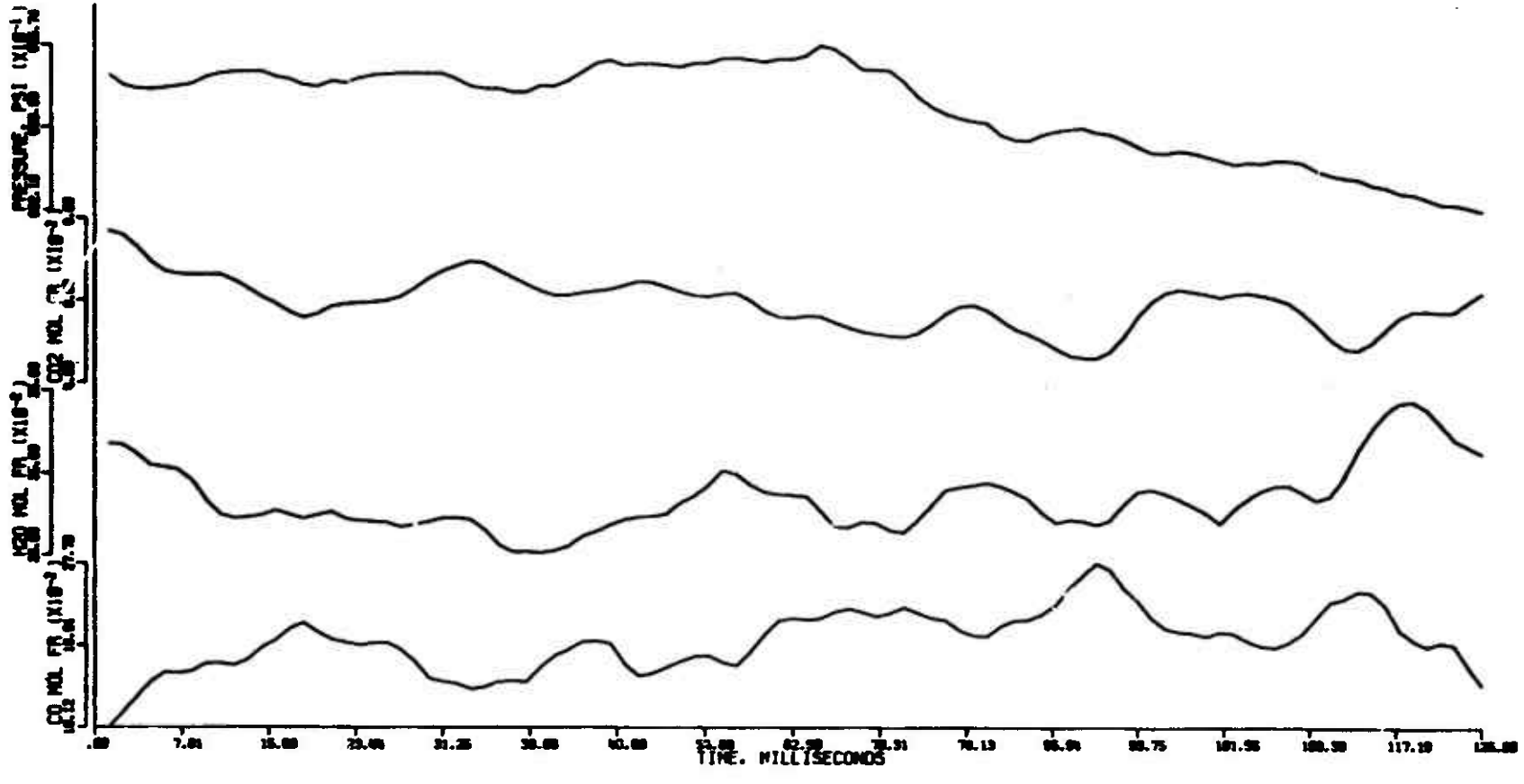

FIGURE G-2. CONCENTRATION PROFILES FROM A CONSTANT PRESSURE TEST. (82 wt. % AP propellant [UFN], 3-5mm, Run No. 6-122873)

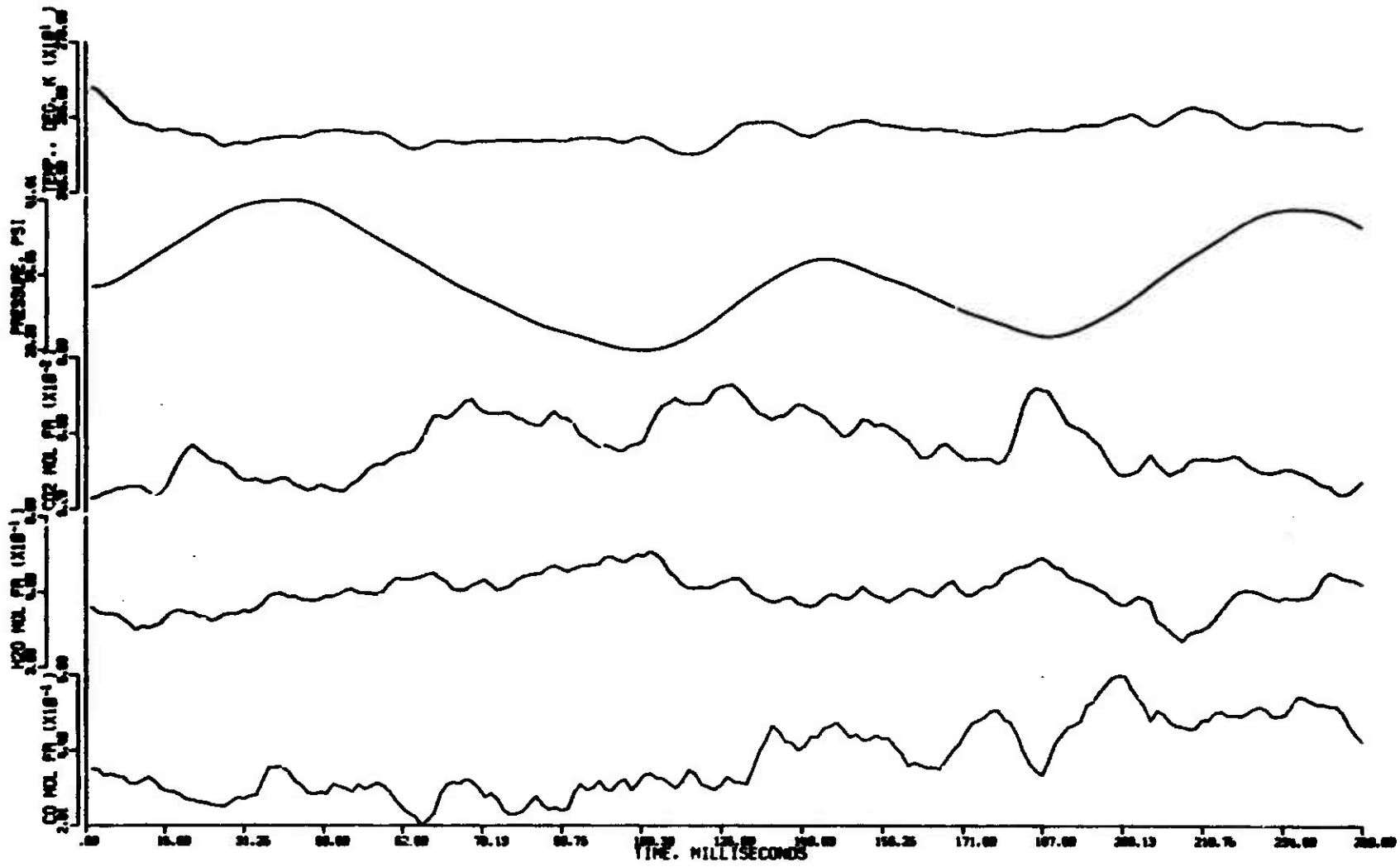

FIGURE G-3. TEMPERATURE AND CONCENTRATION PROFILES FOR A 10 Hz. OSCILLATORY-PRESSURE TEST. (82 wt. % AP propellant [UFP], 3-5 mm, Run No. 1-31474)

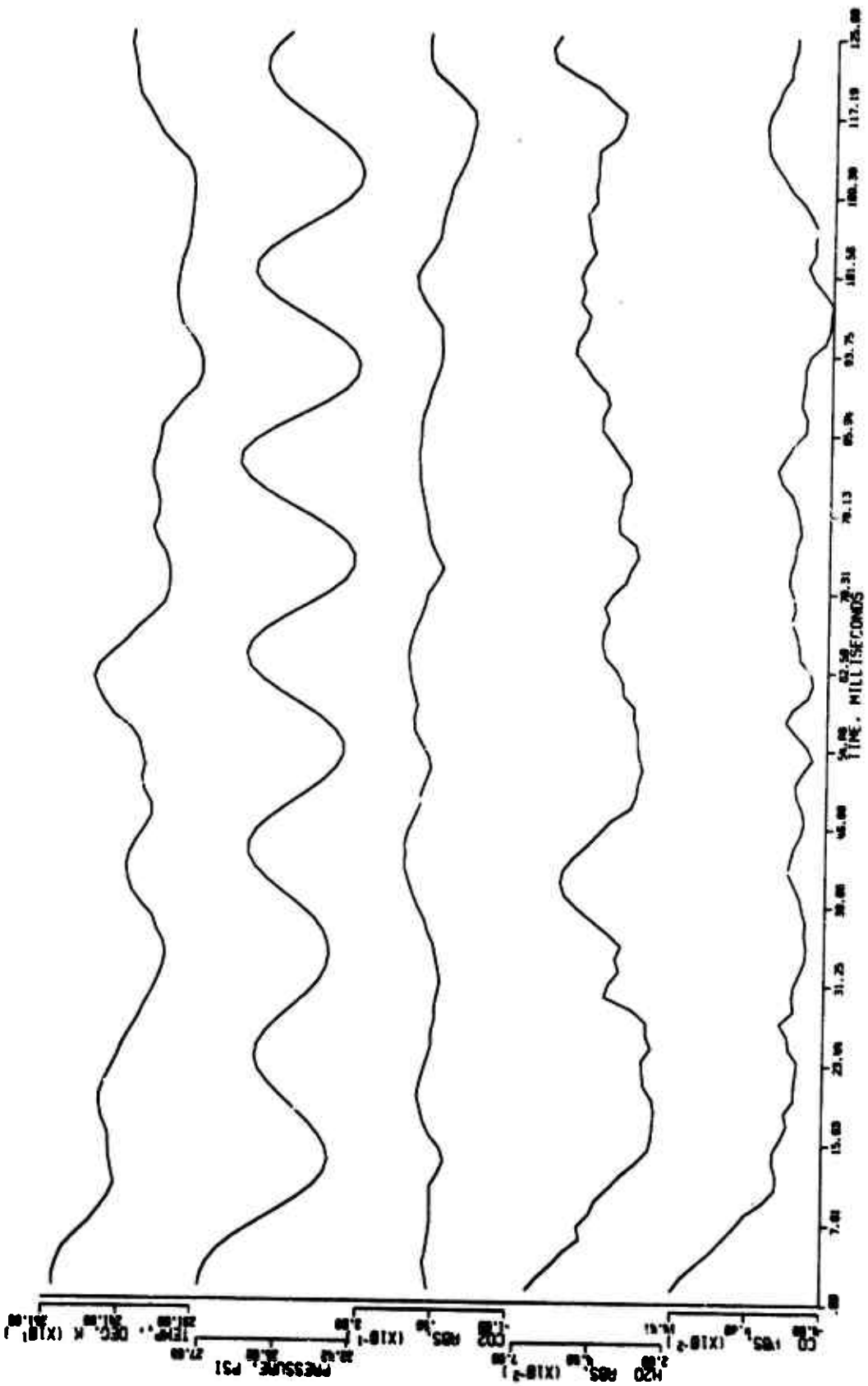

FIGURE G-4. TEMPERATURE AND PRESSURE-CORRECTED ABSORBANCE PROFILES FOR A 50 Hz. OSCILLATORY-PRESSURE TEST. (unimodal 80 wt. % AP propellant [UFO], 3-5 mm, Run No. 7-31574)

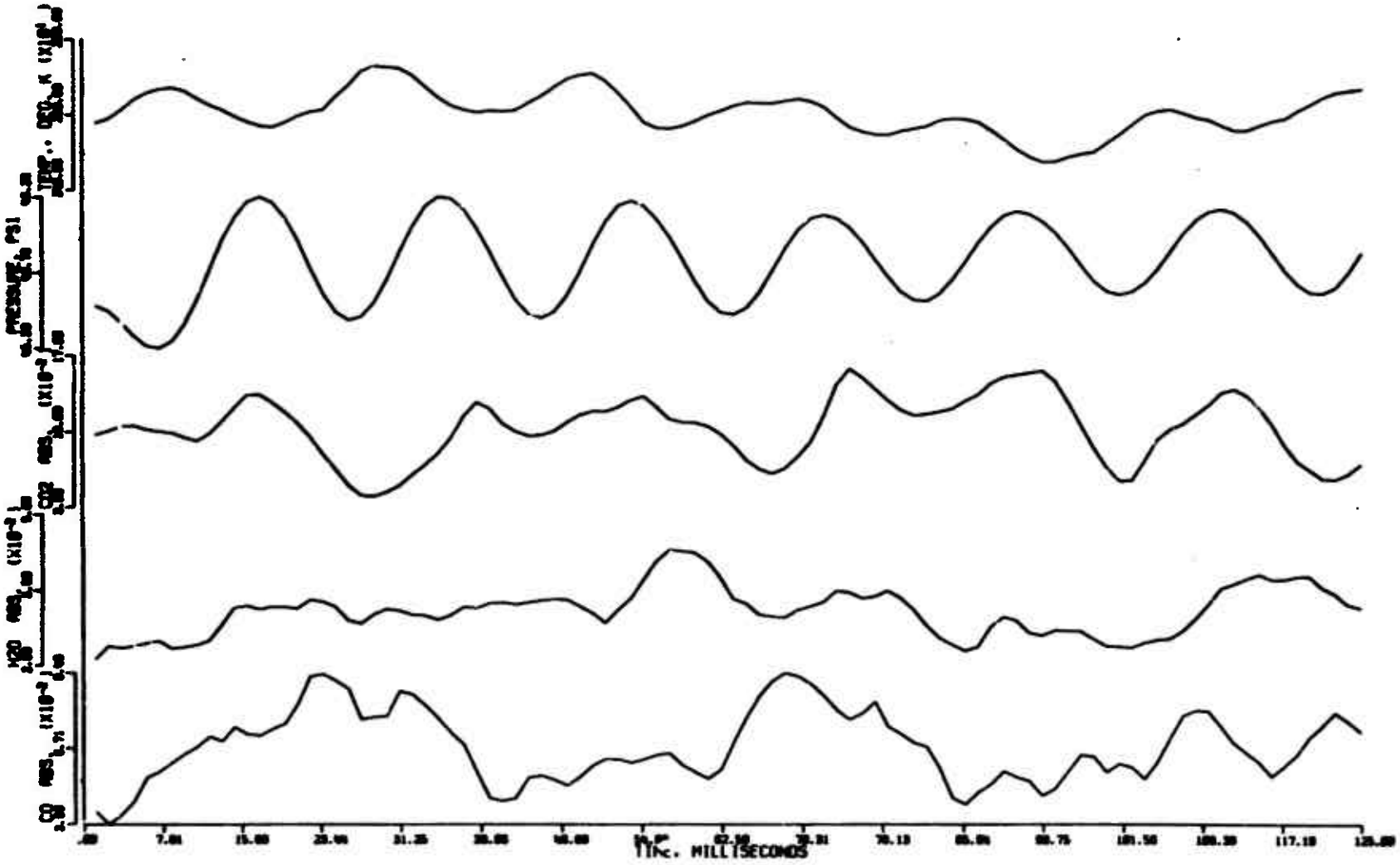

FIGURE G-5. TEMPERATURE AND PRESSURE-CORRECTED ABSORBANCE PROFILES FOR A 51 Hz. OSCILLATORY-PRESSURE TEST. (85 wt. % AP propellant [UFR], 3-5 mm, Run No. 9-4474)

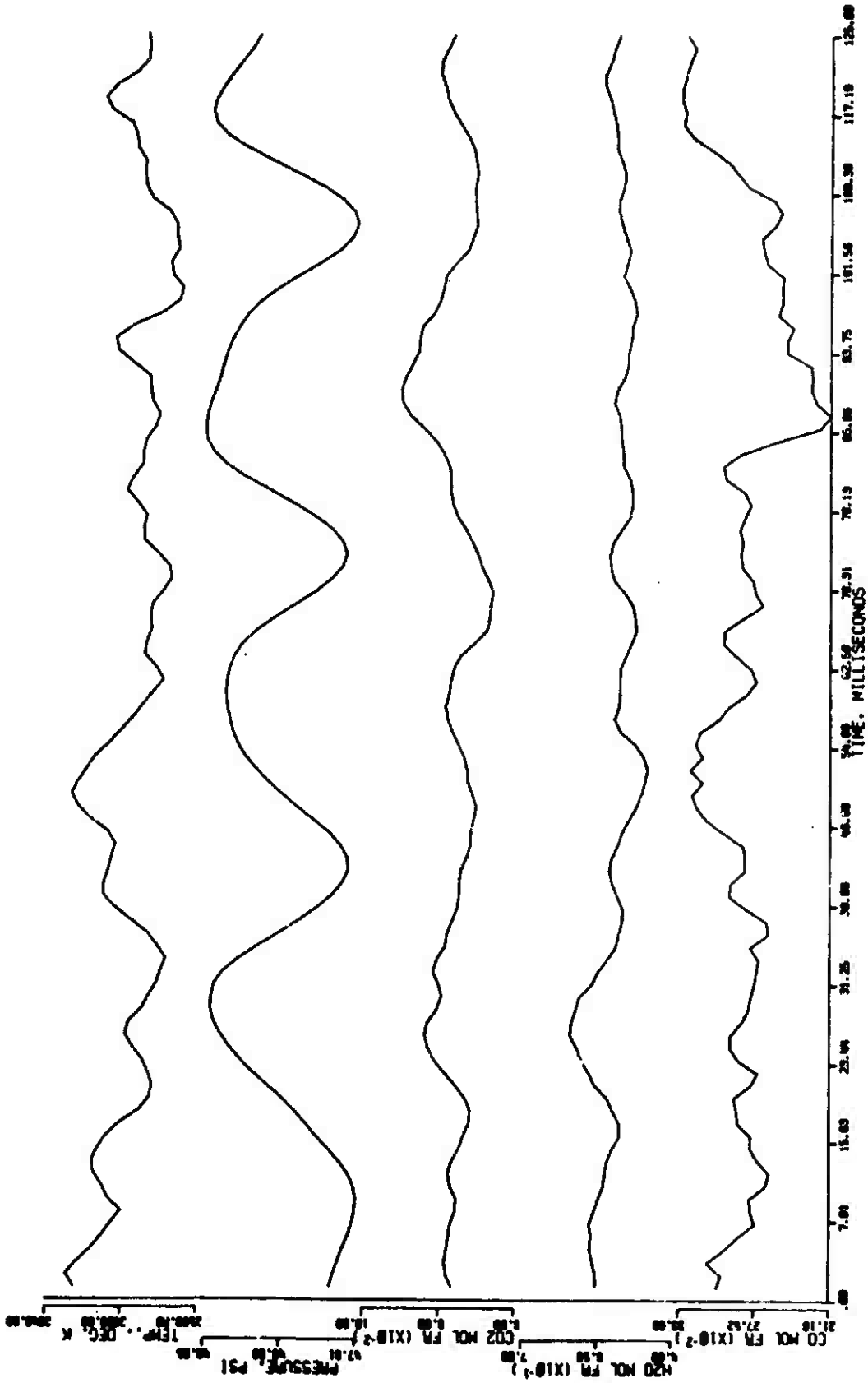

FIGURE G-6. TEMPERATURE AND CONCENTRATION PROFILES FOR A 31 Hz. OSCILLATORY-PRESSURE TEST. (82 wt. % AP propellant [UFN], 3-5 mm, Run No. 7-4374)

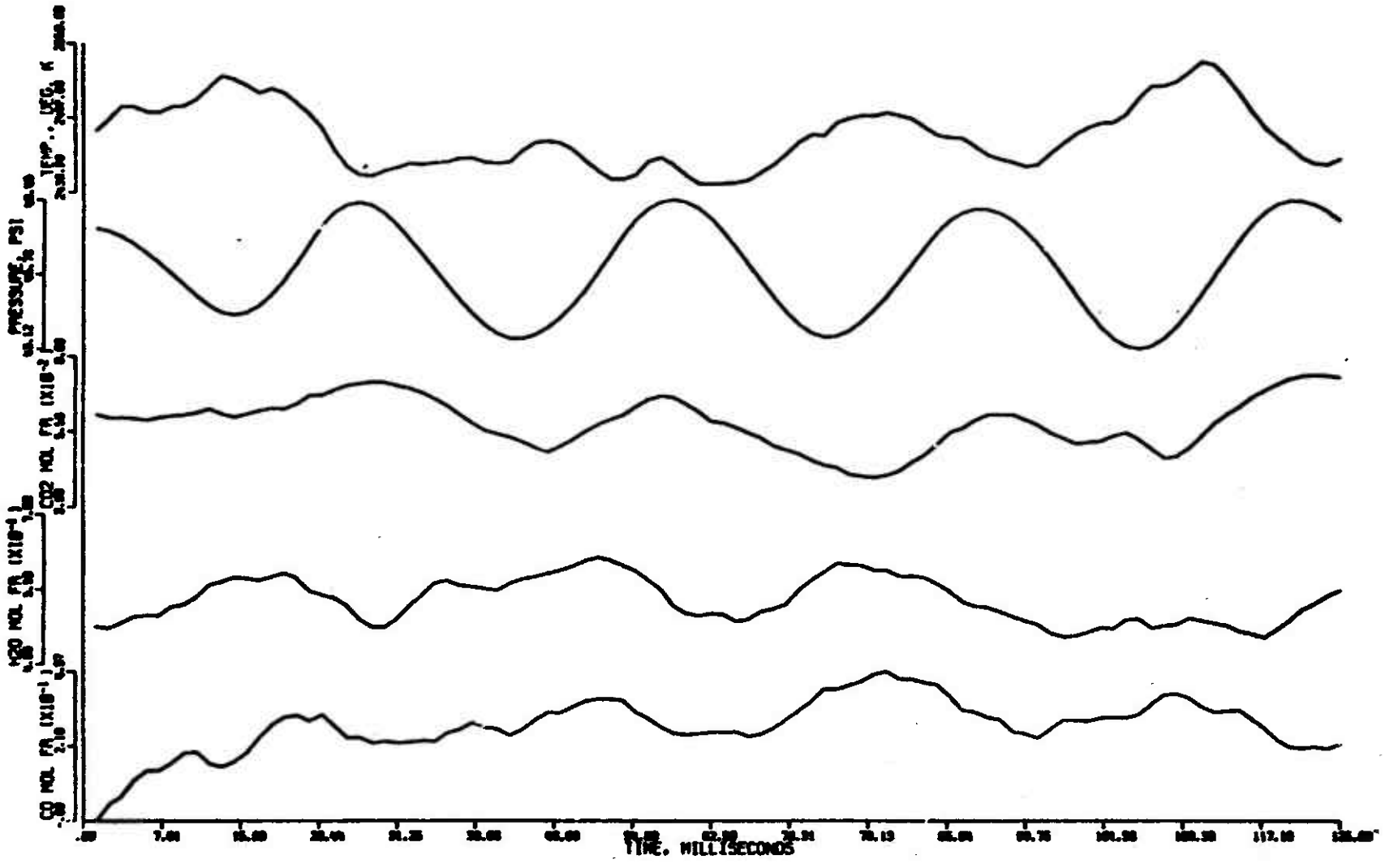

FIGURE G-7. TEMPERATURE AND CONCENTRATION PROFILES FOR A 31 Hz. OSCILLATORY-PRESSURE TEST. (82 wt. % AP propellant [UFP], 3-5 mm, Run No. 3-31474)

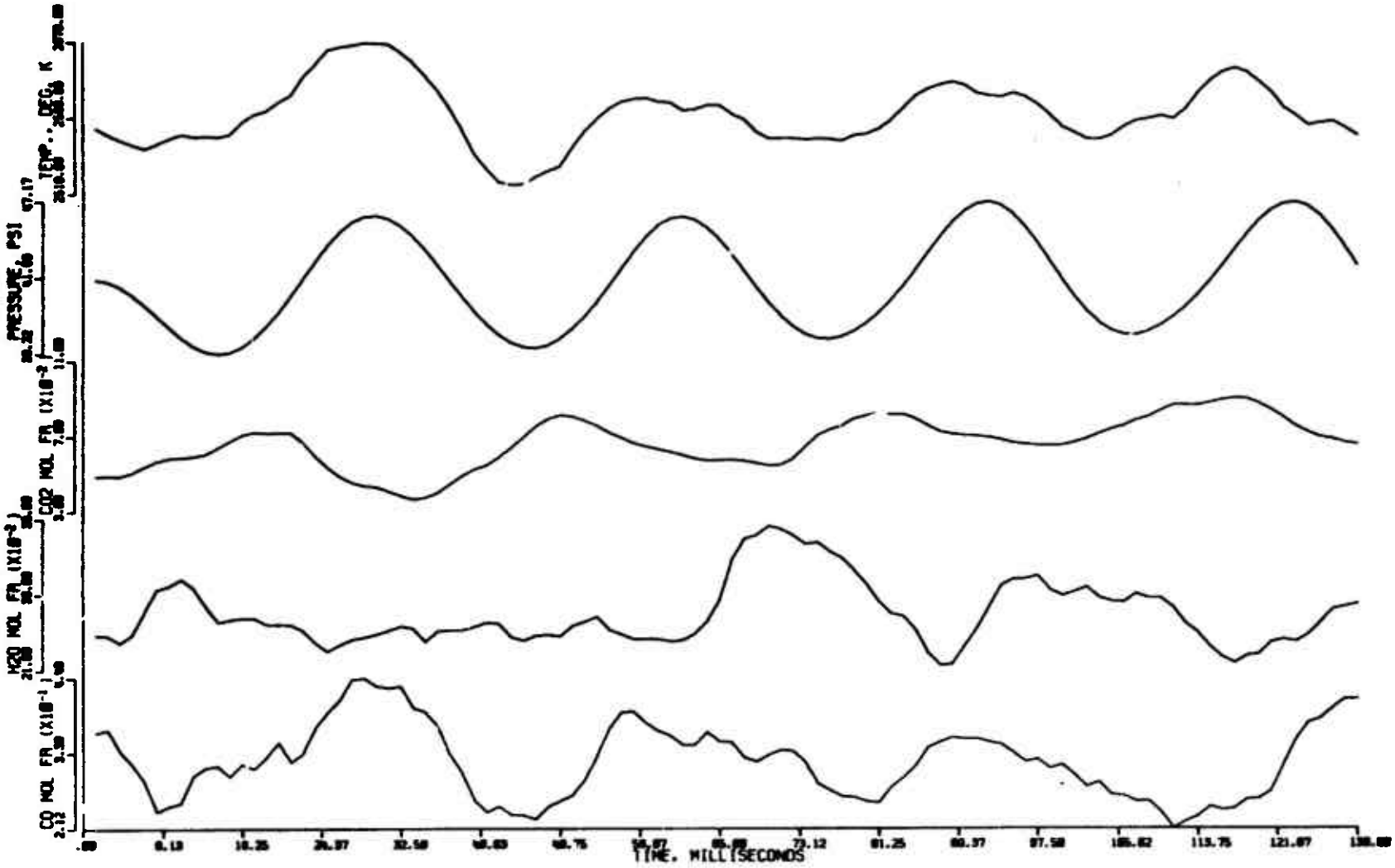

FIGURE G-8. TEMPERATURE AND CONCENTRATION PROFILES FOR A 31 Hz. OSCILLATORY-PRESSURE TEST. (82 wt. % AP propellant [UFP], 3-5 mm, Run No. 5-4374)

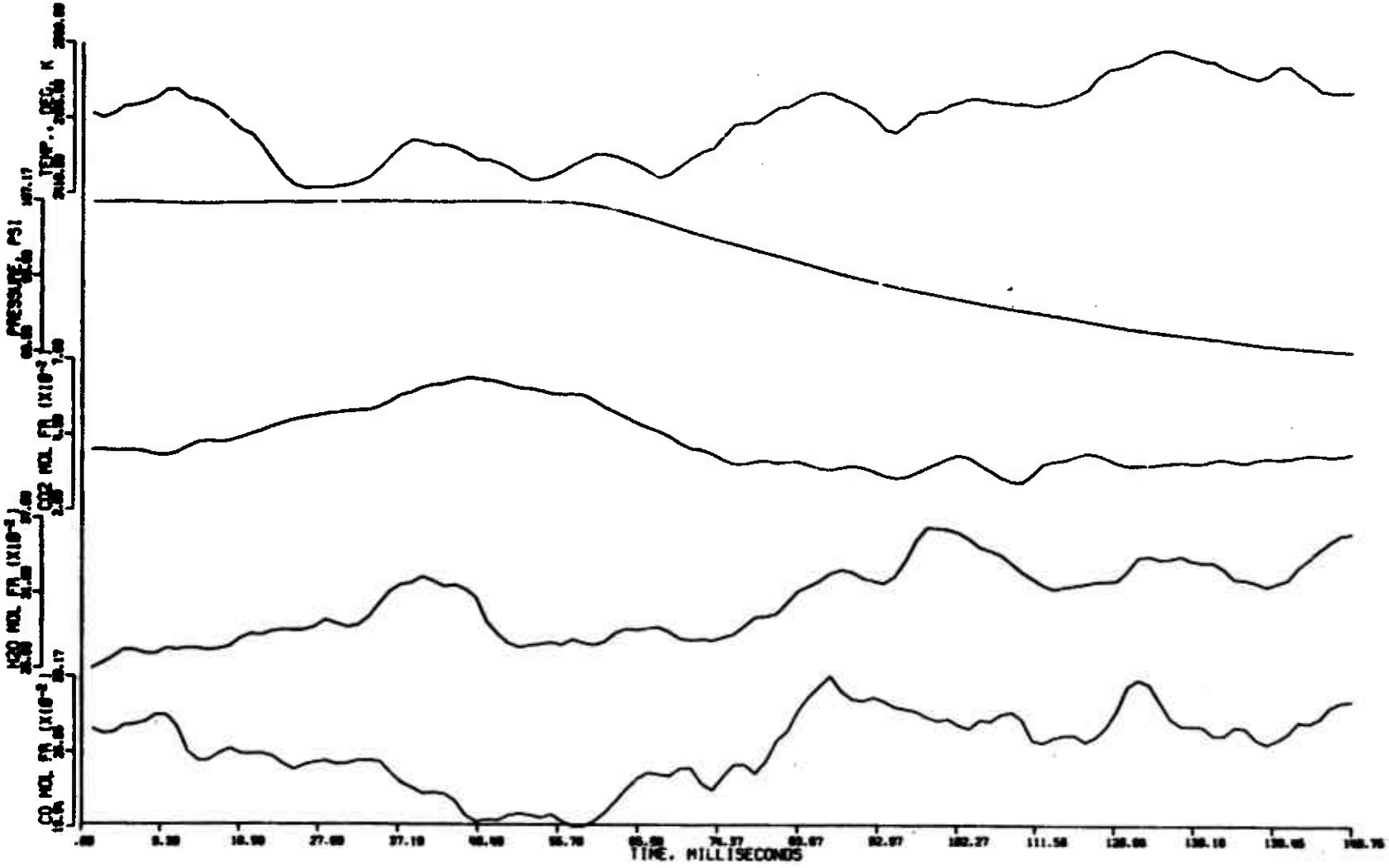

FIGURE G-9. TEMPERATURE AND CONCENTRATION PROFILES FOR A SINGLE-PRESSURE-DECREASE-PULSE TEST. (82 wt. % AP propellant [UFP], 3-5 mm, Run No. 1-31574)

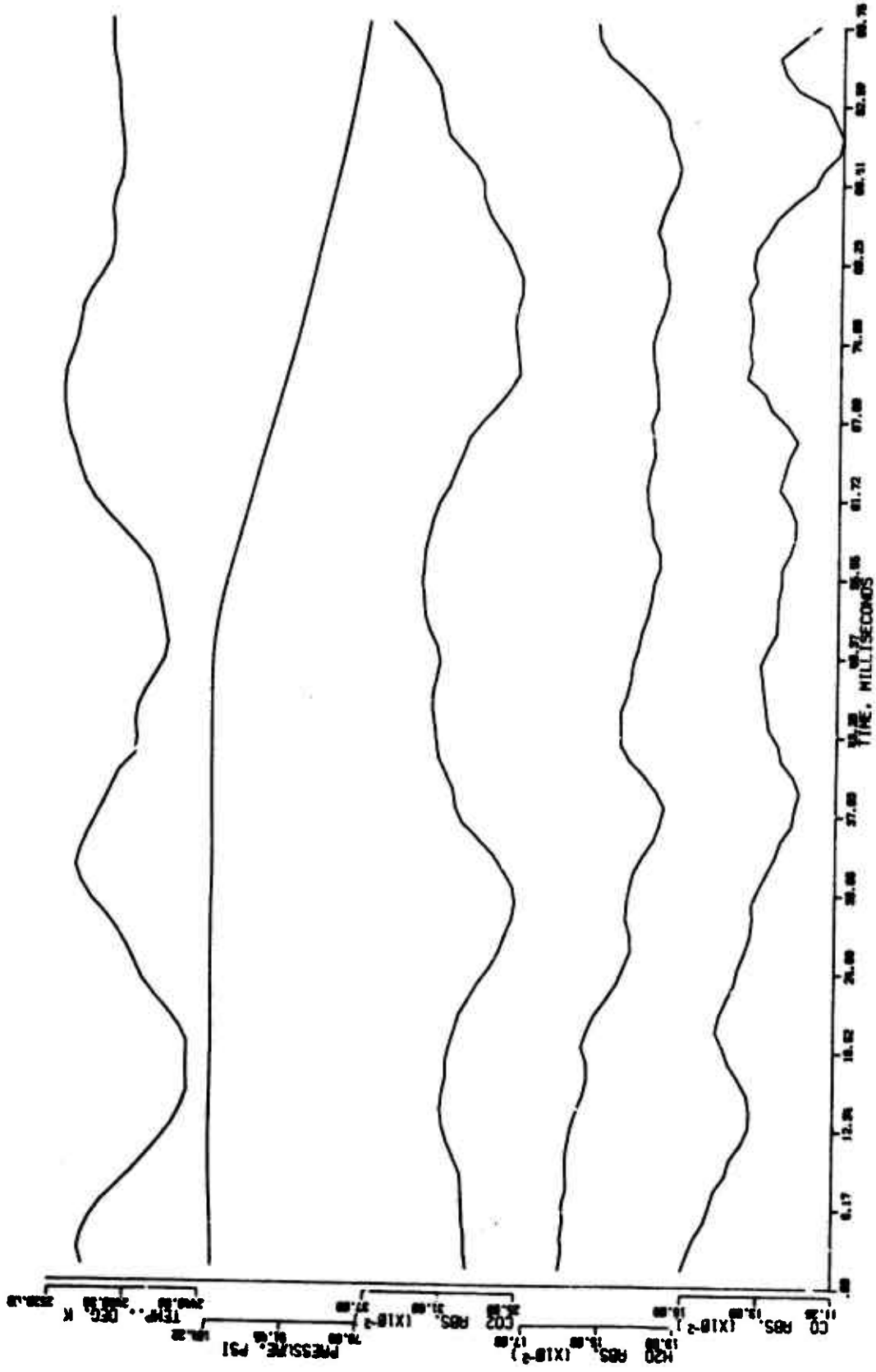

FIGURE G-10. TEMPERATURE AND PRESSURE-CORRECTED ABSORBANCE PROFILES FOR A SINGLE-PRESSURE-DECREASE-PULSE TEST. (80 wt. % AP propellant [UFO], 3-5 mm, Run No. 2-31574)

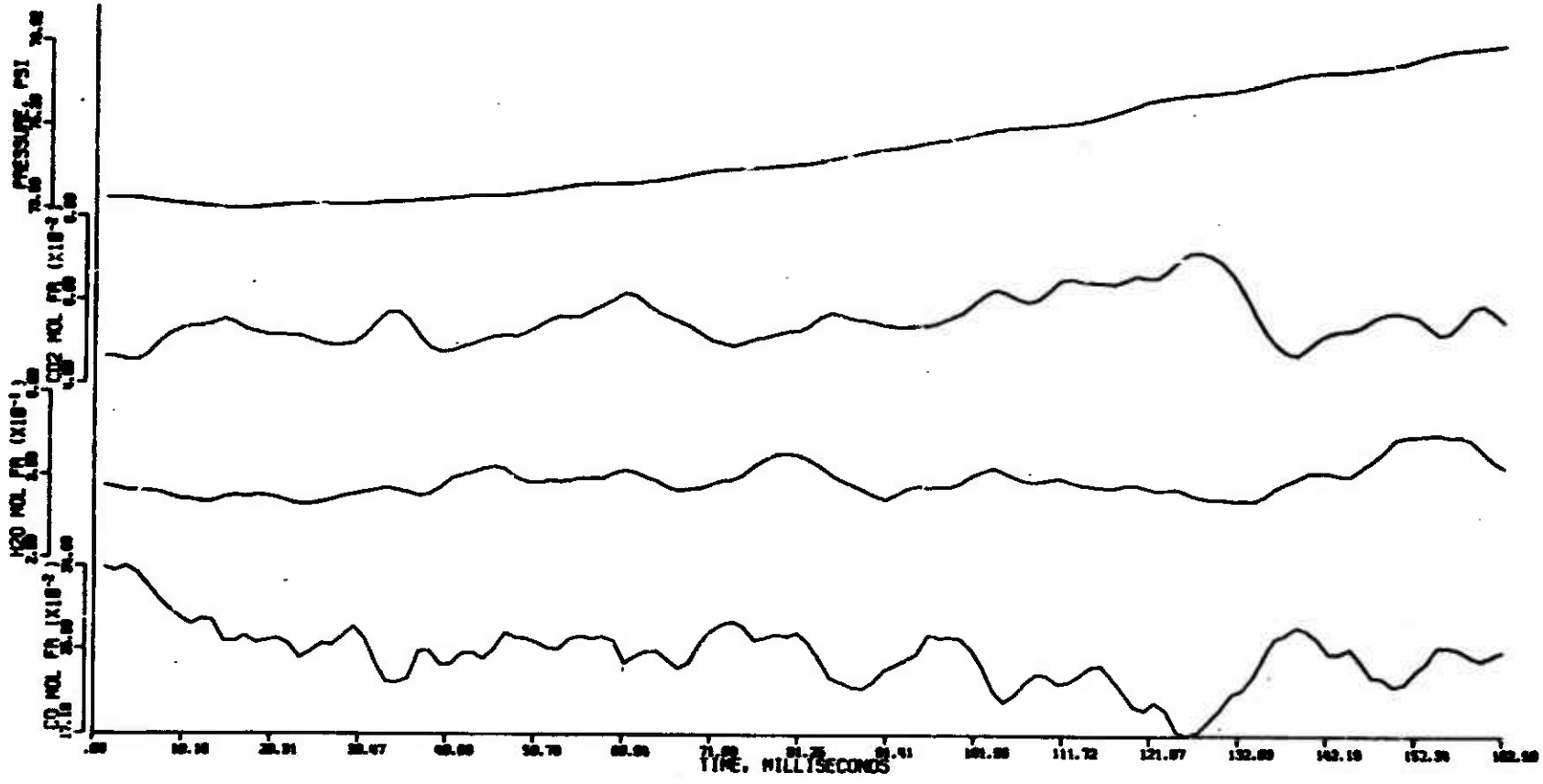

FIGURE G-11. CONCENTRATION PROFILES FOR A SINGLE-PRESSURE-INCREASE-PULSE TEST. (82 wt. % AP propellant [UFN], 12-14 mm, Run No. 6-13074)

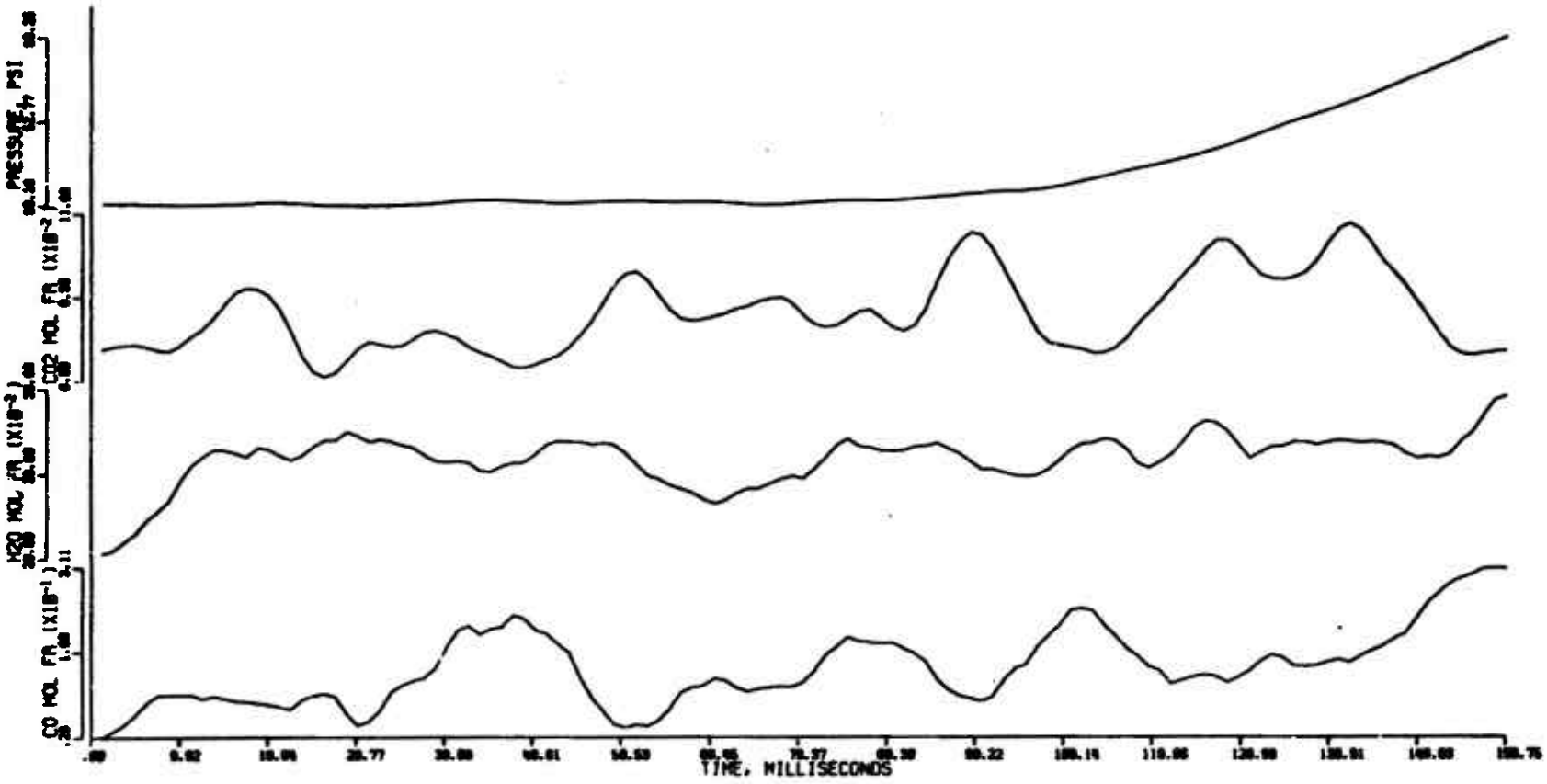

FIGURE G-12. CONCENTRATION PROFILES FOR A SINGLE-PRESSURE-INCREASE-PULSE TEST. (82 wt. % AP propellant [UFN], 12-14 mm, Run No. 2-2674)

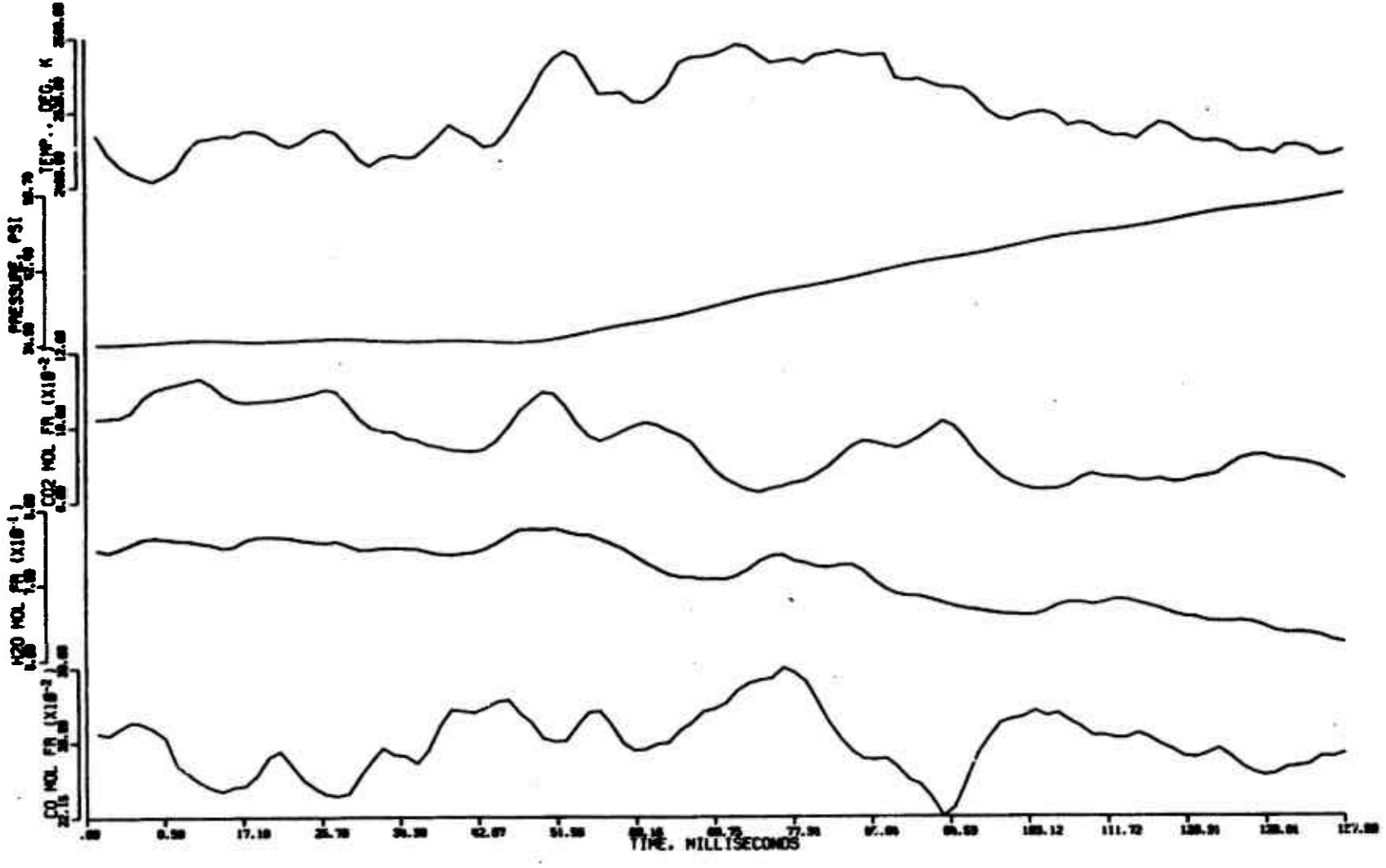

FIGURE G-13. TEMPERATURE AND CONCENTRATION PROFILES FOR A SINGLE-PRESSURE-INCREASE-PULSE TEST. (82 wt. % AP propellant [UFN], 3-5 mm, Run No. 8-4374)

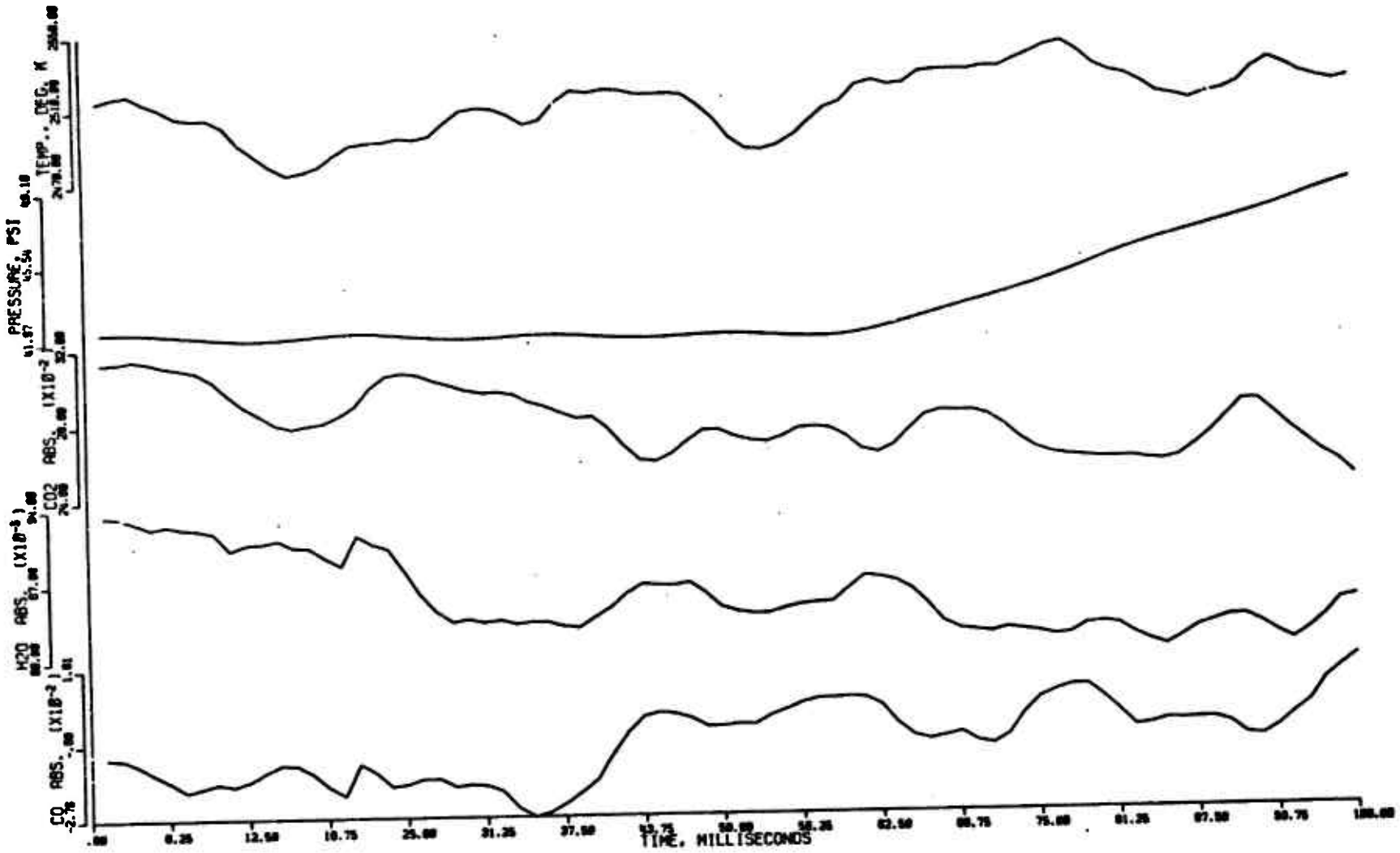

FIGURE G-14. TEMPERATURE AND PRESSURE-CORRECTED ABSORBANCE PROFILES FOR A SINGLE-PRESSURE-INCREASE-PULSE TEST. (80 wt. % AP propellant [UFI], 12-14 mm, Run No. 5-4474)

APPENDIX H

TABULATED DATA

The unfiltered data for all the tests reported are presented in tabular form in this section. The data are labeled with the run number as well as the Figure number where the data, or its filtered counterpart, are presented graphically. Also, the axial position with respect to the propellant surface where the data were measured is given for each test.

The composition data for the 82 weight percent AP propellant are are reported as mole fractions, however, the data for the 80 and 85 weight percent AP propellants are reported as pressure-corrected absorbances. The flame radiation data for the flame-emission-only tests are reported in arbitrary film-reader units. The measured sodium D-line absorptance (absorptivity) is reported for almost all of the tests.

Run No. 1-3774 (Figure 6, p. 42) (82 wt. % AP propellant [UFN], constant pressure)

SCAN NUMBER	PRESSURE	FLAME TEMPERATURE, DEGREES K	H2O MOL FRACTION	CO2 MOL FRACTION	CO MOL FRACTION	H2O/CO ABS.
2	1.	[illegible]	.340	.045	.356	.499
	2	[illegible]	.344	.044	.358	.504
	3	[illegible]	.353	.050	.369	.508
	4	[illegible]	.320	.048	.381	.463
	5	[illegible]	.328	.048	.375	.499
	6	[illegible]	.329	.045	.406	.499
	7	[illegible]	.311	.041	.391	.499
	8	[illegible]	.349	.041	.396	.504
	9	[illegible]	.284	.040	.393	.479
	10	[illegible]	.284	.040	.396	.483
	11	[illegible]	.286	.042	.316	.909
	12	[illegible]	.296	.047	.314	.499
	13	[illegible]	.303	.049	.370	.519
	14	[illegible]	.320	.045	.358	.484
	15	[illegible]	.284	.047	.372	.474
	16	[illegible]	.284	.045	.372	.499
	17	[illegible]	.350	.045	.388	.909
	18	[illegible]	.301	.043	.295	.899
	19	[illegible]	.292	.047	.380	.483
	20	[illegible]	.299	.044	.384	.504
	21	[illegible]	.300	.044	.347	.504
	22	[illegible]	.308	.045	.388	.500
	23	[illegible]	.288	.047	.325	.489
	24	[illegible]	.283	.044	.311	.484
	25	[illegible]	.288	.050	.378	.498
	26	[illegible]	.314	.049	.336	.503
	27	[illegible]	.298	.047	.349	.929
	28	[illegible]	.337	.044	.314	.484
	29	[illegible]	.292	.047	.373	.504

Run No. 1-3774 continued

4 mm

8 mm

Run No. 1-3774 continued

13 mm

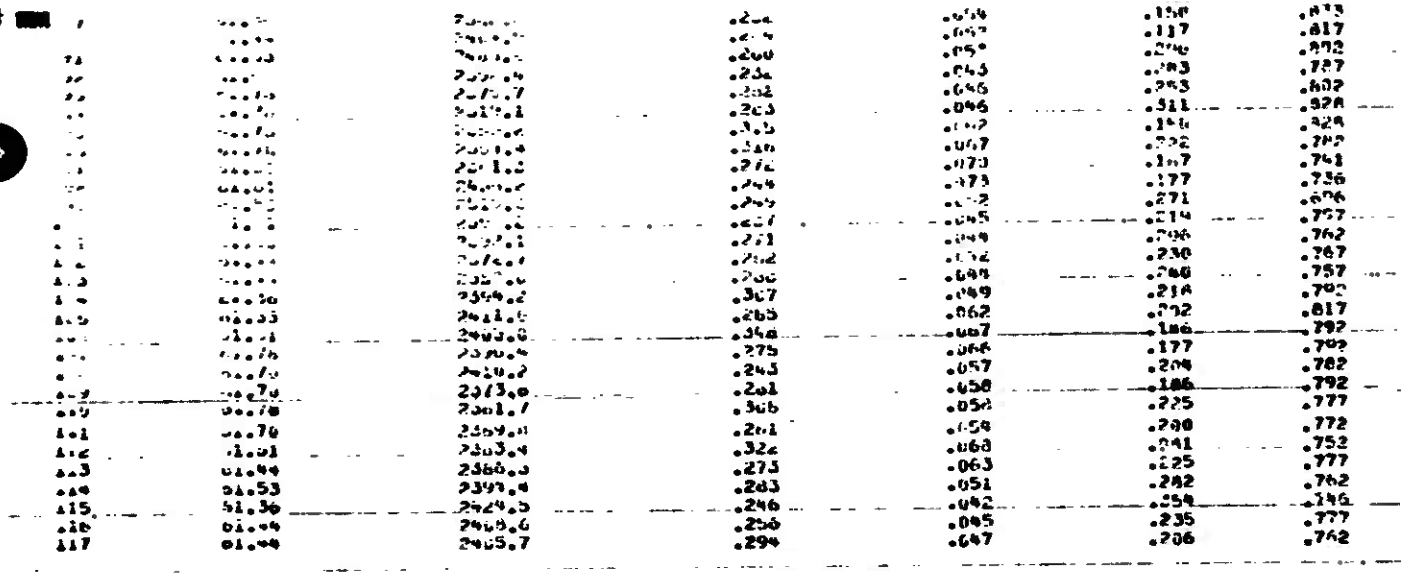

Run No. 1-3772 (Figure 8, p. 47) (82 wt. % AP propellant [UFI], constant pressure, 3-5 mm)

[illegible]	[illegible]	PLANE TE[illegible] KELVIN	H2O MOL FRACTION	CO2 MOL FRACTION	CO MOL FRACTION	[illegible] ABS.
1	[illegible]	2[illegible]	.336	.459	.244	.883
2	[illegible]	[illegible]	.278	.457	.264	.896
3	[illegible]	[illegible]	.242	.455	.271	.833
4	[illegible]	[illegible]	.270	.451	.299	.853
5	[illegible]	[illegible]	.306	.452	.319	.817
6	[illegible]	[illegible]	.320	.450	.349	.854
7	[illegible]	[illegible]	.297	.453	.253	.843
8	[illegible]	[illegible]	.234	.452	.248	.838
9	[illegible]	[illegible]	.245	.445	.301	.888
10	[illegible]	[illegible]	.272	.444	.297	.919
11	[illegible]	[illegible]	.260	.443	.258	.898
12	[illegible]	[illegible]	.318	.454	.265	.863
13	[illegible]	[illegible]	.319	.451	.358	.909
14	[illegible]	[illegible]	.307	.459	.315	.899
15	[illegible]	[illegible]	.284	.450	.320	.843
16	[illegible]	[illegible]	.269	.449	.295	.830
17	[illegible]	[illegible]	.231	.452	.311	.843
18	[illegible]	[illegible]	.297	.453	.344	.903
19	[illegible]	[illegible]	.293	.455	.318	.896
20	[illegible]	[illegible]	.297	.452	.340	.863
21	[illegible]	[illegible]	.282	.448	.340	.873
22	[illegible]	[illegible]	.269	.441	.302	.853
23	[illegible]	[illegible]	.281	.446	.343	.883
24	[illegible]	[illegible]	.307	.454	.275	.873
25	[illegible]	[illegible]	.257	.448	.274	.831 L
26	[illegible]	[illegible]	.275	.459	.244	.863
27	[illegible]	[illegible]	.313	.459	.322	.868
28	[illegible]	[illegible]	.338	.455	.297	.882 L
29	[illegible]	[illegible]	.305	.452	.298	.858
30	[illegible]	[illegible]	.294	.452	.292	.799
31	[illegible]	[illegible]	.283	.449	.311	.887 L
32	[illegible]	[illegible]	.264	.451	.347	.840
33	[illegible]	[illegible]	.314	.456	.256	.836 L
34	[illegible]	[illegible]	.295	.457	.343	.887 L
35	[illegible]	[illegible]	.280	.459	.344	.843
36	[illegible]	[illegible]	.252	.456	.305	.878
37	[illegible]	[illegible]	.302	.458	.297	.904
38	[illegible]	[illegible]	.313	.453	.315	.843
39	[illegible]	[illegible]	.296	.448	.293	.848
40	[illegible]	[illegible]	.297	.453	.298	.853
41	[illegible]	[illegible]	.305	.449	.314	.844
42	[illegible]	[illegible]	.304	.454	.298	.863
43	[illegible]	[illegible]	.304	.452	.295	.873
44	[illegible]	[illegible]	.296	.445	.344	.863
45	[illegible]	[illegible]	.299	.441	.332	.849
46	[illegible]	[illegible]	.290	.451	.298	.878
47	[illegible]	[illegible]	.321	.454	.334	.894
48	[illegible]	[illegible]	.287	.445	.348	.853
49	[illegible]	[illegible]	.323	.451	.362	.853
50	[illegible]	[illegible]	.283	.461	.329	.914
51	[illegible]	[illegible]	.335	.452	.298	.868
52	[illegible]	[illegible]	.351	.448	.328	.888

Run No. 1-3772 continued

[illegible]	79.[illegible]3	2[illegible]	.294	.047	.322	.836
[illegible]	79.[illegible]5	2[illegible]	.349	.056	.272	.787
[illegible]	[illegible]	2[illegible]	.[illegible]	.053	.355	.873
[illegible]	7[illegible]	2[illegible]	.279	.054	.408	.873
57	7[illegible]41	2[illegible]	.342	.052	.312	.859
[illegible]	79.[illegible]9	2[illegible]	.316	.046	.325	.833
[illegible]	[illegible]1	2[illegible]	.293	.055	.298	.835
[illegible]	7[illegible]	2[illegible]	.292	.059	.281	.859
64	[illegible]7	2[illegible]	.324	.063	.227	.848
65	79.[illegible]	2[illegible]	.286	.062	.275	.878
66	[illegible]	2[illegible]	.347	.055	.273	.859
67	[illegible]	2[illegible]	.342	.048	.291	.861
68	[illegible]2	2[illegible]	.331	.051	.265	.847
69	[illegible]4	2[illegible]	.335	.052	.357	.873
70	[illegible]	2[illegible]	.327	.048	.310	.853
71	7[illegible]	2[illegible]	.[illegible]	.050	.354	.868
72	[illegible]	2[illegible]	.314	.051	.300	.812
73	[illegible]1	2[illegible]	.316	.060	.248	.812
74	[illegible]	2[illegible]	.293	.051	.282	.863
75	[illegible]49	2[illegible]	.322	.047	.300	.823
76	[illegible]	2[illegible]	.342	.055	.281	.829
77	[illegible]	2[illegible]	.305	.058	.250	.868
78	[illegible]	2[illegible]	.301	.050	.276	.8[illegible]
79	[illegible]	2[illegible]	.301	.051	.331	.873
80	[illegible]	2[illegible]	.319	.050	.252	.808
81	[illegible]	2[illegible]	.308	.061	.286	.883
82	[illegible]	2[illegible]	.320	.072	.[illegible]09	.873
83	[illegible]	2[illegible]	.294	.067	.29[illegible]	.884
84	[illegible]	2[illegible]	.[illegible]	.062	.[illegible]51	.890
85	[illegible]3	2[illegible]	.[illegible]	.057	.[illegible]79	.873
86	[illegible]	2[illegible]	.318	.061	.292	.873
87	[illegible]	2[illegible]	.[illegible]	.065	.252	.894
88	[illegible]	2[illegible]	.307	.054	.307	.[illegible]
89	[illegible]1	2[illegible]	.[illegible]	.049	.[illegible]1	.899
90	[illegible]	2[illegible]	.[illegible]	.047	.[illegible]75	.863
91	[illegible]	2[illegible]	.[illegible]	.054	.[illegible]3	.884
92	.[illegible]7	2[illegible]	.[illegible]	.053	.[illegible]09	.853
93	[illegible]	2[illegible]	.[illegible]	.058	.[illegible]94	.833
94	[illegible]	2[illegible]	.301	.052	.[illegible]47	.894
95	[illegible]	2[illegible]	.[illegible]	.057	.[illegible]01	.883
96	[illegible]	2[illegible]	.[illegible]	.050	.[illegible]46	.899
97	[illegible]2	2[illegible]	.[illegible]	.[illegible]50	.[illegible]62	.863
98	79.[illegible]	2[illegible]	.286	.053	.279	.865
99	79.[illegible]	2[illegible]	.297	.052	.363	.853
97	79.[illegible]	2[illegible]	.302	.056	.297	.828
98	79.[illegible]	2[illegible]	.278	.056	.335	.843
99	79.[illegible]	2[illegible]	.290	.059	.288	.838

Run No. 1-3774 (Figure 10, p. 49) (82 wt. % AP propellant [UFN], constant pressure, 12-14 mm)

			.297	.054	.266	.741
			.249	.059	.228	.731
			.281	.064	.252	.772
			.313	.057	.271	.726
			.307	.059	.239	.764
			.313	.067	.242	.792
			.287	.058	.228	.772
			.273	.057	.229	.767
			.287	.054	.266	.757
			.267	.046	.234	.823
			.316	.050	.229	.782
			.296	.048	.261	.807
			.249	.044	.301	.777
			.337	.051	.219	.752
			.317	.046	.292	.691
			.335	.051	.277	.726
			.331	.050	.264	.721
			.313	.050	.243	.752
			.294	.056	.205	.796
			.303	.054	.217	.752
			.336	.058	.268	.792
			.257	.055	.228	.767
			.253	.041	.313	.760
			.269	.052	.238	.767
			.250	.045	.266	.767
			.275	.054	.274	.673
			.289	.051	.219	.826
			.257	.046	.283	.736
			.255	.048	.277	.741
			.317	.038	.238	.757
			.322	.041	.229	.752
			.273	.049	.179	.791
			.304	.045	.275	.721
			.257	.048	.319	.752
			.283	.055	.151	.817
			.229	.056	.192	.726
			.265	.038	.306	.735
			.261	.043	.265	.711
			.232	.045	.310	.752
			.308	.042	.210	.823
			.343	.057	.215	.704
			.346	.059	.229	.796
			.255	.052	.274	.777
			.256	.059	.184	.764
			.261	.060	.191	.716
			.234	.056	.159	.746
			.252	.060	.176	.726
			.254	.051	.191	.817
			.268	.049	.280	.817
			.271	.052	.253	.767
		2921.7	.268	.068	.298	.772
		2966.8	.273	.067	.189	.782

Run No. 1-3774 continued

[illegible]	[illegible]	[illegible]	.[illegible]	.059	.038	.824
[illegible]	[illegible]	[illegible]	.206	.043	.295	.787
[illegible]	[illegible]	[illegible]	.[illegible]	.057	.238	.824
[illegible]	[illegible]	[illegible]	.[illegible]	.058	.204	.757
[illegible]	[illegible]	[illegible]	.[illegible]	.056	.234	.782
[illegible]	[illegible]	[illegible]	.[illegible]	.061	.271	.797
[illegible]	[illegible]	[illegible]	.[illegible]	.066	.244	.802
[illegible]	[illegible]	[illegible]	.[illegible]	.063	.245	.741
[illegible]	[illegible]	[illegible]	.[illegible]	.065	.264	.805
[illegible]	[illegible]	[illegible]	.[illegible]	.048	.238	.742
[illegible]	[illegible]	[illegible]	.[illegible]	.055	.185	.797
[illegible]	[illegible]	[illegible]	.[illegible]	.061	.190	.741
[illegible]	[illegible]	[illegible]	.[illegible]	.038	.231	.706
[illegible]	[illegible]	[illegible]	.[illegible]	.057	.[illegible]	.746
[illegible]	[illegible]	[illegible]	.[illegible]	.059	.[illegible]	.762
[illegible]	[illegible]	[illegible]	.[illegible]	.054	.[illegible]	.843
[illegible]	[illegible]	[illegible]	.[illegible]	.054	.150	.833
[illegible]	[illegible]	[illegible]	.[illegible]	.058	.117	.817
[illegible]	[illegible]	[illegible]	.[illegible]	.063	.[illegible]	.802
[illegible]	[illegible]	[illegible]	.[illegible]	.043	.283	.787
[illegible]	[illegible]	[illegible]	.[illegible]	.046	.[illegible]	.802
[illegible]	[illegible]	[illegible]	.[illegible]	.[illegible]	.311	.825
[illegible]	[illegible]	[illegible]	.[illegible]	.062	.150	.823
[illegible]	[illegible]	[illegible]	.[illegible]	.[illegible]	.222	.782
[illegible]	[illegible]	[illegible]	.[illegible]	.070	.167	.741
[illegible]	[illegible]	[illegible]	.[illegible]	.073	.178	.756
[illegible]	[illegible]	[illegible]	.[illegible]	.053	.271	.805
[illegible]	[illegible]	[illegible]	.[illegible]	.045	.214	.797
[illegible]	[illegible]	[illegible]	.[illegible]	.044	.296	.782
[illegible]	[illegible]	[illegible]	.[illegible]	.042	.238	.787
[illegible]	[illegible]	[illegible]	.[illegible]	.044	.240	.757
[illegible]	[illegible]	[illegible]	.[illegible]	.049	.218	.792
[illegible]	[illegible]	[illegible]	.[illegible]	.062	.202	.817
[illegible]	[illegible]	[illegible]	.[illegible]	.057	.190	.792
[illegible]	[illegible]	[illegible]	.[illegible]	.076	.177	.793
[illegible]	[illegible]	[illegible]	.[illegible]	.057	.[illegible]	.782
[illegible]	[illegible]	[illegible]	.[illegible]	.058	.150	.792
[illegible]	[illegible]	[illegible]	.[illegible]	.056	.224	.777
[illegible]	[illegible]	[illegible]	.[illegible]	.054	.[illegible]	.772
[illegible]	[illegible]	[illegible]	.[illegible]	.068	.[illegible]	.752
[illegible]	[illegible]	[illegible]	.[illegible]	.073	.[illegible]	.777
[illegible]	[illegible]	[illegible]	.[illegible]	.051	.[illegible]	.782
[illegible]	[illegible]	[illegible]	.[illegible]	.062	.[illegible]	.746
[illegible]	[illegible]	[illegible]	.[illegible]	.045	.235	.777
[illegible]	[illegible]	[illegible]	.294	.047	.206	.762

Run No. 1-31574 (Figure 12, p. 51) (82 wt. % AP propellant [UFP], constant pressure, 3-5 mm)

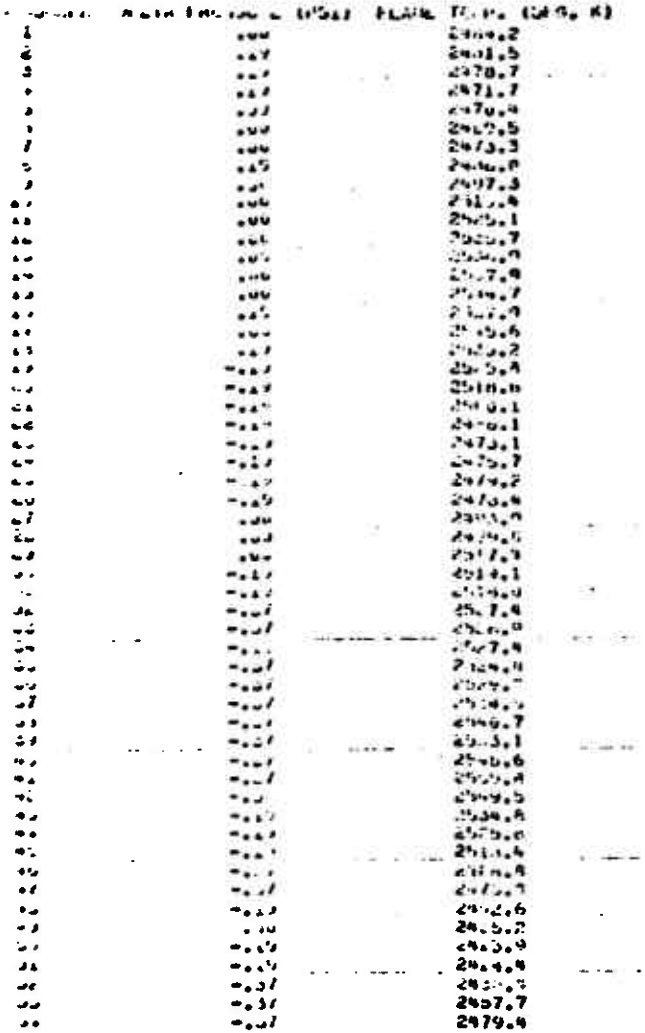

continued

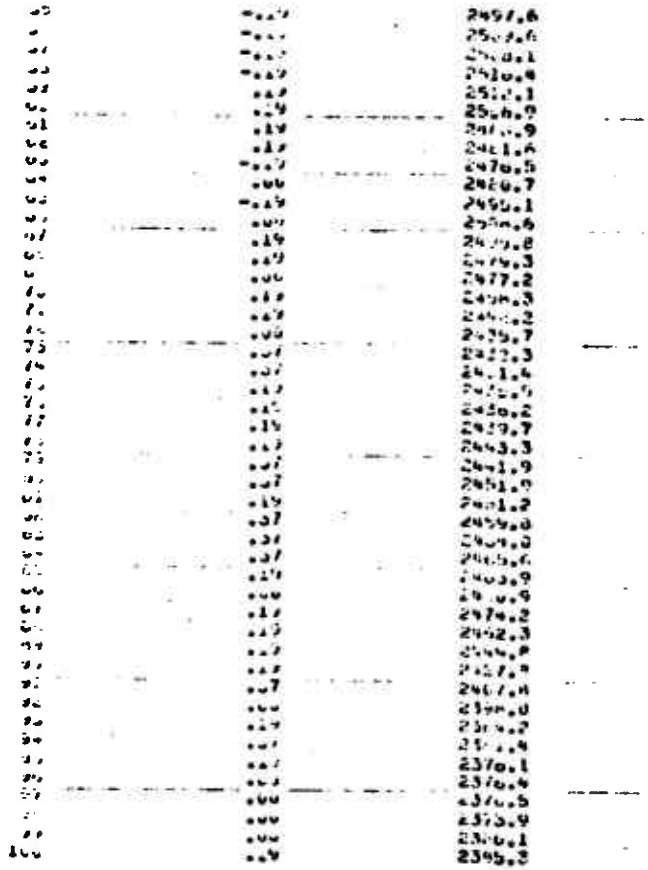

Run No. 5-31474 (Figure 13, p. 52) (82 wt. % AP propellant [UFP], constant pressure, 3-5 mm)

continued

Run No. 1-3774 (Figure 14, p. 56) (82 wt. % AP propellant [UFN], constant pressure, 3-5 mm)

continued

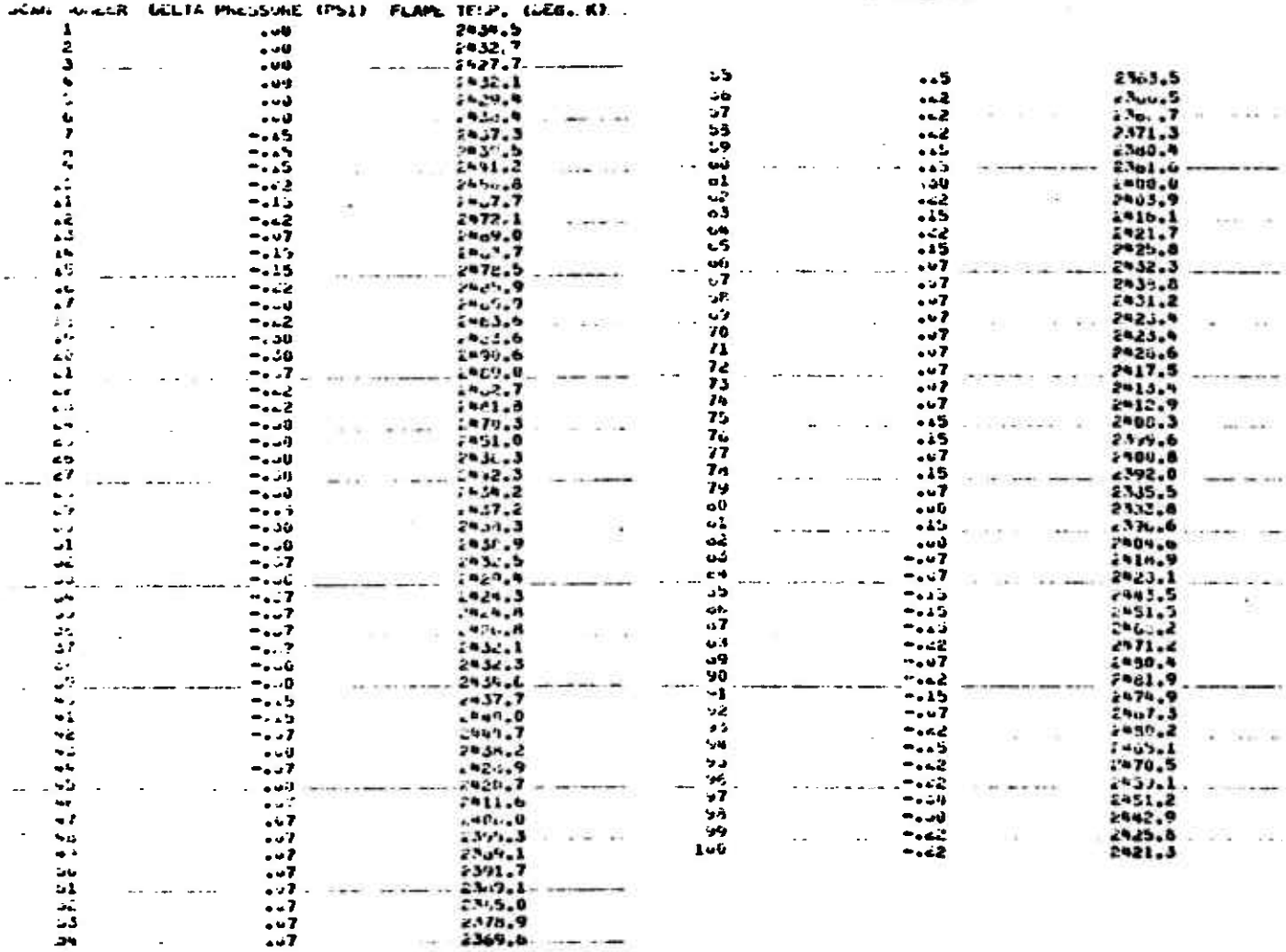

Run No. 1-3774 (Figure 15, p. 57) (82 wt. % AP propellant [UFN], constant pressure, 12-14 mm)

continued

[illegible]	[illegible]	DELTA PRESSURE (PSI)	FLAME TEMP. (DEG. K)
1		.00	2375.1
2		.07	2378.4
3		-.07	2388.4
4		.07	2372.0
5		.07	2391.7
6		.07	2399.2
7		.07	2407.0
8		.00	2411.0
9		.07	2410.1
10		.07	2410.1
11		.07	2407.7
12		.05	2399.9
13		.05	2407.2
14		.07	2394.9
15		.07	2394.9
16		.07	2397.0
17		.05	2391.2
18		.05	2394.0
19		.05	2381.6
20		.05	2394.9
21		.02	2373.7
22		.02	2387.9
23		.07	2383.0
24		.00	2370.7
25		.00	2386.1
26		.00	2383.4
27		.00	2381.5
28		.00	2386.5
29		.03	2391.2
30		.03	2391.1
31		.03	2327.3
32		.02	2332.6
33		.00	2380.5
34		.07	2401.0
35		.00	2395.0
36		.07	2393.0
37		.00	2383.1
38		.04	2392.4
39		.00	2375.3
40		.00	2381.3
41		.02	2352.8
42		.03	2391.-
43		.00	2382.1
44		.04	2397.3
45		.02	2382.7
46		.02	2382.9
47		.02	2361.6
48		.02	2365.7
49		.02	2372.7
50		.05	2382.3
51		.00	2389.0
52		.00	2418.1
53		.00	2440.9
54		.05	2440.9
55		.02	2386.9
56		.02	2386.9
57		.02	2401.8
58		.05	2411.0
59		.05	2405.6
60		.05	2511.0
61		.05	2399.7
62		.05	2473.6
63		.05	2448.2
64		.05	2411.0
65		.05	2401.1
66		.07	2395.6
67		.00	2383.2
68		.05	2388.0
69		.05	2387.9
70		.05	2382.6
71		.07	2384.2
72		.07	2393.3
73		.00	2379.3
74		.00	2386.6
75		.00	2371.8
76		-.07	2383.5
77		-.07	2370.5
78		.00	2377.6
79		-.07	2386.3
80		.00	2382.3
81		-.07	2345.4
82		-.07	2377.6
83		.05	2384.7
84		-.07	2382.1
85		.00	2388.5
86		.00	2386.8
87		.07	2396.2
88		.00	2380.6
89		.00	2380.5
90		.07	2396.8
91		-.07	2403.0
92		-.07	2406.2
93		.00	2407.4
94		.00	2407.4
95		.00	2408.0
96		.00	2415.5
97		.05	2413.0
98		.05	2411.4
99		.02	2407.2
100		.05	2410.7

Run No. 2-22174 (Figure 16, p. 63) (82 wt. % AP propellant [UFN], 31 Hz. oscillatory pressure, 12-14 mm)

SCAN NUMBER	PRESSURE, PSIA	H2O MOL FRACTION	CO2 MOL FRACTION	CO MOL FRACTION
1	45.21	.588	.109	.282
2	45.74	.443	.113	.192
3	46.46	.497	.109	.255
4	46.48	.539	.129	.118
5	46.94	.452	.133	.148
6	47.12	.523	.121	.222
7	47.33	.543	.104	.061
8	47.01	.520	.111	.259
9	46.69	.523	.097	.177
10	46.37	.445	.095	.284
11	46.06	.465	.092	.319
12	45.63	.557	.103	.161
13	45.21	.536	.106	.294
14	44.57	.549	.102	.254
15	44.04	.492	.096	.307
16	43.38	.466	.100	.333
17	42.66	.520	.098	.258
18	42.42	.609	.096	.228
19	41.61	.579	.104	.292
20	42.42	.581	.083	.417
21	42.93	.545	.104	.274
22	43.38	.559	.116	.134
23	44.04	.553	.099	.306
24	44.78	.462	.082	.271
25	45.63	.518	.085	.306
26	46.27	.469	.098	.174
27	46.90	.471	.111	.134
28	47.44	.512	.110	.251
29	47.75	.515	.099	.219
30	47.75	.448	.110	.206
31	47.44	.486	.103	.269
32	46.90	.432	.099	.254
33	46.48	.528	.112	.124
34	46.16	.481	.112	.232
35	45.63	.478	.096	.221
36	45.31	.491	.094	.228
37	44.99	.478	.098	.353
38	44.57	.608	.104	.267
39	44.36	.497	.084	.277
40	43.83	.473	.060	.325
41	43.38	.479	.081	.329
42	42.77	.549	.060	.316
43	42.34	.565	.091	.319
44	42.02	.549	.098	.171
45	41.81	.493	.100	.214
46	42.13	.485	.101	.176
47	42.87	.462	.104	.175
48	43.48	.515	.092	.215
49	44.25	.485	.090	.167
50	45.10	.509	.105	.352
51	45.84	.508	.111	.174
52	46.59	.524	.104	.266

Run No. 2-22174 continued

53	47.22	.520	.100	.220
54	47.44	.466	.098	.153
55	48.67	.457	.090	.255
56	47.75	.452	.086	.243
57	47.41	.480	.002	.320
58	46.46	.484	.004	.301
59	46.05	.461	.092	.235
60	45.63	.381	.083	.111
61	45.10	.521	.076	.345
62	44.74	.518	.071	.366
63	44.40	.560	.086	.359
64	44.15	.487	.106	.147
65	43.72	.467	.115	.178
66	43.40	.483	.117	-.007
67	42.96	.544	.078	.234
68	42.94	.535	.072	.391
69	42.77	.552	.079	.245
70	43.90	.506	.092	.224
71	43.40	.450	.102	.211
72	43.33	.474	.097	.292
73	44.57	.470	.003	.404
74	45.63	.489	.055	.388
75	46.56	.435	.094	.303
76	46.50	.437	.093	.226
77	47.65	.385	.099	.266
78	48.07	.516	.109	.304
79	48.50	.450	.115	.098
80	48.39	.501	.106	.208
81	48.07	.523	.094	.243
82	47.84	.497	.101	.264
83	48.[illegible]	.500	.102	.266
84	49.05	.417	.089	.295
85	45.46	.391	.093	.226
86	44.78	.497	.110	.169
87	44.46	.505	.098	.218
88	44.04	.561	.079	.307
89	43.62	.534	.086	.283
90	43.30	.476	.087	.314
91	42.[illegible]	.510	.091	.212
92	42.77	.553	.104	.278
93	42.45	.623	.107	.239
94	42.34	.648	.098	.351
95	42.66	.581	.099	.270
96	42.77	.526	.100	.219
97	43.30	.554	.099	.342
98	43.83	.541	.105	.297

Run No. 2-11174 (Figure 17, p. 66) (82 wt. % AP propellant [UFN], 7 Hz. oscillatory pressure, 12-14 mm)

SCAN NUMBER	PRESSURE-PSIA	H2O MOL FRACTION	CO2 MOL FRACTION	CO MOL FRACTION
1	62.66	.258	.056	.234
2	62.66	.291	.053	.293
3	62.57	.278	.042	.316
4	62.37	.272	.035	.364
5	62.34	.270	.029	.380
6	62.57	.320	.038	.434
7	62.39	.341	.049	.238
8	62.39	.282	.056	.224
9	62.57	.298	.088	.089
10	62.39	.257	.072	.221
11	62.39	.231	.058	.240
12	62.59	.211	.043	.331
13	62.36	.216	.043	.326
14	62.36	.296	.039	.334
15	62.40	.305	.034	.392
16	62.20	.336	.045	.326
17	62.11	.327	.057	.275
18	62.02	.341	.068	.230
19	61.93	.371	.073	.232
20	61.93	.261	.078	.192
21	62.02	.296	.054	.333
22	61.84	.275	.035	.353
23	61.93	.268	.031	.317
24	62.62	.340	.047	.248
25	61.66	.319	.059	.168
26	61.75	.278	.071	.270
27	61.84	.307	.076	.196
28	61.66	.274	.044	.382
29	61.66	.276	.042	.369
30	61.56	.358	.047	.333
31	61.38	.347	.038	.273
32	61.58	.339	.043	.303
33	61.47	.347	.054	.284
34	61.34	.398	.044	.284
35	61.29	.331	.039	.385
36	61.47	.389	.052	.278
37	61.47	.383	.058	.330
38	61.33	.454	.054	.329
39	61.47	.319	.049	.264
40	61.47	.310	.052	.234
41	61.56	.292	.039	.364
42	61.47	.315	.039	.361
43	61.47	.308	.056	.239
44	61.47	.388	.059	.212
45	61.38	.269	.067	.203
46	61.47	.278	.046	.284
47	61.47	.331	.076	.233
48	61.47	.296	.081	.187
49	61.66	.355	.087	.184
50	61.66	.369	.086	.192
51	61.84	.278	.062	.272
52	61.84	.245	.042	.349

Run No. 2-11174 continued

53	61.84	.387	.052	.249
54	61.93	.315	.069	.281
55	62.11	.315	.070	.323
56	62.11	.294	.060	.315
57	62.11	.272	.052	.390
58	62.20	.292	.052	.382
59	62.20	.278	.067	.280
60	62.30	.305	.080	.133
61	62.30	.315	.076	.186
62	62.48	.257	.066	.271
63	62.57	.265	.063	.243
64	62.66	.265	.046	.354
65	62.74	.287	.044	.378
66	62.75	.313	.066	.177
67	62.84	.299	.055	.315
68	62.94	.361	.056	.236
69	63.12	.276	.061	.243
70	63.12	.312	.072	.215
71	63.03	.312	.078	.229
72	63.21	.293	.083	.243
73	63.12	.227	.051	.380
74	63.21	.267	.043	.331
75	63.39	.308	.046	.298
76	63.39	.315	.052	.366
77	63.58	.281	.050	.304
78	63.67	.309	.041	.402
79	63.67	.367	.054	.267
80	63.67	.336	.061	.232
81	63.76	.331	.059	.171
82	63.85	.297	.057	.389
83	63.76	.321	.055	.314
84	63.76	.291	.053	.299
85	63.76	.294	.054	.281
86	63.85	.256	.038	.404
87	63.67	.295	.042	.318
88	63.76	.355	.053	.260
89	63.85	.351	.050	.260
90	63.85	.321	.049	.287
91	63.85	.301	.051	.227
92	63.85	.266	.051	.324
93	63.85	.317	.054	.304
94	64.03	.302	.052	.325
95	63.94	.327	.046	.317
96	63.94	.308	.048	.325
97	63.76	.301	.036	.314
98	63.85	.294	.025	.430
99	63.76	.387	.033	.336
100	63.85	.371	.030	.497
101	63.85	.368	.024	.430
102	63.85	.302	.039	.295
103	63.85	.342	.045	.340
104	63.85	.321	.035	.408
105	63.85	.345	.045	.234
106	63.76	.321	.053	.253
107	63.76	.275	.049	.274
108	63.67	.250	.038	.355
109	63.67	.306	.041	.287

Run No. 2-11174 continued

110	83.57	.297	.037	.019
111	83.57	.351	.037	.306
112	83.48	.333	.048	.268
113	83.48	.322	.059	.190
114	83.39	.282	.045	.318
115	83.48	.268	.032	.311
116	83.48	.269	.022	.439
117	83.39	.338	.033	.353
118	83.39	.311	.048	.238
119	83.39	.245	.043	.258
120	83.30	.255	.049	.264
121	83.30	.270	.048	.446
122	83.21	.229	.034	.404
123	83.21	.257	.048	.278
124	83.12	.316	.039	.338
125	83.03	.285	.041	.348
126	83.03	.274	.041	.264
127	82.94	.291	.055	.263
128	82.94	.282	.052	.354
129	82.94	.260	.059	.223
130	82.94	.291	.055	.323
131	82.94	.254	.047	.236
132	82.75	.280	.053	.279
133	82.85	.245	.058	.391
134	82.66	.317	.048	.277
135	82.57	.253	.037	.318
136	82.48	.271	.030	.315
137	82.39	.323	.044	.238
138	82.39	.370	.046	.319
139	82.20	.277	.041	.307
140	82.20	.304	.041	.397
141	82.11	.349	.054	.222
142	82.02	.347	.060	.258
143	82.02	.313	.052	.226
144	81.93	.281	.043	.345
145	82.02	.258	.039	.362
146	81.93	.284	.036	.348
147	81.84	.232	.027	.309
148	81.93	.273	.034	.274
149	81.75	.257	.038	.315
150	81.56	.339	.049	.239
151	81.47	.300	.050	.293
152	81.47	.319	.043	.279
153	81.47	.290	.048	.292
154	81.47	.262	.043	.484
155	81.38	.348	.053	.288
156	81.38	.342	.060	.291
157	81.38	.318	.057	.347
158	81.38	.369	.052	.341
159	81.38	.308	.041	.384
160	81.29	.313	.043	.434
161	81.29	.269	.052	.342
162	81.29	.253	.066	.289
163	81.20	.302	.053	.333
164	81.20	.313	.057	.177
165	81.20	.231	.054	.385
166	81.20	.280	.060	.233

Run No. 2-11174 continued

167	61.29	.202	.051	.340
168	61.29	.266	.061	.268
169	61.38	.266	.066	.254
170	61.29	.274	.075	.288
171	61.36	.283	.076	.232
172	61.47	.234	.056	.267
173	61.47	.231	.058	.274
174	61.56	.278	.057	.315
175	61.56	.310	.056	.254
176	61.56	.298	.069	.238
177	61.56	.397	.075	.242
178	61.65	.236	.049	.455
179	61.65	.310	.046	.342
180	61.75	.342	.059	.278
181	61.65	.285	.063	.230
182	61.84	.277	.069	.285
183	62.02	.266	.078	.162
184	62.20	.232	.074	.260
185	62.20	.278	.059	.306
186	62.39	.302	.066	.244
187	62.30	.286	.075	.241
188	62.39	.305	.090	.150
189	62.39	.293	.078	.289
190	62.48	.232	.046	.320
191	62.57	.279	.046	.250
192	62.66	.308	.066	.289
193	62.66	.254	.057	.400
194	62.66	.223	.352	.303
195	62.75	.236	.055	.300
196	63.03	.290	.068	.156
197	62.94	.235	.079	.226
198	63.12	.261	.078	.163
199	63.12	.247	.074	.233
200	63.21	.255	.060	.312
201	63.21	.246	.050	.430
202	63.30	.211	.043	.413
203	63.39	.282	.050	.304
204	63.48	.308	.094	.142
205	63.39	.311	.059	.223
206	63.39	.290	.042	.363
207	63.39	.281	.029	.426
208	63.48	.306	.036	.302
209	63.48	.352	.044	.298

Run No. 2-31474 (Figure 18, p. 67) (80 wt. % AP propellant [UFO], 8 Hz. oscillatory pressure, 3-5 mm)

SCAN NUMBER	PRESSURE,PSIA	FLAME TEMP.,DEG. KELVIN	H2O ABSORBANCE	CO2 ABSORBANCE	CO ABSORBANCE	NA-D ABS.
1	42.06	2368.1	.035	.063	.047	.591
2	42.30	2379.8	.057	.095	.029	.578
3	42.31	2368.5	.050	.102	.038	.581
4	42.09	2374.3	.052	.088	.030	.596
5	42.09	2372.6	.044	.112	-.000	.575
6	41.96	2363.8	.035	.103	.009	.565
7	41.86	2374.3	.044	.098	.035	.555
8	41.88	2368.3	.024	.119	.028	.548
9	41.84	2356.3	.027	.129	.009	.555
10	41.75	2371.6	.041	.119	.028	.548
11	41.71	2379.2	.051	.104	.068	.534
12	41.54	2364.8	.042	.095	.044	.507
13	41.56	2368.9	.036	.081	.038	.497
14	41.28	2360.9	.028	.081	.038	.497
15	41.63	2376.5	.041	.102	.024	.497
16	40.22	2369.6	.029	.082	.031	.507
17	40.74	2394.5	.015	.064	.012	.497
18	40.69	2374.9	.024	.074	.062	.492
19	40.74	2404.7	.033	.071	.020	.476
20	40.65	2396.1	.050	.112	.044	.513
21	40.78	2423.4	.024	.093	.033	.471
22	40.52	2430.3	.042	.068	.048	.471
23	40.91	2421.5	.044	.115	.054	.481
24	41.03	2426.4	.034	.111	-.015	.492
25	41.12	2417.9	.050	.111	.043	.502
26	41.26	2395.9	.024	.093	.061	.502
27	41.37	2409.5	.049	.101	-.004	.492
28	41.42	2413.8	.045	.106	.021	.486
29	41.63	2434.8	.032	.108	.003	.465
30	41.75	2421.4	.053	.105	-.009	.502
31	41.14	2427.4	.045	.124	-.004	.486
32	42.36	2438.3	.026	.127	.058	.497
33	42.99	2459.6	.038	.136	.031	.497
34	43.41	2442.5	.046	.127	.022	.523
35	43.96	2447.3	.022	.109	.064	.528
36	44.39	2473.2	.039	.164	.048	.523
37	44.93	2494.8	.045	.108	.044	.513
38	45.19	2507.2	.053	.101	.038	.492
39	45.57	2496.7	.033	.136	.044	.502
40	46.08	2516.3	.022	.147	.029	.486
41	46.13	2507.5	.031	.113	.038	.518
42	46.51	2511.3	.042	.156	.029	.513
43	46.61	2539.3	.046	.099	.047	.497
44	47.06	2542.3	.044	.147	.009	.529
45	47.33	2475.4	.042	.132	-.018	.575
46	47.91	2477.2	.048	.153	-.017	.586
47	48.28	2469.8	.039	.124	.054	.541
48	48.34	2527.8	.038	.143	.034	.539
49	48.27	2568.6	.028	.148	.044	.513
50	48.49	2555.5	.022	.132	.012	.555
51	50.12	2554.3	.046	.144	.002	.539
52	50.37	2532.9	.025	.122	.034	.602

Run No. 2-31474 continued

53	50.75	2543.2	.033	.150	.019	.578
54	50.[illegible]	2531.7	.027	.136	.019	.591
55	51.69	2521.1	.048	.112	.007	.623
56	51.50	2510.4	.052	.108	.042	.649
57	51.47	2501.8	.045	.134	.019	.[illegible]
58	51.73	2515.0	.044	.154	.049	.628
59	51.[illegible]	2517.0	.031	.140	.033	.624
60	52.11	2501.6	.059	.188	.085	.654
61	52.32	2510.3	.046	.173	.005	.659
62	52.49	2513.0	.040	.152	.027	.654
63	52.[illegible]	2491.5	.042	.152	.029	.686
64	52.38	2482.7	.039	.152	.054	.670
65	52.45	2496.5	.041	.139	.020	.659
66	52.32	2505.7	.042	.140	-.014	.644
67	52.11	2480.0	.030	.154	.029	.659
68	51.77	2477.7	.044	.168	.058	.675
69	51.39	2516.0	.049	.163	-.008	.[illegible]
70	51.65	2382.4	.051	.131	.016	1.220
71	50.75	2513.1	.050	.131	.052	.628
72	50.53	2532.4	.056	.131	.038	.581
73	50.24	2511.1	.050	.112	.059	.628
74	50.03	2530.4	.043	.160	.021	.581
75	49.90	2497.9	.041	.146	.059	.633
76	49.65	2490.2	.043	.153	.045	.612
77	49.44	2510.2	.050	.120	.060	.59[illegible]
78	49.14	2513.6	.043	.081	.068	.565
79	48.80	2502.3	.051	.111	.026	.575
80	48.56	2508.7	.059	.165	-.017	.575
81	48.22	2506.0	.053	.174	.008	.560
82	47.85	2497.1	.054	.152	.053	.549
83	47.50	2493.4	.049	.161	.020	.565
84	47.08	2489.9	.053	.177	.039	.501
85	46.[illegible]	2503.7	.036	.162	.021	.534
86	46.[illegible]	2504.7	.038	.120	.055	.524
87	46.[illegible]	2509.5	.053	.157	.023	.523
88	46.[illegible]	2502.6	.036	.165	-.032	.518
89	46.04	2495.3	.055	.116	.033	.507
90	45.87	2499.5	.029	.138	.050	.492
91	45.66	2478.3	.035	.160	.033	.513
92	45.40	2482.2	.040	.176	.023	.507
93	45.19	2487.2	.051	.148	.014	.539
94	44.77	2496.7	.056	.135	.018	.562
95	44.[illegible]	2500.9	.052	.136	.018	.[illegible]
96	44.49	2506.5	.038	.165	.024	.47[illegible]
97	43.73	2487.8	.065	.152	.004	.48[illegible]
98	43.42	2492.6	.057	.129	.068	.529
99	43.[illegible]	2436.4	.031	.159	-.034	.507
100	43.20	2440.5	.042	.169	-.003	.518
101	43.16	2469.6	.044	.185	-.019	.502
102	43.07	2457.0	.050	.185	-.031	.461
103	42.90	2492.0	.034	.117	.038	.439
104	42.[illegible]	2454.6	.038	.073	.053	.465
105	42.[illegible]	2475.8	.027	.070	.033	.465
106	42.43	2465.0	.040	.117	-.011	.460
107	42.20	2460.0	.043	.125	.052	.455
108	42.01	2461.9	.047	.128	.046	.460
109	41.75	2456.3	.053	.128	.068	.471

Run No. 2-31474 continued

110	41.54	2455.1	.036	.143	.024	.476
111	41.33	2471.2	.037	.152	.017	.469
112	41.44	2459.4	.039	.153	.024	.471
113	41.25	2455.6	.035	.162	.019	.468
114	41.25	2439.2	.042	.139	.034	.476
115	41.25	2435.7	.050	.116	.034	.460
116	41.28	2443.6	.033	.100	.014	.455
117	41.28	2468.5	.029	.148	.022	.434
118	41.28	2467.4	.044	.125	.022	.423
119	41.12	2472.9	.034	.124	.011	.450
120	41.12	2456.8	.032	.122	.024	.444
121	40.99	2449.3	.025	.123	.024	.446
122	40.91	2451.4	.043	.164	.003	.458
123	40.99	2492.4	.034	.146	.009	.397
124	41.03	2485.8	.039	.146	.009	.418
125	41.46	2473.5	.047	.137	.024	.439
126	41.71	2496.7	.046	.128	.004	.423
127	42.05	2503.7	.048	.115	.019	.439
128	42.52	2563.8	.048	.128	-.024	.460
129	42.99	2536.4	.034	.097	.029	.434
130	43.41	2562.5	.041	.132	-.016	.450
131	43.92	2529.8	.048	.138	.003	.455
132	44.22	2545.5	.053	.123	.003	.429
133	44.64	2547.4	.065	.135	-.009	.444
134	44.61	2536.9	.046	.093	.024	.466
135	45.11	2540.1	.034	.113	.003	.465
136	45.45	2539.1	.044	.098	.035	.497
137	45.78	2539.7	.073	.106	.034	.481
138	46.13	2568.4	.045	.125	.019	.471
139	46.55	2574.7	.045	.124	.043	.455
140	47.02	2565.7	.038	.150	.042	.497
141	47.53	2563.6	.043	.155	-.022	.471
142	47.95	2570.2	.050	.175	.014	.502
143	48.33	2569.2	.043	.173	.014	.497
144	48.76	2574.0	.036	.193	.002	.481
145	49.14	2569.1	.021	.193	.046	.492
146	49.48	2607.5	.035	.149	.025	.492
147	49.69	2597.8	.035	.135	.025	.513
148	49.78	2560.9	.031	.149	.033	.523
149	49.99	2566.8	.034	.154	.032	.570
150	50.12	2575.9	.033	.160	.034	.544
151	50.20	2565.2	.034	.160	.014	.575
152	50.37	2581.9	.046	.153	.018	.560
153	50.45	2604.8	.034	.166	.004	.523
154	50.58	2579.1	.026	.139	.023	.539
155	50.50	2546.8	.022	.113	.031	.544
156	50.41	2563.2	.036	.127	.044	.566
157	50.37	2574.2	.026	.129	.023	.549
158	50.37	2569.7	.043	.129	.044	.534
159	49.96	2545.6	.034	.141	.040	.575
160	49.69	2551.1	.041	.128	.054	.549
161	49.18	2529.1	.043	.137	.034	.570
162	48.64	2560.8	.037	.131	-.005	.518
163	48.59	2547.6	.036	.113	.011	.555
164	48.25	2529.1	.036	.105	.040	.570
165	48.08	2515.4	.039	.121	.027	.549
166	47.67	2569.7	.051	.154	.007	.581

Run No. 2-31474 continued

167	47.05	2537.5	.045	.128	.012	.555
168	47.53	2540.2	.049	.148	.033	.523
169	47.49	2529.8	.065	.123	.028	.539
170	47.19	2516.4	.032	.136	.019	.528
171	47.02	2524.3	.029	.128	.064	.528
172	46.76	2534.8	.043	.136	.034	.497
173	46.59	2519.0	.037	.165	.034	.544
174	46.21	2519.6	.046	.188	-.044	.534
175	45.91	2535.0	.056	.158	.003	.481
176	45.62	2512.7	.047	.148	.012	.507
177	45.4	2513.2	.039	.106	.003	.497
178	45.07	2507.9	.047	.087	.020	.507
179	44.90	2504.2	.034	.095	.037	.497
180	44.68	2496.5	.043	.110	.022	.513
181	44.51	2493.6	.048	.137	-.013	.523
182	44.39	2509.7	.050	.139	.022	.492
183	44.17	2497.2	.043	.139	.022	.502
184	44.09	2518.4	.040	.138	.028	.471
185	43.83	2510.3	.049	.154	.062	.486
186	43.58	2488.2	.049	.170	.036	.507
187	43.41	2477.1	.051	.156	-.003	.518
188	43.03	2471.4	.051	.187	-.024	.507
189	42.83	2467.0	.052	.144	.023	.502
190	42.58	2476.6	.055	.139	.025	.497
191	42.31	2502.1	.050	.086	.035	.444
192	42.18	2502.4	.040	.132	.008	.434
193	42.03	2495.1	.040	.111	.016	.429
194	41.97	2498.4	.039	.089	.023	.444
195	41.97	2467.5	.051	.101	.039	.471
196	41.84	2430.8	.069	.113	-.000	.528
197	41.80	2461.3	.052	.169	.832	.476
198	41.75	2493.6	.060	.162	.024	.423
199	41.54	2464.3	.044	.127	.080	.476
200	41.46	2469.0	.032	.148	.024	.444

Run No. 1-22174 (Figure 19, p. 69) (82 wt. % AP propellant [UFN], 22 Hz. oscillatory pressure, 12-14 mm)

SCAN NUMBER	PRESSURE, PSIA	H2O MOL FRACTION	CO2 MOL FRACTION	CO MOL FRACTION
1	45.75	.576	.092	.234
2	45.32	.468	.092	.237
3	44.74	.487	.099	.208
4	44.16	.525	.102	.239
5	43.64	.540	.103	.256
6	43.41	.422	.102	.211
7	42.79	.591	.099	.317
8	42.45	.509	.110	.260
9	42.50	.490	.108	.251
10	42.14	.524	.108	.265
11	41.71	.590	.099	.185
12	41.29	.554	.108	.129
13	40.87	.530	.105	.291
14	40.49	.449	.103	.379
15	39.91	.576	.118	.068
16	39.48	.537	.113	.318
17	39.19	.555	.113	.315
18	39.91	.582	.106	.268
19	45.44	.608	.103	.201
20	46.97	.627	.108	.268
21	41.93	.588	.109	.148
22	42.78	.539	.121	.190
23	43.52	.487	.132	.132
24	44.20	.619	.140	.173
25	44.09	.560	.123	.145
26	45.43	.512	.118	.226
27	45.98	.548	.121	.182
28	46.38	.471	.135	.108
29	46.80	.474	.117	.278
30	46.76	.480	.110	.211
31	46.49	.622	.094	.212
32	46.28	.489	.069	.307
33	45.98	.546	.097	.292
34	45.66	.478	.095	.224
35	45.32	.519	.091	.261
36	45.11	.407	.083	.298
37	44.79	.549	.089	.285
38	44.26	.505	.098	.277
39	43.62	.488	.097	.291
40	43.20	.462	.102	.303
41	42.56	.514	.106	.335
42	41.82	.540	.110	.284
43	41.29	.490	.109	.328
44	40.95	.504	.123	.057
45	40.34	.502	.124	.248
46	39.91	.573	.115	.167
47	39.91	.653	.149	.287
48	44.23	.562	.120	.304
49	46.65	.627	.117	.428
50	41.18	.483	.129	.115
51	41.93	.522	.131	.287
52	42.35	.523	.135	.249

Run No. 1-22174 continued

53	42.49	.558	.131	.210
54	42.41	.562	.126	.172
55	43.94	.469	.114	.135
56	44.37	.473	.119	.184
57	44.90	.594	.127	.142
58	45.43	.534	.122	.236
59	46.07	.534	.118	.225
60	46.49	.484	.107	.193
61	47.55	.468	.104	.074
62	48.40	.460	.110	.127
63	48.82	.500	.120	.093
64	49.25	.397	.124	.034
65	49.24	.492	.128	.003
66	49.64	.442	.130	.060
67	48.72	.362	.115	.048
68	45.19	.52[illegible]	.129	.032
69	47.45	.416	.114	.190
70	46.41	.468	.101	.176
71	46.17	.457	.103	.146
72	45.84	.422	.090	.214
73	45.11	.440	.095	.255
74	44.69	.507	.097	.387
75	44.47	.479	.104	.177
76	44.15	.485	.099	.247
77	43.73	.473	.103	.193
78	43.01	.614	.112	.236
79	42.56	.574	.113	.282
80	42.29	.619	.115	.228
81	41.71	.631	.111	.179
82	41.18	.591	.105	.236
83	40.44	.621	.118	.110
84	39.91	.621	.126	.081
85	39.59	.606	.121	.197
86	39.27	.456	.113	.270
87	39.96	.506	.132	.149
88	38.95	.694	.131	.155
89	38.96	.542	.124	.217
90	38.74	.498	.120	.254

Run No. 11-4474 (Figure 20, p. 70) (85 wt. % AP propellant [UFR], 22 Hz. oscillatory pressure, 3-5 mm)

SCAN NUMBER	PRESSURE,PSIA	FLAME TEMP.,DEG. KELVIN	H2O ABSORBANCE	CO2 ABSORBANCE	CO ABSORBANCE	NA-D ABS.
1	45.34	2610.2	.055	.252	.013	.375
2	45.20	2654.5	.066	.259	.042	.336
3	44.56	2645.8	.064	.262	.038	.353
4	43.97	2642.4	.059	.249	.045	.319
5	43.50	2626.6	.062	.253	.035	.342
6	43.04	2620.4	.066	.262	.019	.342
7	42.74	2646.9	.065	.285	.028	.308
8	42.40	2608.4	.061	.251	.065	.288
9	42.10	2614.8	.057	.253	.034	.342
10	42.02	2570.7	.057	.259	.023	.358
11	41.61	2616.1	.072	.265	.024	.319
12	41.51	2525.0	.066	.211	.032	.408
13	41.34	2613.4	.054	.192	.029	.314
14	41.08	2561.9	.063	.213	.053	.397
15	41.08	2591.4	.066	.189	.064	.353
16	41.17	2582.7	.063	.222	-.010	.356
17	41.25	2628.2	.066	.293	.000	.308
18	41.55	2621.2	.064	.329	.030	.330
19	41.93	2629.6	.053	.339	.037	.356
20	42.44	2625.1	.060	.320	.026	.319
21	43.04	2625.6	.061	.306	.054	.314
22	43.63	2706.3	.066	.277	.039	.258
23	44.22	2646.0	.059	.282	.035	.314
24	44.93	2660.0	.061	.288	.044	.358
25	45.46	2659.9	.070	.336	.007	.314
26	46.05	2702.2	.054	.293	.018	.286
27	46.52	2679.8	.056	.322	.004	.319
28	46.95	2694.8	.058	.337	.036	.319
29	47.41	2641.9	.055	.345	.053	.364
30	47.49	2651.7	.057	.342	.039	.347
31	47.56	2606.6	.054	.329	.016	.353
32	47.64	2614.8	.049	.327	.000	.342
33	47.41	2710.9	.056	.301	.014	.291
34	47.15	2721.5	.057	.252	.041	.297
35	46.86	2620.1	.066	.239	.042	.386
36	46.52	2641.2	.059	.232	.042	.336
37	46.26	2610.9	.060	.235	.026	.364
38	45.84	2673.1	.051	.255	.009	.291
39	45.46	2645.5	.061	.251	.030	.336
40	45.12	2572.0	.057	.267	.049	.425
41	44.65	2597.3	.055	.233	.033	.347
42	44.27	2600.4	.060	.284	.018	.336
43	43.63	2627.2	.060	.300	.031	.297
44	43.12	2564.4	.068	.289	.021	.350
45	42.61	2675.6	.065	.229	.017	.235
46	42.23	2571.8	.066	.207	.012	.330
47	41.97	2568.1	.064	.253	.014	.336
48	41.72	2582.3	.069	.244	.036	.347
49	41.51	2594.3	.071	.274	.002	.336
50	41.47	2588.3	.057	.318	.021	.347
51	41.38	2659.7	.073	.293	.051	.286
52	41.21	2642.7	.062	.223	.041	.297

Run No. 11-4474 continued

53	41.25	2691.3	.057	.193	.047	.258
54	41.36	2646.6	.063	.156	.043	.291
55	41.59	2647.5	.067	.191	.813	.286
56	41.93	2702.3	.072	.223	.814	.269
57	42.14	2665.7	.056	.217	.831	.236
58	42.47	2644.8	.058	.235	.865	.382
59	42.49	2695.3	.056	.242	-.006	.247
60	43.55	2695.5	.059	.285	.848	.286
61	44.14	2654.6	.056	.257	.041	.319
62	44.73	2629.6	.062	.277	.817	.314
63	45.41	2710.8	.055	.268	.054	.263
64	46.05	2610.7	.060	.257	.043	.369
65	46.56	2642.1	.054	.260	.037	.342
66	47.24	2674.5	.053	.279	.818	.297
67	47.62	2706.4	.058	.343	.023	.291
68	47.47	2669.8	.051	.369	.015	.330
69	48.13	2731.6	.052	.351	.018	.252
70	47.79	2694.1	.056	.319	.022	.286
71	47.41	2716.9	.053	.297	.018	.275
72	47.11	2[illegible].6	.045	.262	.854	.388
73	46.69	2702.2	.067	.236	.034	.286
74	46.26	2734.7	.054	.248	.055	.253
75	45.84	2626.2	.059	.282	.026	.347
76	45.45	2674.4	.055	.263	.847	.286
77	45.24	2670.8	.066	.334	.022	.269
78	44.90	2650.7	.064	.299	.034	.319
79	44.46	2682.2	.063	.284	.057	.297
80	44.14	2635.4	.070	.273	.030	.330
81	43.72	2652.8	.063	.266	.021	.308
82	43.33	2631.4	.062	.247	.037	.342
83	42.82	2656.7	.059	.223	.046	.425
84	42.27	2685.8	.059	.217	.041	.353
85	41.85	2621.3	.064	.219	.018	.291
86	41.55	2682.1	.076	.249	.013	.254
87	41.30	2621.7	.049	.272	.032	.325
88	41.21	2697.4	.064	.294	.036	.253
89	41.17	2632.1	.064	.361	.028	.259
90	41.42	2615.4	.063	.332	.028	.330
91	41.72	2689.5	.062	.335	.017	.247
92	42.10	2677.3	.071	.326	.043	.275
93	42.65	2661.5	.061	.317	.002	.291
94	43.12	2649.6	.056	.338	.065	.291
95	43.63	2708.5	.057	.329	.039	.252
96	44.14	2588.5	.053	.314	.034	.353
97	44.59	2684.2	.050	.358	.012	.403
98	44.73	2617.0	.053	.410	-.019	.185
99	45.24	2636.0	.872	.424	-.006	.325
100	45.75	2650.8	.856	.333	.028	.336

Run No. 6-4374 (Figure 21, p. 71) (82 wt. % AP propellant [UFP], 100 Hz. oscillatory pressure, 3-5 mm)

1	[illegible]	[illegible]	.441	.078	.169	.344
[illegible]	[illegible]	[illegible]	.427	.069	.161	.306
[illegible]	[illegible]	[illegible]	.424	.051	.247	.327
[illegible]	[illegible]	[illegible]	.384	.063	.141	.338
[illegible]	[illegible]	[illegible]	.390	.052	.274	.296
[illegible]	[illegible]	[illegible]	.397	.050	.329	.319
7	[illegible]	[illegible]	.397	.062	.196	.378
[illegible]	[illegible]	[illegible]	.396	.069	.176	.322
[illegible]	[illegible]	[illegible]	.438	.064	.262	.327
10	[illegible]	[illegible]	.401	.048	.373	.333
11	[illegible]	[illegible]	.[illegible]	.045	.238	.311
12	[illegible]	[illegible]	.392	.059	.226	.283
13	[illegible]	[illegible]	.400	.060	.281	.298
14	[illegible]	[illegible]	.407	.073	.224	.272
15	[illegible]	[illegible]	.430	.078	.128	.316
16	[illegible]	[illegible]	.383	.072	.269	.355
17	[illegible]	[illegible]	.371	.068	.207	.432
18	[illegible]	[illegible]	.401	.071	.309	.319
19	[illegible]	[illegible]	.412	.075	.318	.261
20	[illegible]	[illegible]	.[illegible]	.063	.[illegible]	.350
21	[illegible]	[illegible]	.[illegible]	.068	.[illegible]	.327
22	[illegible]	[illegible]	.405	.061	.419	.333
23	[illegible]	[illegible]	.[illegible]	.058	.307	.427
24	[illegible]	[illegible]	.[illegible]	.053	.[illegible]	.410
25	[illegible]	[illegible]	.[illegible]	.[illegible]	.[illegible]	.427
26	[illegible]	[illegible]	.407	.054	.[illegible]	.355
27	[illegible]	[illegible]	.377	.056	.405	.350
28	[illegible]	[illegible]	.[illegible]	.063	.[illegible]	.272
29	[illegible]	[illegible]	.[illegible]	.[illegible]	.[illegible]	.300
30	[illegible]	[illegible]	.[illegible]	.055	.[illegible]	.305
31	[illegible]	[illegible]	.[illegible]	.061	.191	.261
32	[illegible]	[illegible]	.[illegible]	.077	.[illegible]	.[illegible]
33	[illegible]	[illegible]	.[illegible]	.067	.[illegible]	.[illegible]
34	[illegible]	[illegible]	.[illegible]	.053	.255	.301
35	[illegible]	[illegible]	.[illegible]	.[illegible]	.[illegible]	.[illegible]
36	[illegible]	[illegible]	.[illegible]	.063	.[illegible]	.311
37	[illegible]	[illegible]	.[illegible]	.[illegible]	.[illegible]	.272
38	[illegible]	[illegible]	.[illegible]	.063	.[illegible]	.327
39	[illegible]	[illegible]	.[illegible]	.052	.[illegible]	.[illegible]
40	[illegible]	[illegible]	.413	.054	.[illegible]	.316
41	[illegible]	[illegible]	.[illegible]	.[illegible]	.[illegible]	.[illegible]
42	[illegible]	[illegible]	.427	.072	.[illegible]	.[illegible]
43	[illegible]	[illegible]	.[illegible]	.053	.260	.[illegible]
44	[illegible]	[illegible]	.[illegible]	.[illegible]	.[illegible]	.[illegible]
45	[illegible]	[illegible]	.407	.058	.[illegible]	.372
46	[illegible]	[illegible]	.[illegible]	.[illegible]	.358	.[illegible]
47	[illegible]	[illegible]	.[illegible]	.074	.270	.[illegible]
48	[illegible]	[illegible]	.[illegible]	.078	.[illegible]	.[illegible]
49	[illegible]	[illegible]	.[illegible]	.[illegible]	.295	.311
50	[illegible]	[illegible]	.[illegible]	.[illegible]	.[illegible]	.[illegible]
51	[illegible]	[illegible]	.374	.[illegible]	.452	.333
52	[illegible]	[illegible]	.401	.056	.461	.305
[illegible]	[illegible]	[illegible]	.374	.[illegible]	.452	.289

Run No. 6-4374 continued

[illegible]	[illegible]	[illegible]	.399	.057	.247	.355
[illegible]	[illegible]	[illegible]	.346	.069	.358	.372
[illegible]	[illegible]	[illegible]	.348	.083	.258	.423
[illegible]	[illegible]	[illegible]	.393	.067	.194	.432
[illegible]	[illegible]	[illegible]	.358	.058	.394	.383
[illegible]	[illegible]	[illegible]	.389	.065	.315	.300
[illegible]	[illegible]	[illegible]	.377	.066	.238	.269
[illegible]	[illegible]	[illegible]	.442	.077	.081	.333
[illegible]	[illegible]	[illegible]	.401	.065	.236	.350
[illegible]	[illegible]	[illegible]	.414	.073	.348	.372
[illegible]	[illegible]	[illegible]	.371	.078	.214	.372
[illegible]	[illegible]	[illegible]	.429	.075	.154	.384
[illegible]	[illegible]	[illegible]	.394	.064	.282	.372
[illegible]	[illegible]	[illegible]	.394	.068	.246	.327
[illegible]	[illegible]	[illegible]	.419	.063	.343	.335
[illegible]	[illegible]	[illegible]	.345	.057	.367	.361
[illegible]	[illegible]	[illegible]	.432	.066	.283	.394
[illegible]	[illegible]	[illegible]	.387	.068	.231	.427
[illegible]	[illegible]	[illegible]	.444	.061	.177	.432
[illegible]	[illegible]	[illegible]	.547	.062	.290	.355
[illegible]	[illegible]	[illegible]	.[illegible]	.044	.196	.305
[illegible]	[illegible]	[illegible]	.374	.058	.420	.316
[illegible]	[illegible]	[illegible]	.[illegible]	.067	.247	.394
[illegible]	[illegible]	[illegible]	.[illegible]	.067	.352	.322
[illegible]	[illegible]	[illegible]	.422	.056	.371	.365
[illegible]	[illegible]	[illegible]	.422	.075	.318	.468
[illegible]	[illegible]	[illegible]	.473	.064	.174	.416
[illegible]	[illegible]	[illegible]	.[illegible]	.065	.424	.344
[illegible]	[illegible]	[illegible]	.449	.057	.204	.350
[illegible]	[illegible]	[illegible]	.[illegible]	.052	.276	.333
[illegible]	[illegible]	[illegible]	.443	.066	.303	.316
[illegible]	[illegible]	[illegible]	.484	.066	.407	.300
[illegible]	[illegible]	[illegible]	.[illegible]	.071	.293	.301
[illegible]	[illegible]	[illegible]	.412	.064	.318	.520
[illegible]	[illegible]	[illegible]	.418	.072	.223	.405
[illegible]	[illegible]	[illegible]	.375	.067	.269	.261
[illegible]	[illegible]	[illegible]	.358	.055	.276	.316
[illegible]	[illegible]	[illegible]	.340	.046	.403	.305
[illegible]	[illegible]	[illegible]	.330	.042	.347	.305
[illegible]	[illegible]	[illegible]	.314	.035	.438	.333
[illegible]	[illegible]	[illegible]	.358	.050	.334	.358
[illegible]	[illegible]	[illegible]	.429	.066	.268	.359
[illegible]	[illegible]	[illegible]	.437	.072	.243	.372
[illegible]	[illegible]	[illegible]	.410	.058	.419	.322
[illegible]	[illegible]	[illegible]	.472	.042	.369	.334
[illegible]	[illegible]	[illegible]	.373	.023	.463	.316
[illegible]	[illegible]	[illegible]	.339	.042	.239	.333
[illegible]	[illegible]	[illegible]	.367	.060	.103	.311
[illegible]	[illegible]	[illegible]	.399	.064	.464	.316
[illegible]	[illegible]	[illegible]	.364	.061	.389	.432
[illegible]	[illegible]	[illegible]	.361	.073	.215	.245

Run No. 5-4374 (Figure 22, p. 73) (82 wt. % AP propellant [UFP], 35 Hz. oscillatory pressure, 3-5 mm) continued

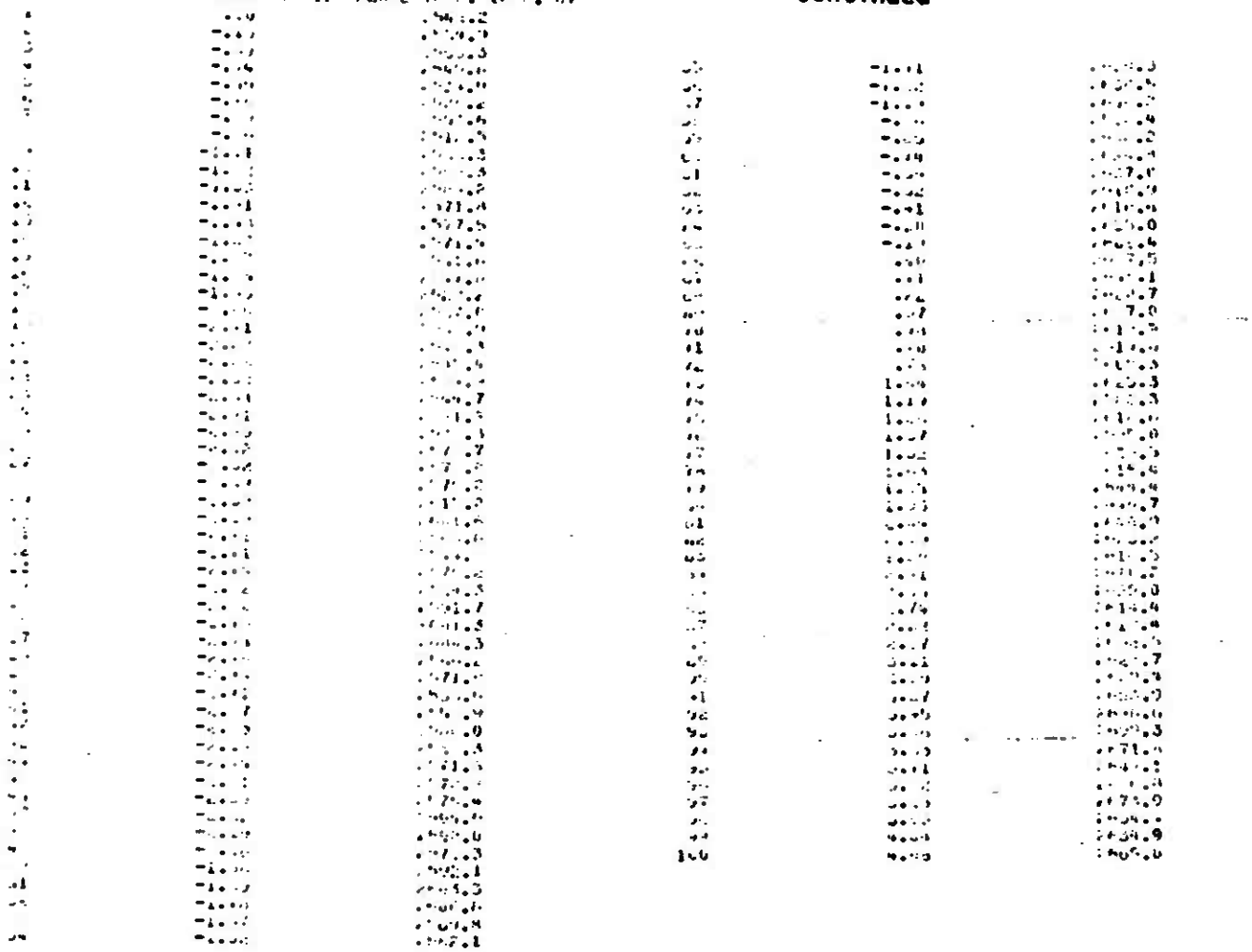

Run No. 6-31574 (Figure 23, p. 74) (82 wt. % AP propellant [UFP], 50 Hz. oscillatory pressure, 3-5 mm)

SCAN NUMBER	DELTA PRESSURE (PSI)	FLAME TEMP. (DEG. K)
1	.08	2461.7
2	.11	2454.7
3	.15	2451.4
4	.22	2448.6
5	.22	2436.6
6	.22	2441.1
7	.26	2466.3
8	.26	2450.2
9	.22	2459.9
10	.22	2441.1
11	.22	2447.8
12	.19	2432.0
13	.15	2427.4
14	.15	2437.8
15	.07	2426.7
16	.07	2424.0
17	.07	2433.8
18	.00	2418.0
19	-.07	2429.4
20	-.07	2420.4
21	-.22	2432.5
22	-.33	2423.1
23	-.37	2424.0
24	-.63	2420.4
25	-.70	2424.0
26	-.82	2436.0
27	-.96	2433.0
28	-1.07	2440.9
29	-1.22	2429.5
30	-1.30	2445.9
31	-1.48	2420.7
32	-1.56	2437.3
33	-1.70	2433.5
34	-1.76	2436.9
35	-1.93	2457.4
36	-2.00	2480.3
37	-2.11	2476.7
38	-2.19	2467.9
39	-2.30	2454.7
40	-2.37	2461.8
41	-2.41	2427.1
42	-2.52	2440.6
43	-2.56	2459.3
44	-2.67	2448.6
45	-2.67	2455.5
46	-2.71	2446.8
47	-2.74	2434.3
48	-2.74	2432.4
49	-2.67	2436.2
50	-2.71	2421.5
51	-2.63	2478.6
52	-2.67	2472.5
53	-2.67	2461.8
54	-2.59	2449.0

continued

55	-2.52	2459.3
56	-2.48	2482.5
57	-2.48	2467.9
58	-2.41	2459.3
59	-2.37	2446.8
60	-2.34	2446.8
61	-2.19	2465.4
62	-2.11	2465.4
63	-2.00	2456.1
64	-1.93	2456.0
65	-1.78	2451.9
66	-1.70	2464.8
67	-1.59	2461.7
68	-1.56	2451.9
69	-1.41	2475.7
70	-1.33	2444.2
71	-1.26	2454.7
72	-1.15	2439.1
73	-1.11	2449.5
74	-1.07	2458.6
75	-.93	2451.0
76	-.89	2454.7
77	-.78	2464.7
78	-.70	2450.5
79	-.63	2490.9
80	-.48	2468.3
81	-.41	2505.7
82	-.37	2493.4
83	-.26	2486.2
84	-.19	2486.2
85	-.15	2509.6
86	-.11	2484.8
87	-.04	2497.5
88	-.04	2502.5
89	.04	2502.5
90	.00	2486.2
91	.04	2512.3
92	.15	2497.9
93	.15	2493.2
94	.19	2500.4
95	.15	2486.2
96	.22	2493.2
97	.19	2495.7
98	.19	2472.3
99	.11	2478.9
188	.04	2445.8

Run No. 5-4474 (Figure 24, p. 76) (80 wt. % AP propellant [UFI], single-pressure-decrease-pulse, 3-5 mm)

SCAN NUMBER	PRESSURE,PSIA	FLAME TEMP.,DEG. KELVIN	H2O ABSORBANCE	CO2 ABSORBANCE	CO ABSORBANCE	HA-N ABS.
1	80.00	2391.5	.140	.334	.046	.920
2	80.00	2410.9	.146	.325	.072	.698
3	80.00	2427.1	.159	.344	.032	.925
4	80.00	2409.6	.135	.312	.067	.856
5	80.00	2441.0	.140	.313	.060	.909
6	80.00	2430.7	.135	.310	.061	.898
7	80.00	2437.8	.135	.339	.035	.904
8	80.00	2421.4	.134	.320	.053	.920
9	80.00	2425.6	.146	.290	.071	.920
10	80.00	2443.3	.147	.271	.080	.904
11	80.00	2409.0	.159	.272	.073	.909
12	80.00	2403.1	.159	.298	.057	.920
13	80.00	2449.3	.139	.303	.059	.936
14	80.00	2443.3	.146	.315	.073	.920
15	80.00	2453.5	.139	.303	.079	.904
16	80.00	2464.5	.127	.325	.072	.914
17	80.00	2491.3	.147	.357	.040	.904
18	80.00	2480.5	.152	.351	.050	.914
19	80.00	2480.0	.152	.335	.071	.941
20	80.00	2411.7	.146	.353	.030	.947
21	80.00	2425.6	.159	.346	.065	.920
22	80.00	2435.2	.140	.338	.059	.914
23	80.00	2425.0	.147	.357	.060	.920
24	80.00	2458.2	.159	.344	.052	.898
25	80.00	2455.2	.146	.208	.144	.904
26	80.00	2459.5	.159	.307	.006	.909
27	80.00	2459.3	.133	.303	.079	.947
28	80.00	2478.5	.134	.296	.084	.888
29	80.00	2457.4	.153	.355	.047	.893
30	80.00	2444.5	.153	.364	.073	.677
31	80.00	2445.1	.159	.332	.060	.888
32	80.00	2432.6	.128	.292	.073	.904
33	79.50	2429.4	.129	.301	.060	.682
34	79.15	2430.2	.146	.318	.073	.893
35	78.73	2443.9	.155	.340	.074	.898
36	78.30	2457.5	.144	.361	.056	.898
37	77.82	2449.2	.145	.341	.070	.872
38	77.11	2405.4	.141	.324	.052	.888
39	76.43	2471.7	.136	.302	.058	.877
40	75.93	2484.3	.149	.277	.071	.845
41	75.42	2466.5	.156	.300	.050	1.173
42	74.99	2511.7	.150	.295	.065	.840
43	74.65	2498.8	.152	.308	.067	.834
44	74.23	2483.6	.147	.274	.081	.850
45	74.14	2507.6	.146	.297	.090	.818
46	73.80	2494.8	.160	.243	.068	.829
47	73.63	2463.2	.140	.250	.059	.866
48	73.46	2436.6	.147	.217	.067	.802
49	73.34	2443.4	.140	.232	.088	.856
50	72.49	2439.1	.155	.234	.081	.861
51	72.11	2452.4	.187	.241	.089	.856
52	71.60	2439.0	.155	.260	.118	.845

Run No. 5-4474 continued

53	71.09	2441.5	.172	.304	.053	.854
54	70.75	2447.4	.166	.299	.083	.859
55	70.28	2445.1	.174	.319	.090	.848
56	70.07	2462.5	.174	.287	.098	.845
57	69.90	2493.4	.162	.270	.107	.807
58	69.47	2473.9	.169	.302	.878	.813
59	69.47	2451.7	.156	.345	.050	.861
60	69.39	2460.9	.151	.269	.087	.861
61	69.13	2453.5	.151	.324	.065	.861
62	68.88	2453.7	.158	.332	.036	.845
63	68.37	2451.6	.160	.289	.067	.818
64	68.12	2477.2	.180	.315	.080	.802
65	67.61	2478.3	.161	.331	.067	.818
66	67.16	2514.1	.162	.326	.051	.807
67	66.84	2514.1	.156	.349	.053	.807
68	66.42	2505.6	.150	.344	.083	.802
69	66.16	2476.7	.151	.315	.061	.829
70	65.99	2453.0	.158	.308	.045	.850
71	65.74	2471.1	.159	.317	.061	.845
72	65.74	2479.4	.159	.317	.084	.845
73	65.48	2445.8	.159	.350	.022	.866
74	65.23	2440.8	.166	.345	.107	.856
75	64.98	2448.3	.165	.311	.098	.845
76	64.63	2453.2	.176	.307	.085	.834
77	64.38	2453.5	.163	.307	.094	.861
78	63.87	2453.5	.170	.335	.062	.861
79	63.45	2448.2	.194	.395	.079	.861

Run No. 8-4374 (Figure 25, p. 77) (82 wt. % AP propellant [UFN], single-pressure-decrease-pulse, 3-5 mm)

SCAN NUMBER	PRESSURE,PSIA	FLAME TEMP.,DEG. KELVIN	H2O MOL FRACTION	CO2 MOL FRACTION	CO MOL FRACTION	NA-D ABS.
1	85.35	2539.6	.459	.047	.276	.541
2	83.61	2527.6	.443	.053	.206	.852
3	82.76	2[illegible].6	.413	.052	.287	.803
4	82.14	25[illegible].4	.456	.057	.253	.639
5	82.87	2560.4	.450	.054	.303	.869
6	82.84	2551.2	.446	.053	.232	.803
7	82.84	2512.9	.416	.049	.296	.809
8	82.93	2517.6	.452	.048	.296	.825
9	83.18	2537.2	.464	.051	.309	.847
10	83.15	2531.6	.480	.053	.297	.814
11	83.27	2548.7	.455	.054	.264	.809
12	83.05	2536.8	.454	.052	.295	.874
13	83.27	2541.3	.457	.054	.253	.847
14	83.03	2503.1	.449	.052	.279	.814
15	83.16	2538.8	.443	.052	.293	.809
16	82.73	2542.9	.476	.056	.215	.792
17	82.76	2573.1	.455	.054	.271	.798
18	82.76	2[illegible]9.8	.471	.050	.273	.716
19	82.93	2565.6	.465	.052	.291	.814
20	82.93	2557.8	.464	.052	.291	.759
21	83.10	2558.6	.435	.051	.267	.792
22	83.05	2567.4	.453	.044	.332	.809
23	83.32	2572.2	.475	.042	.347	.814
24	83.27	2582.4	.491	.044	.303	.701
25	83.15	2543.4	.485	.041	.322	.836
26	82.93	2521.9	.460	.043	.308	.869
27	82.54	2552.1	.503	.054	.231	.787
28	82.37	2563.6	.434	.054	.258	.765
29	82.32	2544.0	.434	.053	.256	.761
30	81.99	2[illegible].3	.443	.055	.249	.798
31	81.82	2575.9	.469	.049	.276	.803
32	81.87	2541.6	.441	.053	.213	.831
33	81.65	253[illegible]	.427	.053	.271	.841
34	80.72	2544.1	.449	.054	.252	.841
35	80.93	2564.9	.470	.056	.244	.791
36	79.96	2546.1	.463	.052	.240	.847
37	79.40	2562.1	.447	.052	.247	.759
38	78.84	2552.8	.455	.051	.263	.803
39	78.34	2554.3	.453	.047	.320	.809
40	77.73	2531.2	.469	.050	.286	.809
41	77.53	2542.2	.461	.049	.243	.776
42	77.24	2538.9	.447	.047	.288	.754
43	76.90	2567.9	.457	.050	.309	.770
44	76.73	2511.3	.469	.045	.291	.770
45	76.45	2[illegible].5	.447	.045	.289	.814
46	76.22	2522.7	.460	.047	.266	.793
47	75.97	2539.6	.462	.045	.315	.819
48	75.54	2541.1	.482	.048	.307	.793
49	75.29	2553.0	.471	.046	.309	.759
50	74.84	2534.1	.489	.050	.292	.809
51	74.48	2572.8	.499	.050	.280	.726
52	73.76	2561.5	.518	.051	.256	.748

Run No. 8-4374 continued

53	73.58	2563.7	.471	.051	.358	.710
54	73.63	2561.7	.490	.055	.321	.759
55	73.70	2553.9	.469	.055	.258	.743
56	72.66	2562.6	.479	.051	.273	.745
57	72.69	2567.7	.523	.052	.310	.721
58	72.69	2568.6	.510	.053	.273	.743
59	72.63	2564.2	.490	.053	.291	.743
60	72.65	2562.0	.491	.051	.279	.703
61	71.69	2561.6	.506	.056	.238	.705
62	71.67	2564.5	.506	.054	.228	.701
63	71.63	2566.1	.510	.054	.243	.770
64	70.70	2561.0	.510	.055	.281	.774
65	70.64	2562.1	.503	.057	.260	.747
66	69.63	2562.9	.544	.058	.271	.765
67	69.63	2557.9	.513	.057	.257	.776
68	69.62	2562.2	.506	.055	.271	.759
69	69.63	2557.2	.507	.057	.274	.726
70	69.61	2562.0	.459	.055	.248	.754
71	69.61	2558.0	.487	.056	.254	.774
72	69.61	2563.3	.486	.057	.195	.747
73	68.62	2564.5	.478	.055	.224	.726
74	68.67	2562.3	.427	.056	.266	.737
75	68.61	2565.6	.492	.053	.338	.743
76	68.64	2563.6	.493	.053	.250	.709
77	67.73	2474.0	.471	.053	.207	.814
78	67.69	2561.3	.484	.054	.237	.773
79	67.61	2561.6	.536	.061	.269	.721
80	66.61	2567.7	.519	.059	.323	.677
81	66.58	2565.3	.535	.059	.317	.683
82	66.61	2555.6	.517	.055	.237	.694
83	66.63	2567.5	.486	.055	.285	.726
84	66.59	2564.0	.485	.050	.234	.737
85	66.63	2568.6	.504	.059	.303	.732
86	66.66	2561.9	.519	.054	.365	.705
87	66.57	2567.0	.491	.053	.314	.694
88	66.62	2561.5	.520	.053	.278	.726
89	65.65	2565.2	.475	.049	.265	.721
90	65.61	2561.3	.494	.048	.279	.737
91	65.56	2571.1	.476	.044	.341	.661
92	64.61	2561.6	.511	.047	.242	.732
93	64.70	2564.7	.540	.047	.268	.732
94	64.66	2561.3	.487	.046	.295	.705
95	64.61	2477.1	.519	.047	.348	.787
96	64.61	2565.2	.536	.048	.343	.757
97	64.63	2567.6	.490	.051	.287	.653
98	64.59	2564.4	.472	.056	.249	.710
99	64.61	2561.2	.513	.060	.269	.737
100	64.62	2567.3	.508	.058	.238	.716
101	64.64	2574.0	.486	.054	.227	.655
102	64.67	2564.3	.448	.053	.276	.633
103	64.64	2564.9	.469	.053	.265	.649
104	63.63	2563.2	.522	.057	.210	.573
105	63.63	2565.8	.500	.059	.321	.606
106	63.62	2567.7	.509	.056	.324	.623
107	63.65	2564.4	.519	.048	.294	.653
108	63.65	2563.2	.548	.051	.314	.628
109	63.65	2564.1	.537	.055	.282	.710

Run No. 8-4374 continued

11c	63.15	2538.5	.500	.057	.305	.716
11d	63.23	2537.7	.499	.056	.238	.661
11e	63.32	2541.5	.516	.057	.267	.623
11f	63.40	2581.0	.487	.060	.261	.573
11g	63.23	2578.7	.496	.051	.299	.623
11h	63.15	2597.6	.511	.059	.326	.694
11i	63.15	2564.9	.490	.061	.300	.612
11j	62.61	2598.9	.520	.060	.235	.601
11k	62.57	2568.7	.464	.056	.244	.561
11m	62.36	2625.8	.489	.057	.281	.672
12J	62.21	2491.5	.506	.057	.207	.765
12A	62.21	2567.2	.523	.062	.310	.606
12C	62.21	2573.4	.518	.057	.270	.666
12D	62.13	2543.2	.556	.063	.297	.770
12E	62.21	2523.0	.468	.064	.212	.710

Run No. 1-31574 (Figure 26, p. 79) (82 wt. % AP propellant [UFP], single-pressure-increase-pulse, 3-5 mm)

[illegible]	[illegible]	PLANE TEMP., DEG. KELVIN	H2O MOL FRACTION	CO2 MOL FRACTION	CO MOL FRACTION	HA-D AUS.
1	[illegible]	2517.3	.447	.038	.494	.539
2	[illegible]	[illegible]	.474	.052	.253	.529
3	[illegible]	[illegible]	.416	.034	.133	.496
4	[illegible]	[illegible]	.489	.043	.164	.490
5	[illegible]	2561.8	.457	.041	.320	.534
6	[illegible]	[illegible]	.497	.038	.405	.529
7	[illegible]	[illegible]	.412	.034	.413	.545
8	[illegible]	2567.7	.402	.044	.367	.464
9	[illegible]	[illegible]	.461	.050	.314	.572
10	[illegible]	2511.2	.351	.036	.452	.545
11	[illegible]	[illegible]	.504	.033	.366	.550
12	[illegible]	[illegible]	.[illegible]	.[illegible]	.331	.[illegible]
13	[illegible]	[illegible]	.352	.034	.474	.457
14	[illegible]	2496.0	.450	.033	.364	.572
15	[illegible]	2474.2	.447	.033	.361	.572
16	[illegible]	2504.4	.474	.033	.454	.572
17	[illegible]	2551.4	.540	.035	.358	.499
18	[illegible]	[illegible]	.496	.045	.262	.534
19	[illegible]	2581.3	.430	.045	.262	.550
20	[illegible]	[illegible]	.540	.050	.224	.501
21	[illegible]	2519.1	.364	.041	.625	.550
22	[illegible]	2544.9	.377	.035	.328	.523
23	[illegible]	2531.4	.316	.141	.229	.537
24	[illegible]	[illegible]	.264	.038	.384	.474
25	[illegible]	2562.6	.545	.045	.361	.529
26	[illegible]	2559.9	.363	.046	.364	.496
27	[illegible]	2541.6	.490	.043	.268	.539
28	[illegible]	2561.4	.405	.050	.359	.512
29	[illegible]	[illegible]	.462	.045	.484	.480
30	[illegible]	2572.3	.502	.038	.484	.507
31	[illegible]	[illegible]	.403	.044	.304	.518
32	[illegible]	[illegible]	.474	.055	.344	.529
33	[illegible]	2574.5	.488	.048	.349	.496
34	[illegible]	2551.5	.364	.049	.067	.523
35	[illegible]	[illegible]	.500	.046	.285	.622
36	[illegible]	[illegible]	.463	.055	.285	.605
37	[illegible]	2561.7	.339	.056	.274	.605
38	[illegible]	[illegible]	.500	.051	.285	.643
39	[illegible]	2551.1	.345	.047	.193	.544
40	[illegible]	2496.5	.403	.056	.317	.[illegible]
41	[illegible]	2567.5	.339	.047	.394	.550
42	[illegible]	2563.2	.396	.055	.236	.644
43	[illegible]	2581.3	.360	.051	.163	.655
44	[illegible]	2582.6	.493	.044	.358	.638
45	[illegible]	2514.3	.364	.043	.314	.605
46	[illegible]	2567.4	.387	.045	.454	.611
47	[illegible]	2535.3	.361	.043	.364	.649
48	[illegible]	2610.3	.504	.045	.398	.561
49	[illegible]	2606.3	.419	.044	.503	.561
50	[illegible]	2596.8	.385	.045	.345	.622
51	54.97	2562.8	.477	.043	.345	.649
52	54.97	2564.2	.449	.051	.346	.622

Run No. 1-31574 continued

53	55.40	2591.3	.354	.045	.385	.545
54	55.40	2551.2	.426	.050	.304	.622
55	55.42	2545.7	.511	.052	.194	.695
56	56.45	2523.4	.555	.055	.339	.677
57	56.67	2558.6	.351	.051	.302	.682
58	57.10	2561.3	.328	.050	.504	.633
59	57.73	2593.4	.284	.046	.339	.600
60	57.79	2600.9	.316	.049	.472	.655
61	58.10	2561.3	.361	.044	.468	.616
62	58.17	2542.9	.339	.046	.299	.671
63	58.38	2521.6	.360	.043	.447	.656
64	58.79	2564.7	.364	.044	.391	.664
65	58.79	2533.9	.340	.047	.453	.688
66	59.14	2561.4	.242	.040	.389	.696
67	59.58	2580.4	.338	.046	.291	.644
68	59.64	2547.7	.448	.043	.358	.648
69	59.70	2561.6	.471	.049	.287	.644
70	60.07	2564.5	.331	.045	.361	.635
71	60.32	2561.5	.441	.039	.384	.647
72	60.42	2571.4	.366	.045	.387	.633
73	61.24	2565.0	.461	.056	.380	.633
74	61.26	2564.0	.333	.043	.367	.666
75	62.19	2595.2	.325	.044	.376	.638
76	62.19	2580.3	.383	.047	.337	.720
77	62.49	2523.5	.334	.039	.395	.737
78	62.60	2523.7	.481	.046	.394	.770
79	62.61	2528.8	.409	.054	.455	.781

Run No. 7-4474 (Figure 27, p. 80) (80 wt. % AP propellant [UFQ], single-pressure-increase-pulse, 12-14 mm)

SCAN NUMBER	PRESSURE,PSIA	FLAME TEMP.,DEG. KELVIN	H2O MOL FRACTION	CO2 MOL FRACTION	CO MOL FRACTION	NA-D ABS.
1	45.00	2531.8	.101	.299	.031	.631
2	45.17	2529.3	.081	.328	-.008	.680
3	45.25	2513.0	.100	.341	.010	.669
4	45.34	2503.4	.104	.313	.005	.680
5	45.42	2519.2	.103	.282	.015	.642
6	45.51	2542.5	.097	.293	.018	.610
7	45.68	2507.5	.105	.339	.008	.669
8	45.59	2505.4	.102	.297	-.002	.680
9	45.59	2481.5	.098	.281	.024	.680
10	45.51	2455.7	.089	.283	.018	.680
11	45.34	2457.2	.094	.288	.014	.658
12	45.17	2464.5	.103	.329	.005	.707
13	45.08	2502.5	.100	.348	.001	.675
14	45.25	2530.7	.098	.331	.008	.642
15	45.51	2502.1	.106	.309	.008	.696
16	45.51	2483.6	.086	.304	.012	.680
17	45.59	2500.6	.101	.282	.018	.675
18	45.68	2518.1	.110	.282	.018	.648
19	45.59	2490.6	.106	.305	.011	.685
20	45.59	2530.6	.105	.341	.017	.658
21	45.51	2554.0	.111	.296	.019	.664
22	45.17	2526.9	.102	.305	.003	.675
23	45.08	2498.5	.093	.318	.022	.685
24	45.17	2504.9	.094	.275	.003	.626
25	45.34	2519.7	.103	.287	.019	.648
26	45.25	2528.2	.099	.264	.005	.620
27	45.51	2520.1	.100	.300	-.021	.664
28	45.76	2510.3	.110	.316	.014	.675
29	45.68	2511.8	.097	.276	-.002	.685
30	45.68	2462.7	.093	.296	-.002	.745
31	45.68	2498.0	.101	.312	-.012	.718
32	45.00	2535.5	.099	.326	.024	.653
33	45.17	2551.5	.099	.314	.024	.604
34	45.25	2535.7	.110	.348	-.003	.637
35	45.42	2519.4	.109	.389	.011	.658
36	45.42	2506.2	.104	.356	.020	.685
37	45.51	2497.8	.104	.333	.020	.669
38	45.68	2451.2	.109	.314	.021	.751
39	45.76	2445.3	.107	.297	.013	.723
40	45.85	2520.1	.096	.302	.027	.604
41	45.85	2513.0	.088	.306	.008	.625
42	45.76	2522.3	.105	.323	.027	.620
43	45.93	2507.6	.092	.301	.012	.669
44	45.93	2530.2	.100	.325	.021	.604
45	46.10	2560.7	.107	.323	-.016	.604
46	46.36	2583.6	.098	.337	.026	.604
47	46.53	2553.2	.107	.346	.011	.653
48	46.95	2532.8	.096	.319	.024	.696
49	47.29	2560.3	.098	.267	.013	.745
50	47.55	2463.0	.085	.266	.036	.783
51	48.06	2472.3	.104	.298	.012	.734
52	48.40	2444.9	.094	.324	.019	.756

Run No. 7-4474 continued

53	48.57	2493.5	.110	.350	.009	.702
54	49.07	2537.0	.102	.372	.011	.658
55	49.47	2554.9	.106	.366	-.007	.669
56	49.24	2552.9	.089	.371	-.003	.723
57	49.41	2542.0	.093	.365	.001	.685
58	49.58	2492.4	.092	.343	.015	.718
59	49.67	2509.3	.096	.351	.000	.707
60	49.92	2536.4	.089	.354	-.003	.680
61	50.18	2516.5	.098	.322	.018	.707
62	50.60	2514.3	.090	.279	.024	.714
63	50.06	2490.5	.081	.247	.022	.718
64	51.20	2490.1	.098	.270	.038	.729
65	51.45	2483.2	.101	.302	.028	.772
66	51.62	2493.9	.103	.319	.008	.772
67	51.96	2541.1	.095	.320	.023	.734
68	52.13	2545.5	.095	.328	.009	.772
69	52.39	2512.2	.094	.334	.008	.810
70	52.56	2483.5	.094	.353	.008	.826
71	52.47	2483.5	.097	.331	.021	.816
72	52.56	2483.3	.100	.308	.033	.848
73	52.41	2483.5	.108	.305	.011	.837
74	52.09	2515.2	.108	.318	.034	.767
75	53.32	2521.9	.107	.309	.023	.723
76	53.57	2551.2	.107	.294	.012	.696
77	53.91	2556.9	.103	.267	.013	.740
78	54.17	2547.4	.111	.283	.031	.734
79	54.34	2549.7	.098	.290	.012	.745
80	54.62	2527.6	.089	.314	.024	.761

Run No. 2-4373 (Figure 28, p. 82) (82 wt. % AP propellant [UFP], 54 Hz. oscillatory pressure, 3-5 mm)

SCAN NUMBER	DELTA PRESSURE (PSI)	FLAME TEMP. (DEG. K)	RADH2O	RADWN1	RADCO2	RADCO	RADWN2	NAD-ABS	WN1/H2O	WN1/CO2	WN1/CO
1	.00	2384.1	.14	.12	.26	.09	.04	.349	.86	.44	1.35
2	-.68	2410.4	.14	.12	.29	.09	.04	.298	.86	.42	1.34
3	-1.06	2376.3	.14	.12	.31	.09	.05	.329	.89	.40	1.35
4	-1.27	2384.4	.14	.12	.31	.09	.05	.313	.86	.39	1.36
5	-1.19	2376.3	.14	.13	.34	.10	.04	.329	.92	.38	1.38
6	-.76	2373.5	.16	.14	.34	.10	.04	.349	.87	.40	1.42
7	-.25	2378.1	.14	.12	.30	.09	.04	.354	.86	.41	1.35
8	.15	2387.6	.16	.14	.34	.10	.05	.359	.85	.41	1.46
9	.72	2383.1	.16	.15	.33	.10	.04	.390	.92	.45	1.48
10	1.15	2395.1	.18	.15	.32	.11	.05	.400	.86	.40	1.41
11	1.53	2374.7	.18	.16	.33	.10	.06	.420	.91	.48	1.54
12	1.70	2386.2	.18	.15	.33	.10	.05	.400	.82	.45	1.42
13	1.44	2396.5	.17	.15	.30	.04	.04	.364	.88	.49	1.76
14	1.06	2380.4	.17	.14	.32	.10	.05	.354	.83	.44	1.40
15	.38	2341.6	.17	.14	.31	.10	.05	.420	.86	.46	1.38
16	-.38	2364.7	.16	.14	.31	.09	.04	.379	.67	.44	1.55
17	-.93	2381.1	.14	.12	.30	.09	.04	.334	.89	.41	1.41
18	-1.32	2429.6	.14	.13	.31	.09	.04	.288	.94	.42	1.50
19	-1.56	2419.9	.14	.12	.32	.00	.04	.303	.86	.38	1.43
20	-1.62	2416.0	.14	.13	.29	.09	.04	.318	.92	.45	1.43
21	-.64	2375.4	.15	.14	.32	.10	.04	.374	.95	.43	1.46
22	-.17	2428.1	.17	.14	.36	.10	.04	.329	.86	.40	1.38
23	.30	2409.4	.16	.14	.33	.10	.04	.369	.08	.43	1.44
24	.81	2431.2	.15	.12	.30	.09	.04	.369	.04	.42	1.35
25	1.27	2412.9	.17	.15	.33	.10	.06	.374	.88	.45	1.42
26	1.44	2391.3	.17	.15	.33	.10	.05	.425	.88	.46	1.46
27	1.44	2364.7	.10	.16	.32	.10	.05	.430	.89	.48	1.56
28	1.15	2359.4	.16	.14	.32	.09	.04	.440	.03	.43	1.55
29	.42	2306.0	.16	.14	.32	.09	.04	.369	.90	.44	1.54
30	-.30	2396.1	.16	.13	.31	.09	.04	.339	.05	.43	1.50
31	-.65	2400.2	.14	.12	.31	.09	.03	.318	.89	.40	1.41
32	-1.27	2386.5	.14	.13	.32	.09	.04	.334	.09	.41	1.45
33	-1.56	2394.0	.14	.12	.32	.09	.04	.310	.06	.39	1.41
34	-1.27	2417.2	.14	.12	.28	.10	.04	.293	.89	.44	1.29
35	-.93	2409.1	.14	.13	.32	.09	.04	.303	.92	.41	1.43
36	-.51	2408.5	.15	.13	.32	.10	.04	.329	.07	.41	1.38
37	.00	2401.2	.16	.14	.34	.10	.05	.390	.07	.40	1.36
38	.51	2409.4	.10	.15	.34	.11	.05	.309	.04	.44	1.37
39	.95	2422.7	.18	.15	.35	.11	.05	.369	.04	.43	1.36
40	1.32	2411.0	.17	.15	.31	.10	.05	.379	.88	.49	1.40
41	1.53	2390.7	.16	.14	.32	.10	.04	.400	.85	.42	1.42
42	1.32	2411.0	.16	.13	.32	.10	.00	.379	.85	.41	1.37
43	.89	2410.4	.15	.12	.30	.09	.03	.349	.82	.42	1.41
44	.30	2396.1	.14	.12	.28	.08	.03	.339	.05	.41	1.30
45	-.34	2417.2	.15	.13	.31	.10	.04	.293	.07	.42	1.38
46	-.85	2404.4	.15	.13	.32	.09	.04	.323	.86	.40	1.39
47	-1.19	2431.2	.14	.12	.30	.09	.05	.283	.08	.39	1.30
48	-1.32	2425.7	.12	.11	.29	.06	.04	.203	.90	.39	1.47
49	-1.06	2457.0	.14	.13	.32	.09	.04	.257	.91	.41	1.45
50	-.72	2452.8	.14	.13	.32	.10	.04	.263	.92	.41	1.30

Run No. 1-4474 (Figure A-3, p. 108) (82 wt. % AP propellant [UFP], constant pressure, 3-5 mm)

SCAN NUMBER	DELTA PRESSURE (PSI)	FLAME TEMP. (DEG. K)	RADH2O	RADWN1	RADCO2	RADCO	RADWN2	NAD-ABS	WN1/H2O	WN1/CO2	WN1/CO
1	.00	2629.2	.37	.30	.35	.19	.08	.808	.80	.84	1.54
2	.00	2640.0	.36	.29	.34	.19	.08	.803	.81	.85	1.53
3	-.04	2626.7	.34	.27	.34	.19	.08	.819	.80	.80	1.42
4	.04	2646.9	.33	.27	.33	.19	.08	.741	.83	.82	1.45
5	.00	2671.0	.30	.24	.32	.17	.08	.725	.79	.75	1.40
6	-.08	2676.8	.28	.23	.31	.16	.07	.710	.83	.74	1.46
7	.04	2679.5	.25	.21	.28	.15	.06	.705	.84	.77	1.39
8	.00	2689.7	.24	.20	.28	.14	.06	.663	.84	.74	1.46
9	.00	2664.4	.24	.19	.28	.14	.06	.715	.80	.70	1.33
10	-.04	2639.9	.21	.17	.25	.13	.05	.746	.81	.69	1.30
11	-.08	2600.3	.24	.19	.26	.15	.06	.803	.81	.74	1.30
12	-.08	2640.5	.23	.19	.25	.15	.06	.736	.83	.77	1.30
13	-.13	2664.4	.23	.19	.24	.14	.06	.715	.81	.80	1.34
14	-.13	2675.2	.24	.19	.25	.15	.06	.694	.78	.75	1.27
15	-.08	2685.4	.25	.20	.27	.16	.06	.699	.78	.73	1.26
16	-.13	2661.1	.26	.22	.28	.16	.06	.715	.85	.80	1.38
17	-.04	2636.5	.26	.21	.28	.16	.07	.767	.80	.76	1.32
18	-.08	2675.7	.28	.22	.27	.16	.07	.710	.80	.81	1.38
19	-.08	2680.6	.25	.21	.26	.15	.06	.705	.84	.82	1.43
20	-.04	2685.5	.25	.19	.25	.14	.06	.689	.77	.77	1.33
21	-.08	2681.1	.23	.18	.24	.14	.06	.710	.79	.76	1.29
22	-.08	2681.7	.22	.17	.23	.13	.05	.694	.76	.74	1.27
23	-.04	2616.9	.21	.17	.22	.14	.05	.777	.79	.78	1.24
24	-.17	2601.5	.24	.19	.24	.15	.06	.798	.77	.80	1.24
25	-.13	2663.0	.28	.22	.27	.17	.06	.731	.81	.82	1.33
26	-.08	2676.3	.28	.22	.29	.17	.06	.736	.80	.77	1.33
27	-.17	2641.5	.28	.22	.28	.17	.06	.756	.76	.76	1.29
28	-.17	2645.3	.27	.22	.28	.17	.07	.731	.79	.76	1.29
29	-.13	2688.6	.28	.22	.30	.17	.06	.663	.77	.72	1.28
30	-.13	2683.4	.29	.23	.30	.17	.07	.689	.78	.75	1.33
31	-.13	2595.1	.25	.20	.27	.14	.06	.751	.79	.73	1.36
32	-.13	2634.4	.22	.18	.24	.14	.06	.674	.82	.76	1.25
33	-.13	2686.7	.24	.19	.24	.14	.06	.642	.80	.77	1.31
34	-.09	2648.2	.24	.18	.26	.14	.05	.658	.77	.72	1.24
35	-.13	2693.1	.25	.19	.26	.14	.06	.637	.77	.75	1.33
36	-.08	2664.7	.24	.20	.26	.15	.06	.674	.82	.78	1.35
37	-.17	2642.1	.25	.21	.28	.16	.06	.689	.84	.76	1.29
38	-.17	2639.9	.28	.23	.29	.17	.07	.725	.81	.79	1.33
39	-.13	2646.9	.30	.24	.31	.18	.07	.741	.80	.79	1.39
40	-.13	2636.5	.31	.26	.31	.18	.08	.746	.84	.84	1.44
41	-.17	2667.6	.30	.25	.30	.17	.07	.668	.83	.84	1.47
42	-.08	2663.1	.26	.22	.27	.16	.07	.679	.85	.82	1.44
43	-.13	2642.5	.27	.22	.28	.16	.06	.684	.81	.79	1.41
44	-.04	2628.6	.28	.21	.26	.16	.06	.715	.77	.80	1.32
45	-.17	2646.3	.26	.21	.27	.16	.06	.663	.80	.79	1.32
46	-.08	2670.7	.26	.20	.26	.16	.06	.627	.77	.74	1.26
47	-.08	2655.0	.23	.18	.23	.14	.06	.663	.79	.79	1.31
48	-.04	2645.4	.23	.19	.23	.14	.06	.694	.81	.81	1.38
49	.00	2687.0	.25	.19	.24	.16	.06	.658	.77	.80	1.23
50	.00	2679.1	.25	.19	.24	.15	.06	.668	.76	.79	1.26

Run No. 3-31574 (Figure A-4, p. 110) (82 wt. % AP propellant [UFP], constant pressure, 3-5 mm)

SCAN NUMBER	DELTA PRESSURE (PSI)	FLAME TEMP. (DEG. R)	RADH2O	RADWN1	RADCO2	RADCO	RADWN2	NAD-ABS	WN1/H2O	WN1/CO2	WN1/CO
1	.00	2315.0	.64	.56	.66	.32	.15	.971	.89	.85	1.78
2	.00	2333.4	.63	.56	.60	.31	.15	.949	.90	.85	1.83
3	.00	2306.9	.61	.54	.64	.30	.15	.977	.88	.83	1.79
4	-.21	2338.5	.56	.49	.63	.28	.14	.954	.87	.78	1.76
5	.21	2311.9	.57	.51	.67	.30	.14	.943	.89	.76	1.72
6	.00	2336.3	.61	.53	.68	.30	.14	.926	.87	.79	1.77
7	.21	2346.6	.59	.50	.65	.30	.14	.943	.86	.78	1.70
8	.21	2331.0	.55	.48	.62	.28	.13	.931	.88	.77	1.71
9	-.21	2292.4	.61	.54	.67	.32	.15	.966	.88	.81	1.71
10	.00	2309.3	.59	.51	.66	.30	.14	.954	.86	.77	1.69
11	-.21	2328.3	.54	.47	.64	.28	.13	.943	.87	.73	1.66
12	.00	2349.2	.57	.50	.65	.30	.14	.920	.87	.77	1.67
13	-.21	2338.9	.59	.52	.65	.30	.14	.926	.87	.79	1.72
14	.00	2355.9	.56	.49	.58	.28	.13	.943	.88	.84	1.73
15	-.21	2374.4	.51	.44	.57	.26	.12	.897	.87	.78	1.69
16	.00	2349.5	.55	.49	.61	.29	.13	.906	.88	.80	1.67
17	.21	2360.4	.59	.52	.67	.30	.14	.949	.87	.77	1.72
18	.00	2350.9	.62	.55	.66	.30	.14	.949	.88	.84	1.85
19	.21	2398.0	.58	.51	.62	.30	.14	.914	.88	.82	1.72
20	.21	2400.5	.63	.55	.64	.32	.15	.908	.89	.86	1.75
21	.21	2392.3	.67	.59	.65	.32	.16	.903	.88	.90	1.81
22	.21	2347.2	.60	.54	.60	.30	.13	.897	.89	.89	1.61
23	.21	2363.3	.58	.50	.63	.30	.14	.874	.87	.80	1.68
24	.00	2396.9	.63	.56	.69	.33	.16	.868	.89	.81	1.71
25	.21	2402.6	.70	.63	.68	.33	.16	.908	.90	.92	1.91
26	.21	2385.6	.62	.56	.60	.30	.14	.903	.90	.93	1.88
27	.21	2386.7	.56	.49	.56	.28	.14	.886	.87	.84	1.74
28	.42	2381.0	.55	.49	.59	.28	.13	.903	.90	.83	1.73
29	.21	2377.2	.60	.54	.62	.31	.15	.931	.89	.87	1.74
30	.42	2385.7	.61	.55	.58	.30	.14	.937	.90	.95	1.84
31	.42	2384.6	.57	.51	.58	.28	.14	.920	.90	.88	1.80
32	.21	2381.0	.60	.53	.60	.30	.15	.903	.88	.87	1.76
33	.21	2434.1	.69	.62	.69	.34	.17	.857	.90	.90	1.85
34	.21	2409.1	.71	.64	.68	.33	.17	.880	.90	.94	1.95
35	.21	2428.6	.62	.57	.62	.30	.15	.891	.91	.91	1.89
36	.42	2434.3	.6_	.56	.62	.30	.15	.874	.91	.90	1.87
37	.21	2442.7	.61	.54	.60	.29	.15	.868	.89	.91	1.85
38	.21	2408.0	.60	.54	.64	.30	.15	.920	.91	.87	1.81
39	.42	2365.5	.63	.56	.62	.32	.15	.937	.89	.90	1.78
40	.00	2363.6	.66	.60	.66	.34	.16	.926	.90	.90	1.79
41	.21	2389.0	.67	.60	.66	.32	.16	.920	.90	.91	1.87
42	.42	2420.7	.62	.56	.63	.31	.15	.868	.90	.89	1.83
43	.04	2416.5	.58	.51	.61	.30	.14	.937	.89	.84	1.73
44	.21	2406.8	.62	.57	.59	.30	.15	.908	.92	.96	1.87
45	.42	2398.0	.59	.53	.60	.30	.14	.914	.90	.89	1.78
46	.00	2405.6	.59	.52	.61	.29	.14	.897	.89	.86	1.82
47	.21	2419.5	.63	.57	.62	.31	.16	.903	.90	.92	1.84
48	.00	2419.5	.62	.56	.61	.30	.15	.903	.90	.92	1.86
49	.21	2386.9	.62	.56	.61	.30	.15	.954	.90	.92	1.84
50	.00	2408.0	.60	.53	.59	.29	.13	.920	.88	.89	1.83

Run No. 3-31574 (Figure A-5, p. 111) (82 wt. % AP propellant [UFP], constant pressure, 3-5 mm)

SCAN NUMBER	DELTA PRESSURE (PSI)	FLAME TEMP. (DEG. K)	RADH2O	RADWN1	RADCO2	RADCO	RADWN2	RAD-ABS	WN1/H2O	WN1/CO2	WN1/CO
1	.00	2482.3	.26	.21	.42	.14	.07	.640	.82	.50	1.51
2	.00	2469.2	.27	.21	.41	.13	.06	.634	.78	.51	1.58
3	.00	2500.9	.26	.22	.41	.14	.07	.554	.62	.52	1.54
4	.00	2480.9	.23	.19	.39	.13	.06	.611	.61	.48	1.47
5	.00	2499.0	.23	.18	.38	.12	.05	.583	.79	.47	1.55
6	.00	2507.5	.23	.20	.40	.13	.06	.577	.84	.49	1.53
7	.00	2492.6	.24	.20	.38	.13	.06	.611	.84	.54	1.55
8	.21	2494.9	.27	.22	.42	.14	.06	.623	.82	.53	1.60
9	.00	2502.2	.30	.26	.45	.16	.06	.600	.86	.58	1.67
10	.00	2489.2	.29	.24	.42	.14	.07	.606	.82	.57	1.67
11	.00	2477.5	.29	.24	.42	.15	.06	.629	.64	.58	1.65
12	.00	2473.3	.30	.25	.42	.15	.06	.651	.83	.60	1.63
13	.00	2515.6	.29	.24	.41	.14	.07	.554	.62	.57	1.69
14	-.21	2505.1	.30	.26	.44	.15	.08	.577	.86	.59	1.68
15	.00	2466.2	.31	.26	.46	.16	.08	.640	.63	.57	1.62
16	.00	2502.2	.31	.26	.44	.15	.08	.549	.84	.59	1.71
17	.00	2453.7	.28	.23	.44	.14	.08	.623	.63	.53	1.66
18	-.21	2480.6	.29	.25	.43	.15	.07	.589	.86	.57	1.68
19	.00	2470.6	.28	.24	.44	.15	.07	.640	.85	.55	1.62
20	.21	2468.5	.25	.21	.41	.14	.06	.611	.84	.52	1.51
21	.00	2461.9	.29	.24	.44	.15	.07	.606	.65	.56	1.65
22	.00	2454.1	.30	.25	.44	.15	.08	.651	.83	.57	1.68
23	.00	2490.5	.30	.25	.45	.15	.06	.600	.84	.55	1.63
24	.00	2503.2	.30	.25	.46	.16	.08	.606	.63	.54	1.59
25	.00	2479.4	.31	.25	.45	.16	.06	.594	.81	.55	1.59
26	.00	2463.2	.29	.23	.43	.14	.06	.600	.79	.53	1.68
27	.00	2466.8	.26	.21	.40	.13	.06	.634	.81	.52	1.62
28	.00	2462.4	.23	.16	.39	.13	.06	.646	.79	.46	1.41
29	.00	2486.0	.25	.20	.42	.13	.06	.611	.81	.48	1.52
30	.00	2505.2	.28	.23	.43	.14	.08	.617	.83	.53	1.58
31	-.21	2515.4	.25	.20	.40	.13	.06	.583	.61	.51	1.59
32	-.21	2470.3	.26	.21	.44	.14	.06	.629	.82	.49	1.56
33	-.21	2473.5	.26	.22	.42	.14	.07	.611	.82	.51	1.59
34	.00	2489.2	.22	.18	.39	.12	.06	.606	.82	.47	1.53
35	-.21	2469.6	.26	.21	.44	.13	.06	.646	.82	.49	1.61
36	.00	2501.2	.27	.22	.45	.14	.06	.594	.82	.49	1.57
37	-.21	2481.0	.30	.26	.48	.15	.07	.623	.84	.55	1.76
38	.00	2494.3	.34	.27	.49	.16	.06	.571	.61	.56	1.70
39	.00	2490.4	.29	.24	.44	.14	.07	.623	.83	.55	1.67
40	.21	2510.0	.26	.21	.43	.14	.07	.606	.82	.50	1.47
41	.00	2515.9	.27	.22	.45	.15	.07	.571	.82	.50	1.51
42	.00	2499.7	.27	.22	.44	.14	.06	.611	.84	.50	1.60
43	.42	2480.9	.29	.25	.44	.15	.08	.611	.85	.57	1.63
44	.41	2456.5	.31	.26	.46	.16	.09	.651	.82	.56	1.60
45	.42	2483.2	.34	.29	.48	.17	.08	.600	.86	.60	1.71
46	.21	2464.9	.31	.26	.47	.15	.07	.617	.84	.56	1.71
47	.00	2451.6	.28	.23	.44	.14	.06	.651	.82	.53	1.71
48	.21	2482.1	.26	.22	.44	.14	.07	.617	.85	.51	1.56
49	.00	2495.1	.27	.22	.44	.14	.07	.611	.82	.50	1.60
50	.21	2497.4	.27	.22	.44	.14	.07	.611	.82	.50	1.60
51	.21	2493.6	.28	.23	.46	.16	.07	.651	.83	.48	1.46

Run No. 6-31574 (Figure D-6, p. 159) (82 wt. % AP propellant [UFP], 55 Hz. oscillatory pressure, 3-5 mm)

[illegible]	[illegible]	[illegible]	[illegible]	H2O MOL FRACTION	CO2 MOL FRACTION	CO MOL FRACTION	HCl MOL FRACTION
[illegible]	[illegible]	[illegible]	.590	.661	.215	.290	
[illegible]	[illegible]	[illegible]	.491	.648	.261	.331	
[illegible]	[illegible]	[illegible]	.472	.636	.413	.419	
[illegible]	[illegible]	[illegible]	.545	.645	.276	.354	
[illegible]	[illegible]	[illegible]	.486	.662	.276	.354	
[illegible]	[illegible]	[illegible]	.487	.662	-.166	.390	
[illegible]	[illegible]	[illegible]	.487	.657	.323	.384	
[illegible]	[illegible]	[illegible]	.538	.660	.191	.401	
[illegible]	[illegible]	[illegible]	.491	.658	.344	.354	
[illegible]	[illegible]	[illegible]	.505	.656	.196	.255	
[illegible]	[illegible]	[illegible]	.427	.660	.141	.284	
[illegible]	[illegible]	[illegible]	.491	.658	.183	.342	
[illegible]	[illegible]	[illegible]	.536	.670	.281	.366	
[illegible]	[illegible]	[illegible]	.559	.658	.340	.274	
[illegible]	[illegible]	[illegible]	.496	.655	.371	.319	
[illegible]	[illegible]	[illegible]	.472	.658	.316	.325	
[illegible]	[illegible]	[illegible]	.533	.669	.268	.325	
[illegible]	[illegible]	[illegible]	.467	.664	.256	.325	
[illegible]	[illegible]	[illegible]	.566	.678	.368	.337	
[illegible]	[illegible]	[illegible]	.487	.667	.177	.337	
[illegible]	[illegible]	[illegible]	.561	.670	.265	.331	
[illegible]	[illegible]	[illegible]	.491	.676	.342	.390	
[illegible]	[illegible]	[illegible]	.442	.671	.431	.331	
[illegible]	[illegible]	[illegible]	.471	.658	.405	.325	
[illegible]	[illegible]	[illegible]	.533	.659	.468	.296	
[illegible]	[illegible]	[illegible]	.487	.664	.225	.296	
[illegible]	[illegible]	[illegible]	.462	.673	.317	.269	
[illegible]	[illegible]	[illegible]	.471	.669	[illegible]	.255	
[illegible]	[illegible]	[illegible]	.473	.648	.368	.296	
[illegible]	[illegible]	[illegible]	.491	.671	.164	.284	
[illegible]	[illegible]	[illegible]	.566	.679	.320	.255	
[illegible]	[illegible]	[illegible]	.487	.662	.370	.337	
[illegible]	[illegible]	[illegible]	.462	.676	.179	.349	
[illegible]	[illegible]	[illegible]	.460	.669	-.452	.343	
[illegible]	[illegible]	[illegible]	.483	.664	.242	.360	
[illegible]	[illegible]	[illegible]	.505	.675	.170	.360	
[illegible]	[illegible]	[illegible]	.484	.666	.074	.372	
[illegible]	[illegible]	[illegible]	.483	.662	.246	.337	
[illegible]	[illegible]	[illegible]	.491	.656	.333	.302	
[illegible]	[illegible]	[illegible]	.509	.662	.256	.261	
[illegible]	[illegible]	[illegible]	.473	.660	.247	.284	
[illegible]	[illegible]	[illegible]	.517	.659	.474	.290	
[illegible]	[illegible]	[illegible]	.487	.666	.256	.290	
[illegible]	[illegible]	[illegible]	.469	.658	.249	.337	
[illegible]	[illegible]	[illegible]	.514	.670	.315	.384	
[illegible]	[illegible]	[illegible]	.455	.675	.427	.313	
[illegible]	[illegible]	[illegible]	.540	.670	-.172	.366	
[illegible]	[illegible]	[illegible]	.515	.668	.200	.401	
[illegible]	[illegible]	[illegible]	.484	.676	.051	.437	
[illegible]	[illegible]	[illegible]	.492	.661	.343	.401	
[illegible]	[illegible]	[illegible]	.560	.676	.274	.366	
[illegible]	[illegible]	[illegible]	.610	.675	.258	.331	

Run No. 6-31574 continued

[illegible]	[illegible]	[illegible]	.557	.072	.221	.284
[illegible]	[illegible]	247[illegible]	.517	.059	.224	.266
[illegible]	[illegible]	[illegible]	.460	.055	.022	.243
[illegible]	[illegible]	[illegible]	.469	.065	.361	.284
[illegible]	[illegible]	[illegible]	.560	.059	.109	.302
[illegible]	[illegible]	[illegible]	.400	.051	.392	.313
[illegible]	[illegible]	[illegible]	.577	.046	.110	.325
[illegible]	[illegible]	247[illegible]	.443	.058	.109	.325
[illegible]	[illegible]	[illegible]	.509	.066	.133	.300
[illegible]	[illegible]	[illegible]	.539	.073	.201	.290
[illegible]	[illegible]	[illegible]	.555	.063	.274	.337
[illegible]	[illegible]	[illegible]	.555	.063	.273	.349
[illegible]	[illegible]	[illegible]	.651	.057	.401	.401
[illegible]	[illegible]	[illegible]	.471	.057	.354	.349
[illegible]	[illegible]	[illegible]	.445	.057	.151	.302
[illegible]	[illegible]	[illegible]	.557	.056	-.102	.290
[illegible]	[illegible]	[illegible]	.453	.056	.113	.313
[illegible]	[illegible]	[illegible]	.440	.054	.094	.278
[illegible]	[illegible]	[illegible]	.554	.052	.284	.313
[illegible]	[illegible]	[illegible]	.519	.046	.407	.325
[illegible]	[illegible]	[illegible]	.527	.050	.056	.319
[illegible]	[illegible]	[illegible]	.601	.051	.438	.337
[illegible]	[illegible]	[illegible]	.503	.058	.358	.396
[illegible]	[illegible]	[illegible]	.443	.041	.524	.331
[illegible]	[illegible]	[illegible]	.524	.057	.544	.407
[illegible]	[illegible]	[illegible]	.468	.067	.457	.361
[illegible]	[illegible]	[illegible]	.567	.074	.420	.354
[illegible]	[illegible]	[illegible]	.424	.061	.250	.349
[illegible]	[illegible]	[illegible]	.539	.070	.261	.331
[illegible]	[illegible]	[illegible]	.443	.072	.256	.295
[illegible]	[illegible]	[illegible]	.464	.061	.235	.290
[illegible]	[illegible]	[illegible]	.493	.058	.190	.266
[illegible]	[illegible]	[illegible]	.509	.041	.157	.284
[illegible]	[illegible]	[illegible]	.502	.058	.288	.313
[illegible]	[illegible]	[illegible]	.506	.071	.284	.284
[illegible]	[illegible]	247[illegible]	.533	.065	.118	.290
[illegible]	[illegible]	[illegible]	.466	.056	.295	.313
[illegible]	[illegible]	248[illegible]	.505	.057	.251	.354
[illegible]	[illegible]	[illegible]	.402	.051	.106	.360
[illegible]	[illegible]	[illegible]	.474	.058	.435	.349
[illegible]	[illegible]	[illegible]	.607	.061	.279	.343
[illegible]	[illegible]	[illegible]	.543	.062	.267	.361
[illegible]	[illegible]	[illegible]	.565	.066	.143	.331
[illegible]	[illegible]	[illegible]	.478	.061	.115	.337
[illegible]	[illegible]	[illegible]	.504	.058	.431	.343
[illegible]	[illegible]	[illegible]	.373	.065	.215	.302
[illegible]	[illegible]	[illegible]	.446	.055	.392	.343
[illegible]	[illegible]	[illegible]	.542	.074	-.104	.284
[illegible]	[illegible]	[illegible]	.553	.063	.156	.278
[illegible]	[illegible]	[illegible]	.549	.066	.058	.266
[illegible]	[illegible]	[illegible]	.510	.056	.177	.319

Run No. 4-122873 (Figure G-1, p. 178) (82 wt. % AP propellant [UFN], constant pressure, 3-5 mm)

SCAN NUMBER	PRESSURE,PSIA	H2O VOL FRACTION	CO2 MOL FRACTION	CO MOL FRACTION
1	96.68	.220	.059	.149
2	97.91	.227	.056	.165
3	96.00	.235	.058	.142
4	98.68	.241	.060	.220
5	97.42	.210	.056	.199
6	97.91	.251	.059	.227
7	98.68	.177	.040	.161
8	98.68	.196	.044	.188
9	97.91	.215	.051	.223
10	97.42	.190	.050	.264
11	97.73	.248	.063	.168
12	97.42	.275	.068	.186
13	97.63	.240	.075	.146
14	97.42	.248	.068	.141
15	97.91	.210	.049	.322
16	97.42	.225	.046	.259
17	97.42	.282	.052	.218
18	98.68	.203	.059	.191
19	98.19	.245	.068	.203
20	98.64	.241	.066	.209
21	98.89	.202	.063	.161
22	97.91	.233	.072	.168
23	98.68	.214	.061	.232
24	98.89	.210	.063	.202
25	98.92	.240	.072	.181
26	97.42	.252	.068	.175
27	97.91	.267	.066	.165
28	97.42	.210	.048	.140
29	97.91	.240	.066	.109
30	98.89	.244	.074	.083
31	98.68	.265	.078	.141
32	97.91	.257	.065	.186
33	98.40	.195	.043	.235
34	98.89	.227	.040	.331
35	98.89	.254	.041	.285
36	98.68	.257	.043	.243
37	97.91	.248	.051	.245
38	97.91	.256	.056	.243
39	97.91	.233	.058	.224
40	97.42	.250	.061	.224
41	98.68	.239	.058	.222
42	97.91	.236	.062	.253
43	97.91	.233	.062	.169
44	98.66	.267	.076	.097
45	98.89	.245	.075	.157
46	98.15	.284	.074	.149
47	98.14	.230	.065	.220
48	98.89	.222	.057	.189
49	98.68	.240	.057	.219
50	98.68	.216	.060	.232
51	98.37	.254	.052	.153
52	98.37	.241	.052	.198

Run No. 4-122873 continued

53	98.10	.234	.054	.180
54	98.00	.220	.049	.230
55	98.14	.212	.041	.261
56	98.00	.215	.037	.274
57	98.09	.278	.049	.222
58	98.10	.250	.049	.264
59	98.09	.263	.048	.214
60	98.14	.220	.045	.275
61	98.27	.238	.046	.232
62	98.27	.245	.047	.180
63	98.27	.244	.056	.210
64	98.27	.225	.059	.231
65	98.00	.230	.066	.138
66	98.09	.243	.078	.124
67	98.09	.209	.063	.278
68	98.14	.255	.053	.277
69	98.09	.251	.049	.268
70	98.00	.253	.051	.241
71	98.14	.240	.055	.146
72	98.27	.260	.054	.212
73	98.09	.247	.055	.213
74	98.09	.223	.053	.214
75	98.27	.232	.058	.212
76	98.27	.219	.063	.202
77	98.27	.240	.063	.183
78	98.27	.243	.057	.140
79	98.27	.243	.054	.204
80	98.27	.228	.054	.223
81	98.27	.220	.054	.252
82	98.00	.230	.058	.273
83	98.10	.233	.057	.297
84	98.00	.244	.058	.144
85	98.10	.233	.052	.214
86	98.14	.223	.064	.188
87	98.27	.213	.067	.151
88	98.27	.246	.067	.199
89	98.00	.204	.058	.204
90	98.27	.224	.062	.102
91	98.27	.252	.060	.104
92	98.27	.237	.065	.165
93	98.27	.228	.059	.161
94	98.09	.201	.067	.189
95	98.27	.253	.071	.178
96	98.05	.248	.064	.152
97	98.14	.240	.066	.094
98	98.14	.217	.063	.142
99	98.00	.243	.064	.184
100	98.27	.238	.060	.277

Run No. 6-122873 (Figure G-2, p. 179) (82 wt. % AP propellant [UFN], constant pressure, 3-5 mm)

SCAN NUMBER	PRESSURE, PSIA	H2O MOL FRACTION	CO2 MOL FRACTION	CO MOL FRACTION
1	[illegible]	.311	.062	.120
4	[illegible]	.305	.072	.204
5	[illegible]	.270	.056	.208
[illegible]	[illegible]	.271	.036	.215
[illegible]	[illegible]	.316	.067	.174
8	[illegible]	.290	.075	.122
[illegible]	[illegible]	.256	.073	.188
[illegible]	[illegible]	.262	.072	.227
[illegible]	[illegible]	.260	.071	.143
10	[illegible]	.291	.057	.154
11	[illegible]	.305	.057	.231
12	[illegible]	.293	.055	.200
[illegible]	[illegible]	.299	.059	.169
14	[illegible]	.247	.031	.267
15	[illegible]	.266	.058	.211
16	[illegible]	.302	.076	.103
17	[illegible]	.264	.076	.178
[illegible]	[illegible]	.237	.061	.201
[illegible]	[illegible]	.280	.063	.182
[illegible]	[illegible]	.276	.065	.214
21	[illegible]	.270	.067	.188
[illegible]	[illegible]	.253	.073	.129
[illegible]	[illegible]	.294	.082	.113
[illegible]	[illegible]	.274	.062	.079
[illegible]	[illegible]	.263	.077	.202
26	[illegible]	.267	.077	.156
27	[illegible]	.269	.078	.118
[illegible]	[illegible]	.327	.065	.191
[illegible]	[illegible]	.216	.038	.154
[illegible]	[illegible]	.[illegible]	.063	.188
[illegible]	[illegible]	.277	.062	.145
[illegible]	[illegible]	.253	.060	.296
33	[illegible]	.276	.068	.208
[illegible]	[illegible]	.277	.072	.190
[illegible]	[illegible]	.301	.072	.229
[illegible]	[illegible]	.283	.068	.171
[illegible]	[illegible]	.[illegible]	.070	.109
[illegible]	[illegible]	.283	.075	.072
[illegible]	[illegible]	.275	.075	.147
[illegible]	[illegible]	.274	.062	.239
[illegible]	[illegible]	.283	.059	.207
[illegible]	[illegible]	.[illegible]	.062	.201
[illegible]	[illegible]	.290	.063	.196
[illegible]	[illegible]	.324	.069	.167
[illegible]	[illegible]	.340	.073	.119
[illegible]	[illegible]	.247	.065	.176
[illegible]	[illegible]	.250	.047	.307
[illegible]	[illegible]	.248	.048	.274
[illegible]	[illegible]	.293	.059	.256
[illegible]	[illegible]	.289	.066	.174
[illegible]	[illegible]	.282	.066	.190
[illegible]	[illegible]	.216	.057	.231

Run No. 6-122873 continued

53	[illegible]	.237	.048	.264
54	[illegible]	.302	.054	.222
55	[illegible]	.300	.054	.178
56	[illegible]	.254	.056	.197
57	[illegible]	.240	.055	.261
58	[illegible]	.274	.055	.252
59	[illegible]	.335	.067	.153
60	[illegible]	.316	.073	.195
61	[illegible]	.322	.076	.219
62	[illegible]	.267	.067	.133
63	[illegible]	.293	.059	.198
64	[illegible]	.299	.049	.215
65	[illegible]	.269	.045	.290
66	[illegible]	.270	.049	.216
67	[illegible]	.267	.056	.192
68	[illegible]	.233	.046	.259
69	[illegible]	.261	.043	.273
70	[illegible]	.310	.045	.335
71	[illegible]	.261	.054	.283
72	[illegible]	.258	.052	.298
73	[illegible]	.302	.067	.162
74	[illegible]	.340	.082	.119
75	[illegible]	.311	.068	.203
76	[illegible]	.266	.073	.132
77	[illegible]	.265	.071	.197
78	[illegible]	.266	.064	.215
79	[illegible]	.263	.059	.205
80	[illegible]	.262	.063	.180
81	[illegible]	.242	.062	.248
82	[illegible]	.306	.076	.172
83	[illegible]	.299	.067	.142
84	[illegible]	.302	.059	.181
85	[illegible]	.293	.062	.198
86	[illegible]	.262	.057	.241
87	[illegible]	.255	.045	.249
88	[illegible]	.265	.043	.302
89	[illegible]	.324	.039	.201
90	[illegible]	.369	.048	.197
91	[illegible]	.382	.060	.261
92	[illegible]	.350	.073	.191
93	[illegible]	.350	.076	.131
94	[illegible]	.337	.073	.066
95	[illegible]	.316	.062	.213
96	[illegible]	.268	.055	.181
97	[illegible]	.273	.058	.252
98	[illegible]	.260	.066	.154
99	[illegible]	.313	.085	.020
100	[illegible]	.291	.076	.097

Run No. 1-31474 (Figure G-3, p. 180) (82 wt. % AP propellant [UFP], 10 Hz. oscillatory pressure, 3-5 mm)

[illegible]	[illegible]	[illegible]	H2O MOL FRACTION	CO2 MOL FRACTION	CO MOL FRACTION	[illegible]
1	35.97	[illegible]	.421	.353	.408	.363
4	34.93	[illegible]	.322	.055	.300	.452
5	34.74	[illegible]	.430	.059	.287	.505
[illegible]	[illegible]	[illegible]	.420	.063	.476	.585
[illegible]	[illegible]	[illegible]	.398	.059	.336	.534
[illegible]	[illegible]	[illegible]	.330	.053	.395	.611
[illegible]	[illegible]	[illegible]	.331	.058	.273	.538
[illegible]	37.[illegible]	[illegible]	.300	.062	.427	.498
[illegible]	37.[illegible]	[illegible]	.413	.055	.488	.515
10	37.[illegible]	[illegible]	.217	.046	.421	.559
11	37.[illegible]	[illegible]	.442	.052	.277	.626
[illegible]	[illegible]	[illegible]	.414	.061	.283	.467
[illegible]	[illegible]	[illegible]	.512	.066	.383	.495
[illegible]	[illegible]	[illegible]	.420	.073	.378	.573
[illegible]	[illegible]	[illegible]	.293	.068	.385	.611
[illegible]	[illegible]	[illegible]	.388	.067	.299	.617
17	[illegible]	[illegible]	.444	.064	.376	.616
[illegible]	[illegible]	[illegible]	.338	.048	.307	.599
[illegible]	[illegible]	[illegible]	.419	.057	.361	.611
23	[illegible]	[illegible]	.302	.056	.294	.652
24	[illegible]	[illegible]	.471	.061	.347	.718
[illegible]	[illegible]	[illegible]	.434	.058	.327	.631
[illegible]	[illegible]	[illegible]	.490	.062	.429	.589
[illegible]	[illegible]	[illegible]	.[illegible]	.060	.382	.652
[illegible]	[illegible]	[illegible]	.[illegible]	.057	.285	.693
[illegible]	[illegible]	[illegible]	.360	.059	.417	.641
27	[illegible]	[illegible]	.470	.058	.355	.565
[illegible]	[illegible]	[illegible]	.495	.060	.409	.589
30	[illegible]	[illegible]	.[illegible]	.057	.304	.590
31	[illegible]	[illegible]	.419	.062	.293	.554
32	[illegible]	[illegible]	.427	.057	.415	.554
33	[illegible]	[illegible]	.358	.053	.313	.565
[illegible]	[illegible]	[illegible]	.407	.048	.261	.565
[illegible]	[illegible]	[illegible]	.362	.056	.306	.621
[illegible]	[illegible]	[illegible]	.406	.051	.269	.549
[illegible]	[illegible]	[illegible]	.428	.060	.406	.568
37	[illegible]	[illegible]	.402	.060	.406	.529
[illegible]	[illegible]	[illegible]	.402	.048	.312	.580
[illegible]	[illegible]	[illegible]	.411	.051	.353	.534
[illegible]	[illegible]	[illegible]	.491	.065	.288	.534
[illegible]	[illegible]	[illegible]	.496	.055	.353	.570
42	[illegible]	[illegible]	.446	.067	.317	.565
[illegible]	[illegible]	[illegible]	.375	.056	.334	.605
[illegible]	[illegible]	[illegible]	.471	.066	.321	.554
[illegible]	27.21	[illegible]	.454	.062	.478	.508
[illegible]	[illegible]	[illegible]	.428	.059	.403	.543
[illegible]	[illegible]	[illegible]	.500	.065	.292	.534
48	[illegible]	[illegible]	.570	.069	.283	.559
49	[illegible]	[illegible]	.499	.063	.259	.559
[illegible]	[illegible]	[illegible]	.414	.061	.286	.549
51	[illegible]	2471.7	.475	.060	.298	.513
52	[illegible]	2514.1	.490	.066	.307	.467

Run No. 1-31474 continued

53	3941.7	2567.9	.503	.076	.177	.457
54	4041.6	2541.4	.501	.079	.475	.416
55	3954.4	2547.6	.499	.078	.394	.401
56	3869.9	2554.4	.508	.058	.424	.442
57	3991.1	2541.2	.466	.062	.357	.414
58	3341.6	2541.6	.507	.074	.358	.467
59	4061.7	2541.6	.497	.076	.313	.467
60	4076.6	2538.3	.477	.077	.489	.452
61	3969.3	2536.7	.535	.069	.293	.431
62	4069.8	2531.7	.473	.054	.283	.421
63	3916.9	2542.6	.501	.058	.256	.442
64	3916.1	2541.9	.352	.070	.506	.431
65	3969.4	2541.4	.506	.069	.288	.421
66	3916.4	2541.1	.531	.071	.186	.401
67	3961.3	2541.0	.476	.068	.358	.421
68	3966.4	2538.8	.552	.059	.371	.411
69	3961.7	2541.3	.491	.070	.364	.384
70	3969.1	2539.1	.481	.061	.443	.386
71	3961.6	2541.4	.465	.067	.405	.416
72	4176.4	2541.6	.494	.068	.137	.375
73	4196.8	2541.7	.488	.080	.317	.349
74	4161.7	2542.1	.499	.073	.409	.401
75	4196.75	2542.4	.421	.051	.262	.411
76	4201.2	2541.2	.466	.072	.376	.370
77	4246.6	2537.9	.474	.059	.626	.355
78	4296.6	2541.6	.412	.049	.379	.385
79	4241.2	2542.3	.497	.063	.184	.411
80	4261.9	2541.9	.504	.059	.471	.364
81	4261.8	2541.1	.506	.069	.471	.390
82	4246.8	2536.4	.537	.070	.140	.375
83	4246.9	2541.9	.463	.057	.424	.406
84	4261.7	2542.1	.482	.058	.527	.462
85	4261.9	2541.7	.505	.066	.357	.393
86	4241.3	2537.5	.492	.071	.161	.349
87	4241.71	2541.5	.506	.059	.585	.349
88	4241.7	2542.1	.447	.067	.482	.421
89	4241.7	2541.4	.531	.067	.347	.426
90	4246.3	2542.3	.482	.076	.288	.477
91	4241.1	2541.2	.497	.073	.424	.506
92	4241.1	2540.7	.345	.068	.243	.529
93	4241.4	2541.3	.487	.077	.368	.498
94	4241.4	2541.4	.503	.069	.537	.518
95	4241.4	2539.6	.486	.071	.531	.472
96	4241.3	2541.1	.484	.074	.232	.503
97	4241.4	2541.2	.483	.069	.229	.467
98	4261.4	2537.4	.426	.077	.457	.442
99	4261.4	2541.7	.508	.067	.358	.411
100	4261.4	2541.1	.524	.071	.474	.390
101	4261.4	2538.4	.461	.073	.495	.421
102	4261.6	2537.9	.505	.074	.221	.447
103	4261.7	2541.3	.449	.061	.418	.442
104	4241.4	2537.8	.362	.065	.362	.524
105	4241.5	2538.9	.359	.061	.666	.503
106	4261.2	2541.2	.477	.065	.378	.467
107	4261.7	2538.1	.337	.070	.508	.490
108	4261.3	2538.1	.435	.062	.638	.508
109	4241.4	2541.4	.461	.079	.238	.554

Run No. 1-31474 continued

[illegible]	[illegible]	[illegible]	.[illegible]	.365	.348	.385
[illegible]	[illegible]	[illegible]	.[illegible]	.379	.316	.576
[illegible]	[illegible]	[illegible]	.[illegible]	.374	.329	.595
[illegible]	[illegible]	[illegible]	.[illegible]	.363	.583	.549
[illegible]	[illegible]	[illegible]	.[illegible]	.362	.588	.544
[illegible]	[illegible]	[illegible]	.[illegible]	.368	.357	.477
[illegible]	[illegible]	[illegible]	.[illegible]	.365	.643	.435
[illegible]	[illegible]	[illegible]	.[illegible]	.357	.437	.457
[illegible]	[illegible]	[illegible]	.[illegible]	.363	.539	.508
[illegible]	[illegible]	[illegible]	.[illegible]	.357	.316	.529
[illegible]	[illegible]	[illegible]	.[illegible]	.374	.395	.395
[illegible]	[illegible]	[illegible]	.[illegible]	.375	.593	.411
[illegible]	[illegible]	[illegible]	.[illegible]	.377	.332	.452
[illegible]	[illegible]	[illegible]	.[illegible]	.358	.517	.477
[illegible]	[illegible]	[illegible]	.[illegible]	.350	.538	.539
[illegible]	[illegible]	[illegible]	.[illegible]	.375	.584	.513
[illegible]	[illegible]	[illegible]	.[illegible]	.360	.442	.431
[illegible]	[illegible]	[illegible]	.[illegible]	.361	.263	.426
[illegible]	[illegible]	[illegible]	.[illegible]	.359	.405	.411
[illegible]	[illegible]	[illegible]	.[illegible]	.360	.261	.406
[illegible]	[illegible]	[illegible]	.[illegible]	.352	.577	.421
[illegible]	[illegible]	[illegible]	.[illegible]	.333	.342	.411
[illegible]	[illegible]	[illegible]	.[illegible]	.366	.391	.421
[illegible]	[illegible]	[illegible]	.[illegible]	.369	.436	.411
[illegible]	[illegible]	[illegible]	.[illegible]	.373	.388	.452
[illegible]	[illegible]	[illegible]	.[illegible]	.360	.385	.417
[illegible]	[illegible]	[illegible]	.[illegible]	.348	.470	.390
[illegible]	[illegible]	[illegible]	.[illegible]	.358	.488	.447
[illegible]	[illegible]	[illegible]	.[illegible]	.356	.614	.442
[illegible]	[illegible]	[illegible]	.[illegible]	.366	.596	.395
[illegible]	[illegible]	[illegible]	.[illegible]	.359	.460	.411
[illegible]	[illegible]	[illegible]	.[illegible]	.360	.535	.405
[illegible]	[illegible]	[illegible]	.[illegible]	.359	.387	.375
[illegible]	[illegible]	[illegible]	.[illegible]	.362	.472	.406
[illegible]	[illegible]	[illegible]	.[illegible]	.369	.530	.385
[illegible]	[illegible]	[illegible]	.[illegible]	.376	.529	.389
[illegible]	[illegible]	[illegible]	.[illegible]	.369	.504	.395
[illegible]	[illegible]	[illegible]	.[illegible]	.390	.253	.390
[illegible]	[illegible]	[illegible]	.[illegible]	.376	.356	.370
[illegible]	[illegible]	[illegible]	.[illegible]	.370	.340	.385
[illegible]	[illegible]	[illegible]	.[illegible]	.365	.384	.393
[illegible]	[illegible]	[illegible]	.[illegible]	.371	.677	.375
[illegible]	[illegible]	[illegible]	.[illegible]	.355	.633	.401
[illegible]	[illegible]	[illegible]	.[illegible]	.360	.465	.467
[illegible]	[illegible]	[illegible]	.[illegible]	.367	.459	.393
[illegible]	[illegible]	[illegible]	.[illegible]	.370	.460	.394
[illegible]	[illegible]	[illegible]	.[illegible]	.365	.537	.416
[illegible]	[illegible]	[illegible]	.[illegible]	.368	.759	.447
[illegible]	[illegible]	[illegible]	.[illegible]	.366	.453	.447
[illegible]	[illegible]	[illegible]	.[illegible]	.359	.673	.447
[illegible]	[illegible]	[illegible]	.[illegible]	.366	.662	.385
[illegible]	[illegible]	[illegible]	.[illegible]	.351	.632	.401
[illegible]	[illegible]	[illegible]	.[illegible]	.354	.548	.442
[illegible]	[illegible]	[illegible]	.[illegible]	.361	.543	.442
[illegible]	[illegible]	[illegible]	.[illegible]	.362	.365	.401
[illegible]	[illegible]	[illegible]	.[illegible]	.369	.480	.606
[illegible]	[illegible]	[illegible]	.[illegible]	.372	.467	.590

Run No. 1-31474 continued

[illegible]	[illegible]	[illegible]	.372	.067	.523	.524
[illegible]	[illegible]	[illegible]	.118	.037	.010	.452
[illegible]	[illegible]	[illegible]	.469	.055	.365	.471
[illegible]	[illegible]	[illegible]	.305	.053	.344	.431
[illegible]	[illegible]	[illegible]	.342	.069	.470	.426
[illegible]	[illegible]	[illegible]	.314	.038	.506	.442
[illegible]	[illegible]	[illegible]	.343	.071	.451	.467
[illegible]	[illegible]	[illegible]	.350	.048	.512	.534
[illegible]	[illegible]	[illegible]	.379	.058	.625	.626
[illegible]	[illegible]	[illegible]	.440	.060	.433	.524
[illegible]	[illegible]	[illegible]	.485	.058	.624	.534
[illegible]	[illegible]	[illegible]	.494	.062	.474	.[illegible]
[illegible]	[illegible]	[illegible]	.496	.062	.612	.[illegible]
[illegible]	[illegible]	[illegible]	.495	.063	.564	.595
[illegible]	[illegible]	[illegible]	.455	.045	.472	.554
[illegible]	[illegible]	[illegible]	.434	.050	.567	.[illegible]
[illegible]	[illegible]	[illegible]	.437	.057	.571	.493
[illegible]	[illegible]	[illegible]	.511	.065	.517	.483
[illegible]	[illegible]	[illegible]	.465	.059	.450	.503
[illegible]	[illegible]	[illegible]	.424	.058	.408	.411
[illegible]	[illegible]	[illegible]	.434	.060	.568	.554
[illegible]	[illegible]	[illegible]	.497	.051	.539	.524
[illegible]	[illegible]	[illegible]	.307	.055	.649	.533
[illegible]	[illegible]	[illegible]	.435	.054	.603	.543
[illegible]	[illegible]	[illegible]	.455	.056	.439	.539
[illegible]	[illegible]	[illegible]	.447	.053	.477	.472
[illegible]	[illegible]	[illegible]	.[illegible]96	.050	.518	.472
[illegible]	[illegible]	[illegible]	.408	.054	.545	.524
[illegible]	[illegible]	[illegible]	.407	.046	.486	.549
[illegible]	[illegible]	[illegible]	.396	.043	.[illegible]1	.539
[illegible]	[illegible]	[illegible]	.433	.057	.540	.575
[illegible]	[illegible]	[illegible]	.486	.058	.335	.540
[illegible]	[illegible]	[illegible]	.467	.062	.433	.484
[illegible]	[illegible]	[illegible]	.485	.061	.404	.447

Run No. 7-31574 (Figure G-4, p. 181) (80 wt. % AP propellant [UFO], 50 Hz. oscillatory pressure, 3-5 mm)

SCAN NUMBER	PRESSURE, PSIA	FLAME TEMP., DEG. KELVIN	H2O ABSORBANCE	CO2 ABSORBANCE	CO ABSORBANCE	NA-D ABS.
1	25.76	2428.1	.051	.064	.057	.403
2	25.46	2427.5	.036	.001	.010	.385
3	25.03	2408.2	.030	.077	.002	.409
4	24.81	2404.4	.041	.036	.005	.403
5	24.02	2375.3	.032	.059	.010	.365
6	23.91	2373.8	.057	.059	-.003	.397
7	23.50	2390.2	.027	.068	.003	.361
8	23.34	2368.0	.043	.065	-.047	.349
9	23.46	2392.2	.026	.062	-.005	.343
10	23.85	2424.9	.033	.002	.028	.331
11	24.19	2404.7	.026	.040	.028	.373
12	24.05	2397.3	.030	.104	-.004	.385
13	24.43	2401.5	.039	.125	-.030	.391
14	25.16	2426.8	.036	.074	-.009	.379
15	25.42	2405.2	.033	.072	.028	.427
16	25.54	2396.6	.038	.084	-.054	.421
17	25.54	2386.2	.044	.045	.014	.433
18	25.37	2379.5	.033	.052	-.012	.438
19	24.86	2381.0	.036	.049	-.004	.421
20	24.44	2385.2	.023	.050	.042	.355
21	24.02	2364.8	.048	.082	-.013	.373
22	23.72	2366.7	.032	.033	.036	.355
23	23.55	2373.0	.055	.076	-.006	.355
24	23.91	2358.1	.065	.040	.040	.379
25	23.68	2365.4	.019	.046	-.014	.367
26	23.43	2363.0	.030	.084	-.028	.391
27	24.14	2371.5	.051	.072	-.017	.367
28	24.80	2369.2	.029	.069	-.002	.367
29	24.65	2404.7	.061	.100	.005	.373
30	25.08	2379.5	.053	.073	-.019	.434
31	25.59	2429.5	.053	.111	.014	.397
32	25.76	2405.2	.052	.090	-.002	.427
33	25.84	2387.5	.044	.004	.019	.415
34	25.59	2390.0	.041	.098	.014	.432
35	25.20	2372.5	.035	.067	-.026	.409
36	24.65	2363.0	.034	.093	-.012	.391
37	24.34	2358.1	.036	.057	-.028	.379
38	23.59	2360.0	.034	.049	-.005	.361
39	23.42	2401.6	.022	.057	.013	.301
40	23.21	2416.3	.043	.006	.016	.319
41	23.25	2377.1	.038	.041	-.010	.325
42	23.51	2363.0	.032	.048	-.043	.391
43	23.60	2406.3	.044	.105	-.035	.337
44	24.40	2393.0	.037	.116	.038	.373
45	24.95	2423.9	.036	.100	.037	.379
46	25.46	2459.0	.043	.063	.023	.355
47	25.93	2407.2	.035	.040	-.056	.415
48	26.05	2419.0	.053	.115	-.063	.379
49	25.93	2411.6	.033	.095	.005	.391
50	25.54	2373.2	.047	.086	.014	.403
51	24.86	2351.4	.051	.084	.038	.385
52	24.27	2359.1	.039	.066	-.024	.367

Run No. 7-31574 continued

53	23.63	2370.1	.039	.060	.007	.379
54	23.12	2338.9	.035	.051	.017	.379
55	22.87	2351.4	.051	.061	-.030	.385
56	22.91	2382.8	.029	.064	.018	.331
57	23.29	2377.5	.028	.012	.017	.367
58	23.60	2376.3	.041	.044	-.015	.361
59	24.23	2391.0	.031	.138	-.017	.391
60	24.91	2406.6	.046	.005	.002	.391
61	25.42	2380.9	.057	.071	-.020	.427
62	25.28	2341.9	.031	.059	.016	.456
63	25.26	2387.4	.035	.090	.007	.379
64	25.22	2393.5	.041	.085	.016	.409
65	25.68	2396.4	.030	.086	.044	.403
66	25.37	2368.8	.045	.072	.002	.391
67	24.92	2356.1	.050	.083	-.042	.379
68	23.59	2377.1	.045	.060	-.018	.325
69	23.12	2374.6	.049	.084	-.041	.343
70	22.74	2325.3	.035	.065	.014	.397
71	22.63	2344.8	.034	.044	.025	.391
72	23.68	2316.0	.050	.066	-.023	.355
73	23.89	2363.6	.057	.041	-.012	.385
74	24.19	2388.8	.047	.051	-.000	.391
75	24.74	2371.5	.052	.068	-.029	.367
76	25.29	2392.6	.037	.075	-.071	.415
77	25.80	2395.7	.036	.062	-.002	.427
78	25.97	2359.9	.046	.131	-.011	.427
79	26.05	2376.6	.058	.107	-.024	.427
80	25.71	2364.3	.035	.096	.032	.438
81	25.06	2359.5	.053	.067	.018	.432
82	24.48	2380.9	.036	.021	-.005	.415
83	23.68	2348.5	.037	.034	-.054	.432
84	23.25	2360.2	.055	.045	.010	.355
85	23.00	2385.4	.043	.079	-.023	.367
86	22.83	2356.6	.046	.050	.029	.373
87	23.12	2359.7	.031	.035	.019	.361
88	23.53	2360.8	.051	.053	.039	.349
89	24.02	2372.8	.040	.015	.014	.349
90	24.52	2387.4	.045	.026	.035	.379
91	24.86	2425.3	.043	.034	.027	.373
92	25.29	2398.5	.022	.037	.002	.409
93	25.99	2396.5	.042	.029	.019	.385
94	26.67	2403.6	.042	.062	-.002	.379
95	26.63	2412.7	.061	.122	-.015	.385
96	26.33	2387.5	.050	.111	.006	.415
97	25.63	2367.5	.067	.124	-.025	.415
98	24.57	2404.7	.058	.062	.022	.373
99	23.89	2401.5	.041	.057	-.016	.361
100	23.55	2377.5	.038	.066	.009	.367

Run No. 9-4474 (Figure G-5, p. 182) (85 wt. % AP propellant [UFR], 51 Hz. oscillatory pressure, 3-5 mm)

SCAN NUMBER	PRESSURE-PSIA	FLAME TEMP.-DEG. KELVIN	H2O ABSORBANCE	CO2 ABSORBANCE	CO ABSORBANCE	NA-D ABS.
1	46.49	2590.3	.025	.100	.054	.398
2	45.90	2655.9	.040	.120	.028	.342
3	45.43	2696.1	.018	.117	.083	.309
4	45.43	2710.3	.030	.096	.073	.303
5	45.73	2654.6	.029	.081	.093	.353
6	46.32	2643.1	.028	.102	.050	.381
7	46.72	2636.8	.018	.100	.074	.420
8	47.51	2564.4	.032	.078	.075	.470
9	48.19	2550.1	.028	.091	.073	.482
10	48.57	2577.4	.031	.144	.082	.465
11	48.70	2590.9	.042	.148	.050	.454
12	48.23	2547.5	.041	.146	.103	.504
13	47.69	2564.4	.024	.149	.043	.448
14	47.38	2567.6	.026	.090	.074	.459
15	46.79	2595.5	.036	.078	.086	.381
16	46.24	2606.9	.029	.066	.076	.337
17	45.73	2654.8	.030	.078	.108	.365
18	45.34	2619.5	.042	.059	.114	.370
19	45.51	2606.1	.025	.042	.061	.381
20	45.85	2606.9	.026	.052	.064	.220
21	46.49	2701.1	.019	.035	.071	.309
22	47.13	2780.6	.033	.058	.024	.264
23	47.76	2642.3	.042	.067	.108	.409
24	48.32	2625.8	.032	.094	.073	.429
25	48.06	2662.4	.026	.092	.125	.376
26	46.53	2578.2	.027	.115	.048	.487
27	48.19	2541.8	.032	.103	.050	.456
28	47.59	2561.1	.026	.118	.060	.470
29	47.00	2578.9	.037	.147	.055	.443
30	46.49	2609.4	.037	.172	.061	.431
31	46.07	2603.2	.026	.129	.022	.392
32	45.73	2650.8	.037	.050	.035	.359
33	45.51	2586.1	.030	.051	.077	.443
34	45.60	2628.8	.029	.101	.064	.381
35	46.11	2717.1	.035	.096	.047	.298
36	46.70	2673.3	.033	.115	.045	.353
37	47.25	2717.3	.032	.117	.051	.326
38	47.93	2701.9	.031	.138	.054	.314
39	46.32	2662.4	.024	.123	.083	.376
40	46.66	2657.2	.027	.112	.077	.365
41	48.40	2540.1	.022	.099	.067	.521
42	47.89	2526.0	.050	.137	.058	.554
43	47.30	2505.6	.037	.139	.058	.571
44	46.63	2480.6	.047	.122	.075	.613
45	46.36	2614.7	.045	.053	.071	.415
46	46.15	2615.7	.040	.078	.066	.392
47	45.77	2626.6	.030	.120	.039	.409
48	45.60	2642.9	.036	.112	.061	.404
49	45.77	2647.6	.028	.089	.054	.365
50	46.28	2625.9	.023	.070	.087	.387
51	46.79	2652.5	.019	.057	.111	.348
52	47.25	2631.5	.038	.046	.095	.431

Run No. 9-4474 continued

53	47.61	2584.9	.021	.075	.094	.493
54	48.23	2624.7	.034	.080	.088	.404
55	48.27	2657.0	.031	.115	.083	.381
56	48.02	2636.3	.039	.129	.069	.426
57	47.54	2573.5	.031	.139	.069	.482
58	47.17	2555.0	.034	.168	.064	.509
59	46.96	2491.1	.042	.219	.059	.593
60	46.58	2527.5	.025	.127	.070	.498
61	46.24	2503.7	.027	.052	.096	.443
62	46.62	2567.0	.038	.089	.092	.487
63	45.98	2538.2	.038	.090	.013	.426
64	46.17	2552.6	.022	.096	.082	.392
65	46.49	2586.1	.023	.107	.059	.443
66	46.63	2602.3	.019	.130	.069	.443
67	47.47	2657.6	.024	.120	.026	.392
68	47.41	2576.6	.027	.121	.022	.504
69	47.34	2571.8	.024	.147	.073	.448
70	46.39	2557.6	.034	.133	.088	.515
71	47.28	2490.8	.047	.166	.063	.588
72	47.72	2490.0	.030	.129	.079	.583
73	47.34	2478.4	.021	.125	.038	.546
74	47.00	2509.9	.018	.136	.060	.487
75	46.63	2511.1	.032	.137	.034	.526
76	46.53	2561.5	.035	.073	.087	.448
77	46.19	2542.1	.025	.042	.087	.431
78	46.02	2555.3	.026	.049	.082	.459
79	46.02	2551.6	.020	.037	.046	.487
80	46.47	2575.2	.024	.049	.034	.342
81	46.63	2567.0	.030	.059	.096	.404
82	47.00	2601.5	.026	.112	.049	.381
83	47.47	2606.4	.033	.177	.042	.431
84	47.63	2597.5	.028	.151	.108	.493
85	48.10	2597.8	.027	.147	.098	.476
86	47.89	2561.3	.035	.107	.093	.532
87	47.31	2591.1	.034	.136	.063	.465
88	47.13	2594.6	.040	.138	.068	.426
89	47.55	2627.8	.042	.158	.042	.515
90	46.99	2556.6	.030	.108	.056	.467
91	46.70	2616.7	.037	.060	.064	.420
92	46.29	2615.1	.036	.070	.055	.365
93	46.67	2615.2	.027	.057	.045	.426
94	46.62	2597.7	.037	.032	.097	.443
95	46.44	2595.2	.038	.063	.077	.353
96	46.53	2646.4	.033	.060	.091	.392
97	46.98	2600.5	.022	.055	.075	.331
98	47.38	2650.9	.032	.096	.090	.392
99	47.98	2624.7	.024	.103	.044	.437
100	48.47	2654.6	.033	.117	.059	.398

Run No. 7-4374 (Figure G-6, p. 183) (82 wt. % AP propellant [UFN], 31 Hz. oscillatory pressure, 3-5 mm)

SCAN NUMBER	PRESSURE-PSIA	FLAME TEMP.-DEG. KELVIN	H2O MOL FRACTION	CO2 MOL FRACTION	CO MOL FRACTION	NA-D ABS.
1	48.57	2611.5	.536	.076	.297	.658
2	48.51	2634.2	.539	.086	.277	.603
3	48.41	2565.0	.568	.076	.374	.691
4	48.31	2584.2	.554	.072	.186	.674
5	48.23	2592.3	.515	.077	.264	.625
6	48.31	2596.3	.565	.075	.242	.669
7	48.36	2563.1	.484	.071	.335	.696
8	48.46	2651.8	.517	.078	.278	.575
9	48.41	2661.2	.497	.086	.201	.641
10	48.74	2606.0	.536	.076	.292	.625
11	48.75	2598.9	.508	.069	.337	.659
12	49.06	2587.7	.471	.069	.288	.669
13	49.08	2563.4	.465	.074	.263	.652
14	49.06	2572.0	.555	.078	.345	.685
15	49.15	2568.2	.583	.076	.264	.708
16	49.42	2584.8	.545	.083	.298	.669
17	49.59	2591.4	.634	.065	.202	.663
18	49.53	2603.8	.539	.086	.286	.674
19	49.59	2600.4	.599	.086	.386	.674
20	49.47	2613.7	.564	.081	.287	.630
21	49.59	2606.6	.612	.080	.266	.680
22	49.63	2574.2	.507	.074	.239	.658
23	49.46	2561.6	.525	.069	.278	.702
24	49.49	2598.2	.540	.079	.287	.652
25	49.49	2574.2	.432	.086	.270	.658
26	48.47	2585.5	.537	.085	.277	.658
27	48.53	2575.6	.462	.069	.274	.702
28	48.35	2611.1	.474	.089	.323	.636
29	48.19	2664.8	.562	.081	.174	.663
30	48.08	2625.5	.492	.071	.321	.603
31	48.14	2620.0	.518	.072	.365	.625
32	48.14	2617.8	.569	.077	.324	.680
33	48.31	2583.3	.547	.076	.247	.625
34	48.43	2596.2	.516	.074	.226	.652
35	48.74	2591.3	.482	.067	.315	.641
36	48.75	2583.4	.458	.073	.293	.658
37	49.12	2607.5	.499	.076	.374	.647
38	49.42	2641.2	.449	.070	.332	.614
39	49.53	2619.2	.457	.072	.313	.647
40	49.42	2617.9	.470	.080	.308	.658
41	49.30	2548.0	.471	.078	.245	.719
42	49.19	2594.9	.472	.072	.391	.674
43	49.30	2592.4	.536	.078	.222	.674
44	49.19	2574.4	.596	.082	.364	.713
45	49.36	2567.2	.617	.081	.270	.669
46	49.25	2577.7	.497	.079	.224	.663
47	49.42	2582.4	.430	.077	.289	.663
48	49.30	2574.2	.527	.070	.231	.674
49	49.19	2571.9	.514	.078	.278	.702
50	49.19	2624.3	.505	.073	.326	.641
51	49.09	2611.6	.449	.068	.341	.647
52	48.73	2584.3	.469	.059	.318	.674

Run No. 7-4374 continued

53	[illegible]	2577.7	.473	.064	.259	.663
54	[illegible]	2[illegible]	.532	.077	.208	.597
55	[illegible]	2[illegible]	.511	.071	.232	.680
56	[illegible]	2[illegible]	.576	.068	.357	.713
57	[illegible]	2574.0	.582	.070	.276	.674
58	[illegible]	2[illegible]	.508	.077	.323	.641
59	[illegible]	2[illegible]	.507	.074	.273	.630
60	[illegible]	2[illegible]	.480	.079	.271	.630
61	[illegible]	257[illegible]	.442	.080	.305	.696
62	[illegible]	25[illegible]	.456	.062	.256	.609
63	[illegible]	2[illegible]	.521	.078	.268	.619
64	[illegible]	2[illegible]	.510	.076	.325	.647
65	[illegible]	25[illegible]	.523	.075	.360	.685
66	[illegible]	257[illegible]	.562	.080	.266	.663
67	[illegible]	2[illegible]	.471	.065	.202	.630
68	[illegible]	25[illegible]	.529	.066	.149	.674
69	[illegible]	2567.4	.505	.091	.149	.691
70	[illegible]	25[illegible]	.522	.093	.290	.669
71	[illegible]	2[illegible]	.561	.085	.340	.619
72	[illegible]	25[illegible]	.456	.080	.242	.713
73	[illegible]	25[illegible]	.441	.077	.237	.647
74	[illegible]	2[illegible]	.469	.077	.241	.551
75	[illegible]	2[illegible]	.522	.078	.363	.619
76	[illegible]	2[illegible]	.480	.085	.214	.625
77	[illegible]	2564.7	.509	.078	.235	.680
78	[illegible]	25[illegible]	.449	.066	.348	.625
79	[illegible]	2[illegible]	.536	.078	.215	.653
80	[illegible]	25[illegible]	.534	.073	.278	.630
81	[illegible]	2[illegible]	.547	.077	.261	.641
82	[illegible]	2[illegible]	.450	.069	.347	.735
83	[illegible]	2[illegible]	.489	.066	.255	.724
84	[illegible]	2[illegible]	.485	.075	.278	.641
85	[illegible]	257[illegible]	.526	.071	.206	.685
86	[illegible]	2[illegible]	.525	.078	.270	.663
87	[illegible]	2[illegible]	.490	.073	.319	.603
88	[illegible]	2[illegible]	.467	.073	.375	.702
89	[illegible]	25[illegible]	.511	.070	.276	.685
90	[illegible]	2[illegible]	.559	.077	.313	.669
91	[illegible]	2567.4	.551	.075	.354	.619
92	[illegible]	25[illegible]	.486	.081	.354	.680
93	[illegible]	25[illegible]	.529	.080	.314	.652
94	[illegible]	2[illegible]	.540	.081	.262	.586
95	[illegible]	25[illegible]	.535	.080	.334	.685
96	[illegible]	2565.1	.563	.078	.300	.685
97	[illegible]	256[illegible]	.496	.082	.300	.730
98	[illegible]	25[illegible]	.460	.074	.304	.630
99	[illegible]	2[illegible]	.516	.069	.291	.652
100	[illegible]	2[illegible]	.475	.073	.362	.680

Run No. 3-31474 (Figure G-7, p. 184) (82 wt. % AP propellant [UFP], 31 Hz. oscillatory pressure, 3-5 mm)

[illegible]	[illegible]	[illegible] TEMP. [illegible] KELVIN	H2O MOL FRACTION	CO2 MOL FRACTION	CO MOL FRACTION	NA-D ABS.
1	[illegible]	2477.4	.498	.060	.094	.599
[illegible]	[illegible]	[illegible]	.476	.052	.444	.502
[illegible]	[illegible]	[illegible]	[illegible]	.062	.144	.574
[illegible]	[illegible]	[illegible]	.547	.057	.405	.625
[illegible]	[illegible]	[illegible]	.491	.056	.214	.597
[illegible]	[illegible]	[illegible]	.499	.065	.113	.560
[illegible]	[illegible]	[illegible]	.617	.060	.357	.514
[illegible]	[illegible]	[illegible]	.497	.059	.353	.560
[illegible]	[illegible]	[illegible]	.595	.063	.159	.502
[illegible]	[illegible]	[illegible]	.633	.065	-.027	.529
[illegible]	[illegible]	[illegible]	.514	.048	.263	.549
[illegible]	[illegible]	[illegible]	[illegible]	.059	.356	.661
[illegible]	[illegible]	[illegible]	.521	.060	.360	.629
[illegible]	[illegible]	[illegible]	.535	.063	.473	.652
[illegible]	[illegible]	[illegible]	.601	.062	.388	.545
[illegible]	[illegible]	[illegible]	.502	.058	.336	.679
[illegible]	[illegible]	[illegible]	.479	.071	.274	.657
[illegible]	[illegible]	[illegible]	.450	.073	.172	.647
[illegible]	[illegible]	[illegible]	.565	.056	.503	.663
[illegible]	[illegible]	[illegible]	.522	.073	.005	.727
[illegible]	[illegible]	[illegible]	.457	.068	.165	.679
[illegible]	[illegible]	[illegible]	.416	.065	.390	.647
[illegible]	[illegible]	[illegible]	.400	.066	.149	.631
[illegible]	[illegible]	[illegible]	[illegible]	.064	.350	.577
[illegible]	[illegible]	[illegible]	.599	.060	.213	.604
[illegible]	[illegible]	[illegible]	.610	.063	.296	.562
[illegible]	[illegible]	[illegible]	.570	.058	.285	.657
[illegible]	[illegible]	[illegible]	.624	.056	.227	.562
[illegible]	[illegible]	[illegible]	.510	.054	.457	.593
[illegible]	[illegible]	[illegible]	.479	.051	.262	.563
[illegible]	[illegible]	[illegible]	.557	.051	.397	.557
[illegible]	[illegible]	[illegible]	.527	.051	.136	.663
[illegible]	[illegible]	[illegible]	.532	.057	.364	.593
[illegible]	[illegible]	[illegible]	.651	.053	.166	.599
[illegible]	[illegible]	[illegible]	.561	.049	.462	.556
[illegible]	[illegible]	[illegible]	.502	.047	.422	.609
[illegible]	[illegible]	[illegible]	.582	.051	.387	.652
[illegible]	[illegible]	[illegible]	.576	.046	.226	.663
[illegible]	[illegible]	[illegible]	.593	.062	.363	.705
[illegible]	[illegible]	[illegible]	.607	.064	.342	.673
[illegible]	[illegible]	[illegible]	.502	.062	.334	.652
[illegible]	[illegible]	[illegible]	.525	.061	.324	.647
[illegible]	[illegible]	[illegible]	.529	.062	.376	.591
[illegible]	[illegible]	[illegible]	.532	.072	.106	.577
[illegible]	[illegible]	[illegible]	.486	.067	.310	.524
[illegible]	[illegible]	[illegible]	.567	.062	.195	.647
[illegible]	[illegible]	[illegible]	.404	.057	.248	.679
[illegible]	[illegible]	[illegible]	.527	.051	.313	.609
[illegible]	[illegible]	[illegible]	.523	.053	.312	.615
[illegible]	[illegible]	[illegible]	.550	.048	.245	.593
[illegible]	[illegible]	[illegible]	.486	.064	.267	.593
[illegible]	[illegible]	[illegible]	.440	.050	.293	.593

Run No. 3-31474 continued

53	44.34	2452.5	.567	.051	.175	.609
54	45.03	2471.0	.585	.051	.377	.582
55	44.[illegible]	2477.[illegible]	.585	.045	.378	.577
56	44.[illegible]	2475.[illegible]	.538	.053	.414	.556
57	44.[illegible]	2475.[illegible]	.607	.049	.411	.550
58	44.[illegible]	2476.[illegible]	.576	.043	.437	.576
59	44.71	2480.[illegible]	.591	.047	.517	.673
60	45.42	2481.1	.614	.050	.246	.534
61	45.21	2479.[illegible]	.518	.038	.457	.625
62	46.[illegible]	2479.[illegible]	.585	.050	.422	.665
63	46.41	2478.[illegible]	.517	.048	.504	.684
64	46.[illegible]	2479.[illegible]	.582	.043	.527	.594
65	47.[illegible]	2484.7	.494	.035	.221	.668
66	47.[illegible]	2481.2	.588	.041	.459	.652
67	47.[illegible]	2481.[illegible]	.538	.057	.231	.673
68	47.[illegible]	2481.[illegible]	.490	.046	.369	.620
69	47.[illegible]	2481.[illegible]	.498	.047	.156	.593
70	47.[illegible]	2481.[illegible]	.504	.058	.187	.[illegible]
71	47.[illegible]	2481.[illegible]	.531	.048	.431	.663
72	48.[illegible]	2480.[illegible]	.530	.062	.282	.663
73	48.[illegible]	2481.[illegible]	.501	.054	.324	.604
74	48.[illegible]	2482.7	.480	.[illegible]0	.072	.615
75	48.[illegible]	2481.[illegible]	.[illegible]	.050	.357	.625
76	48.44	2481.[illegible]	.489	.052	.203	.577
77	48.[illegible]	2482.[illegible]	.[illegible]	.048	.503	.513
78	48.[illegible]	2481.[illegible]	.[illegible]	.053	.384	.566
79	48.[illegible]	2481.7	.[illegible]	.049	.219	.550
80	48.[illegible]	2481.[illegible]	.[illegible]	.[illegible]02	.267	.577
81	48.[illegible]	2481.[illegible]	.[illegible]	.055	.382	.577
82	48.[illegible]	2481.[illegible]	.[illegible]	.053	.291	.593
83	48.[illegible]	2481.[illegible]	.[illegible]	.057	.294	.534
84	48.[illegible]	2481.[illegible]	.[illegible]	.048	.388	.529
85	48.[illegible]	2481.[illegible]	.[illegible]	.043	.409	.513
86	48.[illegible]	2481.[illegible]	.[illegible]	.044	.455	.582
87	48.[illegible]	2481.[illegible]	.[illegible]	.043	.275	.559
88	48.[illegible]	2481.[illegible]	.[illegible]	.[illegible]	.275	.529
89	47.[illegible]	2481.7	.[illegible]	.[illegible]	.194	.534
90	47.[illegible]	2481.[illegible]	.493	.048	.314	.657
91	47.77	2482.[illegible]	.537	.[illegible]	.397	.636
92	48.[illegible]	2482.[illegible]	.[illegible]	.055	.335	.[illegible]
93	47.[illegible]	2481.[illegible]	.493	.[illegible]72	.134	.657
94	47.[illegible]	2481.[illegible]	.[illegible]	.[illegible]	.282	.[illegible]
95	47.[illegible]	2481.[illegible]	.[illegible]	.070	.135	.[illegible]
96	47.[illegible]	2481.[illegible]	.[illegible]	.070	.213	.615
97	48.[illegible]	2482.[illegible]	.[illegible]	.[illegible]	.[illegible]	.[illegible]
98	48.[illegible]	2481.7	.527	.[illegible]06	.282	.609
99	48.[illegible]	2471.3	.578	.065	.198	.631
100	48.[illegible]	2481.[illegible]	.557	.064	.361	.577

Run No. 3-31474 continued

53	44.61	2463.5	.567	.351	.175	.609
54	44.73	2467.0	.580	.351	.377	.582
55	44.84	2477.0	.595	.345	.378	.577
56	44.96	2481.2	.604	.353	.414	.556
57	45.07	2486.5	.609	.349	.411	.559
58	45.19	2490.8	.571	.343	.437	.572
59	45.31	2495.9	.591	.347	.417	.573
60	45.42	2501.1	.614	.350	.446	.534
61	45.54	2507.3	.614	.338	.487	.525
62	45.65	2511.3	.585	.350	.422	.603
63	45.77	2517.0	.617	.348	.504	.604
64	45.89	2523.5	.585	.343	.507	.599
65	46.00	2527.7	.634	.335	.721	.648
66	46.12	2532.2	.588	.341	.459	.652
67	46.23	2536.1	.536	.357	.531	.673
68	46.35	2540.5	.630	.366	.369	.620
69	46.46	2545.3	.598	.307	.156	.593
70	46.58	2549.4	.604	.334	.167	.600
71	46.69	2554.6	.591	.368	.431	.602
72	46.81	2560.5	.630	.362	.222	.663
73	46.92	2565.9	.601	.354	.324	.604
74	47.04	2571.7	.620	.360	.272	.615
75	47.15	2581.0	.602	.340	.357	.625
76	47.27	2587.5	.589	.352	.205	.577
77	47.38	2592.8	.582	.346	.563	.513
78	47.50	2598.0	.595	.353	.384	.566
79	47.61	2603.7	.619	.349	.218	.550
80	47.73	2609.2	.624	.362	.267	.577
81	47.84	2614.3	.625	.355	.382	.577
82	47.96	2619.1	.603	.291	.291	.593
83	48.07	2625.1	.605	.357	.294	.534
84	48.19	2630.4	.608	.340	.388	.609
85	48.30	2636.1	.591	.353	.400	.513
86	48.42	2641.4	.579	.344	.456	.566
87	48.53	2647.6	.606	.363	.275	.589
88	48.65	2651.8	.587	.360	.274	.529
89	48.76	2657.7	.615	.369	.198	.534
90	48.88	2663.1	.623	.368	.313	.657
91	48.99	2667.8	.607	.364	.397	.636
92	49.11	2673.0	.611	.365	.335	.631
93	49.22	2678.3	.593	.372	.134	.657
94	49.34	2683.9	.602	.367	.202	.670
95	49.45	2689.4	.609	.370	.135	.624
96	49.57	2695.2	.590	.370	.213	.615
97	49.68	2699.8	.596	.367	.307	.652
98	49.80	2705.7	.627	.366	.282	.609
99	49.91	2711.3	.578	.365	.196	.631
100	50.03	2717.0	.597	.364	.361	.577

Run No. 5-4374 (Figure G-8, p. 185) (82 wt. % AP propellant [UFP], 31 Hz. oscillatory pressure, 3-5 mm)

[illegible]	[illegible]	FLAME TEMPERATURE, KELVIN	H2O MOL FRACTION	CO2 MOL FRACTION	CO MOL FRACTION	NA-D AVG.
1	41[illegible]	29[illegible]	.2[illegible]	.057	.343	.427
4	[illegible]	294 .2	.266	.059	.373	.433
[illegible]	[illegible]	[illegible]	.219	.054	.141	.363
[illegible]	[illegible]	[illegible]	.358	.068	.298	.359
[illegible]	[illegible]	[illegible]	.396	.071	.214	.336
7	37[illegible]	[illegible]	.[illegible]	.067	.102	.293
[illegible]	37[illegible]	[illegible]	.247	.063	.450	.299
[illegible]	37[illegible]	[illegible]	.[illegible]	.060	.284	.329
[illegible]	[illegible]	[illegible]	.245	.065	.513	.379
11	3[illegible]	29[illegible]	.234	.080	.295	.400
12	[illegible]	[illegible]	.[illegible]	.077	.208	.374
13	[illegible]	[illegible]	.271	.077	.467	.342
14	[illegible]	[illegible]	.267	.069	.215	.395
15	[illegible]	[illegible]	.[illegible]	.063	.437	.400
16	[illegible]	[illegible]	.[illegible]	.073	.408	.368
17	[illegible]	[illegible]	.[illegible]	.068	.[illegible]	.395
18	[illegible]	[illegible]	.[illegible]	.040	.477	.347
19	[illegible]	[illegible]	.[illegible]	.040	.514	.433
[illegible]	[illegible]	[illegible]	.[illegible]	.049	.[illegible]	.368
[illegible]	[illegible]	[illegible]	.[illegible]	.047	.403	.454
24	[illegible]	[illegible]	.272	.051	.508	.411
[illegible]	[illegible]	[illegible]	.[illegible]	.054	.314	.416
[illegible]	[illegible]	[illegible]	.[illegible]	.[illegible]	.[illegible]	.405
[illegible]	[illegible]	[illegible]	.[illegible]	.042	.[illegible]	.384
28	41[illegible]	[illegible]	.[illegible]	.045	.[illegible]	.[illegible]
[illegible]	[illegible]	[illegible]	.[illegible]	.045	.185	.395
30	[illegible]	[illegible]	.[illegible]	.060	.414	.374
[illegible]	[illegible]	[illegible]	.[illegible]	.[illegible]	.255	.358
32	[illegible]	[illegible]	.237	.071	.154	.384
33	[illegible]	[illegible]	.[illegible]	.[illegible]	.277	.395
34	37.[illegible]	[illegible]	.291	.065	.137	.400
35	37.[illegible]	[illegible]	.265	.062	.290	.363
[illegible]	[illegible]	[illegible]	.[illegible]	.078	.[illegible]	.427
[illegible]	[illegible]	[illegible]	.[illegible]	.079	.177	.374
[illegible]	[illegible]	[illegible]	.[illegible]	.065	.[illegible]	.395
[illegible]	[illegible]	[illegible]	.[illegible]	.[illegible]	.[illegible]	.[illegible]
[illegible]	[illegible]	[illegible]	.251	.079	.[illegible]	.436
[illegible]	[illegible]	[illegible]	.[illegible]	.075	.[illegible]	.427
[illegible]	[illegible]	[illegible]	.[illegible]	.[illegible]	.[illegible]	.[illegible]
41	[illegible]	[illegible]	.[illegible]	.064	.[illegible]	.411
[illegible]	[illegible]	[illegible]	.[illegible]	.064	.[illegible]	.422
[illegible]	[illegible]	[illegible]	.171	.059	.467	.416
[illegible]	[illegible]	[illegible]	.[illegible]	.063	.[illegible]	.[illegible]
[illegible]	[illegible]	[illegible]	.246	.068	.[illegible]	.459
[illegible]	[illegible]	[illegible]	.[illegible]	.064	.[illegible]	.427
47	[illegible]	[illegible]	.[illegible]	.063	.[illegible]	.433
[illegible]	[illegible]	[illegible]	.249	.060	.[illegible]	.436
[illegible]	[illegible]	[illegible]	.272	.059	.[illegible]	.502
[illegible]	[illegible]	[illegible]	.[illegible]	.057	.[illegible]	.[illegible]
54	[illegible]	[illegible]	.329	.062	.446	.358
55	40.[illegible]	[illegible]	.375	.065	.[illegible]	.384

Run No. 5-4373 continued

			.493	.603	.407	.406
			.356	.057	.203	.325
			.234	.356	.347	.390
			.361	.057	.396	.325
			.234	.065	.437	.342
			.381	.076	.298	.284
			.293	.069	.231	.306
			.365	.065	.174	.247
			.256	.070	.325	.400
			.302	.074	.262	.345
			.239	.069	.306	.388
			.273	.073	.247	.462
			.225	.060	.290	.264
			.285	.065	.425	.374
			.400	.060	.314	.379
			.132	.062	.366	.400
			.150	.060	.425	.438
			.239	.063	.302	.416
			.289	.071	.355	.400
			.309	.069	.302	.443
			.329	.060	.344	.470
			.234	.067	.306	.454
			.302	.082	.324	.465
			.267	.061	.272	.405
			.289	.067	.249	.404
			.321	.065	.375	.400
			.197	.068	.228	.390
			.298	.067	.385	.379
			.175	.065	.206	.329
			.311	.074	.241	.374
			.260	.070	.391	.347
			.296	.076	.158	.354
			.293	.075	.325	.306
			.345	.063	.240	.395
			.304	.076	.312	.395
			.301	.069	.174	.379
			.245	.065	.177	.459
			.207	.069	.300	.352
			.261	.079	.279	.379
			.195	.066	.334	.400
			.249	.064	.202	.400
			.241	.060	.305	.411
			.211	.076	.251	.470
			.297	.066	.253	.465
			.220	.068	.340	.465
			.235	.062	.408	.507
			.230	.059	.418	.433
			.314	.066	.305	.401
			.325	.064	.313	.363
			.324	.070	.431	.390
			.294	.060	.401	.403
			.293	.066	.335	.368

Run No. 1-31574 (Figure G-9, p. 186) (82 wt. % AP propellant [UFP], single-pressure-decrease-pulse, 3-5 mm)

SCAN NUMBER	PRESSURE,PSIA	FLAME TEMP.,DEG. KELVIN	H2O MOL FRACTION	CO2 MOL FRACTION	CO MOL FRACTION	NA-D ABS.
1	103.50	2468.8	.261	.040	.263	.775
2	103.50	2458.7	.294	.041	.239	.846
3	103.50	2534.5	.287	.038	.279	.693
4	103.71	2528.0	.296	.041	.297	.764
5	103.29	2476.7	.249	.041	.252	.619
6	103.08	2514.0	.250	.036	.278	.748
7	103.29	2521.7	.274	.034	.299	.720
8	102.66	2556.8	.307	.041	.250	.660
9	102.66	2475.0	.246	.046	.207	.770
10	102.86	2440.5	.286	.052	.159	.759
11	103.29	2512.5	.266	.045	.267	.622
12	103.50	2478.8	.264	.041	.274	.608
13	103.71	2454.8	.286	.037	.281	.775
14	103.71	2434.9	.283	.047	.258	.770
15	103.71	2440.9	.326	.050	.214	.759
16	103.50	2472.4	.264	.049	.242	.737
17	103.71	2367.6	.261	.049	.253	.786
18	103.71	2304.6	.318	.053	.232	.792
19	103.08	2356.2	.261	.050	.212	.797
20	103.29	2419.4	.278	.052	.236	.814
21	103.29	2441.3	.269	.050	.240	.836
22	103.71	2441.3	.304	.050	.247	.803
23	103.92	2420.9	.322	.054	.246	.814
24	103.71	2437.5	.245	.051	.224	.836
25	103.92	2426.6	.279	.051	.258	.808
26	103.71	2450.4	.309	.052	.260	.744
27	103.71	2463.5	.335	.051	.238	.770
28	103.71	2496.3	.354	.059	.241	.731
29	103.50	2501.2	.342	.062	.183	.715
30	103.29	2490.7	.313	.064	.218	.720
31	103.29	2472.5	.305	.053	.230	.786
32	103.29	2460.3	.349	.065	.214	.753
33	103.50	2444.8	.272	.058	.248	.742
34	103.50	2479.5	.293	.057	.219	.753
35	103.71	2439.3	.359	.064	.193	.819
36	103.71	2427.8	.282	.062	.157	.814
37	103.71	2424.8	.269	.055	.224	.803
38	103.92	2472.0	.175	.055	.240	.764
39	103.71	2426.6	.284	.056	.202	.825
40	103.50	2421.8	.260	.053	.246	.852
41	103.50	2403.0	.278	.053	.211	.852
42	103.08	2430.5	.299	.059	.204	.808
43	103.08	2401.9	.277	.052	.247	.753
44	103.29	2456.1	.262	.051	.239	.781
45	103.08	2465.0	.256	.055	.170	.786
46	102.44	2474.4	.317	.056	.204	.749
47	101.17	2465.1	.240	.052	.224	.759
48	100.32	2470.9	.274	.041	.238	.797
49	99.47	2436.0	.304	.042	.247	.814
50	98.41	2437.8	.322	.047	.260	.781
51	97.35	2427.8	.285	.043	.262	.775
52	96.71	2428.7	.262	.041	.253	.786

Run No. 1-31574 continued

53	95.44	2413.9	.304	.042	.244	.803
54	94.60	2419.4	.284	.043	.213	.814
55	93.74	2491.7	.254	.037	.236	.715
56	93.16	2491.6	.254	.031	.281	.737
57	92.45	2479.1	.269	.038	.226	.720
58	91.82	2472.6	.291	.043	.156	.698
59	91.19	2461.1	.266	.032	.239	.704
60	90.98	2546.0	.304	.028	.317	.600
61	89.71	2517.1	.290	.034	.270	.698
62	89.07	2449.0	.325	.041	.214	.797
63	88.22	2489.8	.320	.044	.194	.698
64	87.56	2538.2	.272	.036	.330	.638
65	86.95	2517.5	.308	.031	.330	.671
66	86.10	2476.0	.360	.043	.252	.715
67	85.46	2538.3	.343	.036	.350	.638
68	84.81	2523.0	.385	.028	.381	.669
69	83.76	2499.6	.334	.032	.300	.682
70	83.14	2486.9	.349	.037	.314	.698
71	82.49	2464.9	.320	.041	.145	.720
72	82.07	2485.8	.298	.034	.278	.693
73	81.35	2488.1	.290	.029	.291	.726
74	81.22	2434.9	.317	.028	.302	.770
75	80.79	2483.0	.310	.027	.249	.737
76	79.94	2499.1	.368	.034	.257	.666
77	79.73	2545.0	.396	.038	.278	.611
78	79.09	2539.0	.420	.044	.267	.627
79	78.58	2463.7	.361	.042	.246	.687
80	78.03	2498.1	.307	.043	.267	.605
81	77.62	2537.0	.344	.044	.286	.589
82	77.18	2511.0	.333	.041	.230	.671
83	76.76	2513.6	.316	.028	.264	.649
84	75.91	2484.6	.309	.023	.318	.655
85	75.70	2477.4	.339	.029	.239	.611
86	75.49	2502.5	.320	.025	.308	.660
87	75.27	2488.9	.288	.030	.266	.633
88	75.06	2503.0	.300	.037	.225	.627
89	74.64	2479.3	.304	.054	.175	.660
90	74.08	2510.9	.296	.051	.209	.611
91	73.56	2513.4	.306	.032	.208	.627
92	72.94	2511.4	.341	.036	.260	.655
93	72.32	2523.8	.314	.047	.254	.583
94	71.68	2538.8	.319	.043	.223	.605
95	71.04	2509.0	.322	.032	.304	.539
96	71.03	2531.3	.313	.031	.299	.627
97	71.03	2513.8	.319	.031	.328	.644
98	70.39	2536.7	.373	.035	.364	.605
99	70.01	2559.8	.378	.041	.259	.578
100	70.18	2501.3	.300	.036	.248	.539
101	69.97	2538.2	.305	.040	.203	.609
102	69.76	2530.7	.346	.037	.230	.622
103	69.33	2508.4	.345	.039	.275	.622
104	69.12	2524.0	.292	.031	.281	.600
105	68.91	2510.9	.333	.040	.263	.638
106	68.06	2531.4	.333	.044	.217	.611
107	67.63	2483.5	.287	.037	.281	.649
108	67.21	2520.9	.277	.030	.307	.638
109	67.21	2503.6	.344	.038	.238	.644

Run No. 1-31574 continued

110	67.00	2509.1	.302	.047	.293	.600
111	66.79	2559.2	.297	.038	.261	.539
112	66.79	2570.7	.349	.034	.293	.567
113	67.00	2498.9	.325	.040	.280	.615
114	66.36	2453.9	.387	.044	.308	.605
115	66.36	2497.7	.341	.039	.230	.559
116	66.15	2469.6	.367	.037	.298	.627
117	65.94	2526.7	.362	.036	.319	.572
118	65.94	2515.9	.360	.043	.273	.616
119	65.51	2502.7	.336	.044	.271	.638

Run No. 2-31574 (Figure G-10, p. 187) (80 wt. % AP propellant [UFO], single-pressure-decrease-pulse, 3-5 mm)

SCAN NUMBER	PRESSURE,PSIA	FLAME TEMP.,DEG. KELVIN	H2O MOL FRACTION	CO2 MOL FRACTION	CO MOL FRACTION	NA-D ABS.
1	103.00	2502.2	.159	.289	.159	.960
2	103.00	2526.2	.153	.305	.142	.949
3	103.05	2472.0	.164	.286	.146	.960
4	103.04	2472.7	.152	.307	.135	.954
5	103.05	2456.8	.164	.289	.150	.966
6	103.05	2434.0	.147	.295	.145	.972
7	103.04	2439.8	.164	.301	.123	.949
8	103.04	2448.4	.158	.342	.149	.960
9	103.04	2428.7	.151	.327	.118	.972
10	103.21	2432.1	.153	.318	.136	.954
11	103.21	2441.6	.146	.305	.148	.966
12	103.42	2439.1	.146	.290	.148	.972
13	103.21	2463.4	.152	.287	.162	.977
14	103.21	2444.5	.159	.321	.161	.972
15	103.21	2444.5	.165	.277	.148	.954
16	103.05	2489.0	.155	.278	.162	.937
17	103.04	2494.2	.141	.283	.138	.954
18	103.05	2506.7	.130	.294	.133	.949
19	103.05	2497.4	.135	.252	.133	.932
20	103.04	2477.7	.141	.221	.145	.977
21	103.04	2500.9	.135	.253	.128	.949
22	103.04	2509.0	.152	.254	.135	.972
23	103.42	2527.1	.153	.236	.141	.960
24	103.42	2542.0	.136	.256	.145	.949
25	103.00	2513.2	.137	.288	.117	.972
26	103.42	2509.6	.136	.315	.122	.977
27	103.05	2470.2	.124	.310	.122	.949
28	103.06	2480.6	.123	.357	.128	.966
29	103.05	2476.0	.135	.346	.104	.966
30	103.05	2472.3	.132	.292	.136	.932
31	103.05	2473.4	.156	.293	.117	.949
32	103.04	2467.0	.158	.349	.150	.949
33	103.04	2421.9	.164	.342	.157	.966
34	103.05	2504.4	.146	.305	.122	.954
35	103.05	2491.2	.135	.310	.157	.954
36	103.05	2453.1	.147	.331	.128	.954
37	103.06	2441.6	.129	.309	.139	.966
38	103.42	2437.5	.142	.289	.139	.954
39	102.79	2441.0	.143	.304	.140	.972
40	102.15	2407.7	.131	.350	.112	.943
41	100.08	2462.7	.139	.366	.120	.926
42	100.45	2478.2	.129	.329	.143	.949
43	99.39	2472.7	.137	.318	.132	.954
44	98.53	2475.7	.137	.333	.123	.943
45	97.58	2468.2	.125	.310	.136	.943
46	96.65	2526.1	.145	.324	.106	.932
47	96.41	2522.6	.152	.299	.125	.954
48	95.57	2530.7	.132	.306	.134	.937
49	94.94	2528.4	.148	.289	.146	.926
50	94.51	2515.6	.137	.262	.152	.909
51	93.86	2511.5	.131	.294	.103	.926
52	92.81	2517.2	.131	.276	.124	.926

Run No. 2-31574 continued

53	91.75	2552.1	.146	.279	.111	.920
54	91.12	2516.9	.143	.218	.178	.937
55	90.48	2518.1	.119	.214	.144	.920
56	89.94	2511.2	.146	.234	.133	.900
57	89.99	2507.7	.140	.230	.180	.932
58	88.88	2483.2	.143	.304	.104	.932
59	87.72	2499.7	.137	.266	.156	.926
60	87.51	2507.9	.127	.266	.130	.960
61	88.87	2502.5	.126	.236	.145	.937
62	88.23	2470.4	.133	.231	.152	.960
63	85.81	2484.5	.140	.273	.113	.915
64	85.39	2476.2	.146	.304	.161	.915
65	84.84	2501.3	.134	.285	.128	.915
66	83.76	2500.4	.149	.323	.108	.932
67	83.65	2499.8	.119	.310	.124	.915
68	82.63	2470.2	.127	.290	.097	.949
69	82.20	2487.9	.121	.270	.090	.954
70	81.35	2492.9	.134	.340	.126	.909
71	81.14	2493.6	.147	.372	.083	.926
72	80.72	2495.1	.144	.349	.127	.926
73	80.29	2493.7	.133	.293	.143	.915
74	79.87	2489.0	.156	.325	.128	.937
75	79.44	2489.8	.163	.329	.203	.920
76	79.44	2504.6	.169	.380	.121	.903
77	78.81	2500.0	.172	.371	.130	.903
78	78.38	2485.6	.151	.388	.069	.909
79	77.96	2493.0	.146	.413	.094	.897

Run No. 6-13074 (Figure G-11, p. 188) (82 wt. % AP propellant [UFN], single-pressure-increase-pulse, 12-14 mm)

SCAN NUMBER	PRESSURE,PSIA	H2O MOL FRACTION	CO2 MOL FRACTION	CO MOL FRACTION
1	74.10	.333	.048	.327
4	74.10	.301	.048	.299
[illegible]	74.[illegible]	.310	.043	.375
[illegible]	73.91	.335	.049	.257
[illegible]	73.[illegible]	.332	.050	.240
[illegible]	73.[illegible]	.304	.045	.246
[illegible]	73.91	.280	.037	.208
[illegible]	73.[illegible]	.288	.034	.262
[illegible]	74.[illegible]	.324	.054	.264
10	73.[illegible]	.292	.052	.348
11	73.[illegible]	.320	.059	.250
12	73.93	.371	.060	.113
13	73.91	.315	.045	.341
14	73.91	.298	.045	.321
15	73.91	.350	.054	.183
16	74.[illegible]	.290	.050	.314
17	73.91	.291	.045	.270
18	74.[illegible]	.275	.031	.212
19	73.94	.302	.052	.284
20	74.[illegible]	.326	.045	.356
21	74.[illegible]	.335	.048	.301
22	73.[illegible]	.333	.052	.218
23	74.[illegible]	.349	.053	.310
24	74.91	.324	.053	.311
25	74.[illegible]	.334	.045	.133
26	74.[illegible]	.345	.068	.110
27	73.91	.3[illegible]3	.064	.190
28	74.[illegible]	.281	.049	.298
29	74.[illegible]	.309	.059	.273
30	74.[illegible]	.284	.033	.439
31	74.[illegible]	.308	.045	.157
32	74.[illegible]	.397	.052	.140
33	74.[illegible]	.424	.055	.304
34	74.[illegible]	.328	.056	.358
35	74.[illegible]	.300	.032	.[illegible]
36	74.[illegible]	.343	.057	.[illegible]
37	74.[illegible]	.306	.054	.357
38	74.[illegible]	.313	.051	.304
39	74.[illegible]	.255	.050	.159
40	74.[illegible]	.346	.062	.284
41	74.[illegible]	.306	.059	.229
42	74.[illegible]	.309	.062	.234
43	74.37	.317	.056	.277
44	74.[illegible]	.303	.051	.354
45	74.[illegible]	.309	.059	.240
46	74.[illegible]	.329	.068	.248
47	74.[illegible]	.344	.061	.291
48	74.[illegible]	.420	.066	.224
49	74.[illegible]	.362	.066	.095
50	74.[illegible]	.303	.050	.393
51	74.46	.299	.046	.264
52	74.37	.327	.051	.244

Run No. 6-13074 continued

55	74.40	.270	.054	.184
56	74.50	.334	.052	.218
57	74.64	.372	.050	.321
58	74.70	.350	.045	.290
59	74.80	.306	.046	.298
60	74.90	.301	.053	.283
61	74.96	.329	.049	.276
62	75.05	.415	.059	.223
63	75.14	.445	.056	.185
64	75.20	.392	.052	.344
65	75.30	.405	.056	.286
66	75.44	.351	.055	.239
67	75.54	.301	.052	.211
68	75.64	.323	.063	.163
69	75.74	.305	.066	.175
70	75.81	.291	.057	.162
71	75.91	.311	.048	.266
72	75.96	.324	.052	.209
73	76.01	.287	.057	.235
74	76.01	.284	.052	.292
75	76.10	.300	.052	.304
76	76.21	.414	.054	.232
77	76.31	.376	.056	.269
78	76.40	.335	.055	.263
79	76.50	.280	.054	.352
80	76.61	.359	.061	.169
81	76.71	.329	.061	.258
82	76.81	.399	.061	.250
83	76.91	.410	.070	.185
84	77.00	.364	.067	.163
85	77.11	.376	.064	.110
86	77.20	.269	.050	.217
87	77.30	.318	.053	.323
88	77.40	.319	.057	.302
89	77.50	.372	.068	.254
90	77.60	.366	.074	.194
91	77.70	.363	.073	.171
92	77.77	.279	.057	.280
93	77.87	.325	.056	.265
94	77.93	.363	.064	.278
95	78.03	.330	.063	.230
96	78.14	.335	.061	.131
97	78.24	.372	.070	.168
98	78.33	.333	.069	.159
99	78.42	.286	.057	.237
100	78.54	.314	.065	.208
101	78.64	.364	.079	.118
102	78.74	.352	.079	.064
103	78.83	.251	.071	.238
104	78.94	.311	.065	.236
105	79.04	.316	.062	.274
106	79.12	.329	.057	.248
107	79.23	.301	.050	.285
108	79.31	.321	.041	.204
109	79.41	.309	.037	.328
110	79.50	.305	.041	.349
111	79.59	.413	.045	.320

Run No. 6-13074 continued

11.	7[illegible].19	.352	.047	.237	.669
11A	7[illegible].19	.369	.052	.323	.622
11[illegible]	7[illegible].19	.405	.068	.242	.648
11[illegible]	7[illegible].19	.313	.060	.216	.593
11[illegible]	7[illegible]	.351	.054	.185	.595
11[illegible]	7[illegible].1	319	.053	.313	.591
.[illegible]	7[illegible].19	.366	.053	.[illegible]05	.575
.[illegible]	7[illegible]	.407	.062	.136	.543
1[illegible]	7[illegible].1	.420	.065	.172	.593
[illegible]	7[illegible]	.[illegible]31	.[illegible]5[illegible]	.[illegible]64	.583
[illegible]	7[illegible]	.[illegible]	.[illegible]56	.165	.60[illegible]
1[illegible]	7[illegible]	.381	.052	.202	.[illegible]85
[illegible]	7[illegible]	.[illegible]85	.053	.327	.693
.23	7[illegible]	.413	.062	.[illegible]64	.740
[illegible]	7[illegible]	.[illegible]37	.040	.341	.[illegible]69
[illegible]	7[illegible]	.373	.064	.[illegible]85	.553
[illegible]	7[illegible]	.[illegible]54	.[illegible]73	.[illegible]50	.512
[illegible]	7[illegible]	.345	.071	.219	.[illegible]36
12[illegible]	7[illegible].[illegible]	.[illegible]04	.052	.[illegible]48	.522
1[illegible]	7[illegible]	.310	.043	.308	.525
13[illegible]	7[illegible].5	.350	.045	.277	.654

Run No. 2-2674 (Figure G-12, p. 189) (82 wt. % AP propellant [UFN], single-pressure-increase-pulse, 12-14 mm)

SCAN NUMBER	PRESSURE,PSIA	H2O MOL FRACTION	CO2 MOL FRACTION	CO MOL FRACTION
1	50.50	.223	.072	.049
2	50.50	.246	.078	.136
3	50.50	.281	.073	.109
4	50.56	.263	.072	.152
5	50.61	.311	.067	.177
6	50.63	.267	.067	.126
7	50.61	.302	.072	.068
8	50.70	.370	.086	.100
9	50.83	.330	.088	.112
10	50.83	.308	.082	.060
11	50.70	.319	.095	.158
12	50.69	.277	.100	.060
13	50.66	.279	.097	.084
14	50.59	.279	.083	.101
15	50.59	.379	.078	.085
16	50.69	.260	.072	.084
17	50.61	.256	.057	.074
18	50.50	.267	.046	.068
19	50.41	.345	.041	.235
20	50.41	.340	.059	.094
21	50.41	.321	.072	.106
22	50.56	.265	.081	.051
23	50.69	.374	.090	-.104
24	50.61	.255	.095	.034
25	50.67	.280	.075	.195
26	50.61	.348	.060	.184
27	50.63	.264	.070	.268
28	50.59	.289	.078	.090
29	50.59	.290	.088	.140
30	50.70	.255	.083	.129
31	50.84	.280	.072	.249
32	50.84	.305	.065	.356
33	50.85	.307	.068	.277
34	50.68	.270	.060	.146
35	50.59	.242	.068	.049
36	50.59	.364	.068	.322
37	50.50	.335	.061	.187
38	50.50	.290	.062	.340
39	50.50	.287	.073	.094
40	50.50	.351	.076	.078
41	50.50	.344	.075	.217
42	50.50	.297	.075	.070
43	50.59	.289	.086	.126
44	50.63	.319	.091	-.124
45	50.59	.298	.096	.020
46	50.59	.325	.105	.060
47	50.59	.289	.107	-.022
48	50.59	.251	.093	.115
49	50.59	.231	.084	.120
50	50.50	.250	.065	.031
51	50.50	.292	.063	.168
52	50.59	.240	.057	.184

Run No. 2-2674 continued

53	50.59	.268	.075	.241
54	50.59	.260	.085	.079
55	50.50	.231	.085	.101
56	50.50	.256	.084	.210
57	50.50	.301	.084	.057
58	50.41	.300	.088	.034
59	50.41	.270	.083	.114
60	50.50	.257	.091	.174
61	50.59	.309	.085	.116
62	50.50	.294	.084	.114
63	50.59	.287	.089	.107
64	50.59	.246	.080	.168
65	50.68	.307	.073	.244
66	50.59	.336	.080	.285
67	50.41	.350	.086	.167
68	50.68	.308	.091	.254
69	50.59	.251	.089	.064
70	50.59	.322	.076	.100
71	50.68	.282	.080	.170
72	50.68	.311	.086	.104
73	50.77	.305	.079	.090
74	50.68	.332	.085	.136
75	50.77	.296	.112	.083
76	50.77	.322	.100	-.031
77	50.77	.255	.113	.091
78	51.77	.296	.108	.098
79	51.77	.290	.101	.109
80	50.77	.301	.093	.086
81	50.86	.316	.097	.171
82	50.77	.290	.084	.304
83	50.68	.273	.082	.183
84	50.68	.285	.059	.124
85	51.04	.290	.056	.255
86	51.05	.341	.072	.214
87	51.14	.320	.080	.257
88	51.14	.339	.071	.334
89	51.14	.311	.089	.144
90	51.14	.292	.085	.173
91	51.41	.334	.077	.050
92	51.41	.279	.091	.140
93	51.41	.320	.090	.088
94	51.41	.227	.090	.142
95	51.50	.305	.092	.068
96	51.50	.302	.093	.148
97	51.50	.320	.084	-.013
98	51.77	.300	.101	.262
99	51.77	.372	.104	.147
100	52.05	.316	.112	.137
101	52.14	.287	.104	.098
102	52.14	.263	.087	.058
103	52.51	.243	.075	.237
104	52.42	.252	.073	.186
105	52.69	.318	.080	.227
106	52.69	.324	.093	.177
107	52.78	.280	.091	.085
108	52.68	.335	.095	.058
109	52.95	.291	.097	.197

Run No. 2-2674 continued

110	52.97	.288	.113	.160
111	53.15	.333	.122	.189
112	53.[illegible]	.314	.113	.164
113	53.[illegible]	.293	.098	.094
114	53.[illegible]	.305	.060	.265
115	53.[illegible]	.317	.073	.194
116	53.[illegible]	.296	.073	.192
117	53.79	.232	.064	.240
118	53.[illegible]7	.291	.071	.212
119	53.47	.293	.065	.357
120	54.[illegible]	.322	.062	.324
121	54.[illegible]	.288	.059	.207
122	54.[illegible]	.327	.060	.317
123	54.81	.364	.072	.264
124	54.[illegible]1	.329	.076	.293
125	54.[illegible]	.411	.075	.320
126	54.72	.[illegible]	.073	.244
127	54.[illegible]	.313	.072	.204

Run No. 8-4374 (Figure G-13, p. 190) (82 wt. % AP propellant [UFN], single-pressure-increase-pulse, 3-5 mm)

SCAN NUMBER	PRESSURE-PSIA	FLAME TEMP.-DEG. KELVIN	H2O MOL FRACTION	CO2 MOL FRACTION	CO MOL FRACTION	NA-D ABS.
1	36.63	2505.7	.810	.101	.314	.519
2	36.71	2429.3	.769	.103	.293	.509
3	36.78	2490.4	.806	.101	.309	.535
4	36.85	2467.8	.803	.112	.346	.595
5	36.85	2490.2	.806	.106	.276	.579
6	36.84	2483.8	.811	.110	.280	.530
7	36.72	2521.6	.790	.107	.263	.486
8	36.74	2513.2	.817	.109	.295	.551
9	36.72	2504.4	.824	.113	.330	.608
10	36.67	2516.8	.791	.112	.291	.540
11	36.70	2471.8	.815	.094	.254	.540
12	36.70	2511.6	.774	.093	.260	.530
13	36.71	2507.3	.802	.104	.317	.595
14	36.69	2534.2	.810	.107	.258	.486
15	36.73	2501.8	.828	.109	.360	.540
16	36.74	2491.9	.818	.105	.331	.562
17	36.74	2481.5	.822	.107	.268	.584
18	36.73	2506.9	.816	.108	.344	.540
19	36.73	2532.4	.796	.108	.215	.508
20	36.72	2532.4	.821	.109	.258	.503
21	36.71	2511.5	.821	.113	.241	.584
22	36.72	2498.3	.806	.097	.271	.557
23	36.68	2487.8	.744	.092	.286	.568
24	36.70	2467.9	.782	.087	.411	.540
25	36.70	2496.8	.851	.096	.332	.530
26	36.71	2545.8	.836	.101	.349	.459
27	36.69	2492.5	.806	.101	.188	.551
28	36.69	2497.4	.803	.085	.314	.568
29	36.72	2506.5	.809	.100	.228	.551
30	36.72	2537.1	.757	.087	.448	.524
31	36.74	2533.8	.796	.097	.461	.497
32	36.69	2551.5	.814	.098	.372	.497
33	36.71	2496.9	.827	.096	.253	.432
34	36.69	2504.5	.815	.094	.323	.568
35	36.74	2477.2	.804	.100	.284	.595
36	36.63	2536.1	.787	.110	.372	.519
37	36.68	2504.9	.806	.117	.333	.503
38	36.69	2507.8	.837	.121	.213	.497
39	36.71	2535.4	.796	.107	.293	.503
40	37.15	2534.4	.833	.115	.218	.464
41	37.49	2534.7	.806	.094	.340	.524
42	37.74	2546.9	.785	.091	.325	.513
43	38.08	2526.1	.814	.079	.44	.502
44	38.19	2474.5	.806	.090	.376	.564
45	38.42	2468.9	.775	.098	.288	.573
46	38.42	2504.7	.786	.110	.195	.491
47	38.50	2527.0	.774	.106	.218	.568
48	38.38	2486.7	.734	.104	.316	.628
49	38.76	2538.7	.742	.102	.340	.540
50	38.93	2535.9	.744	.092	.341	.540
51	39.33	2562.7	.736	.090	.294	.551
52	39.61	2599.4	.771	.094	.414	.480

Run No. 8-4374 continued

53	39.[illegible]	2521.3	.784	.087	.330	.590
54	4[illegible].9	2536.3	.740	.073	.397	.557
[illegible]	4[illegible]	2547.8	.764	.078	.309	.563
[illegible]	4[illegible]	2561.1	.756	.083	.374	.557
57	40.97	2561.1	.827	.085	.434	.557
58	41.[illegible]	2521.9	.859	.081	.366	.617
[illegible]	41.[illegible]	2516.0	.871	.086	.357	.612
60	41.72	2516.9	.841	.096	.364	.584
61	41.[illegible]	2504.4	.777	.087	.453	.546
62	41.[illegible]	2501.3	.696	.092	.282	.562
63	41.73	2521.1	.864	.083	.301	.633
64	41.[illegible]	2505.7	.745	.100	.219	.535
65	42.[illegible]	2534.2	.800	.093	.239	.612
66	42.[illegible]	2551.0	.845	.105	.282	.579
67	42.[illegible]	2[illegible].2	.775	.105	.263	.644
68	42.[illegible]	2547.4	.687	.097	.265	.595
69	43.17	2551.9	.654	.088	.311	.568
70	43.[illegible]	2541.8	.712	.090	.309	.579
71	43.71	2440.8	.720	.094	.203	.600
72	43.77	2575.7	.751	.107	.267	.533
73	43.17	2543.8	.740	.105	.280	.590
74	43.77	2511.4	.692	.107	.163	.623
75	43.[illegible]	2524.2	.696	.109	.145	.612
76	43.[illegible]	2534.4	.697	.081	.401	.595
77	44.[illegible]	2523.4	.705	.076	.458	.593
78	44.33	2491.3	.715	.076	.404	.623
79	44.70	2467.8	.692	.087	.338	.650
80	45.[illegible]	2519.4	.699	.078	.276	.601
81	45.[illegible]	2522.4	.713	.086	.291	.628
82	45.47	2541.4	.696	.083	.332	.595
83	45.72	2521.5	.716	.086	.375	.606
84	45.[illegible]	2511.3	.702	.089	.262	.622
85	45.[illegible]	2501.6	.706	.087	.376	.633
86	45.[illegible]	2511.3	.719	.093	.244	.644
87	45.09	2545.4	.730	.100	.300	.568
88	45.[illegible]	2502.4	.697	.089	.265	.633
89	46.[illegible]	2483.7	.709	.079	.351	.666
90	46.[illegible]	2511.1	.702	.089	.[illegible]87	.601
91	46.[illegible]	2511.4	.699	.089	.321	.606
92	46.[illegible]	2492.1	.686	.082	.353	.644
93	46.[illegible]	2551.4	.730	.091	.290	.535
94	47.[illegible]	2522.5	.699	.091	.[illegible]66	.666
95	47.42	2470.9	.684	.080	.275	.650
96	47.[illegible]	2480.4	.694	.091	.268	.651
97	47.[illegible]	2492.1	.711	.095	.318	.644
98	47.[illegible]	2518.1	.654	.088	.329	.612
99	48.61	2517.3	.711	.092	.327	.655
100	47.93	2492.0	.699	.104	.209	.655
101	47.[illegible]	2470.7	.703	.097	.234	.688
102	48.61	2516.3	.667	.091	.271	.625
103	48.10	2508.3	.648	.092	.273	.655
104	48.35	2462.6	.635	.084	.306	.672
105	48.61	2547.3	.688	.094	.325	.584
106	48.78	2488.9	.694	.090	.267	.650
107	49.03	2492.3	.664	.089	.295	.623
108	49.12	2477.4	.643	.087	.348	.677
109	49.37	2518.6	.616	.062	.251	.694

Run No. 5-4474 (Figure G-14, p. 191) (82 wt. % AP propellant [UFI], single-pressure-increase-pulse, 12-14 mm)

SCAN NUMBER	PRESSURE,PSIA	FLAME TEMP.,DEG. KELVIN	H2O ABSORBANCE	CO2 ABSORBANCE	CO ABSORBANCE	NA-D ABS.
1	42.50	2515.3	.093	.311	-.012	.487
2	42.42	2538.9	.091	.315	-.015	.460
3	42.42	2519.1	.089	.322	-.027	.465
4	42.25	2487.7	.089	.293	-.027	.503
5	42.08	2501.6	.097	.294	-.025	.460
6	42.08	2479.2	.086	.307	-.031	.513
7	41.99	2516.6	.092	.298	.000	.491
8	41.91	2512.7	.089	.272	-.014	.513
9	41.99	2460.4	.078	.252	-.030	.604
10	42.08	2424.1	.102	.266	-.003	.604
11	42.25	2474.0	.089	.275	-.003	.524
12	42.50	2453.8	.093	.258	-.007	.513
13	42.50	2466.1	.083	.283	-.024	.497
14	42.50	2511.1	.092	.302	-.033	.465
15	42.67	2499.7	.092	.294	-.037	.497
16	42.58	2529.5	.086	.309	-.026	.465
17	42.42	2507.1	.114	.317	.065	.497
18	42.16	2479.0	.071	.361	-.071	.503
19	41.99	2489.9	.090	.310	-.038	.503
20	41.99	2508.4	.072	.291	.002	.465
21	41.91	2476.4	.076	.287	-.009	.471
22	42.08	2515.8	.081	.280	-.023	.476
23	42.08	2561.6	.082	.294	-.036	.439
24	42.16	2531.2	.090	.283	-.006	.476
25	42.33	2491.7	.080	.294	-.024	.444
26	42.42	2497.9	.087	.305	-.031	.433
27	42.50	2479.0	.079	.293	-.055	.503
28	42.42	2470.5	.067	.261	-.026	.540
29	42.25	2545.4	.082	.287	-.006	.433
30	42.16	2592.1	.080	.266	-.009	.412
31	41.99	2524.4	.084	.272	-.007	.465
32	41.91	2460.3	.093	.303	-.005	.497
33	41.99	2553.3	.088	.220	.030	.444
34	41.99	2508.2	.093	.215	.011	.503
35	42.08	2499.7	.088	.238	.006	.535
36	42.25	2525.3	.082	.280	-.012	.487
37	42.42	2521.3	.087	.300	-.011	.492
38	42.42	2507.9	.089	.312	-.012	.476
39	42.33	2462.5	.076	.294	-.018	.540
40	42.25	2459.7	.078	.250	.004	.540
41	42.16	2483.5	.080	.241	-.001	.631
42	41.99	2483.4	.088	.267	-.009	.529
43	41.91	2507.9	.085	.272	.017	.476
44	41.91	2512.7	.088	.298	-.000	.460
45	41.91	2526.9	.086	.301	.007	.433
46	42.08	2548.4	.065	.262	.002	.433
47	42.16	2537.8	.085	.266	-.003	.433
48	42.67	2505.6	.096	.239	.001	.503
49	42.75	2585.3	.092	.225	-.003	.433
50	43.18	2501.1	.080	.276	-.017	.529
51	43.43	2487.3	.084	.309	-.037	.535
52	43.52	2540.3	.081	.327	-.015	.471

Run No. 5-4474 continued

53	43.72	2570.8	.077	.310	-.004	.455
54	43.94	2564.0	.075	.271	.003	.540
55	44.11	2525.3	.084	.269	-.004	.487
56	44.28	2524.0	.084	.287	-.034	.524
57	44.45	2545.2	.081	.259	-.007	.513
58	44.71	2520.2	.087	.242	.014	.529
59	45.05	2567.4	.079	.231	.033	.446
60	45.13	2550.3	.081	.250	.009	.497
61	45.64	2560.6	.080	.261	-.001	.487
62	45.98	2540.4	.085	.262	.006	.529
63	46.15	2478.7	.089	.260	-.003	.631
64	46.49	2485.5	.088	.254	-.026	.626
65	46.66	2524.3	.081	.261	-.020	.572
66	46.74	2527.1	.075	.263	-.024	.545
67	47.00	2486.3	.079	.243	.015	.604
68	47.00	2485.0	.079	.260	.001	.588
69	47.17	2524.1	.090	.277	-.012	.540
70	47.42	2496.9	.087	.307	-.003	.636
71	47.59	2553.7	.083	.301	-.007	.535
72	47.85	2513.1	.085	.320	-.018	.523
73	48.02	2543.6	.082	.322	-.029	.519
74	48.27	2564.6	.076	.250	.000	.497
75	48.61	2537.1	.077	.218	.014	.594
76	49.04	2474.0	.079	.238	.013	.668
77	49.21	2497.5	.093	.246	.008	.594
78	49.38	2519.2	.089	.232	.039	.567
79	45.46	2513.9	.092	.245	.008	.588
80	49.03	2547.3	.080	.207	.020	.578

NOMENCLATURE

Symbol	Description	Units
A_{ox}	exposed surface area of the oxidizer per total propellant surface area	cm^2
A_{fuel}	exposed surface area of the fuel per total propellant surface area	cm^2
C	proportionality constant of electro-optical hot-gas pyrometer system	
c	concentration of absorbing component	moles/liter
c_1	physical constant	3.74×10^{-12} $\cdot (watts/cm^2)$
c_2	physical constant	1.439°K cm
D_f	hot-gas pyrometer signal due to flame emission	mv
D_T	hot-gas pyrometer signal due to flame-transmitted radiation from the background radiation source	mv
D_s	hot-gas pyrometer signal due to background radiation source	mv
K_λ	Beer-Lambert spectral absorption coefficient at wavelength λ	ℓ/cm moles
L	characteristic length associated with initially depleting the propellant surface of one ingredient during depressurization	cm
ℓ	optical path length in flame	cm
m_λ	ratio of incident radiant power at wavelength λ to the incident radiant power at 3.90 μm	dimensionless
n_λ	ratio of flame emission at 3.9 μm to the flame emission at wavelength λ	dimensionless

$N_{ps}(\lambda_D, T_{ps})$	spectral radiance of the projected image of the background radiation source over the Na D-line filter spectral bandwidth	$\frac{\text{watts}}{\text{cm}^2 \cdot \text{Sr} \cdot \mu\text{m}}$
$N^b(\lambda_D, T_f)$	spectral radiance of a blackbody at the true flame temperature over the Na D-line filter spectral bandwidth	$\frac{\text{watts}}{\text{cm}^2 \cdot \text{Sr} \cdot \mu\text{m}}$
$N^b(\lambda_D, T^b_{ps})$	spectral radiance of a blackbody at the brightness temperature of the projected image of the background radiation source over the Na D-line filter spectral bandwidth	$\frac{\text{watts}}{\text{cm}^2 \cdot \text{Sr} \cdot \mu\text{m}}$
$N_s(\lambda_p, T^p_s)$	spectral radiance of the tungsten filament at the optical pyrometer wavelength	$\frac{\text{watts}}{\text{cm}^2 \cdot \text{Sr} \cdot \mu\text{m}}$
$N_s(\lambda_D, T^b_s)$	spectral radiance of the tungsten filament at the Na D-line wavelength	$\frac{\text{watts}}{\text{cm}^2 \cdot \text{Sr} \cdot \mu\text{m}}$
p^o_λ	incident radiant power at wavelength λ from the infrared radiation source	watts
p_λ	transmitted radiant power at wavelength λ from the infrared radiation source	watts
o_λ	flame emission at wavelength λ	watts
$\bar{o}_\lambda$	time-average value of the flame emission	watts
p'_λ	fluctuating component of p_λ	watts
r	characteristic mean regression rate associated with depleting the propellant surface of one ingredient during the initial depressurization	cm/sec
T_{ps}	true temperature of projected image of the background radiation source	°K
T^p_{ps}	brightness temperature measured at λ_p of the projected image of the background radiation source	°K
T^b_{ps}	brightness temperature measured at λ_D of the projected image of the background radiation source	°K
T_s	true temperature of tungsten filament	°K

T_s^p	brightness temperature measured at λ_p of the tungsten filament (optical pyrometer reading)	°K
T_s^b	brightness temperature measured at λ_D of the tungsten filament	°K
T_f	true flame temperature	°K
T_{ss}	sampling time interval associated with taking digital data	msec
v_{ox}	oxidizer gasification rate per exposed surface area of oxidizer	$\frac{gm}{sec.cm}$
v_{fuel}	fuel gasification rate per exposed surface area of fuel	$\frac{gm}{sec.cm}$
$x(t)$	output signal from filter	
x_n	present input value to digital-lag filter	
$y(t)$	input signal to filter	
y_n	present output value from digital-lag filter	
y_{n-1}	previous output value from digital-lag filter	

Greek Letters

τ	characteristic time of propellant during depressurization	msec
ω	characteristic frequency associated with initial gas-phase composition fluctuation during depressurization	Hz.
λ	wavelength	μm
λ_D	Na D-line wavelength	0.5896-μm
λ_p	optical pyrometer wavelength	0.653-μm
$\Delta\lambda_D$	spectral bandwidth of the Na D-line interference filter	μm
$\epsilon_{f\lambda}$	effective flame emissivity over the spectral bandwidth of the Na D-line interference filter	dimensionless
$\alpha_{f\lambda}$	effective absorptance of the flame over the spectral bandwidth of the Na D-line filter	dimensionless

ε_p	emissivity of tungsten at the optical pyrometer wavelength	dimension-less
ε_D	emissivity of tungsten at the Na D-line wavelength	dimension-less
τ_f	time constant of the digital-lag filter	msec
α	weighting function of the digital-lag filger	dimension-less

REFERENCES

1. Derr, R. L. and Osborn, J. R., "Composite Propellant Combustion," *AIAA Journal, Vol. 8,* No. 8, 1488 (August, 1970).

2. Bastress, E. K., Hall, K. P., and Summerfield, M. "Modification of the Burning Rates of Solid Propellants by Oxidizer Particle Size Control," Preprint 1597-61, February, 1961, American Rocket Society; Rept. 536, March, 1961, Princeton University.

3. Boggs, T. L., Derr, R. L., and Beckstead, M. W., "Surface Structure of Ammonium Perchlorate Composite Propellants," *AIAA Journal, Vol. 8,* No. 2, 370 (February, 1970).

4. Derr, R. L. and Boggs, T. L., "Role of Scanning Electron Microscopy in the Study of Solid Propellant Combustion: Part III. The Surface Structure and Profile Characteristics of Burning Composite Solid Propellants," *Combustion Science and Technology, Vol. 2,* No. 2, 219 (1970).

5. Baer, A. D., Ryan, N. W., and Schulz, E. B., "Spectra and Temperature of Propellant Flames During Depressurization," *AIAA Journal, Vol. 9,* No. 5, 869 (May, 1971).

6. Bastress, E. K., "Modification of the Burning Rates of Composite Propellants by Oxidizer Particle Size Control," Ph.D. Thesis, Dept. of Aeronautical Eng., Princeton University, (1961).

7. Schulz, E. M., "Propellant-Flame Spectra during Depressurization," Ph.D. Thesis, Dept. of Chem. Eng., University of Utah, (1970).

8. Gaydon, A. G. and Wolfhard, H. G., *Flames: Their Structure, Radiation and Temperature,* London, Chapman and Hall Ltd.,(1970).

9. Gaydon, A. G., *The Spectroscopy of Flames,* London, Chapman and Hall Ltd., (1957).

10. Wolfhard, H. G. and Parker, W. G., "A New Technique for the Spectroscopic Examination of Flames at Normal Pressures," *Proc. Phys. Soc. A, 62,* 722 (1949).

11. Wolfhard, H. G. and Parker, W. G., "Influence of Sulfur on Carbon Formation in Diffusion Flames," *Fuel, 29,* 235 (1950).

12. Wolfhard, H. G. and Parker, W. G., "A Spectroscopic Investibation into the Structure of Diffusion Flames," *Proc. Phys. Soc. A, 65,* 2 (1952).

13. Spokes, G. N. and Gaydon, A. G., "Absorption Spectra of Flat Flames Using a Multiple-Reflexion Technique," *Nature, Vol. 180,* No. 4595, 1114 (November, 1957).

14. Donovan, R. E. and Agnew, W. G., "Infrared Spectrum of Two-Stage Cool Flame of Diethyl Ether," *J. Chem. Phy., Vol. 23,* No. 9, 1592 (September, 1955).

15. Donovan, R. E., "Infrared Spectrum of the Two-Stage Cool Flame of Acetaldehyde,"

16. Cole, D. J. and Minkoff, G. J., "Carbon Formation in Diffusion Flames and the Role of Acetylene," *Proc. Roy. Soc. A., 239,* 280 (1957).

17. Cole, D. J. and Minkoff, G. J., "Experimental Techniques for the Study of Flat Flames by Infrared Spectroscopy," *Combustion and Flame, 1,* 241 (1957).

18. Smith, L. G., "A New Source for Infrared Spectrometers," *Rev. Sci. Instr., 13,* 63 (1942).

19. Buckingham, W. D. and Deibert, C. R., "The Concentrated-Arc Lamp," *J. Opt. Soc. Am., 36,* 245 (1946).

20. Rupert, C. S. and Strong, J., "The Carbon-Arc as an Infra-Red Source," *J. Opt. Soc. Am., 40,* 455 (1950).

21. Taylor, J. H., Rupert, C. S., and Strong, J., "An Incandescent Tungsten Source for Infrared Spectroscopy," *J. Opt. Soc. Am., 41,* 626 (1951).

22. Eisel, J. "Flame Spectra of Solid Propellants During Unstable Combustion," Ph.D. Thesis, Dept. of Chem. Eng., University of Utah, (1972).

23. Heath, G. A. and Hirst, R., "Some Characteristics of the High Pressure Combustion of Double-Base Propellants," *Eighth Symposium (International) on Combustion,* Baltimore, Md.: Williams and Wilkins Co., 711 (1962).

24. Diederichsen, J. and Gould, R. D., "Combustion Instability of Solid Propellants: Radiation from Cordite Burning Under Conditions of Oscillating Pressure," Rocket Propulsion Establishment (Westcott), T.M. 278, (May, 1966).

25. Kimball, G. H. and Brownlee, W. G., "Status Report of Optical Studies of Combustion Instability at CARDE," Canadian Armament Research and Development Establishment, CARDE T.M. 1784/68, (March, 1968).

26. Eisel, J. L., Ryan, N. W., and Baer, A. D., "Combustion of NH_4ClO_4-Polyurethane Propellants: Pressure, Temperature, and Gas-Phase Composition Fluctuations," *AIAA Journal, Vol. 10,* No. 12, 1655 (1972).

27. Boggs, T. L., and Beckstead, M. W., "Failure of Existing Theories to Correlate Experimental Nonacoustic Combustion Instability Data," *AIAA Journal, Vol. 8,* No. 4, 626 (April, 1970).

28. Law, R. J., Manuscript under preparation, Ph.D. Thesis, Dept. of Chem. Eng., University of Utah, (1974).

29. Millar, G. H., Winans, J. G., Uyehara, O. A., and Myers, P. S., "A Fast, Electro-optical, Hot Gas Pyrometer," *J. Opt. Soc. A., Vol. 43,* No. 7, 609 (July, 1953).

30. Tourin, R. H., *Spectroscopic Gas Temperature Measurement,* London, Elsevier Publishing Co., (1966).

31. Hertzberg, G., *Molecular Spectra and Molecular Structure, Vol. 1 and 2,* D. Van Nostrand Co., (1968).

32. Singh, T. and Sawyer, R. F., "CO Reactions in the Afterflame Region of Ethylene/Oxygen and Ethane/Oxygen Flames," *Thirteenth Symposium (International) on Combustion,* The Combustion Institute, 403, Pittsburgh, Pa. (1971).

33. Fristrom, R. M. and Westenberg, A. A., *Flame Structure,* New York, McGraw-Hill, (1965).

34. Brabbs, T. A., Belles, F. E., and Brokaw, R. S., "Shock-tube Measurements of Specific Reaction Rates in the Branched-chain H_2-CO-O_2 System," *Thirteenth Symposium (International) on Combustion,* The Combustion Institute, Pittsburgh, (1971).

35. Stewart, J. E., *Infrared Spectroscopy,* New York, Marcel Dekker Inc., (1970).

36. Angstrom, K., *Ann. Phys. Chem., 39,* 267 (1890).

37. Tourin, R. H., "Measurements of Infrared Spectral Emissivities of Hot Carbon Dioxide in the 4.3-μ Region," *J. Opt. Soc. A., Vol. 51,* No. 2, 175 (February, 1971).

38. Tourin, R. H., "Spectral Emissivities of Hot CO_2-H_2O Mixtures in the 2.7-μ Region," *J. Opt. Soc. A., Vol. 51*, No. 7, 799 (July, 1961).

39. Tourin, R. H., "Some Spectral Emissivities of Water Vapor in The 2.7-μ Region," *J. Opt. Soc. A., Vol 51*, No. 11, 1225 (November, 1961).

40. Steinberg, M. and Davies, W. O., "High-temperature Absorption of Carbon Dioxide at 4.40μ," *J. Chem. Physics, Vol. 34*, No. 4, 1373 (April, 1961).

41. Tourin, R. H. and Barbrov, H. J., "Note on Absorption Coefficients of Hot CO_2 at 4.40μ," *J. Chem. Physics, Vol. 37*, No. 3, 581 (1962).

42. Penzias, G. J. and Tourin, R. H., "Methods of Infra-red Analysis of Rocket Falmes in Situ," *Combustion and Flame, Vol. 6*, 147 (1962).

43. Babrov, H. J. and Tourin, R. H., "Methods of Predicting Infrared Radiance of Flames by Extrapolation From Laboratory Measurements," *Journal Quant. Spectrosc. Radiation Transfer, Vol. 3*, 15 (1963).

44. Schmidt, Ann. *Physik, Vol. 29*, 971 (1909).

45. Silverman, S., "The Determination of Flame Temperatures by Infra-red Radiation," *J. Opt. Soc. A., Vol. 39*, No. 4, 275 (April, 1949).

46. Forsythe, N. E. and Worthing, A. G., "The Properties of Tungsten and the Characteristics of Tungsten Lamps," *Astrophysical Jour., 61*, 146 (1925).

47. Groher, H., Erk, S., and Grigull, V. *Heat Transfer*, New York, McGraw Hill Co., Inc., 428 (1961).

48. Jursik, J., "Rejecting Common Mode Noise in Process Data Systems," *Control Eng.*, 61 (August, 1963).

49. Goff, K. W., "A Systematic Approach to DDC Design," *Inst. Soc. Amer. Jour.*, 44 (December, 1966).

50. Smith, C. L., *Digital Computer Process Control*, San Francisco, Intext Educational Publishers (1972).